THE BIOMECHANICAL EFFECT OF PROSTHETIC DESIGN FOR TRANSFEMORAL AMPUTEES

A COMBINED EXPERIMENTAL AND COMPUTATIONAL STUDY

Diana Toderiţă
Supervisor: Prof. Anthony MJ Bull

This thesis is submitted in the degree of Doctor of Philosophy of Imperial College London.

Department of Bioengineering
Imperial College London
United Kingdom
November 2022

Acknowledgments

Deepest thanks to my supervisor, Prof. Anthony MJ Bull, for his unconditional and invaluable guidance. Many thanks go to Clément Favier, an exceptional colleague and friend, for all the support and encouragement - thank you for always advising me in difficult times. Clém, Dave Henson and Vassia Vardakastani - my dream team - have helped me so much and working with them has been a pleasure. I will always be grateful for Fearghal Behan and Lance Rane's friendship, they have always been there for me. Also, many thanks to Shuqiao Xie, Christian Klemt, Pouya Amiri, Phatsimo Kgwarae, Hristo Dimitrov, Andra Topan, Giovanni Milandri and Răzvan Gălăţeanu. The PhD would not have been the same without these fantastic friends. Last but not least, huge thanks go to my beautiful family, Marian, Vasilica and Marius, for their never-ending love, encouragement and support. Vă mulţumesc şi vă iubesc!

A huge thank you to all participants for their help, this work could not have been possible without them. The financial support from the Royal British Legion Centre for Blast Injury Studies is gratefully acknowledged.

Declaration of Originality

I declare that this project is entirely my own work, except where explicit reference is made to the work of others. To the best of my knowledge, the work is not plagiarised.

Copyright Declaration

The copyright of this thesis rests with the author. Unless otherwise indicated, its contents are licensed under a Creative Commons Attribution-Non Commercial 4.0 International Licence (CC BY-NC).

Under this licence, you may copy and redistribute the material in any medium or format. You may also create and distribute modified versions of the work. This is on the condition that: you credit the author and do not use it, or any derivative works, for a commercial purpose.

When reusing or sharing this work, ensure you make the licence terms clear to others by naming the licence and linking to the licence text. Where a work has been adapted, you should indicate that the work has been changed and describe those changes.

Please seek permission from the copyright holder for uses of this work that are not included in this licence or permitted under UK Copyright Law.

Abstract

Lower limb prosthesis prescription is based on anecdotal evidence and manufacturer claims, with little research-based evidence of their effect on the musculoskeletal system. Amputees are at a high risk of musculoskeletal health complications, which may be avoided through adequate prosthesis design and prescription. This thesis aims to understand the bilateral above/through-knee (BTF) and unilateral above/through-knee amputee (UTF) function and loading with various prostheses in order to support informed decision-making in prosthesis prescription.

The thesis presents a method to create amputee musculoskeletal models based on anatomical datasets derived from magnetic resonance scans, where linear scaling to a model with the most similar pelvis width, body mass index and stump length to pelvis width ratio resulted in predictions of hip joint contact forces with minimal errors (average 0.4 BW). This method then enabled musculoskeletal modelling to be used in the remainder of the thesis, where new datasets of amputee gait were obtained from a number of different prostheses. Analysis of the biomechanical outcomes found that BTF with full-length articulated prostheses presented higher hip contact forces by 3.5 BW than non-articulated stubby prostheses and that reduced flexor muscle volume and residual limb length might limit the use of full-length articulated prostheses. When investigating UTF function with microprocessor knees (MPK), the analysis identified higher lateral intact knee impulse by 27.7 BW.s than able-bodied persons, and this may explain the incidence of intact knee osteoarthritis in the UTF population. As the vast majority of amputees are in low-to-middle-income countries, it was important to also assess the biomechanical effect of more affordable prostheses. Therefore, this thesis analysed UTF function with the International Committee of the Red Cross (ICRC) polycentric knee, where amputees presented with ICRC lower walking speeds (by 0.2 m/s) and higher loading of the intact knee (by 14.9 BW.s/m) and intact ankle (by 24.1 BW.s/m) with ICRC than MPK. The spring extension assist mechanism in polycentric knees is a key feature that influences amputee function, and this thesis showed that a novel extension assist, which links the top and bottom knee parts, improves walking speeds by 0.1 m/s and symmetry between the intact and prosthetic knee flexion angles by 5.5% compared to the conventional extension assist used by ICRC.

Finally, regression analysis was used to generalize learning of amputee function and loading, and identified the prosthesis type, age, stump length and body mass index to be significant predictors of cadence and speed. Prosthesis type was the only significant predictor of BTF hip and UTF lateral intact knee loading. Appropriate prosthetic design and prescription may reduce the risk of musculoskeletal complications, whilst maintaining appropriate functional levels. The studies in this thesis form the basis for future improvements of prosthesis design.

Contents

1 Context of research **21**
- 1.1 Overview of problem statement and motivation . . . 22
- 1.2 Thesis aim and significance . . . 25
- 1.3 Thesis objectives . . . 25
- 1.4 Thesis outline . . . 26

2 An anatomical atlas-based scaling study for quantifying muscle and hip joint contact forces in above and through-knee amputees using validated musculoskeletal modelling **27**
- 2.1 Introduction . . . 28
- 2.2 Methods . . . 29
  - 2.2.1 Experimental data . . . 29
  - 2.2.2 Anatomical geometry . . . 32
  - 2.2.3 Musculoskeletal modelling and data analysis . . . 35
- 2.3 Results . . . 40
  - 2.3.1 Predictors of discrepancies in muscle and hip joint contact forces . 41
- 2.4 Discussion . . . 43
  - 2.4.1 Validation of subject-specific models . . . 43
  - 2.4.2 Predictors of discrepancies in hip joint contact forces . . . 44
  - 2.4.3 Predictors of discrepancies in muscle forces . . . 45
  - 2.4.4 Predictors of discrepancies in muscle and hip joint contact forces . 45
  - 2.4.5 Limitations . . . 46
- 2.5 Conclusion . . . 48

3 Biomechanical assessment of bilateral transfemoral amputee gait with stubbies and microprocessor- controlled knees **49**
- 3.1 Introduction . . . 50
- 3.2 Aims and hypotheses . . . 51
- 3.3 Methods . . . 52
  - 3.3.1 Data acquisition and processing . . . 52
  - 3.3.2 Musculoskeletal modelling . . . 56
  - 3.3.3 Data analysis . . . 57
- 3.4 Results . . . 58
  - 3.4.1 Prosthesis type analysis . . . 58

3.4.2 Comparison between stubbies and full-length prostheses for amputees who could use both . . . 78
3.4.3 Stubby prostheses analysis . . . 90
3.5 Discussion . . . 102
3.6 Limitations . . . 105
3.7 Conclusion . . . 106

4 Understanding the musculoskeletal function and loading of unilateral transfemoral amputees 107
4.1 Introduction . . . 108
4.2 Methods . . . 111
4.2.1 Data acquisition and processing . . . 111
4.2.2 Anthropometry and body segment parameters . . . 114
4.2.3 Musculoskeletal modelling . . . 114
4.2.4 Data analysis . . . 115
4.3 Results . . . 116
4.3.1 Temporal and spatial gait characteristics . . . 116
4.3.2 Kinematics . . . 116
4.3.3 Kinetics . . . 127
4.3.4 Joint contact forces . . . 136
4.3.5 Case study . . . 141
4.4 Discussion . . . 144
4.4.1 Case study discussion . . . 148
4.5 Limitations . . . 148
4.6 Conclusion . . . 149

5 Biomechanical differences between high- and low-cost prostheses for transfemoral amputees 150
5.1 Introduction . . . 151
5.2 Methods . . . 153
5.2.1 Data acquisition and processing . . . 153
5.2.2 Anthropometry and body segment parameters . . . 156
5.2.3 Musculoskeletal modelling . . . 156
5.2.4 Data analysis . . . 157
5.3 Results . . . 157
5.3.1 Prosthetic components parameters . . . 157
5.3.2 Temporal and spatial gait characteristics . . . 158
5.3.3 Kinematics . . . 160
5.3.4 Kinetics . . . 170
5.4 Discussion . . . 184
5.5 Limitations . . . 187
5.6 Conclusion . . . 187

6 The effect of spring extension assist mechanisms in polycentric prosthetic knees 188
6.1 Introduction . . . 189
6.2 Methods . . . 191
6.2.1 Data acquisition and processing . . . 191
6.2.2 Anthropometry and body segment parameters . . . 193
6.2.3 Musculoskeletal modelling . . . 194
6.2.4 Data analysis . . . 195
6.3 Results . . . 195
6.3.1 SAT-PRO questionnaires . . . 195
6.3.2 Prosthetic inertial parameters . . . 196
6.3.3 Temporal and spatial gait characteristics . . . 197
6.3.4 Kinematics . . . 198
6.3.5 Kinetics . . . 207
6.4 Discussion . . . 222
6.5 Limitations . . . 224
6.6 Conclusion . . . 224

7 Conclusion. Generalizing learning of amputee musculoskeletal function and loading 225
7.1 Thesis summary and motivation for generalizing learning . . . 226
7.2 Database and analytical approach . . . 229
7.3 Results . . . 233
7.3.1 Individuals with bilateral transfemoral amputation . . . 233
7.3.2 Individuals with unilateral transfemoral amputation . . . 234
7.4 Thesis discussion and concluding remarks . . . 236
7.4.1 Individuals with bilateral transfemoral amputation . . . 236
7.4.2 Individuals with unilateral transfemoral amputation . . . 237
7.5 Future work . . . 241
7.6 Broader context . . . 242

Appendices 244

A Detailed muscle parameters of each anatomical dataset 245

B Validation of each subject-specific musculoskeletal model 263

C SAT-PRO prosthesis satisfaction questionnaire 269

D List of publications and conference presentations 273

List of Figures

1.1 Musculoskeletal modelling pipeline. 25

2.1 EMG sensor locations. 31
2.2 Lower limb 2D axial plane MRI scan of a representative subject. 32
2.3 Lower limb anatomy of a representative subject (one limb of a bilateral above-knee amputee): (a) pelvis, femoral remnants and muscle 3D reconstruction. (b) muscle lines-of-action (red), hip joint centre (yellow point), wrapping object (yellow cylinder). 33
2.4 Musculoskeletal model of one transfemoral amputee model. (a) Frontal view (b) Lateral view. 35
2.5 Reaction board method with moment equilibrium (reproduced with permission from Henson, 2020). 36
2.6 Musculoskeletal simulation pipeline for model 1. 38
2.7 Predicted muscle activations (solid line) and normalised EMG data (shaded area) for the adductor longus, gluteus maximus, gluteus medius and rectus femoris muscles for a representative model. 40

3.1 Representative study participants with different prostheses. 54
3.2 Pelvic orientations and coordinate system. 56
3.3 Left: Ankle dorsiflexion (DF)/plantar flexion (PF) angles. Right: Statistical parametric mapping results. BTF Sidekicks - green. BTF Genium - blue. AB - black. 60
3.4 Left: Hip joint abduction (Abd)/adduction (Add) angles. Right: Statistical parametric mapping results. BTF Sidekicks - green. BTF Genium - blue. AB - black. 62
3.5 Left: Hip joint extension (Ext)/flexion (Fle) angles. Right: Statistical parametric mapping results. BTF Sidekicks - green. BTF Genium - blue. AB - black. 63
3.6 Left: Hip internal (Int)/external (Ext) rotation (Rot) angles. Right: Statistical parametric mapping results. BTF Sidekicks - green. BTF Genium - blue. AB - black. 64
3.7 Left: Pelvic anterior (Ant)/posterior (Post) tilt angles. Right: Statistical parametric mapping results. BTF Sidekicks - green. BTF Genium - blue. AB - black. 65

3.8 Left: Pelvic obliquity angles. Positive angles describe an increase in the vertical height of the contralateral hip. Right: Statistical parametric mapping results. BTF Sidekicks - green. BTF Genium - blue. AB - black. . . 66
3.9 Left: Pelvic internal (Int)/external (Ext) rotation (Rot) angles. Right: Statistical parametric mapping results. BTF Sidekicks - green. BTF Genium - blue. AB - black. 67
3.10 Left: Ground reaction forces (GRF). Right: Statistical parametric mapping results. BTF Sidekicks - green. BTF Genium - blue. AB - black. . . 68
3.11 Left: Abduction (Abd)/adduction (Add) hip moments (Mom). Right: Statistical parametric mapping results. BTF Sidekicks - green. BTF Genium - blue. AB - black. 69
3.12 Left: Extension (Ext)/flexion (Fle) hip moments (Mom). Right: Statistical parametric mapping results. BTF Sidekicks - green. BTF Genium - blue. AB - black. 71
3.13 Left: Generated (Gen)/absorbed (Abs) hip joint power (Pow). Right: Statistical parametric mapping results. BTF Sidekicks - green. BTF Genium - blue. AB - black. 72
3.14 Left: Hip contact forces. Right: Statistical parametric mapping results. BTF Sidekicks - green. BTF Genium - blue. AB - black. 73
3.15 Left: Ankle dorsiflexion (DF)/plantar flexion (PF). Right: Statistical parametric mapping results. Cohort 1_Sidekicks - green. Cohort 1_Genium - blue. 79
3.16 Left: Hip joint angles (a) Hip abduction (Abd)/adduction (Add). (b) Hip extension (Ext)/flexion (Fle). (c) Hip internal (Int)/external (Ext) rotation (Rot). Right: Statistical parametric mapping results. Cohort 1_Sidekicks - green. Cohort 1_Genium - blue. 80
3.17 Left: Pelvic angles (a) Pelvic anterior (Ant)/posterior (Post) tilt. (b) Pelvic obliquity, where positive angles describe an increase in the vertical height of the contralateral hip. (c) Pelvic internal (Int)/external (Ext) rotation (Rot). Right: Statistical parametric mapping results. Cohort 1_Sidekicks - green. Cohort 1_Genium - blue. 82
3.18 Left: Ground reaction forces (GRF). Right: Statistical parametric mapping results. Cohort 1_Sidekicks - green. Cohort 1_Genium - blue. 83
3.19 Left: Hip joint moments and power (a) Abduction (Abd)/ adduction (Add) hip moments (Mom). (b) Extension (Ext)/flexion (Fle) hip moments (Mom). (c) Generated (Gen)/absorbed (Abs) hip joint power (Pow). Right: Statistical parametric mapping results. Cohort 1_Sidekicks - green. Cohort 1_Genium - blue. 84
3.20 Left: Hip joint contact forces. Right: Statistical parametric mapping results. Cohort 1_Sidekicks - green. Cohort 1_Genium - blue. 85
3.21 Left: Ankle dorsiflexion (DF)/plantar flexion (PF) angles. Right: Statistical parametric mapping results. Cohort 1_Sidekicks - orange. Cohort 2 - purple. 91

3.22 Left: Hip joint angles (a) Hip abduction (Abd)/adduction (Add). (b) Hip extension (Ext)/flexion (Fle). (c) Hip internal (Int)/external (Ext) rotation (Rot). Right: Statistical parametric mapping results. Cohort 1_Sidekicks - orange. Cohort 2 - purple. 92
3.23 Left: Pelvic angles (a) Pelvic anterior (Ant)/posterior (Post) tilt angles. (b) Pelvic obliquity angles, where positive angles describe an increase in the vertical height of the contralateral hip. (c) Pelvic internal (Int)/external (Ext) rotation (Rot) angles. Right: Statistical parametric mapping results. Cohort 1_Sidekicks - orange. Cohort 2 - purple. 94
3.24 Left: Ground reaction forces (GRF). Right: Statistical parametric mapping results. Cohort 1_Sidekicks - orange. Cohort 2 - purple. 95
3.25 Left: Hip joint moments and power (a) Abduction (Abd)/ adduction (Add) hip moments (Mom). (b) Extension (Ext)/flexion (Fle) hip moments (Mom). (c) Generated (Gen)/absorbed (Abs) hip joint power (Pow). Right: Statistical parametric mapping results. Cohort 1_Sidekicks - orange. Cohort 2 - purple. 96
3.26 Left: Hip joint contact forces. Right: Statistical parametric mapping results. Cohort 1_Sidekicks - orange. Cohort 2 - purple. 97
3.27 Subject-specific flexor muscle parameters (length, volume, PCSA). *Statistically significant differences between cohorts ($p<.05$). Cohort 1 - orange. Cohort 2 - blue. 101

4.1 Marker placement for one representative unilateral above-knee amputee. The labels highlight the marker and cluster positions as listed in Table 4.2. 113
4.2 Top: Ankle dorsiflexion (DF)/plantar flexion (PF) angles of UTF (blue) and AB (black). Bottom: Statistical parametric mapping results. 117
4.3 Top: Knee flexion (Fle)/extension (Ext) angles of UTF (blue) and AB (black). Bottom: Statistical parametric mapping results. 118
4.4 Top: Knee angular velocity of UTF (blue) and AB (black). Bottom: Statistical parametric mapping results. 119
4.5 Top: Hip flexion (Fle)/extension (Ext) angles of UTF (blue) and AB (black). Bottom: Statistical parametric mapping results. 120
4.6 Top: Hip abduction (Abd)/adduction (Add) angles of UTF (blue) and AB (black). Bottom: Statistical parametric mapping results. 121
4.7 Top: Hip internal (Int)/external (Ext) rotation (Rot) angles of UTF (blue) and AB (black). Bottom: Statistical parametric mapping results. 122
4.8 Top: Pelvic anterior (Ant)/posterior (Post) tilt angles of UTF (blue) and AB (black). Bottom: Statistical parametric mapping results. 123
4.9 Top: Pelvic obliquity angles of UTF (blue) and AB (black). Positive angles describe an increase in the vertical height of the contralateral hip. Bottom: Statistical parametric mapping results. 124
4.10 Top: Pelvic internal (Int)/external (Ext) rotation (Rot) angles of UTF (blue) and AB (black). Bottom: Statistical parametric mapping results. . 125
4.11 AB (left) and UTF (right) body orientations in the intact limb stance phase. Top: Front view. Bottom: Lateral view. 126

4.12 Top: Net ground reaction forces (GRF) of UTF (blue) and AB (black). Bottom: Statistical parametric mapping results. 127
4.13 Top: Ankle plantar flexion (PF)/dorsiflexion (DF) moments of UTF (blue) and AB (black). Bottom: Statistical parametric mapping results. 128
4.14 Top: Intact knee external adduction moment of UTF (blue) and AB (black). Bottom: Statistical parametric mapping results. 129
4.15 Top: Knee external flexion (Fle)/extension (Ext) moments of UTF (blue) and AB (black). Bottom: Statistical parametric mapping results. 130
4.16 Top: Hip abduction (Abd)/adduction (Add) moments of UTF (blue) and AB (black). Bottom: Statistical parametric mapping results. 131
4.17 Top: Hip flexion (Fle)/extension (Ext) moments of UTF (blue) and AB (black). Bottom: Statistical parametric mapping results. 132
4.18 Top: Ankle generated (Gen)/absorbed (Abs) power (Pow) of UTF (blue) and AB (black). Bottom: Statistical parametric mapping results. 133
4.19 Top: Knee generated (Gen)/absorbed (Abs) power (Pow) of UTF (blue) and AB (black). Bottom: Statistical parametric mapping results. 134
4.20 Top: Hip generated (Gen)/absorbed (Abs) power (Pow) of UTF (blue) and AB (black). Bottom: Statistical parametric mapping results. 135
4.21 Top: Intact ankle joint contact forces of UTF (blue) and AB (black). Bottom: Statistical parametric mapping results. 136
4.22 Top: Medial intact knee joint contact forces of UTF (blue) and AB (black). Bottom: Statistical parametric mapping results. 137
4.23 Top: Lateral intact knee joint contact forces of UTF (blue) and AB (black). Bottom: Statistical parametric mapping results. 138
4.24 Top: Total intact knee joint contact forces of UTF (blue) and AB (black). Bottom: Statistical parametric mapping results. 139
4.25 Top: Hip joint contact forces of UTF (blue) and AB (black). Bottom: Statistical parametric mapping results. 140
4.26 Case study GRF subjects UTF 1 and UTF 6 over the course of one complete intact and prosthetic side gait cycle. Intact side - blue. Prosthetic side - orange. 141
4.27 Case study results comparing UTF 1 (green) and UTF 6 (red) to the UTF cohort results (blue). 142

5.1 UTF study participant. The labels highlight the marker and cluster positions as listed in Table 4.2, Chapter 4. Top: MPK unit and dynamic response foot. Bottom: ICRC knee and SACH foot. 155
5.2 ICRC prosthesis system. 156
5.3 Top: Ankle dorsiflexion (DF)/plantar flexion (PF) angles of UTF with MPK (blue) and ICRC (black) prostheses. Bottom: Statistical parametric mapping results. 160
5.4 Top: Knee flexion (Fle)/extension (Ext) angles of UTF with MPK (blue) and ICRC (black) prostheses. Bottom: Statistical parametric mapping results. 161

5.5 Top: Prosthetic knee angular velocity and acceleration of UTF with MPK (blue) and ICRC (black) prostheses. Bottom: Statistical parametric mapping results. . . . 162
5.6 Top: Hip flexion (Fle)/extension (Ext) angles of UTF with MPK (blue) and ICRC (black) prostheses. Bottom: Statistical parametric mapping results. . . . 163
5.7 Top: Prosthetic side hip angular velocity and acceleration of UTF with MPK (blue) and ICRC (black) prostheses. Bottom: Statistical parametric mapping results. . . . 164
5.8 Top: Hip Abduction (Abd)/Adduction (Add) angles of UTF with MPK (blue) and ICRC (black) prostheses. Bottom: Statistical parametric mapping results. . . . 165
5.9 Top: Hip Internal (Int)/External (Ext) Rotation (Rot) angles of UTF with MPK (blue) and ICRC (black) prostheses. Bottom: Statistical parametric mapping results. . . . 166
5.10 Top: Pelvic Anterior (Ant)/Posterior (Post) tilt angles of UTF with MPK (blue) and ICRC (black) prostheses. Bottom: Statistical parametric mapping results. . . . 167
5.11 Top: Pelvic obliquity angles of UTF with MPK (blue) and ICRC (black) prostheses. Positive angles describe an increase in the vertical height of the contralateral hip. Bottom: Statistical parametric mapping results. . . . 168
5.12 Top: Pelvic Internal (Int)/External (Ext) Rotation (Rot) angles of UTF with MPK (blue) and ICRC (black) prostheses. Bottom: Statistical parametric mapping results. . . . 169
5.13 Top: Ground reaction forces of UTF with MPK (blue) and ICRC (black) prostheses. Bottom: Statistical parametric mapping results. . . . 170
5.14 Top: Ankle Plantar flexion (PF)/Dorsiflexion (DF) Moments of UTF with MPK (blue) and ICRC (black) prostheses. Bottom: Statistical parametric mapping results. . . . 171
5.15 Top: Intact knee Extension (Ext)/Flexion (Fle) Moments of UTF with MPK (blue) and ICRC (black) prostheses. Bottom: Statistical parametric mapping results. . . . 172
5.16 Top: External intact knee adduction moments of UTF with MPK (blue) and ICRC (black) prostheses. Bottom: Statistical parametric mapping results. . . . 173
5.17 Top: Hip Extension (Ext)/Flexion (Fle) Moments of UTF with MPK (blue) and ICRC (black) prostheses. Bottom: Statistical parametric mapping results. . . . 174
5.18 Top: Hip Abduction (Abd)/Adduction (Add) Moments of UTF with MPK (blue) and ICRC (black) prostheses. Bottom: Statistical parametric mapping results. . . . 175
5.19 Top: Ankle Generated (Gen)/Absorbed (Abs) Power of UTF with MPK (blue) and ICRC (black) prostheses. Bottom: Statistical parametric mapping results. . . . 176

5.20 Top: Knee Generated (Gen)/Absorbed (Abs) Power of UTF with MPK (blue) and ICRC (black) prostheses. Bottom: Statistical parametric mapping results. 177
5.21 Top: Hip Generated (Gen)/Absorbed (Abs) Power of UTF with MPK (blue) and ICRC (black) prostheses. Bottom: Statistical parametric mapping results. 178
5.22 Top: Intact side intact ankle joint contact forces of UTF with MPK (blue) and ICRC (black) prostheses. Bottom: Statistical parametric mapping results. 179
5.23 Top: Intact side medial knee joint contact forces of UTF with MPK (blue) and ICRC (black) prostheses. Bottom: Statistical parametric mapping results. 180
5.24 Top: Intact side lateral knee joint contact forces of UTF with MPK (blue) and ICRC (black) prostheses. Bottom: Statistical parametric mapping results. 181
5.25 Top: Intact side total knee joint contact forces of UTF with MPK (blue) and ICRC (black) prostheses. Bottom: Statistical parametric mapping results. 182
5.26 Top: Hip joint contact forces of UTF with MPK (blue) and ICRC (black) prostheses. Bottom: Statistical parametric mapping results. 183

6.1 Prosthetic knee extension assist mechanisms. (a) Conventional extension assist that links the rear bar to the body of the prosthesis. (b) Novel extension assist that links the top and bottom knee parts. 190
6.2 UTF study participant. The labels highlight the marker and cluster positions in Table 4.2, Chapter 4. Top: ICRC knee and SACH foot. Bottom: TaKeuP knee and SACH foot. 192
6.3 ICRC prosthesis system. 194
6.4 TaKeuP prosthesis system. 194
6.5 Top: Ankle DF (Dorsiflexion)/Plantar flexion (PF) angles with ICRC (black) and TaKeuP (green) prostheses. Bottom: Statistical parametric mapping results. 198
6.6 Top: Knee Flexion (Fle)/Extension (Ext) angles with ICRC (black) and TaKeuP (green) prostheses. Bottom: Statistical parametric mapping results. 199
6.7 Top: Prosthetic knee angular velocity and acceleration with ICRC (black) and TaKeuP (green) prostheses. Bottom: Statistical parametric mapping results. 200
6.8 Top: Hip Flexion (Fle)/Extension (Ext) angles with ICRC (black) and TaKeuP (green) prostheses. Bottom: Statistical parametric mapping results. 201
6.9 Top: Hip Abduction (Abd)/Adduction (Add) angles of UTF with ICRC (black) and TaKeuP (green) prostheses. Bottom: Statistical parametric mapping results. 202
6.10 Top: Hip Internal (Int)/External (Ext) Rotation (Rot) angles with ICRC (black) and TaKeuP (green) prostheses. Bottom: Statistical parametric mapping results. 203

6.11 Top: Pelvic Anterior (Ant)/Posterior (Post) tilt angles with ICRC (black) and TaKeuP (green) prostheses. Bottom: Statistical parametric mapping results. 204
6.12 Top: Pelvic obliquity angles with ICRC (black) and TaKeuP (green) prostheses. Bottom: Statistical parametric mapping results. 205
6.13 Top: Pelvic Internal (Int)/External (Ext) Rotation (Rot) angles with ICRC (black) and TaKeuP (green) prostheses. Bottom: Statistical parametric mapping results. 206
6.14 Top: Ground reaction forces (GRF) with ICRC (black) and TaKeuP (green) prostheses. Bottom: Statistical parametric mapping results. . . . 207
6.15 Top: Ankle Plantar flexion (PF)/Dorsiflexion (DF) moments with ICRC (black) and TaKeuP (green) prostheses. Bottom: Statistical parametric mapping results. 208
6.16 Top: Knee Flexion (Fle)/Extension (Ext) moments with ICRC (black) and TaKeuP (green) prostheses. Bottom: Statistical parametric mapping results. 209
6.17 Top: External intact knee adduction moments with ICRC (black) and TaKeuP (green) prostheses. Bottom: Statistical parametric mapping results. 210
6.18 Top: Hip Extension (Ext)/Flexion (Fle) moments with ICRC (black) and TaKeuP (green) prostheses. Bottom: Statistical parametric mapping results. 211
6.19 Top: Hip Abduction (Abd)/Adduction (Add) moments with ICRC (black) and TaKeuP (green) prostheses. Bottom: Statistical parametric mapping results. 212
6.20 Top: Ankle Generated (Gen)/Absorbed (Abs) power with ICRC (black) and TaKeuP (green) prostheses. Bottom: Statistical parametric mapping results. 213
6.21 Top: Knee Generated (Gen)/Absorbed (Abs) power with ICRC (black) and TaKeuP (green) prostheses. Bottom: Statistical parametric mapping results. 214
6.22 Top: Hip Generated (Gen)/Absorbed (Abs) power with ICRC (black) and TaKeuP (green) prostheses. Bottom: Statistical parametric mapping results. 215
6.23 Top: Intact ankle joint contact forces of UTF with ICRC (black) and TaKeuP (green) prostheses. Bottom: Statistical parametric mapping results. 216
6.24 Top: Medial compartment of the intact knee joint contact forces with ICRC (black) and TaKeuP (green) prostheses. Bottom: Statistical parametric mapping results. 217
6.25 Top: Lateral compartment of the intact knee joint contact forces with ICRC (black) and TaKeuP (green) prostheses. Bottom: Statistical parametric mapping results. 218
6.26 Top: Total intact knee joint contact forces with ICRC (black) and TaKeuP (green) prostheses. Bottom: Statistical parametric mapping results. . . . 219
6.27 Top: Hip joint contact forces with ICRC (black) and TaKeuP (green) prostheses. Bottom: Statistical parametric mapping results. 220
6.28 Thigh length discrepancy of one unilateral through-knee amputee fitted with ICRC and TaKeuP prosthetic knees. 223

B.1 Predicted muscle activations (solid line) and normalised EMG data (shaded area) for model 2. M, P and C represent the magnitude, phase and combined Sprague and Geers errors. 263
B.2 Predicted muscle activations (solid line) and normalised EMG data (shaded area) for model 3. M, P and C represent the magnitude, phase and combined Sprague and Geers errors. 264
B.3 Predicted muscle activations (solid line) and normalised EMG data (shaded area) for model 4. M, P and C represent the magnitude, phase and combined Sprague and Geers errors. 264
B.4 Predicted muscle activations (solid line) and normalised EMG data (shaded area) for model 5. M, P and C represent the magnitude, phase and combined Sprague and Geers errors. 265
B.5 Predicted muscle activations (solid line) and normalised EMG data (shaded area) for model 6. M, P and C represent the magnitude, phase and combined Sprague and Geers errors. 265
B.6 Predicted muscle activations (solid line) and normalised EMG data (shaded area) for model 7. M, P and C represent the magnitude, phase and combined Sprague and Geers errors. 266
B.7 Predicted muscle activations (solid line) and normalised EMG data (shaded area) for model 9. M, P and C represent the magnitude, phase and combined Sprague and Geers errors. 266
B.8 Predicted muscle activations (solid line) and normalised EMG data (shaded area) for model 10. M, P and C represent the magnitude, phase and combined Sprague and Geers errors. 267
B.9 Predicted muscle activations (solid line) and normalised EMG data (shaded area) for model 11. M, P and C represent the magnitude, phase and combined Sprague and Geers errors. 267
B.10 Predicted muscle activations (solid line) and normalised EMG data (shaded area) for model 12. M, P and C represent the magnitude, phase and combined Sprague and Geers errors. 268

List of Tables

2.1 Study participant details. 30
2.2 Muscle parameters of a representative transfemoral amputee model. . . . 34
2.3 Sprague and Geers metric interpretation (Klemt et al. 2019) 37
2.4 S&G metric magnitude (M), phase (P) and combined (C) errors between the EMG signals and muscle activity predictions from all validated subject-specific models (n=12). 40
2.5 Correlations between differences in predicted hip joint contact forces, muscle forces and percentage differences in anthropometric parameters from the subject-specific model. 41
2.6 Multiple linear regression models relating percentage differences in significant anthropometric predictors to RMSD values in predicted internal forces. 42
2.7 Differences in hip joint contact force predictions between the scaled and subject-specific model output for all models (n=18) using different regression models. 43

3.1 Study participant details. 53
3.2 Marker placement locations. 55
3.3 Leg length details. 59
3.4 Temporospatial characteristics. 59
3.5 Sagittal plane ankle kinematics. 61
3.6 Coronal plane hip kinematics. 62
3.7 Sagittal plane hip kinematics. 63
3.8 Transverse plane hip kinematics. 64
3.9 Sagittal plane pelvic kinematics. 65
3.10 Coronal plane pelvic kinematics. 66
3.11 Transverse plane pelvic kinematics. 67
3.12 Ground reaction forces (GRF). 68
3.13 Coronal plane hip moments. 70
3.14 Sagittal plane hip moments. 71
3.15 Sagittal plane hip power. 72
3.16 Hip joint contact forces (HJCF) and impulse. 74
3.17 Muscle forces. 75
3.18 Muscle force impulse. 76
3.19 Normalised muscle force impulse. 76

3.20 Leg length details of Cohort 1. 78
3.21 Temporospatial measures of Cohort 1. 78
3.22 Sagittal plane ankle kinematics of Cohort 1. 79
3.23 Hip kinematics of Cohort 1. 81
3.24 Pelvic kinematics of Cohort 1. 82
3.25 Ground reaction forces (GRF) of Cohort 1. 83
3.26 Hip moments and power of Cohort 1. 85
3.27 Hip joint contact forces (HJCF) and impulse of Cohort 1. 85
3.28 Muscle forces of Cohort 1. 86
3.29 Muscle force impulse of Cohort 1. 87
3.30 Muscle force impulse normalised by walked distance of Cohort 1. 88
3.31 Leg length details of stubby prostheses users. 90
3.32 Temporospatial characteristics of stubby prostheses users. 90
3.33 Sagittal plane ankle kinematics of stubby prostheses users. 91
3.34 Hip kinematics of stubby prostheses users. 93
3.35 Pelvic kinematics of stubby prostheses users. 94
3.36 Ground reaction forces (GRF) of stubby prostheses users. 95
3.37 Hip moments and power of stubby prostheses users. 97
3.38 Hip joint contact forces and impulse of stubby prostheses users. 97
3.39 Muscle forces of stubby prostheses users. 98
3.40 Muscle force impulse of stubby prostheses users. 99
3.41 Muscle force impulse normalised by walked distance of stubby prostheses users. 100
3.42 Key findings of the biomechanical effect of full-length articulated and non-articulated stubby prostheses for BTF. 103

4.1 Study participant details. 112
4.2 Marker placement locations. 113
4.3 Temporal and spatial parameters characteristics. 116
4.4 Sagittal plane ankle kinematics. 117
4.5 Sagittal plane knee kinematics. 118
4.6 Peak sagittal plane knee angular velocity in terminal stance. 119
4.7 Sagittal plane hip kinematics. 120
4.8 Coronal plane hip kinematics. 121
4.9 Transverse plane hip kinematics. 122
4.10 Sagittal plane pelvic kinematics. 123
4.11 Coronal plane pelvic kinematics. 124
4.12 Transverse plane pelvic kinematics. 125
4.13 Ground reaction forces (GRF). 127
4.14 Sagittal plane ankle moments. 128
4.15 Coronal plane intact knee moments and loading rate. 129
4.16 Sagittal plane knee moments. 130
4.17 Coronal plane hip moments. 131
4.18 Sagittal plane hip moments. 132
4.19 Sagittal plane ankle power. 133

4.20 Sagittal plane knee power. . . . 134
4.21 Sagittal plane hip power. . . . 135
4.22 Intact ankle joint contact forces and impulse. . . . 136
4.23 Medial compartment of the intact knee contact forces and impulse. . . . 137
4.24 Lateral compartment of the intact knee contact forces and impulse. . . . 138
4.25 Medial intact knee impulse to lateral intact knee impulse ratio. . . . 139
4.26 Total intact knee contact forces and impulse. . . . 139
4.27 Hip joint contact forces and impulse. . . . 140
4.28 Case study biomechanical results. . . . 142
4.29 Case study joint loading results. . . . 143
4.30 Key findings of the UTF musculoskeletal function and loading. . . . 144

5.1 UTF study participants details. . . . 153
5.2 Prosthetic components masses. . . . 158
5.3 Spatial and temporal characteristics 159
5.4 Sagittal plane ankle kinematics. . . . 160
5.5 Sagittal plane knee kinematics. . . . 161
5.6 Peak sagittal plane prosthetic knee angular velocity and acceleration in swing. . . . 162
5.7 Sagittal plane hip kinematics. . . . 163
5.8 Peak prosthetic side hip angular velocity and acceleration in late swing. . . . 164
5.9 Coronal plane hip kinematics. . . . 165
5.10 Transverse plane hip kinematics. . . . 166
5.11 Sagittal plane pelvic kinematics. . . . 167
5.12 Coronal plane pelvic kinematics. . . . 168
5.13 Transverse plane pelvic kinematics. . . . 169
5.14 Ground reaction forces (GRF). . . . 170
5.15 Sagittal plane ankle moments. . . . 171
5.16 Sagittal plane intact knee moments. . . . 172
5.17 Coronal plane intact knee moments and loading rate. . . . 173
5.18 Sagittal plane hip moments. . . . 174
5.19 Coronal plane hip moments. . . . 175
5.20 Sagittal plane ankle power. . . . 176
5.21 Sagittal plane knee power. . . . 177
5.22 Sagittal plane hip power. . . . 178
5.23 Intact ankle joint contact forces and impulse. . . . 179
5.24 Medial compartment of the intact knee contact forces and impulse. . . . 180
5.25 Lateral compartment of the intact knee contact forces and impulse. . . . 181
5.26 Total intact knee contact forces and impulse. . . . 182
5.27 Hip joint contact forces and impulse. . . . 183
5.28 Key differences between the biomechanical effects of MPK and ICRC prostheses on UTF function and loading. . . . 184

6.1 UTF study participant details. . . . 191
6.2 SAT-PRO prosthesis satisfaction questionnaire scores. . . . 196

6.3 Prosthesis components masses. 197
6.4 Temporal and spatial gait characteristics. 197
6.5 Sagittal plane ankle kinematics. 198
6.6 Sagittal plane knee kinematics. 199
6.7 Peak prosthetic knee angular velocity and acceleration in late swing. . . . 200
6.8 Sagittal plane hip kinematics. 201
6.9 Coronal plane hip kinematics. 202
6.10 Transverse plane hip kinematics. 203
6.11 Sagittal plane pelvic kinematics. 204
6.12 Coronal plane pelvic kinematics. 205
6.13 Transverse plane pelvic kinematics. 206
6.14 Ground reaction forces (GRF). 207
6.15 Sagittal plane ankle moments. 208
6.16 Sagittal plane knee moments. 209
6.17 Coronal plane intact knee moments and loading rate. 210
6.18 Sagittal plane hip moments. 211
6.19 Coronal plane hip moments. 212
6.20 Sagittal plane ankle power. 213
6.21 Sagittal plane knee power. 214
6.22 Sagittal plane hip power. 215
6.23 Intact ankle joint contact forces and impulse. 216
6.24 Medial compartment of the intact knee contact forces and impulse. . . . 217
6.25 Lateral compartment of the intact knee contact forces and impulse. . . . 218
6.26 Total intact knee contact forces and impulse. 219
6.27 Hip joint contact forces and impulse. 221
6.28 Key differences between the biomechanical effect of the TaKeuP and ICRC prosthetic knees. 222

7.1 BTF database details. 229
7.2 UTF database details. 230
7.3 Multilevel regression model (n=16). Dependent variable: self-selected walking speed (m/s). 233
7.4 Multilevel regression model (n=16). Dependent variable: cadence (steps/min). 234
7.5 Multilevel regression model (n=32). Dependent variable: second peak hip joint contact force (BW). 234
7.6 Multilevel regression model (n=32). Dependent variable: normalised hip joint impulse (BW.s/m). 234
7.7 Multilevel regression model (n=25). Dependent variable: cadence (steps/min). AIC=146.509 235
7.8 Multilevel regression model (n=25). Dependent variable: cadence (steps/min). AIC=148.347 235
7.9 Multilevel regression model (n=25). Dependent variable: self-selected walking speed (m/s). AIC = -34.742. 235
7.10 Multilevel regression model (n=25). Dependent variable: self-selected walking speed (m/s). AIC=-32.816. 236

7.11 Multilevel regression model (n=23). Dependent variable: fast walking speed (m/s). 236
7.12 Multilevel regression model (n=25). Dependent variable: normalised lateral knee impulse (BW.s/m). 236

A.1 Muscle parameters of anatomical dataset 1. 246
A.2 Muscle parameters of anatomical dataset 2. 247
A.3 Muscle parameters of anatomical dataset 3. 248
A.4 Muscle parameters of anatomical dataset 5. 249
A.5 Muscle parameters of anatomical dataset 6. 250
A.6 Muscle parameters of anatomical dataset 7. 251
A.7 Muscle parameters of anatomical dataset 8. 252
A.8 Muscle parameters of anatomical dataset 9. 253
A.9 Muscle parameters of anatomical dataset 10. 254
A.10 Muscle parameters of anatomical dataset 11. 255
A.11 Muscle parameters of anatomical dataset 12. 256
A.12 Muscle parameters of anatomical dataset 13. 257
A.13 Muscle parameters of anatomical dataset 14. 258
A.14 Muscle parameters of anatomical dataset 15. 259
A.15 Muscle parameters of anatomical dataset 16. 260
A.16 Muscle parameters of anatomical dataset 17. 261
A.17 Muscle parameters of anatomical dataset 18. 262

List of abbreviations

2D Two-dimensional.
3D Three-dimensional.
AB Able-bodied.
Abd Abduction.
Add Adduction.
AIC Akaike information criterion.
BMD Bone mineral density.
BMI Body mass index.
BTF Bilateral transfemoral.
BW Bodyweight.
CI Confidence interval.
DF Dorsiflexion.
DOF Degree of freedom.
EMG Electromyography.
Ext Extension.
Ext Rot External rotation.
Fle Flexion.
GRF Ground reaction force.
HJCF Hip joint contact force.
IC Ischial containment.
ICRC International Committee of the Red Cross.
Int Rot Internal rotation.
ISO International Organization for Standardization.
LMIC Low to middle income country.
LP Low profile.
MPK Microprocessor knee.
MRI Magnetic resonance imaging.
Mom Moment.
PF Plantarflexion.
P&O Prosthetics and orthotics.
PCSA Physiological cross-sectional area.
P2P Peak-to-peak.
PW Pelvis width.
Quad Quadrilateral.
ROM Range of motion.

RMSD Root-mean-square deviation.
S&G Sprague and Geers.
SACH Solid-ankle-cushioned-heel.
SD Standard deviation.
SI Symmetry index.
SPM Statistical parametric mapping.
ST Stance.
SW Swing.
TF Transfemoral.
TK Through-knee.
UK United Kingdom.
UTF Unilateral transfemoral.
UTT Unilateral transtibial.

Chapter 1

Context of research

This chapter presents an overview of the subject matter of this thesis and introduces the thesis aims, objectives and structure.

1.1 Overview of problem statement and motivation

The 2020 Global Burden of Disease presented 28.9 million unilateral and 6.4 million bilateral lower limb traumatic amputees (Mcdonald et al. 2020). The reasons for amputation among the civilian population include falls, road injuries and mechanical forces (Mcdonald et al. 2020). Additionally, the 2003 - 2014 Afghanistan conflict has resulted in 265 major lower limb amputations in the United Kingdom military, where 153 military casualties sustained transfemoral amputations (Edwards et al. 2015) caused by improvised explosive devices, mines, gunshots, grenades and arms fire (Edwards et al. 2015). Amputations can be surgically induced (e.g. due to cancer), due to trauma, or through other conditions, such as vascular diseases or diabetes. Whilst vascular disease is the primary cause of amputations in developed countries (Abou-Zamzam et al. 2003), developing countries show trauma as the leading cause of amputations (66% in Tanzania, 46% in Iran) (Shaw et al. 2018, Rouhani & Mohajerzadeh 2013), which, due to being acute, requires immediate medical attention. Another difference between traumatic and non-traumatic amputees is that traumatic (including surgically induced trauma) amputees are generally younger and highly active, and non- traumatic amputations are commonly performed later in life.

Lower limb amputations can be performed at different levels: toe, mid-foot, through-ankle, below-knee, through-knee, above-knee or hip disarticulation. Based on the loss of joints, muscle mass and normal physiological muscle attachment locations, the overall musculoskeletal function is disrupted, with the degree of disability increasing with the level of amputation. According to the Hospital Episodes Statistics database, 52% of the total major lower limb amputations performed in England between 2011 and 2020 were at the above/through-knee level (Hospital episode statistics NHS digital 2020). It has been demonstrated that above/through-knee amputees present increased functional limitations (as determined by walking speed, stride length and cadence) compared to other types of amputees (Jarvis et al. 2017). Moreover, transfemoral amputees showed the highest level of energy consumption during level-ground walking (Jarvis et al. 2017). Therefore, this thesis will focus on the above/through-knee amputee group.

The decision on which type of amputation to perform is based on the degree of injury, quality of bone and surrounding tissue. Through-knee surgeries were initially less commonly performed compared to above-knee amputations due to cosmesis issues and socket fitting (Smith 2004, Behr et al. 2009, Mensch 1983). However, these have gained more attention over the years as it has been demonstrated that through-knee amputations may improve functionality. The ability to load bear through the bony distal end, stump shape, more residual muscle volume and strength (Smith 2004) can all reduce pain and improve power generation capabilities to complete a motion task.

The musculoskeletal system disruption can have a profound impact on the amputee's locomotion, quality of life and wellbeing, introducing functional limitations within certain activities of daily living. Return to physical activity is achieved through the use of prosthetic devices and intensive, on-going rehabilitation care. Firstly, the post-amputation

outcomes are highly dependent on the rehabilitation pathway, which is different between the civilian and military amputee population. British military amputees receive intensive care from the initial injury in the battlefield to surgery and undergo intensive rehabilitation in the United Kingdom at the Defence Medical Rehabilitation Centre. Conversely, civilian amputees are offered rehabilitation services through the National Health Service. Nonetheless, although the pathways might differ between institutions, all rehabilitation protocols focus on gait training with the prosthesis and improvement of the neuromusculoskeletal capacity.

The prosthetic devices required by above- and through-knee amputees include the prosthetic foot, knee, socket, connectors and liner. Alternatively, the prosthesis can be fixed to the residual limb using an osseointegrated implant (Brånemark et al. 2001). The choice of prosthesis and fixation method requires an inter-disciplinary collaboration between the prosthetist, physiotherapist, consultant and prosthesis user (Hanspal 2003), and is often based on manufacturer driven research and anecdotal evidence. Commercially available prosthetic knees include microprocessor and monocentric or polycentric mechanically-controlled knees. Prosthetic feet designs include powered, dynamic response and solid-ankle-cushioned-heel feet. Despite the wide range of available prosthetic devices, there are discrepancies in prosthesis prescription between high- and low-to-middle-income countries (LMICs), as amputees in LMICs often lack financial resources to cover the cost of high-cost advanced prosthetic devices. Additionally, high-cost prostheses are often not appropriate for the specific requirements in LMICs as some may be not waterproof or dustproof, and require regular charging. This is despite the fact that the vast majority of traumatic amputees are in LMICs (Mcdonald et al. 2020).

Currently there is no in-depth understanding of the biomechanical effect of prosthetic use and design on amputee functional abilities and internal loading (muscle and joint contact forces), and this thesis aims to address this. The lack of evidence-based prescription, as well as lack of adequate prostheses in LMICs, may make persons with lower limb loss more susceptible to degenerative physical conditions such as osteoarthritis (Burke et al. 1978, Struyf et al. 2009), osteopenia (Rush et al. 1994) and low back pain (Ephraim et al. 2005). This thesis assesses the musculoskeletal function and loading of above/through-knee amputees with different types of prosthetic devices. This investigation will then allow for the proposition of mitigation strategies (e.g. improvements in prosthetic design, informed prosthesis prescription, exercise interventions) to improve functional abilities and long-term musculoskeletal health.

In addition to the selection of the prosthetic components, it is also important to consider the complexity and user specific variability in prosthetic design and component behaviour, socket design and alignment. Prosthetic sockets are custom made to fit the shape of the stump and ensure comfort and the necessary support. Inadequate prosthetic socket and liner fit might lead to pain, discomfort, difficulty in stabilizing the stump in the prosthetic socket, and so an inability to make full use of the prosthetic knee and foot. Moreover, the alignment of the prosthetic components plays an important role in the overall function and comfort - misalignment may influence the load transfer from

the prosthetic socket to the stump, ultimately affecting the health of the stump. Other considerations regard variability in prosthetic characteristics that influence component behaviour. For example, mechanical prosthetic knees have features that could be adjusted to meet the specific requirements of amputees (e.g. spring stiffness, flexion resistance, extension resistance). For some prosthetic knees, such as ICRC, the range of motion could be adjusted by adding plates on the back of the knee to change the maximum extension position, thus enabling the amputee to unlock the knee easier. In this thesis, prosthetic knee features have not been modified for any participant, and the focus was on differences in function and loading between prosthetic components. Additionally, the prosthetic sockets were not changed when participants tested more than one prosthesis and the prosthetic alignment was not modified.

Various methods can be used to investigate the musculoskeletal system function and loading. For instance, instrumented hip prostheses (required in hip replacement surgeries) allow for the *in vivo* measurement of physiological joint contact forces during activities of daily life, removing the constraint of the laboratory setting. However, traumatic amputees are generally young and unlikely to be in need of a hip replacement surgery. Longitudinal cohort studies combine gait analysis and radiography, which allow for the in-depth analysis of musculoskeletal disorders and the loading characteristics contributing to their progression. Although longitudinal data are exceptionally valuable, this method requires a large participant sample size, long time frame and considerable expenditure.

Computational simulations allow for the assessment of musculoskeletal system function and loading in a time and cost-efficient manner. Musculoskeletal modelling is a robust biomechanical tool that has been widely used to investigate muscle and joint contact forces in the able-bodied population (Cleather & Bull 2012, Ding et al. 2016, 2019), below-knee amputee population (Ding et al. 2020) and above/through-knee amputee population (Henson 2020). The analysis of joint contact forces is important as loading magnitudes and rates relate to joint health, and can be indicative of osteoarthritis development and progression (Ding et al. 2020, Felson 2013, Morgenroth et al. 2012). The findings can be then used to propose strategies to ensure optimal musculoskeletal health outcomes in the lower limb amputee population. The overview of the musculoskeletal modelling pipeline is presented in Figure 1.1. This modelling pipeline will be used throughout this thesis.

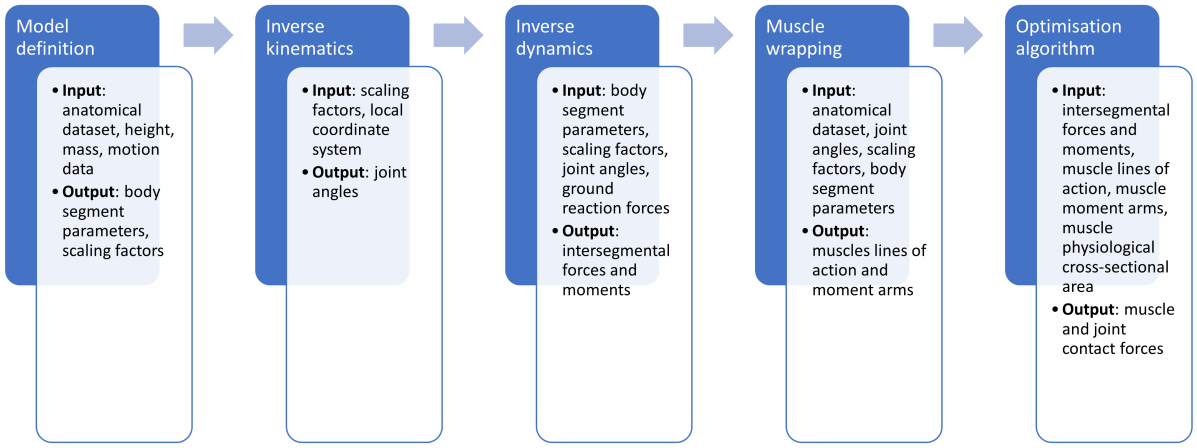


Figure 1.1: Musculoskeletal modelling pipeline.

1.2 Thesis aim and significance

The aim of this thesis is to use established biomechanical tools to understand the musculoskeletal function and loading of bilateral and unilateral above/through-knee traumatic amputees during level-ground walking with different lower limb prosthesis designs. This thesis allows for the proposition of strategies to improve functional abilities whilst reducing gait deviations and the risk of comorbidities such as osteoarthritis, osteopenia and low back pain. The findings of this thesis may provide guidance in making informed decisions for adequate prosthesis prescription to ensure optimal functional and health outcomes. Additionally, the presented findings represent research contributions to knowledge.

1.3 Thesis objectives

The objectives of this thesis are to:

- create technology to accurately predict muscle and hip joint contact forces, through developing and validating subject-specific above/through-knee amputee musculoskeletal models;
- develop datasets of the musculoskeletal function of above/through-knee amputees;
- use the musculoskeletal models and datasets to investigate musculoskeletal function and muscle and joint loading for the following prostheses: full-length articulated, non-articulated stubbies, microprocessor knees with dynamic response feet, and mechanical knees with solid ankle cushioned heel feet; and
- identify significant prosthetic and anatomical parameters that predict functional abilities (walking speed, cadence) and internal loading (muscle and joint contact forces) for traumatic above/through-knee amputees.

1.4 Thesis outline

This thesis is organized in seven chapters.

Chapter 1 presents the context of research, thesis aims and objectives.

Chapter 2 presents an anatomical atlas-based scaling study for accurately quantifying muscle and hip joint contact forces in above- and through-knee traumatic amputees using electromyography-validated musculoskeletal modelling. This chapter also explains the development of an anatomical atlas through manual digitisation of model parameters from high-resolution magnetic resonance imaging (MRI).

Chapter 3 utilises the MRI-based anatomical dataset from Chapter 2 to assess the musculoskeletal function and loading of bilateral above/through-knee amputees using full-length articulated and fore-shortened non-articulated stubby prostheses.

Chapter 4 investigates the musculoskeletal function and loading of traumatic unilateral above/through-knee amputees and explains the risk of intact knee osteoarthritis in this amputee population.

Chapter 5 assesses the above/through-knee amputee musculoskeletal function and loading when walking with high-cost microprocessor-controlled prosthetic knees and low-cost mechanical polycentric International Committee of the Red Cross (ICRC) prosthetic knees.

Chapter 6 uses the developed biomechanics tools to investigate the effect of different spring extension assist mechanisms of two low-cost mechanical polycentric prosthetic knees: ICRC and a novel prosthetic knee for LMICs.

Chapter 7 uses multilevel regression statistical analyses to identify significant prosthetic design and anatomical parameters that explain functional abilities (as determined by walking speed and cadence) and intact joint contact forces and impulse. Additionally, this chapter presents the overall discussion of this thesis and proposes future work.

Chapter 2

An anatomical atlas-based scaling study for quantifying muscle and hip joint contact forces in above and through-knee amputees using validated musculoskeletal modelling

In order to address the first objective of the thesis, to "create technology to accurately predict muscle and hip joint contact forces", in this chapter a magnetic resonance imaging (MRI)-based anatomical atlas of 18 above/through-knee lower limb amputee models is presented. Laboratory motion data are obtained, and musculoskeletal modelling used to quantify muscle and joint forces. Validation is performed using electromyography (EMG) and then these validated models are used to derive multiple linear regression models to enable the anatomical atlas of MRI data to be used as a basis for musculoskeletal models of any other traumatic amputee.

This work was published in part as: 'An anatomical atlas-based scaling study for quantifying muscle and hip joint contact forces in above and through-knee amputees using validated musculoskeletal modelling', with authors: Diana Toderita, David P. Henson, Christian Klemt, Ziyun Ding, Anthony MJ Bull. IEEE Transactions on Biomedical Engineering. 2021. 68(11):3447-3456.

2.1 Introduction

The Afghanistan conflict has led to 265 major lower limb amputations in the UK military from 2003 to 2014 (Edwards et al. 2015). Through a rigorous rehabilitation program, this cohort of traumatic amputees achieve high levels of functional performance, with similar physical abilities to those of able-bodied individuals (Jarvis et al. 2017, 2020). Return to physical activity is achieved through intensive rehabilitation care and use of prosthetic devices, which comes at a compensatory cost, as it introduces different muscle recruitment patterns and joint loading profiles, when compared to able-bodied individuals (Ding et al. 2020). Depending on individual objectives and capabilities, amputees can adopt very distinct movement strategies, which, although beneficial in the short term, can cause detrimental loading of the joints and increased risk of developing comorbidities such as osteoarthritis (Norvell et al. 2005, Burke et al. 1978), osteopenia (Rush et al. 1994) and lower back pain (Ephraim et al. 2005).

A significant increase in the medial knee joint contact forces has been reported in the sound limb of unilateral below-knee amputees (Ding et al. 2020). This is a result of asymmetrical gait, often observed in unilateral amputees for all levels of amputation, including transtibial, transfemoral and through-knee (Isakov et al. 2000, Jaegers et al. 1995, Summers et al. 1987). In order to maximise stability during movement and minimize energy consumption and residual limb pain, the amputated side tends to be under-loaded, as opposed to the joints of the intact limb, which may be overloaded (compared to normal physiological levels). The increased intact knee contact forces are thought to be linked to the high incidence of osteoarthritis in the sound limb of unilateral amputees (Ding et al. 2020). Similarly, high occurrence rates of osteopenia on the amputated side have been reported for unilateral above-knee amputees (Rush et al. 1994) due to the increased reliance on the intact limb and hypothesized inability of the femoral remnant to bear axial loads. However, there is a lack of understanding of the muscle and joint loading patterns in bilateral above and through-knee traumatic amputees. Therefore, there is an immediate need for the investigation of the kinetic profiles of amputees to allow for the development of solutions which mitigate the risk of developing comorbidities in the long term, and at the same time improve the amputee's functional performance.

Comprehensive descriptions of the mechanical effects of the lower extremity amputation on internal forces during movement can be obtained through musculoskeletal modelling, which requires the subject's anatomical geometry as input. This is usually obtained through the time- and cost-efficient linearly scaled generic models (Cleather & Bull 2012), which allow for geometric variation across subjects through linear scaling, based on the three-dimensional (3D) locations of anatomical landmarks (Kaptein & Van Der Helm 2004). However, these do not account for inter-individual anatomical variations (Duda et al. 1996). Linear scaling to a generic model has been shown to lead to significant errors in force predictions for both upper and lower limb models (Klemt et al. 2019, Ding et al. 2019, Scheys et al. 2008). Additionally, amputees have a much wider anthropometric and anatomical variability (and deficit) than able-bodied subjects and so, there are likely to be considerably greater errors in linear scaling from one subject. The accuracy of a

musculoskeletal model is strongly dependent on the anatomical geometry (bony landmarks and muscle parameters), which can be obtained from MRI scans. However, the development of subject-specific models is both time and computationally intensive, and furthermore, MRI scans may not be performed on those military amputees with shrapnel fragments left in the body from the blast injury.

Linear scaling to a musculoskeletal model with anthropometric similarity has been shown to improve model predictions in muscle and joint contact forces in able-bodied lower (Ding et al. 2019) and upper extremities (Klemt et al. 2019). However, there is no existing approach for linear scaling of lower limb amputee musculoskeletal models. In this chapter, an MRI-based anatomical atlas for above and through-knee traumatic amputees is presented, and it was hypothesized that linear scaling to a model with anthropometric similarity can predict muscle and joint contact forces with clinically insignificant errors. If the hypothesis is shown to be correct, then this enables this technique to be used to assess the musculoskeletal function of a variety of amputees with a range of different prostheses.

2.2 Methods

2.2.1 Experimental data

This study received ethical approval by Imperial College Research Ethics Committee (Reference 16IC3562) and the NHS Research Ethics Committee (Reference 16/LO/1715). Written informed consent was obtained from nine bilateral above and through-knee traumatic male amputees (Table 2.1). Six participants were fitted with full-length articulated prostheses: microprocessor-controlled Genium prosthetic knee units and dynamic response Triton prosthetic feet (Ottobock, Germany). Three participants were fitted with Sidekicks stubbies (College Park Sidekicks, Michigan, USA), which are foreshortened prostheses with no articulated knee joints. Participants used quadrilateral and ischial bearing prosthetic sockets. High resolution MRI scans were obtained using a 3.0 T MRI scanner (MAGNETOM Verio, Siemens, Germany) with a 3D T1-weighted spoiled gradient echo sequence with the following settings: 450×450 mm^2 field of view, 1.17×1.17 mm axial plane resolution, 1 mm slice thickness. All subjects were scanned from the top of the iliac crest to the most distal point of the longer residual limb such that both stumps are included in the scans. Therefore, the anatomical atlas consists of two subject-specific unilateral (left and right) models for each study participant.

Part. No.	Age (y)[a]	Body mass (kg)[b]	Adjusted body mass (kg)[c]	Height (m)[d]	Left stump length (cm)	Right stump length (cm)	Prosth. knee[e]	Prosth. foot[e]
1	32	86	88	1.85	52.4 (TK)	39.9 (TF)	Genium	Triton Low Profile
2	27	81	85	1.78	34.3 (TF)	43.4 (TF)	Genium X3	Triton
3	36	90	94	1.86	49.8 (TK)	32.8 (TF)	Genium X3	Triton Low Profile
4	38	83	95	1.80	38.6 (TF)	25.0 (TF)	N/A	Sidekicks stubbies
5	33	90	97	1.82	44.8 (TK)	47.9 (TK)	Genium	Triton Low Profile
6	32	97	103	1.85	48.5 (TK)	47.7 (TK)	Genium X3	Triton Low Profile
7	31	69	71	1.71	35.0 (TF)	35.9 (TF)	Genium X3	Triton
8	30	67	80	1.75	40.6 (TF)	13.9 (TF)	N/A	Sidekicks stubbies
9	27	76	80	1.75	47.0 (TK)	46.4 (TK)	N/A	Sidekicks stubbies

Table 2.1: Study participant details.
[a]Age at time of testing. y, years. [b]Body mass with prosthetic components. [c]Calculated according to previous literature (Tzamaloukas et al. 1994). [d]Pre-injury height available from military records. [e]All subjects had been using their prostheses for a minimum of two years. TF, transfemoral amputation. TK, through-knee amputation.

Gait data were collected from all subjects using a 10-camera VICON motion analysis system (VICON, Oxford Metrics Group, U.K.) with two force plates (Kistler Type 9286B, Kistler Instrumente AG, Winterthur, Switzerland). Retro reflective markers were placed on anatomical landmarks of the lower limb: left/right anterior and posterior superior iliac spine, medial and lateral sides of the prosthetic knee joint centre of rotation (analogous to the medial and lateral femoral epicondyles), medial and lateral sides of the ankle joint centre of rotation (analogous to the medial and lateral malleoli), second/fifth metatarsal head (placed at the front edge of the foot, above the second/fifth toe), posterior calcaneus (placed on the back of the heel at toe height), midfoot superior (placed on top of the foot, anterior to the pylon base). Additionally, two clusters of three markers each were placed on the thigh segment (on the lateral side of the prosthetic socket) and shank segment (on the lateral side of the pylon) (Duffell et al. 2014). All participants performed a static calibration trial and gait trials at self-selected speeds. Three successful trials were

collected and analysed for each study participant. The marker positions and ground reaction forces were filtered in MATLAB (The Mathworks Inc., Natick, MA,USA) using a zero phase-lag, fourth order Butterworth filter with 6 Hz cut-off frequency prior to model input (Yu et al. 1999).

Surface EMG (Delsys Incorporated, Natick, MA, USA) was recorded during the gait trials of six subjects from the gluteus medius, gluteus maximus, adductor longus and rectus femoris muscles. The EMG sensors locations are presented in Figure 2.1. The sensors were positioned to avoid mechanical interference with the prosthetic socket, therefore resulting in different sensor placements than those recommended in the literature (Perotto 2011). The raw EMG data were corrected for DC offsets, high-pass filtered at 30 Hz with a fourth order Butterworth filter, full-wave rectified and low pass filtered at 10 Hz (Arnold et al. 2013). EMG data were not collected for the remaining three study participants due to the unfeasible placement of the EMG sensors on the residual limbs.

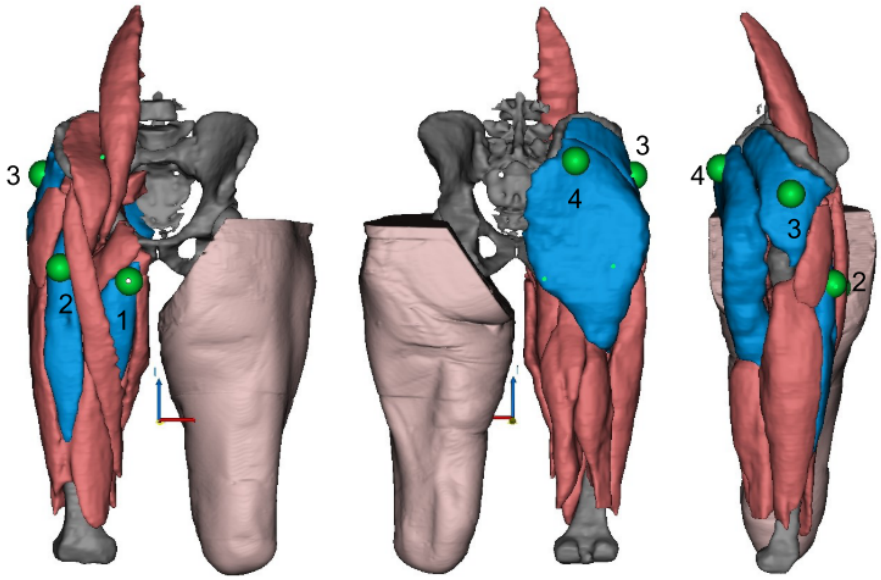


Figure 2.1: EMG sensor locations.
1 - Adductor longus. 2 - Rectus femoris. 3 - Gluteus medius. 4 - Gluteus maximus.
(reproduced with permission from Henson, 2020).

The motion capture, EMG and MRI data used in study were collected as part of a previous study (Henson 2020).

2.2.2 Anatomical geometry

The acquired MRI scans were processed in Mimics (Mimics 19.0, Materialise, Belgium). 2D contours were manually segmented in the axial plane to reconstruct the 3D surfaces of the pelvis, femoral remnant and residual muscles. Figure 2.2 presents one MRI scan slice in the axial plane for one representative subject.

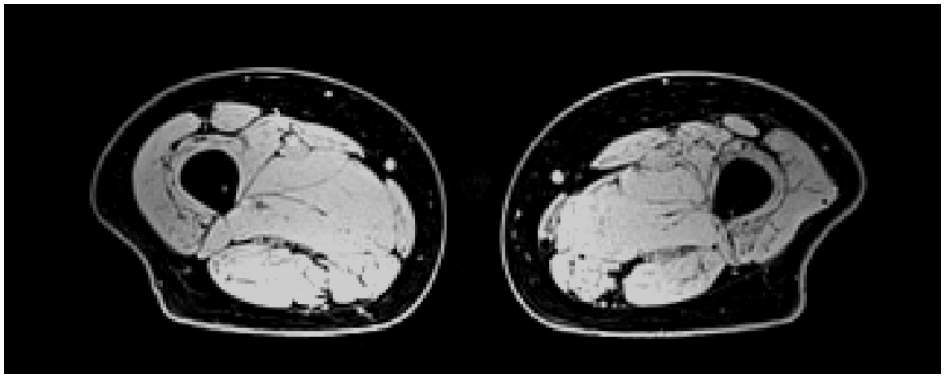
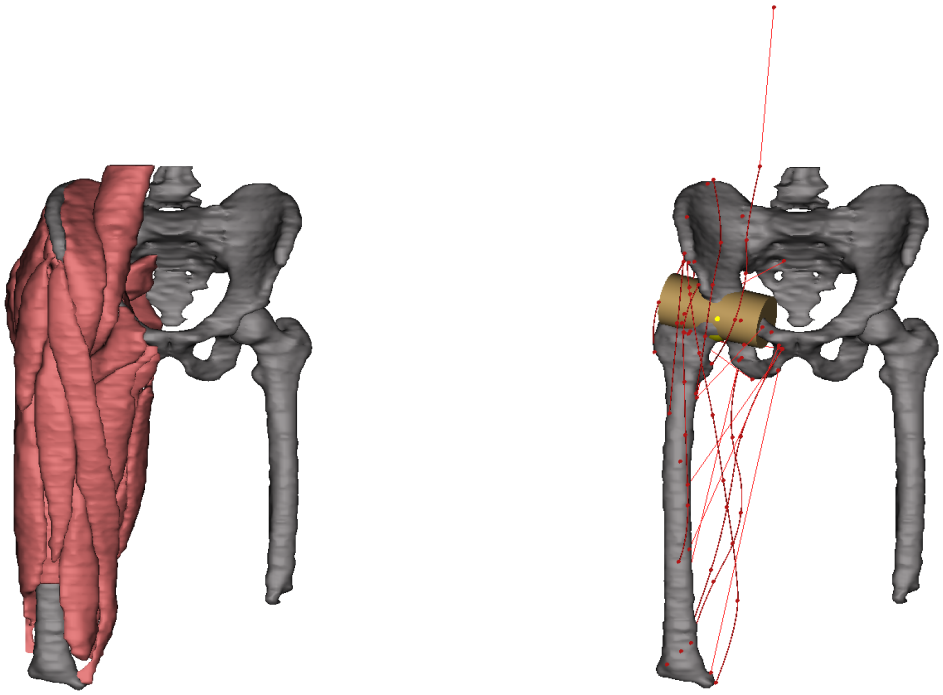


Figure 2.2: Lower limb 2D axial plane MRI scan of a representative subject.

The 3D reconstructions for one representative subject are illustrated in Figure 2.3a. The muscle segmentation procedure has been previously validated using cadaveric measurements, with reported errors of less than 3%, thus demonstrating its reliability (Mitsiopoulos et al. 1998). The anterior and posterior superior iliac spine anatomical landmarks were manually digitised on the bone surface. The hip joint center coordinates were assigned to the coordinates of the centre of a sphere fitted to the femoral head. Additionally, the lines-of-action of 21 muscles were described by the origin, via and insertion points (Klein Horsman et al. 2007), all manually digitised in the MRI scans. The origins of the psoas muscle elements, located on the 12th thoracic vertebra (T12), more proximal than the MRI scans, were approximated using the length of the fifth lumbar vertebra and the intervertebral disc. The psoas muscle volume was obtained using a cone approximation, where the cone diameter was the diameter of the psoas muscle in the most proximal available imaging slice and the cone height was represented by the distance between the centre of the psoas muscle's most proximal slice and T12's approximated location. A cylindrical wrapping object was assigned to the iliacus and psoas muscles, which are free to glide over the pubis, and identified in the imaging scans based on the curvature of the muscle lines-of-action. The joint and muscle representations are shown in Figure 2.3b.



(a) **(b)**

Figure 2.3: Lower limb anatomy of a representative subject (one limb of a bilateral above-knee amputee): (a) pelvis, femoral remnants and muscle 3D reconstruction. (b) muscle lines-of-action (red), hip joint centre (yellow point), wrapping object (yellow cylinder).

Each muscle's physiological cross-sectional area (PCSA) was computed using Equation 2.1 (Handsfield et al. 2014).

$$PCSA = \frac{V_m \times cos\theta}{L_m \times \frac{L_f}{L_m} \times \frac{2.7}{L_s}} \tag{2.1}$$

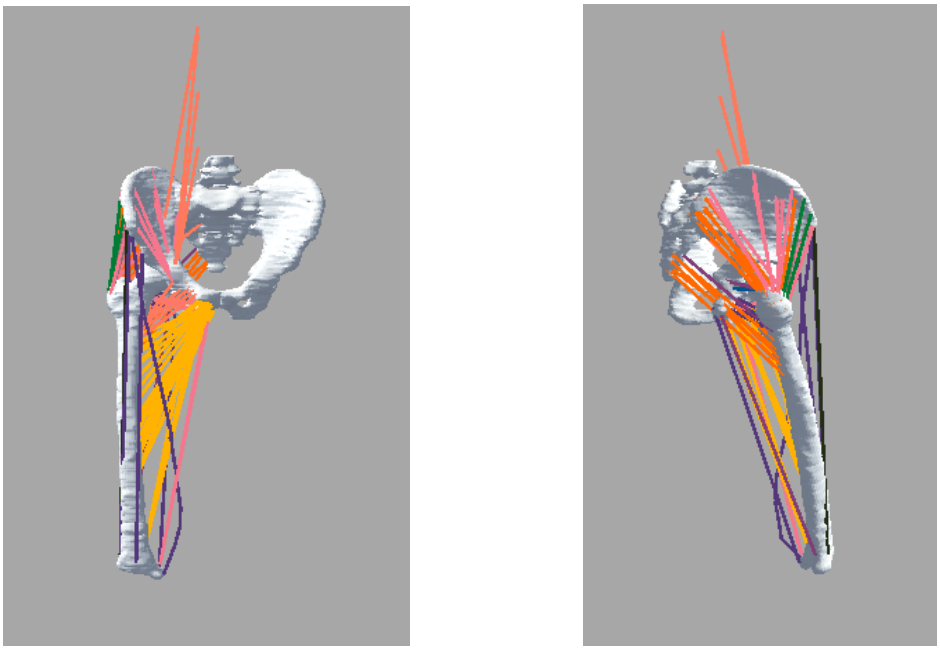
The muscle volume, V_m, was obtained from the rendered 3D geometry of each muscle. The muscle length, L_m, was calculated using the 3D Euclidean distance between axial centroids in the MRI scans, in concordance with previous literature (Handsfield et al. 2014). Values for the pennation angle θ, fibre length to muscle length ratio, $\frac{L_f}{L_m}$, and optimal sarcomere length, L_s, were obtained from cadaveric data (Ward et al. 2009). For the muscles not investigated in the literature, θ was set to 0, $\frac{L_f}{L_m}$ to 1 and L_s to 2.70 μm (Ding et al. 2019, Lieber et al. 1994). Table 2.2 presents muscle parameters for one representative subject. For the gemellus, gluteus minimus, obturator externus, obturator internus, pectineus, quadratus femoris and tensor fasciae latae muscles, which have not been reported in the literature (Ward et al. 2009), the fibre length to muscle length ratio was set to 1.00, the pennation angle was set to 0.00° and the sarcomere length to 2.70 μm, respectively (Ding et al. 2019, Lieber et al. 1994). The psoas minor physiological cross-sectional area (PCSA) was obtained from literature (Klein Horsman et al. 2007). 12 out of 18 subject-specific models were developed as part of previous work (Henson 2020).

Muscle	Muscle group	Muscle volume (V_m, cm^3)	Muscle length (L_m, cm)	Fibre length/ muscle length (L_f/L_m)	Pennation angle (θ,°)	Sarcomere length (L_s, μM)	PCSA (cm^2)
Adductor brevis	Adductor	143.02	19.23	0.68	6.10	2.91	11.72
Adductor longus	Adductor, Int. rot.	211.92	25.65	0.50	7.10	3.00	18.22
Adductor magnus	Adductor	550.35	38.12	0.39	15.50	2.19	28.94
Biceps femoris long head	Extensor	217.68	32.74	0.28	11.60	2.35	20.24
Gemellus	Ext. rot.	1.54	6.81	1.00	0.00	2.70	0.23
Gluteus maximus	Extensor, Ext. rot.	1174.09	27.78	0.62	21.90	2.60	60.91
Gluteus medius	Abductor, Int. rot.	488.77	19.54	0.37	20.50	2.40	56.29
Gluteus minimus	Abductor, Int. rot.	165.93	12.27	1.00	0.00	2.70	13.52
Gracilis	Adductor	78.54	25.20	0.79	8.20	3.24	4.69
Iliacus	Flexor	311.63	28.28	0.56	14.30	3.02	21.33
Obturator externus	Ext. rot.	61.31	11.01	1.00	0.00	2.70	5.57
Obturator internus	Ext. rot.	110.29	14.51	1.00	0.00	2.70	7.60
Pectineus	Adductor	89.96	13.21	1.00	0.00	2.70	6.81
Piriformis	Ext. rot.	66.46	12.54	1.00	0.00	2.70	5.30
Psoas minor	Flexor						1.10
Psoas major	Flexor	244.13	25.73	0.50	10.60	3.11	21.48
Quadratus femoris	Ext. rot.	43.81	8.77	1.00	0.00	2.70	4.99
Rectus femoris	Flexor	185.74	31.36	0.21	13.90	2.42	24.54
Sartorius	Flexor	186.40	49.44	0.90	1.30	3.11	4.82
Semimem-branosus	Extensor, Int. rot.	317.77	32.46	0.24	15.10	2.61	38.07
Tensor fasciae latae	Abductor	107.76	18.29	1.00	0.00	2.70	5.89

Table 2.2: Muscle parameters of a representative transfemoral amputee model. Int, internal. Ext, external. Rot, rotator. Parameters for all amputees are presented in Appendix A.

2.2.3 Musculoskeletal modelling and data analysis

Internal forces during the gait trials were quantified using Freebody v2.1, a segment based musculoskeletal model (Ding et al. 2016, Cleather & Bull 2015) adapted for above and through-knee amputee use (Henson 2020). The model has four rigid segments: pelvis, thigh, shank and foot, where the stump, stump liner and prosthetic socket were combined to model the thigh segment. The pelvis and thigh segments are articulated at the hip joint (spherical joint with 3 degrees of freedom) and actuated by 92 muscle elements, illustrated in Figure 2.4. Inverse kinematics and inverse dynamics simulations were used to obtain moments at the hip joint for the recorded gait trials. Each segment's locations and orientations are derived from the coordinates of the reflective markers placed on the previously presented anatomical landmarks.



(a) **(b)**

Figure 2.4: Musculoskeletal model of one transfemoral amputee model. (a) Frontal view (b) Lateral view.

The one-step static load sharing optimisation algorithm, presented in Equation 2.2, was implemented to compute the forces in each muscle element (F_i) and the resultant contact force at the hip joint. The algorithm aimed to minimize the sum of cubed muscle activations (J) (Crowninshield & Brand 1981). Each muscle element's maximum force, $F_{max,i}$, was computed as the multiplication of the muscle element PCSA, PCSA multiplier and maximum muscle stress, 31.39 N/cm^2 (Yamaguchi 2005). Muscles that cross the absent joint were removed or adjusted for their new insertions and their contribution to the static optimisation was adjusted accordingly. The prosthesis' contribution to the net joint moment was computed using inverse dynamics. The torques were presented at the midpoint between the medial and lateral malleoli on the prosthetic foot and between the medial and lateral epicondyles on the prosthetic knee, respectively.

$$min(J) = min(\sum_{i=1}^{M}(\frac{F_i}{F_{max,i}})^3) \tag{2.2}$$

Anthropometry and body segment parameters (mass, centre of mass location, moment of inertia) served as input to the musculoskeletal model. DeLeva calculations (De Leva 1996) were used to determine the pelvic and stump segment parameters. The stump length was measured from the MRI scans as the distance from the hip joint centre to the most distal point on the residual limb. The mass of the stump was obtained by multiplying the stump volume (rendered 3D geometry from the MRI scans) by density (1.42 g/cm^3 for bone, 1.03 g/cm^3 for soft tissue (White et al. 1987)). This calculation was made under the assumption that the body is formed of two parts, bone and soft tissue, both of uniform densities (Valente et al. 2014). The prosthetic components' inertial parameters were determined using the reaction board method (Smith et al. 2014) with moment equilibrium. The prosthetic component was fixed at the proximal end, and the distal end was placed on a scale, as shown in Figure 2.5, where x_1 is the total segment length, x_2 is the centre of mass location, m_2 is the total segment mass, m_s is the scale reading, R_1 and R_2 are the reaction forces at the distal and proximal ends of the prosthetic component, and g is the gravitational acceleration. Equation 2.3 and Equation 2.4 were used to calculate the center of mass location. The moment of inertia was then calculated using Equation 2.5. The total moment of inertia (I) of the thigh segment was obtained by adding the moment of inertia of the stump to that of the prosthetic components (liners, socket, connectors) using the Huygens-Steiner parallel axis theorem.

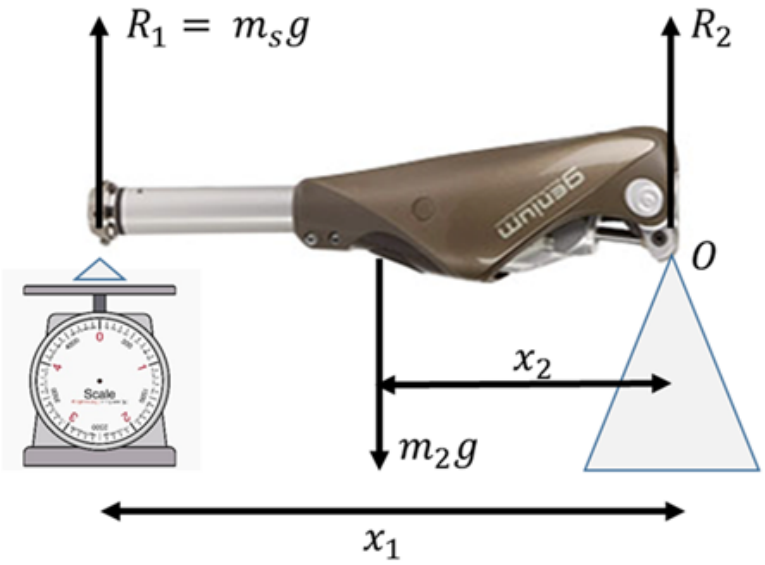


Figure 2.5: Reaction board method with moment equilibrium (reproduced with permission from Henson, 2020).

$$\sum M_O = R_1 x_1 + R_2 0 - m_2 g x_2 = 0 \tag{2.3}$$

$$x_2 = \frac{m_s x_1}{m_2} \tag{2.4}$$

$$I = m_2 x_2^2 \tag{2.5}$$

The intact mass (W_1) was estimated using Equation 2.6 (Tzamaloukas et al. 1994), where W_2 represents the weight without prosthetic components and $\sum \frac{\Delta W}{W_1}$ represents the percentage bodyweight lost through amputation.

$$W_1 = \frac{W_2}{1 - \sum \frac{\Delta W}{W_1}} \tag{2.6}$$

The atlas consists of a total of 18 subject-specific anatomical models, where each subject-specific model is composed of the subject's marker trajectory, force plate and MRI-based anatomical data (skeletal geometry and muscle properties). 12 subject-specific models were validated using the recorded EMG signals. The evaluation was performed by comparing the EMG data and predicted muscle activations. For each model, EMG data were normalised to the maximum recording in the gait trial to obtain activation values from 0 to 1. The predicted muscle activations were defined from 0 to 1 as the predicted muscle force normalised by the maximum force in the gait trial. The Sprague and Geers (S&G) metric (Sarin et al. 2010), defined in Table 2.3, was used to quantify the magnitude (M), phase (P) and combined (C) errors, where the combined measure accounts for both M and P errors.

Error interval	Similarity
0 - 0.15	excellent
0.15 - 0.30	very good
0.30 - 0.45	good
0.45 - 0.60	moderate
> 0.60	none

Table 2.3: Sprague and Geers metric interpretation (Klemt et al. 2019)

Whereas 12 limb-specific models (6 subjects $\times$ 2 limbs) were validated, the overall scaling process included all 18 models (9 subjects $\times$ 2 limbs). The two limbs (left and right sides) for each study participant were analysed separately, as the Freebody v2.1 musculoskeletal model simulates unilateral models only. Therefore, each limb in the atlas had a customised model and 17 further models created through linear scaling to the remaining anatomical datasets. The linear scaling factors were the ratios of the intersegmental length and width measured from the subject in the static trial to the intersegmental length and width in the dataset used for scaling. These factors were used to scale the muscle lines-of-action, wrapping object parameters and hip joint rotation centre. In total, there were 972 simulations (18 models $\times$ 18 anatomical datasets $\times$ 3 gait trials). Figure 2.6 presents the cross-validation process for one model, where M1 represents the anthropometric, force plate and marker trajectory data and A_i represents the i^{th} anatomical dataset.

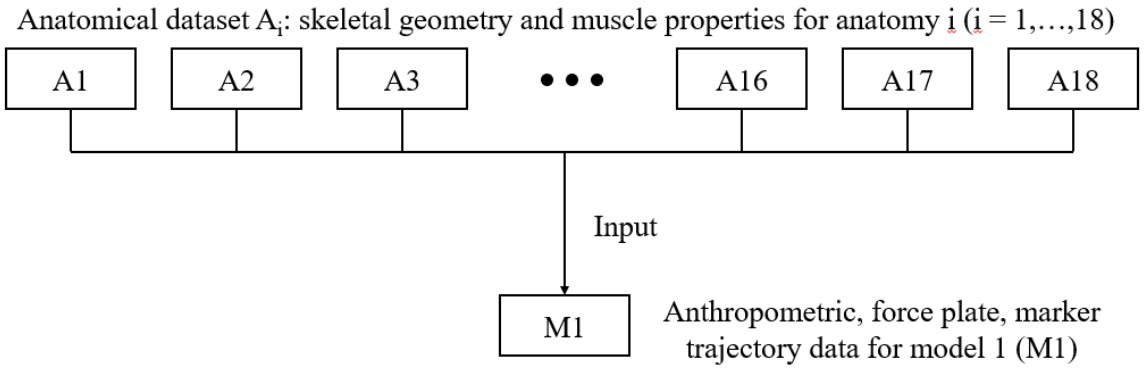


Figure 2.6: Musculoskeletal simulation pipeline for model 1.
The limb-specific model was formed of model 1's anatomy (A1) and anthropometric, force plate and marker trajectory data (M1). The anatomical datasets A2 - A18 served as input to the musculoskeletal model consisting of model M1's data, therefore completing the remaining 17 linearly scaled models.

The computed muscle and hip joint contact forces were expressed as a gait cycle percentage from 0% at heel strike to 100% at the consecutive heel strike in intervals of 1% and averaged over three trials. Muscles were grouped based on their function into six categories: adductors, abductors, extensors, flexors, internal rotators and external rotators. The total force in one muscle group was calculated by adding the forces for all muscles that possess the corresponding function. The root-mean-square difference (RMSD, Equation 2.7 (Ding et al. 2019)), normalised by the mean force in the gait cycle (as presented in a previous study (Ding et al. 2019)) from the subject-specific model ($\overline{F_{ss}}$), was used to quantify the differences between the scaled and subject-specific model output for the hip joint contact and muscle group forces, where the subject-specific model output was considered ground truth. F^i_{ss} and F^i_{sm} represent the forces from the subject-specific and scaled model output, respectively, for each time frame (i).

$$RMSD = \frac{\sqrt{\frac{\sum_{i=0}^{100}(F^i_{ss}-F^i_{sm})^2}{100}}}{\overline{F_{ss}}}(\%) \tag{2.7}$$

To assess the dependency of the musculoskeletal model predictions on the amputee anatomy, the effects of the following anthropometric parameters were investigated: mass without prosthetic components, intact mass, intact body mass index (BMI) calculated using the intact mass (Tzamaloukas et al. 1994), pre-amputation height, stump length (distance from the hip joint centre to the distal end of the residual limb), pelvis width (distance between the left and right anterior iliac spine anatomical landmarks), stump length to pelvis width ratio and prosthesis type parameter, which was assigned a 1 if the residual limb was fitted with a stubby prosthesis and 0 otherwise. The choice of mass and height was based on the previous finding that muscle properties scale with these measurements (Handsfield et al. 2014). The stump length is an indication of the residual muscle volume. Differences in BMI and pelvis width have been shown to introduce significant differences in force predictions for able-body lower limb models (Ding et al. 2019).

Finally, it was hypothesized that differences in fitted prosthetic components introduce discrepancies in force predictions.

Linear regression analysis was used to identify relationships between differences in individual anthropometric parameters and RMSD values for the hip joint and muscle forces in the presence of all investigated parameters. The final multiple linear regression models were identified using stepwise regression analysis. Three regression models were developed, each aiming to minimize the errors in: 1. hip joint contact forces 2. muscle forces and 3. combined hip joint and muscle forces (for which a compound measure was created by obtaining the average of the force errors across all muscle groups and then averaging it with the errors in the predicted hip joint contact forces). The combined regression model was created in order to equally account for the accuracy in both muscle and hip joint contact force predictions (Klemt et al. 2019). To assess the effect of the weighting distribution of the hip and muscle force errors in the combined regression model, all weights from 0% to 100% were considered. The three models were then used to identify the model in the anatomical atlas with the closest predictions to the subject-specific model output. To assess the robustness of the models, the variance was checked for normal distribution by plotting the histogram of residuals.

2.3 Results

Figure 2.7 compares the normalised predicted muscle forces to the normalised EMG curve for one representative model. Results for all models are presented in Appendix B.

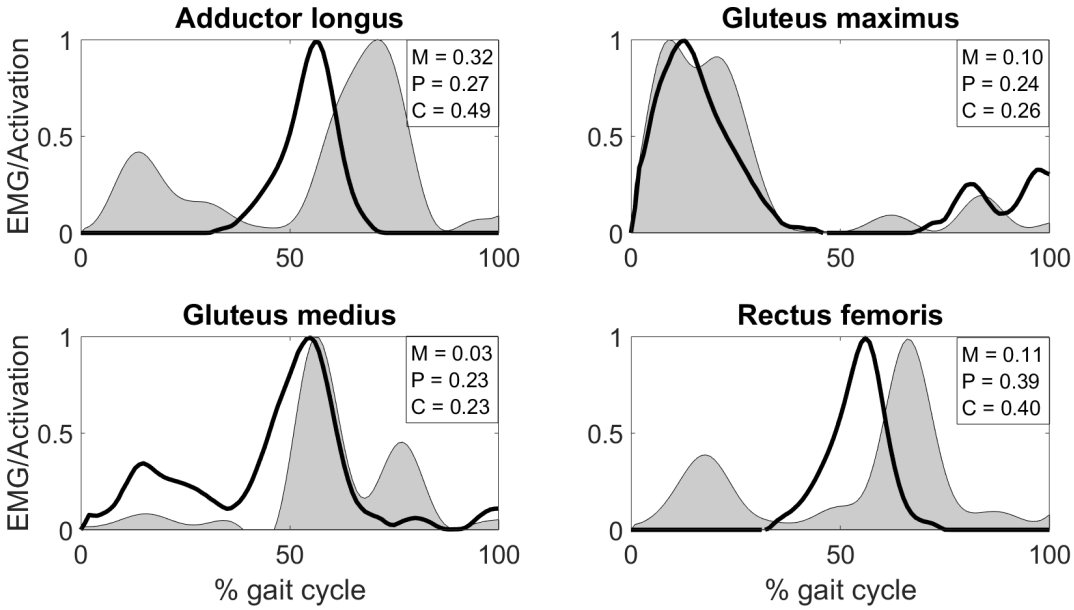


Figure 2.7: Predicted muscle activations (solid line) and normalised EMG data (shaded area) for the adductor longus, gluteus maximus, gluteus medius and rectus femoris muscles for a representative model.
M, P and C represent the magnitude, phase and combined errors, respectively, quantified using the Sprague and Geers metric.

The observed differences between the predicted and recorded muscle activations for 12 subject-specific models are shown in Table 2.4. The magnitude errors ranged from 0.13 ($\pm$0.10) for gluteus maximus to 0.24 ($\pm$0.11) for adductor longus. The phase errors ranged from 0.23 ($\pm$0.09) for gluteus maximus to 0.34 ($\pm$0.06) for rectus femoris. Finally, the combined errors from 0.28 ($\pm$0.10) for gluteus maximus to 0.42 ($\pm$0.11) for the adductor longus muscle. All results were excellent, very good or good, demonstrating that the models were able to accurately predict muscle activations.

	M	P	C
Muscle	Mean $\pm$ SD	Mean $\pm$ SD	Mean $\pm$ SD
Adductor longus	0.24 $\pm$ 0.11	0.33 $\pm$ 0.09	0.42 $\pm$ 0.11
Gluteus maximus	0.13 $\pm$ 0.10	0.23 $\pm$ 0.09	0.28 $\pm$ 0.10
Gluteus medius	0.14 $\pm$ 0.13	0.27 $\pm$ 0.05	0.33 $\pm$ 0.07
Rectus femoris	0.21 $\pm$ 0.10	0.34 $\pm$ 0.06	0.41 $\pm$ 0.09

Table 2.4: S&G metric magnitude (M), phase (P) and combined (C) errors between the EMG signals and muscle activity predictions from all validated subject-specific models (n=12). C<0.15 indicates excellent, 0.15<C<0.30 very good and 0.30<C<0.45 good similarity.

2.3.1 Predictors of discrepancies in muscle and hip joint contact forces

The RMSD values, normalised by the maximum force from the subject-specific model, were analysed in relation to percentage differences in anthropometric parameters from the subject-specific dataset. Table 2.5 presents the correlations between differences in each individual anthropometric parameter and RMSD values, in the presence of all investigated parameters, for the hip joint, muscle and 50:50 combined hip contact and muscle forces.

	Hip joint		Muscle groups		Hip joint & Muscle groups	
Parameter	R^2 (%)	p value	R^2 (%)	p value	R^2 (%)	p value
ΔPW[a]	9.01	<.001	9.87	<.001	12.12	<.001
ΔBMI	7.12	<.001	3.89	<.001	5.87	<.001
Δintact mass	4.22	<.001	5.71	<.001	6.65	<.001
Δintact height	2.99	.0018	5.09	<.001	5.63	<.001
Δmass (without prosth.)	2.06	.0096	4.13	<.001	4.40	<.001
Δprosthesis	1.57	.02	0.51	.20	.04	.71
Δstump length	0.04	.73	3.76	<.001	2.34	.0058
Δratio[b]	0.01	.85	3.69	<.001	2.38	.0054

Table 2.5: Correlations between differences in predicted hip joint contact forces, muscle forces and percentage differences in anthropometric parameters from the subject-specific model.
[a]PW, pelvis width. [b]stump length to pelvis width ratio.

Linear scaling to the models in the atlas introduced RMSD values in hip joint force predictions varying from 5.7% to 102.1%. Statistically significant correlations ($p<.05$) were identified between discrepancies in internal force predictions and percentage differences in all anthropometric parameters, with the exception of the stump length and stump length to pelvis width ratio for the hip joint contact force, and prosthesis type for the muscle and combined forces. Differences in pelvis width presented the strongest and most significant correlation with discrepancies in hip joint contact, muscle and combined forces, explaining 9.0% ($p<.001$), 9.9% ($p<.001$) and 12.1% ($p<.001$), respectively, of the total variability.

Table 2.6 presents the three identified multiple linear regression models, which aim to minimize the differences in the hip joint, muscle groups and overall internal force predictions.

Hip joint contact forces min(RMSD) = min(11.98 + 3.26 ×ΔPW + 1.91 ×ΔBMI - 0.26 ×ΔBMI ×ΔPW) R^2 = 27.27%, adjusted R^2 = 26.79%, p<.001				
Predictor	Coefficient	Standard error	p value	95% CI[a]
intercept	11.98	1.96	<.001	(8.13 15.84)
ΔPW[b]	3.26	0.35	<.001	(2.58 3.95)
ΔBMI	1.91	0.22	<.001	(1.47 2.35)
ΔBMI × ΔPW	-0.26	0.03	<.001	(-0.32 -0.20)
Muscle forces min(RMSD) = min(36.82 + 6.55 ×ΔPW + 2.85 ×ΔBMI + 0.29 ×Δratio - 0.38 ×ΔBMI ×ΔPW) R^2 = 19.76%, adjusted R^2 = 26.79%, p<.001				
Predictor	Coefficient	Standard error	p value	95% CI
intercept	38.82	5.93	<.001	(25.15 48.49)
ΔPW	6.55	1.00	<.001	(4.59 8.51)
ΔBMI	2.85	0.64	<.001	(1.58 4.11)
Δratio[c]	0.29	0.08	<.001	(0.13 0.45)
ΔBMI × ΔPW	-0.38	0.09	<.001	(-0.56 -0.20)
50:50 combined muscle and hip joint contact forces min(RMSD) = min(24.82 + 4.93 ×ΔPW + 2.39 ×ΔBMI + 0.13 ×Δratio - 0.32 ×ΔBMI ×ΔPW) R^2 = 25.55%, adjusted R^2 = 24.62%, p<.001				
Predictor	Coefficient	Standard error	p value	95% CI
intercept	24.82	3.39	<.001	(17.96 31.68)
ΔPW	4.93	0.59	<.001	(3.78 6.08)
ΔBMI	2.39	0.38	<.001	(1.65 3.14)
Δratio	0.13	0.05	.0098	(0.03 0.22)
ΔBMI × ΔPW	-0.32	0.05	<.001	(-0.43 -0.22)

Table 2.6: Multiple linear regression models relating percentage differences in significant anthropometric predictors to RMSD values in predicted internal forces.
[a]CI, confidence interval. [b]PW, pelvis width. [c]stump length to pelvis width ratio.

Stepwise multiple regression analysis identified significant predictors of RMSD values in force predictions to be: differences in pelvis width (coefficient B = 3.26, p<.001), BMI(B = 1.91, p<.001) and their multiplication (B = -0.26, p<.001) for the hip joint contact forces; differences in pelvis width (B = 6.55,p<.001), BMI (B = 2.85, p<.001), their multiplication (B = -0.38, p<.001) and stump length to pelvis width ratio (B = 0.29, p<.001) for the muscle forces; differences in pelvis width (B = 4.93, p<.001), BMI (B = 2.39, p<.001), their multiplication (B = -0.32, p<.001) and stump length to pelvis

width ratio (B = 0.13, p=.0098) for the combined forces. The inclusion of the remaining parameters in the multiple regression models increased the R^2 value by 1.6% for the hip joint contact forces, 0.8% for the muscle groups forces and 0.7% for the overall internal forces.

The muscle force regression equation led to the choice of the same anatomy to be used from the atlas as the hip joint force equation in 15 cases out of the total of 18, whereas the 50:50 combined hip and muscle force regression equation led to the choice of the same anatomy as the hip joint force model. All combined models with a weighting of muscle forces of less than 50% resulted in the same anatomy choice as the hip joint force model. The difference in R^2 value between the two extreme cases with 0% and 100% weighting of muscle force errors in the combined model was 8%. Table 2.7 shows the RMSD values in hip joint contact forces (one of the key musculoskeletal health-related variables) resulting from scaling to the closest anatomical model in the atlas using the 50:50 combined, hip joint and muscle forces regression models.

	RMSD (%)		
Regression model	Mean ± SD	Minimum	Maximum
50:50 combined	18.03 ± 5.84	10.97	29.03
Hip joint	18.03 ± 5.84	10.97	29.03
Muscle	20.07 ± 8.48	10.97	40.71

Table 2.7: Differences in hip joint contact force predictions between the scaled and subject-specific model output for all models (n=18) using different regression models. RMSD, root-mean-square difference.

2.4 Discussion

2.4.1 Validation of subject-specific models

The accuracy of twelve subject-specific models was evaluated by comparing the recorded and predicted muscle activations from the musculoskeletal model. The Sprague and Geers metric was used to quantify the magnitude, phase and combined errors. According to the metric, very good similarity was observed between the predicted and recorded gluteus maximus activations, as the combined error was less than 0.30. With combined errors of less than 0.45, there was good similarity for the gluteus medius, rectus femoris and adductor longus muscles. These findings compare well to able-body lower limb models, with combined magnitude and phase S&G errors of 0.31 (±0.10) and 0.44 (±0.12) for the gluteus medius and rectus femoris muscles, respectively (Ding et al. 2019).

The sub-optimal placement of the EMG sensors, combined with possible cross talk between adjacent muscles, may have reduced the quality of the received signal. The electromechanical delay between the force onset and EMG signal (Cavanagh & Komi 1979) was not accounted for in the musculoskeletal model, as the magnitude of the delay is

not known in atrophied muscles of amputees. Phase delays were most visible in the rectus femoris and adductor longus activity, with S&G metric phase errors of 0.34 (±0.06) and 0.33 (±0.09), respectively. Previous studies have implemented the EMG delay for able-body models (Arnold et al. 2013). However, as an accurate quantification of the delay was not possible for the current cohort, no correction was applied in this study. Use of prosthetic sockets with cut-outs, which allow for the optimal EMG placement recommended in the literature (Perotto 2011), would increase the fidelity of the model validation. However, given that all magnitude, phase and combined S&G errors were less than 0.45, therefore indicating good similarity between the recorded and predicted muscular activations, the validation of the 12 subject-specific models was considered successful. The remaining 6 models could not be validated due to the inability to optimally position the EMG sensors on the stumps.

2.4.2 Predictors of discrepancies in hip joint contact forces

The hip joint contact force is considered a key variable as its magnitude is linked to the likelihood of developing musculoskeletal diseases such as osteoarthritis. When direct measurements, such as instrumented implants, are not available, musculoskeletal modelling using linear scaling can enable the quantification of internal forces (Cleather & Bull 2012). However, linear scaling to a generic lower limb amputee model can produce significant inaccuracies in the predicted hip joint forces since it does not account for anatomical inter-individual variability (Duda et al. 1996). This is confirmed by the large range of RMSD values (from 5.7% to 102.1%) between the hip joint contact forces from the scaled and subject-specific model output. The differences in pelvis width and BMI were the primary predictors of RMSD in hip joint forces, each explaining 9.0% ($p<.001$) and 7.1% ($p<.001$) of the total variability, respectively. Moreover, it was noted that the mass and height differences accounted for inaccuracies in the hip joint forces output. The fact that the mass and inertial properties of the intact segments were not scaled in a subject-specific manner, but rather generically through the DeLeva regression equations (De Leva 1996), may have contributed to inaccuracies in hip joint contact forces. Future work should consider scaling of these parameters.

Unexpectedly, the percentage differences in stump length presented no significant correlation with discrepancies in hip joint forces. This wide variability among traumatic amputees is caused by different factors. Firstly, the muscle re-insertion locations differ from subject to subject, and the surgical procedure introduces the possibility of shorter stumps having stronger musculature than longer residual limbs through the preservation of muscle tension during reattachment (Ranz et al. 2017). Secondly, the rehabilitation and prosthetic training process greatly influences the amputee's musculoskeletal function – different training protocols can improve the functional capacity of different muscle groups. As a result, amputees adopt very distinct movement strategies in order to maximise comfort, performance, endurance, or minimise energy consumption and pain.

The final multiple linear regression model described 27.5% (adjusted $R^2 = 26.8\%$, $p<.001$) of the differences in hip joint contact forces. The anthropometric parameters that were

not included in the multiple regression model accounted for less than 2% of the variability, suggesting that the pelvis width and BMI are the most significant parameters that have to be considered in the analysis of hip joint contact forces from musculoskeletal modelling using a non-subject-specific anatomical dataset. Previous work identified the differences in limb length, mass and gender to be the most significant indicators of discrepancies in predicted hip joint forces during gait of able-bodied individuals, the final regression model accounting for 33.3% of the variance of differences in computed forces (Ding et al. 2019). The lower proportion of variance explained by the amputee model may be justified by the wider anatomical variability found in this cohort compared to persons without limb loss.

2.4.3 Predictors of discrepancies in muscle forces

The primary predictor of differences in the computed muscle forces was the difference in pelvis width (R^2 = 9.9%, p<.001), as was the case for the predicted hip joint contact forces, and the intact mass and height were the following most significant predictors. Muscle properties have been shown to scale with subject mass and limb length (Handsfield et al. 2014). In this study, it was found that the percentage differences in the pre- and post-amputation mass accounted for 5.7% (p<.001) and 4.1% (p<.001), respectively. The percentage differences in the pre-injury height (proportional to intact limb length) accounted for 5.1% (p<.001) of the variability and the stump length for 3.8% (p<.001). These numbers are significant when compared to the degree of variability that the pelvis width is accounting for. This study's cohort of amputees presents a small range of pre-injury height values (1.71 - 1.86 m). With a larger variability, a stronger correlation may be observed between the discrepancies in pre-injury height values and differences in internal force predictions.

The multiple regression model described 19.8% (adjusted R^2 = 18.8%, p<.001) of the variance of discrepancies in muscle force predictions. The model identified the same anthropometric parameters as the hip joint model to be significant predictors of discrepancies in force predictions (differences in pelvis width and BMI), with the addition of differences in the stump length to pelvis width ratio parameter, which did not significantly improve the R^2 value of the hip joint regression model.

2.4.4 Predictors of discrepancies in muscle and hip joint contact forces

The final 50:50 combined multiple linear regression model accounted for 25.5% (adjusted 24.6%, p<.001) of the variance of RMSD in muscle and hip joint contact forces. The addition of the remaining parameters in the multiple regression model increased the R^2 value by less than 1%, demonstrating the pelvis width, BMI and stump length to pelvis width ratio to be the most significant anthropometric parameters that have to be considered for musculoskeletal modelling using non-subject-specific geometries. Scaling using the closest model, identified by the multiple linear regression model, introduced an average RMSD value of 18% in the predicted hip joint loading, which is the key variable. This

RMSD value equates to 0.38 bodyweight difference for the hip joint contact forces, and is at the lower end of the total range of errors obtained from linear scaling to one model (5.7 – 102.1%). A previous study (Ding et al. 2019) found that linear scaling of able-body lower limb models to the closest anatomical dataset produced an average error of 16% (0.37 BW) in joint contact force calculations. The 2% difference may be attributed to the wider anthropometric and anatomical variability in amputees than able-bodied individuals.

The input parameters of the subject-specific models include bony landmarks, joint centres of rotation, muscle geometry, maximum muscle stress; the uncertainties in these could influence the musculoskeletal model outcomes. A previous study investigated this effect by perturbing model parameters according to their uncertainty and used these to build 500 able-bodied lower limb musculoskeletal models (Valente et al. 2014). The results showed that the uncertainties in the input parameters introduced a maximum standard deviation of 0.3 BW in muscle and joint contact forces, which is smaller than the mean difference identified by this chapter's model (0.38 BW) and considerably smaller than the maximum hip joint contact forces reported for bilateral above/through-knee amputees (7.83 BW (Henson 2020). This suggests that the use of the musculoskeletal model developed in this chapter to infer statistical differences should be confined to differences greater than those presented in Valente et al. (2014).

The choice of which regression model to use is based on both the purpose of the model (which application is to be considered) and the differences in errors. As the hip joint contact force is heavily dependent on the estimated muscle forces, an argument can be made to select the model only based on muscle forces. However, the hip joint regression model had the strongest explanatory and statistical power of all presented regression models. The R^2 value of the 50:50 combined model was 2% lower than of the hip joint model, and both models led to the same choice of anatomical dataset to scale to.

The muscle force regression equation led to the choice of the same anatomy to be used from the atlas as the hip joint and 50:50 combined models in 83.3% of the cases. Scaling to the closest dataset, identified by the muscle regression model, increased the errors in the hip joint force predictions, a key variable for the general assessment of musculoskeletal health, by 2% when compared to the use of the combined regression model. In order to accurately predict hip joint forces, as well as muscle forces, it is recommended that the combined regression model, with equal weighting distribution, is used to choose the closest anatomical dataset to scale to. This is what is used in the remainder of this thesis. The full anatomical atlas (bone .stl files, joint, muscle and wrapping object parameters, muscle lines-of-action, bony landmarks coordinates) is available at http://www.msksoftware.org.uk.

2.4.5 Limitations

The static optimisation algorithm implemented in this study is based on the minimisation of energy expenditure, as lower limb amputees have been shown to walk at self-selected

speeds that aim to minimize energy expenditure per metre walked (Inman 1966). This cost function has previously been validated in the musculoskeletal modelling framework for transtibial amputee and able-bodied gait (Ding et al. 2016, 2020) and so, it was assumed that this algorithm also applies for through-knee and transfemoral amputees. However, this young and motivated cohort of military bilateral lower limb amputees may have different objectives and some prior work shows that they walk at speeds different from the energy efficient ones (Jaegers et al. 1993). Therefore, maximisation of performance or stability, minimisation of pain or impact at heel strike could potentially be considered.

Secondly, the prosthetic socket, stump liner and the residual limb were modelled as a single rigid segment, without considering the angular and axial movement at the socket-stump interface (Tang et al. 2015). Although these movements are typically very small, in the order of 12° and 36 mm (Tang et al. 2015), the effect of this simplification in the model could also be investigated. Moreover, the model assumed that the external load is axially transmitted through the distal end of the residual limb. Whilst this is representative of amputees with end-bearing quadrilateral sockets, ischial containment sockets distribute the weight more proximally to the ischium. The prosthetic inertial parameters were determined using the reaction board method (Smith et al. 2014, Henson 2020), and this approach is only adequate for identifying the centre of mass in the longitudinal direction. Moreover, similar to non-amputated segments, the inertial parameters of the residual thigh were approximated using DeLeva calculations. Nonetheless, the residuum centre of mass might vary with length. Future work should investigate the effect of these limitations.

The current study analysed gait only and did not include other activities of daily living. Therefore, using the identified linear regression models in musculoskeletal modelling of other motion tasks may lead to errors in model predictions. However, this thesis will focus only on gait as a key variable that does not comprehensively assess function, but does relate to overall function and is a key task that amputees describe as being one that causes fatigue (Yeung et al. 2012). Furthermore, the identified multiple linear regression models only apply to musculoskeletal modelling using the linear scaling law and different scaling methods may change the regression models. Non-linear scaling, based on a morphing technique, has been shown to improve the model predictions when compared to the ones obtained through linear scaling (Nolte et al. 2016). However, the majority of lower limb musculoskeletal models utilise linear scaling. As a future improvement, the non-linear method could be implemented on the available dataset to generate outputs with increased accuracy.

Muscle force predictions have been shown to be sensitive to the variation in muscle properties (Carbone et al. 2016, Zuk et al. 2018). In this study, the pennation angle, fibre length to muscle length ratio and sarcomere length parameters were not subject-specific, but instead obtained from studies based on elderly cadavers (Ward et al. 2009, Lieber et al. 1994). As these values cannot be acquired from imaging scans, assigning these parameters values from in-vivo cadaveric studies is common in the literature (Klemt

et al. 2019, Ding et al. 2019). Furthermore, the muscle moment arms were defined using imaging scans capturing the standard position of the subjects in the MRI scanner and so, changes in muscle moment arms during dynamic conditions were not included in the model. Future work could perform a model sensitivity analysis to investigate the dependency of the musculoskeletal model and regression models on input parameters. A convergence study could also be performed to investigate the generalization of the anatomical atlas and its sample size.

Finally, this anatomical atlas consists of only male subjects and does not account for gender differences in pelvic shape (Nakahara et al. 2011) and distal femur (Griffin et al. 2000) (in the case of through-knee amputees). A previous study, which used an anatomical atlas to improve scaling of musculoskeletal lower limb modelling for able-bodied individuals (Ding et al. 2019), found that gender differences improve the regression fit of RMSDs in hip joint contact forces by 2%. Future work could develop anatomical datasets for female subjects in order to account for gender differences. However, this thesis is focused primarily on UK military amputees and, as such, the main application is for male subjects.

2.5 Conclusion

This study presents the first EMG-validated musculoskeletal model for bilateral through- and above-knee amputees. An anatomical atlas of 18 datasets is presented and used to show that linear scaling to an anatomy with anthropometric similarity (the most similar pelvis width, estimated intact body mass index and stump length to pelvis width ratio) can accurately predict muscle and joint contact forces for gait, thus enabling such models to be used pervasively without recourse to expensive imaging-derived anatomies. The anatomical atlas in now used throughout the remainder of this thesis to quantify musculoskeletal internal loading (muscle and joint contact forces) for traumatic amputees for a range of prostheses.

Chapter 3

Biomechanical assessment of bilateral transfemoral amputee gait with stubbies and microprocessor-controlled knees

Prosthesis prescription for lower limb amputees is often based on anecdotal evidence and manufacturer claims, with little available in-depth analysis of the biomechanical effect of prosthetic design on the amputee musculoskeletal system. This chapter aims to identify differences in function and internal loading (muscle and joint contact forces) of bilateral above/through-knee male traumatic amputees during level-ground walking with foreshortened non-articulated stubbies and full-length articulated prostheses. Motion capture and force plate data were collected, and musculoskeletal modelling was performed using the anatomical datasets and regression equations developed in Chapter 2. The findings of this chapter may provide beneficial guidance in making informed decisions for adequate prosthesis prescription.

3.1 Introduction

The Afghanistan conflict presented a total of 265 major lower limb UK military amputees from 2003 to 2014 (Edwards et al. 2015). Whilst the injured personnel sustained different locations, levels and number of amputations, the most common type of bilateral amputation was at the transfemoral level (Edwards et al. 2015). The post-injury musculoskeletal function is disrupted as the loss of joints, muscle volume (Henson et al. 2021) and physiological muscle attachments lead to muscular adaptations required for successful task completion, which in turn increase the strain on the musculoskeletal system. Detrimental loading of the joints and residual muscles can lead to musculoskeletal disorders including osteoarthritis (Burke et al. 1978, Struyf et al. 2009), osteopenia (Rush et al. 1994) and low back pain (Ephraim et al. 2005).

Return to physical activity is achieved through the use of prosthetic devices and rehabilitation. Prosthesis prescription is often based on manufacturer driven research and anecdotal evidence, with little research-based evidence of the biomechanical effect of prosthetic design on the amputee musculoskeletal function and loading. Commercially available prostheses for bilateral above/through-knee (BTF) amputees include the foreshortened non-articulated stubbies (e.g. College Park Sidekicks, College Park, Michigan, USA) and advanced microprocessor-controlled knee units (e.g. Genium X3, Ottobock, Germany) coupled with dynamic response feet (e.g. Triton, Ottobock, Germany). These two types of prostheses are considered the two ends of the spectrum. There are other prosthetic devices within the spectrum, such as mechanically-controlled prosthetic knees and solid-ankle-cushioned-heel prosthetic feet, and the thesis will investigate these in the later chapters. This chapter focuses on the two extremes: stubbies (with no articulated knee joints) and microprocessor knees coupled with dynamic response feet. These two types of lower limb prostheses were analysed in this chapter as these are the only prostheses prescribed to BTF amputees. Mechanically-controlled articulated prostheses are not common in this amputee population.

Following bed rest and wheelchair use post amputation and any additional surgical interventions, stubby prostheses are used for immediate training of BTF amputees. For successful functional outcomes, the rehabilitation protocol after an amputation focuses on neuromusculoskeletal capacity improvement through gait training with the prosthesis. Once successful in efficiently walking with stubbies, amputees proceed to walk with full-length articulated prostheses. However, several amputees permanently use stubbies after the rehabilitation process. Additionally, some amputees who regularly use full-length articulated prostheses also use stubbies on occasion. The more complex microprocessor knees can reproduce the power absorption phases of gait in the knee (Czerniecki 1996) and replicate the eccentric function of the quadriceps at heel strike and early swing, and of the hamstrings at the end of the swing phase. The enhanced function of microprocessor knees allows amputees to achieve similar physical abilities to those of non-amputees (Jarvis et al. 2017, 2020). However, even if able to walk with prosthetic knees, there is anecdotal evidence that some amputees choose to use stubbies when they feel tired.

Previous studies have evaluated the functional performance of military traumatic BTF amputees, and the results demonstrated notable function and efficient gait patterns (Jarvis et al. 2017, 2020). However, all participants had microprocessor knees and dynamic response feet, and the biomechanical effect of different prosthetic designs on the BTF musculoskeletal function has not been analyzed. The amputee biomechanics with stubby prostheses has been previously presented in case studies, which showed, in comparison to full-length articulated prostheses, reduced walking speeds (Carroll et al. 2018, Fiodorenko-Dumas et al. 2021, Perry et al. 2004) and increased oxygen cost when used for long distances (Perry et al. 2004). The aforementioned studies focused on spatiotemporal, metabolic, kinematics and dynamics measures, excluding other relevant physiological aspects such as muscle and joint forces, that are related to pathology. Whilst the previous measures can evaluate the functional outcome, muscle and joint contact forces can be used to assess musculoskeletal health (Felson 2013).

There is limited understanding of the biomechanical effect of full-length articulated prostheses and stubbies use on the BTF musculoskeletal system loading. Additionally, there are no studies in the literature which investigate the biomechanics of amputees who are only able to walk with stubby prostheses. Musculoskeletal modelling is a widely used tool that can provide comprehensive descriptions of muscle and joint contact forces during movement (Cleather & Bull 2012, Ding et al. 2016, 2020). The analysis of functional, as well as biomechanical loading measures, allows for the development of strategies to reduce the risk of musculoskeletal health-related diseases, whilst also considering functional performance.

3.2 Aims and hypotheses

The primary aim of this study is to use biomechanical tools to understand the musculoskeletal function and loading of persons with BTF amputations walking with stubbies and microprocessor knees coupled with dynamic response feet, and how these compare to persons without limb loss. Additionally, the study aims to identify biomechanical differences between BTF amputees who are able to walk with both stubbies and prosthetic knees, and those who cannot use prosthetic knees.

This study hypothesizes that although stubbies present lower functional abilities compared to prosthetic knees, they improve (reduce) the loading of the hip joint. Moreover, it is hypothesized that reduced muscle volume and residuum length are the primary causes of the inability to stabilize on prosthetic knees. The findings of this study may provide guidance in making informed decisions for adequate prosthesis prescription to ensure optimal rehabilitation and long-term musculoskeletal health. A prosthesis is deemed adequate if it can be used to achieve the amputee's desired functional abilities and ensures optimal musculoskeletal health.

3.3 Methods

3.3.1 Data acquisition and processing

Data were collected under separate ethical approvals from the Imperial College Research Ethics Committee (Reference 16IC3562, 18IC4677, 20IC6268). Written informed consent was obtained from 12 BTF male traumatic amputees (1 civilian, 11 ex-military) and 8 able-bodied (AB) males (Table 3.1) with no known musculoskeletal or neurological condition. Among the BTF cohort, 4 were able to walk with both Genium and Sidekicks prostheses (Cohort 1), 4 participants were only able to walk with Sidekicks (Cohort 2) and 4 completed walking trials with Genium knees only (Cohort 3). All BTF had been prosthesis users for a minimum of two years. BTF able to use prosthetic knees were group matched to AB persons based on intact adjusted mass (calculated using Equation 2.6, Chapter 2) and pre-injury height. There were no significant differences in adjusted mass (p=.878), height (p=.798) and age (p=.798) between the two groups. This was checked with Mann-Whitney U tests with a .05 significance level. Additionally, there were no significant differences in adjusted mass (p=.778), pre-injury height (p=.326), age (p=.480), left stump length (p=.694) and right stump length (p=.246) between the 3 amputee cohorts. This was checked with the Kruskal-Wallis test with a .05 significance level. The stump length was calculated as the distance from the hip joint centre to the distal end of the residual limb. The hip joint centre location was available from MRI scans from the dataset presented in Chapter 2. For the study participants without MRI scans, the stump length was measured in the laboratory.

The able-bodied data are a subset of a previously collected dataset (Jarvis et al. 2020). Data from eight BTF study participants were collected as part of a previous study (Henson 2020). Cohort 1_Sidekicks indicates Cohort 1 when walking with Sidekicks, and Cohort 1_Genium indicates Cohort 1 when walking with Genium prosthetic knees. The BTF Sidekicks full cohort comprises Cohort 1_Sidekicks and Cohort 2. The BTF Genium full cohort comprises Cohort 1_Genium and Cohort 3.

Cohort	Age (y)	Adj. mass (kg)	Pre-injury height (m)	Left stump length (cm) (level)	Right stump length (cm) (level)	Prosth. socket	Prosth. foot	Prosth. knee
Cohort 1 BTF Sidekicks and Genium (n=4)	36	89	1.87	52.4 (TK)	39.9 (TF)	Quad	Triton LP	Genium X3
	32	68	1.71	35.0 (TF)	35.9 (TF)	IC	Taleo	Genium X3
	34	84	1.80	36.0 (TF)	47.0 (TK)	IC (L) Quad (R)	Triton LP	Genium X3
	41	86	1.87	49.8 (TK)	32.8 (TF)	Quad	Triton LP	Genium X3
Mean ± SD	36 ± 3	82 ± 8	1.81 ± 0.07	43.3 ± 7.9	39.9 ± 5.3			
Cohort 2 BTF Sidekicks only (n=4)	38	95	1.80	38.6 (TF)	25.0 (TF)	IC	Sidekicks	N/A
	31	78	1.70	33.7 (TF)	36.1 (TF)	IC	Sidekicks	N/A
	27	80	1.75	47.0 (TK)	46.4 (TK)	Quad	Sidekicks	N/A
	33	80	1.75	40.6 (TF)	13.9 (TF)	IC	Sidekicks	N/A
Mean ± SD	32 ± 4	83 ± 7	1.75 ± 0.04	42.1 ± 3.6	28.4 ± 13.5			
Cohort 3 BTF Genium (n=4)	41	64	1.64	35.5 (TF)	39.0 (TF)	IC	Triton LP	Genium X3
	27	85	1.85	34.3 (TF)	43.4 (TF)	IC	Triton LP	Genium X3
	40	93	1.80	41.5 (TF)	40.8 (TF)	IC	Triton LP	Genium X3
	33	97	1.82	44.8 (TK)	47.9 (TK)	Quad	Triton LP	Genium X3
Mean ± SD	35 ± 6	85 ± 13	1.78 ± 0.08	39.0 ± 4.3	42.8 ± 3.3			
Control AB (n=8) Mean ± SD	35 ± 4	81.6 ± 9.8	1.82 ± 0.05					

Table 3.1: Study participant details.
Cohort 1 (n=4): Bilateral transfemoral amputees (BTF) able to walk with both Genium and Sidekicks prostheses; Cohort 2 (n=4): BTF able to walk with Sidekicks stubbies only; Cohort 3 (n=4): BTF who completed walking trials with Genium prosthetic knees only; AB (n=8): able-bodied controls. Quad, quadrilateral. IC, ischial containment. LP, low profile. L, left. R, right.

Motion data were collected at an acquisition rate of 120 Hz using a 10-camera VICON motion analysis system (VICON 2.10.3, Oxford Metrics Group, UK). The force plate data were collected with two force plates (Kistler Type 9286B, Kistler Instrumente AG, Winterthur, Switzerland) at an acquisition rate of 1000 Hz. Figure 3.1 shows two representative study participants with full-length articulated prostheses and stubby prostheses. Table 3.2 shows the locations of the retro-reflective markers placed on the lower limbs (Ding et al. 2019, Duffell et al. 2014).



(a) Full-length articulated prostheses. **(b)** Stubby prostheses.

Figure 3.1: Representative study participants with different prostheses.

Marker name	Anatomical landmark
RASIS/LASIS	Right/Left anterior superior iliac spine
RPSIS/LPSIS	Right/Left posterior iliac spine
RFME/LFME	Right/Left medial femoral epicondyle prosthetic knee equivalent: medial side of the knee centre of rotation stubbies equivalent: medial side of the pylon, below the prosthetic socket
RFLE/LFLE	Right/Left lateral femoral epicondyle prosthetic knee equivalent: lateral side of the knee centre of rotation stubbies equivalent: lateral side of the pylon, below the prosthetic socket
RFAM/LFAM	Right/Left lateral malleoli prosthetic equivalent: lateral side of the ankle centre of rotation
RTAM/LTAM	Right/Left medial malleoli prosthetic equivalent: medial side of the ankle centre of rotation
RFM2/LFM2	Right/Left second metatarsal head prosthetic equivalent: front edge of the foot above second toe
RFM5/LFM5	Right/Left fifth metatarsal head prosthetic equivalent: front edge of the foot above fifth toe
RFCC/LFCC	Right/Left posterior calcaneus prosthetic equivalent: heel at toe height
RTF/LTF	Right/Left midfoot superior prosthetic equivalent: top of the foot, anterior to the pylon base
R/L T1/T2/T3	Right/Left thigh segment cluster
R/L C1/C2/C3	Right/Left shank segment cluster

Table 3.2: Marker placement locations.

Static calibration and level ground self-selected speed walking trials, with complete foot placement on the force plate, were collected for all study participants. VICON Nexus (VICON 2.10.3, Oxford Metrics Group, UK) was used to identify the gait cycle events (foot strike, toe off, consecutive foot strike) for both left and right sides, label the reflective markers and fill the marker trajectory gaps using the rigid body gap filling algorithm. The marker trajectories and ground reaction forces were filtered in MATLAB (The Mathworks Inc., Natick, MA, USA) using a zero phase-lag, fourth order Butterworth filter with 6 Hz cut-off frequency (Yu et al. 1999) prior to the musculoskeletal model input.

The orientations of the pelvis were calculated in reference to the anatomical position (Figure 3.2) using the spatial coordinates of the four markers attached on anatomical landmarks of the pelvis (Henson 2020, Nakahara et al. 2011, Leardini et al. 2013). Pelvic tilt was calculated as the rotation angle between the PSIS and ASIS markers in the global sagittal plane (Equation 3.1). Pelvic obliquity was defined as the rotation angle in the coronal plane, and determined using Equation 3.2, where X, Y and Z represent the coordinates of the ASIS markers, SW is the swing limb and ST is the stance limb. Pelvic rotation (Equation 3.3) was defined as the rotation angle in the transverse plane between the left and right ASIS markers.

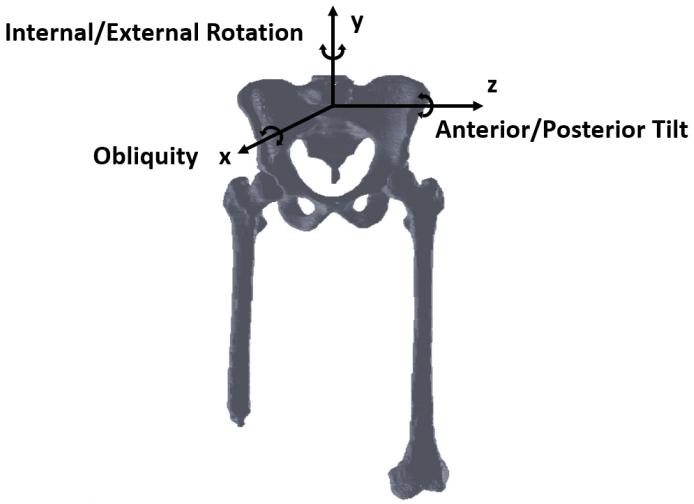


Figure 3.2: Pelvic orientations and coordinate system.

$$Pelvic\ tilt = \frac{180}{\pi} tan^{-1} \frac{PSIS_y - ASIS_y}{ASIS_x - PSIS_x} \tag{3.1}$$

$$Pelvic\ obliquity = \frac{180}{\pi} tan^{-1} \frac{Y_{SW} - Y_{ST}}{\sqrt{(X_{SW} + X_{ST})^2 + (Z_{SW} + Z_{ST})^2}} \tag{3.2}$$

$$Pelvic\ rotation = \frac{180}{\pi} tan^{-1} \frac{RASIS_x - LASIS_x}{RASIS_z - LASIS_z} \tag{3.3}$$

3.3.2 Musculoskeletal modelling

Freebody v2.1 was used to perform inverse kinematics, inverse dynamics and musculoskeletal modelling simulations. The validated above/through-knee amputee model presented in Chapter 2 was used in this chapter. Briefly, it consists of two rigid segments (thigh, pelvis) articulated at the hip joint with three rotational degrees of freedom (DOFs). The residual limb, prosthetic liner, socket and connectors represent the thigh segment. The able-body model is comprised of four rigid segments (foot, shank, thigh, pelvis), three joints (ankle, knee, hip), 163 muscle elements and the patellar tendon. Whilst the hip joint possesses three rotational DOFs, the ankle and knee joints are modelled with six DOFs (three rotational, three translational).

Eight out of twelve amputee models were subject-specific, where the joint and muscle parameters were obtained from the MRI scans analysis performed in Chapter 2. These were 3 participants in Cohort 1, 3 participants in Cohort 2 and 2 participants in Cohort 3 (Table 3.1). The anatomical geometries for the remaining amputee musculoskeletal models were obtained through linear scaling using the regression models and anatomical datasets developed in Chapter 2. The closest datasets for the amputee models were chosen based on similar pelvis width, estimated intact body mass index and stump length to pelvis width ratio in order to accurately predict muscle and hip joint contact forces.

Similarly, the closest datasets for the able-body models were chosen based on similar mass, gender and limb length to pelvis width ratio in order to predict joint contact forces with clinically insignificant errors (Ding et al. 2019). The linearly scaled anatomical parameters were the following: muscle and ligaments lines-of-action, muscle wrapping parameters, joint centres and contact points (Ding et al. 2016). The muscle physiological cross-sectional areas (PCSAs) were equal to those in the datasets the models were scaled to.

The forces (F_i) produced by each muscle element, i, were computed using a one-step static load-sharing optimization algorithm (Equation 3.4) that aims to minimize the sum of muscle activations cubed (J). M represents the total number of muscle elements, where M = 163 for the the able-body model, and M = 92 for the amputee model. $F_{max,i}$ represents the maximum capacity force for each muscle element, and was defined as the multiplication of the muscle element PCSA (determined in the anatomical dataset) and maximum muscle stress (31.39 N/cm^2 (Yamaguchi 2005)).

$$min(J) = min(\sum_{i=1}^{M}(\frac{F_i}{F_{max,i}})^3) \tag{3.4}$$

3.3.3 Data analysis

The leg length was calculated as the sum of thigh and shank segment lengths. The thigh length was calculated as the distance from the hip joint centre to the midpoint of the femoral epicondyles, and the shank length was calculated as the distance from the midpoint of the femoral epicondyles to the midpoint of the malleoli. Step width was calculated as the medial-lateral distance between the FCC marker position at heel strike and the contralateral limb FCC marker position at the contralateral heel strike. Stride length was calculated as the anterior-posterior distance between the FCC marker location at heel strike and the ipsilateral FCC marker location at the consecutive ipsilateral heel strike. Step length was calculated as the anterior-posterior distance between the FCC marker location at heel strike and the contralateral limb FCC marker location at the contralateral heel strike.

Symmetry (SI) in gait (between the left and right step length) and hip joint loading (between left and right first/second peak of the hip joint contact force) was assessed using Equation 3.5 (Agrawal et al. 2009), where X is the variable of interest and 100% represents perfect symmetry.

$$SI = 100 - 100 \times |\frac{X_{left} - X_{right}}{X_{left} + X_{right}}| \tag{3.5}$$

Statistical analysis of walking characteristics was performed using IBM SPSS Statistics 27.0.0 (IBM Corp. Armonk, NY). Parametric data were compared between groups by one-way ANOVA with post-hoc Bonferroni. One-way ANOVA with repeated measures was used to identify differences between prostheses for Cohort 1. Data normality was

checked using the Shapiro-Wilk statistical test.

The computed whole-time data series were expressed as a gait cycle percentage from 0% at heel strike to 100% at the consecutive heel strike in intervals of 1% and averaged over three trials. Statistical parametric mapping (SPM) (Friston et al. 2007, Papi et al. 2020, Pataky et al. 2013) was used to compare the whole time-series data between groups. Depending on data normality, parametric or non-parametric two-tailed independent sample t-tests were performed to first identify biomechanical differences between the three full cohorts: BTF Sidekicks (Cohort 1_Sidekicks and Cohort 2), BTF Genium (Cohort 1_Genium and Cohort 3) and AB controls, and thereafter between Cohort 1_Sidekicks and Cohort 2. One-way ANOVA with repeated measures was used to compare walking characteristics with prosthetic knees and stubbies for Cohort 1. p values of less than .05 were considered to indicate statistical significance.

3.4 Results

The first analysis compares BTF Sidekicks (Cohort 1_Sidekicks and Cohort 2), BTF Genium (Cohort 1_Genium and Cohort 3) and AB controls (Section 3.4.1 - Prosthesis type analysis). The second comparison compares Cohort 1_Sidekicks and Cohort 1_Genium (Section 3.4.2 - Comparison between stubbies and full-length articulated prostheses for amputees who could use both). The third comparison compares Cohort 1_Sidekicks and Cohort 2 (Section 3.4.3 - Stubby prostheses analysis). The kinetic results are normalised to the measured body mass. All biomechanical parameters are presented for the right limb. Normally distributed data are presented as Mean ± SD and non-normally distributed data are presented as Median [95% Confidence Interval]. At the end of each section the key statistically and clinically significant results are summarised. In this thesis, clinically significant results are defined as differences of 10% or higher. Except for walking speed (Carse et al. 2021), the minimal clinically important difference for bilateral transfemoral amputee biomechanical data has not been investigated.

The whole-time data are presented over the course of the gait cycle. SPM results are presented for identification of significant differences between cohorts, where grey threshold clusters indicate statistically significant differences, and red dashed lines represent critical thresholds.

3.4.1 Prosthesis type analysis

This section compares the biomechanical gait data of amputees with Sidekicks (Cohort 1_Sidekicks and Cohort 2), amputees with full-length articulated prostheses (Cohort 1_Genium and Cohort 3) and able-bodied persons. Table 3.3 presents the leg length details for the full cohorts: BTF Sidekicks, BTF Genium, AB. The leg length of BTF Sidekicks were lower by 0.15 m than BTF Genium (p=.011) and 0.14 m than AB persons (p=.020). There were no differences between BTF Genium and AB.

Biomechanical parameter	BTF Sidekicks Mean ± SD	BTF Genium Mean ± SD	AB Mean ± SD
Leg length (m)	0.73 ± 0.14 ***p=.011** ****p=.020**	0.88 ± 0.06	0.87 ± 0.03

Table 3.3: Leg length details.
*Statistically significant differences from BTF Genium (p<.05). **Statistically significant differences from AB controls (p<.05).

Table 3.4 presents the calculated temporospatial parameters for the full cohorts. The step width (base-of-support) was significantly larger in both amputee groups than AB (p<.001), with no significant difference between BTF Sidekicks and BTF Genium. The step length, stride length and self-selected walking speed of BTF Genium were comparable to those of AB, and were greater by 0.2 m (p<.001), 0.4 m (p<.001), and 0.3 m/s (p<.001), respectively, than BTF Sidekicks. There was no significant difference in cadence and gait symmetry index between the three cohorts. BTF Sidekicks spent shorter time in stance than BTF Genium by 2.9% (p<.001) and AB by 3.8% (p<.001).

Biomechanical parameter	BTF Sidekicks Mean ± SD	BTF Genium Mean ± SD	AB Mean ± SD
Step width (m)	0.26 ± 0.06 ****p<.001**	0.22 ± 0.03 ****p<.001**	0.09 ± 0.02
Step length (m)	0.53 ± 0.04 ***p<.001** ****p<.001**	0.70 ± 0.05	0.72 ± 0.03
Gait SI (%)	96.75 ± 1.15	96.21 ± 1.55	96.61 ± 1.95
Stride length (m)	1.01 ± 0.11 ***p<.001** ****p<.001**	1.41 ± 0.09	1.42 ± 0.10
Cadence (steps/min)	102.98 ± 13.76	99.61 ± 5.57	105.00 ± 2.33
Walking speed (m/s)	0.86 ± 0.12 ***p<.001** ****p<.001**	1.17 ± 0.11	1.25 ± 0.07
Stance time (% cycle)	61.14 ± 1.08 ***p<.001** ****p<.001**	64.05 ± 2.05	64.97 ± 1.21

Table 3.4: Temporospatial characteristics.
SI, symmetry index. *Statistically significant differences from BTF Genium (p<.05). **Statistically significant differences from AB controls (p<.05).

Figure 3.3 shows the ankle joint angles over the course of the gait cycle. SPM reported significantly lower ankle plantar flexion angles for BTF Genium and BTF Sidekicks than AB in early swing (p<.001). SPM identified significantly higher dorsiflexion angles for BTF Genium and AB than BTF Sidekicks in late stance (p<.001). When comparing discrete points in Table 3.5, BTF Genium showed higher peak dorsiflexion angles by 5.5° compared to 3.6° for BTF Sidekicks (p=.001).

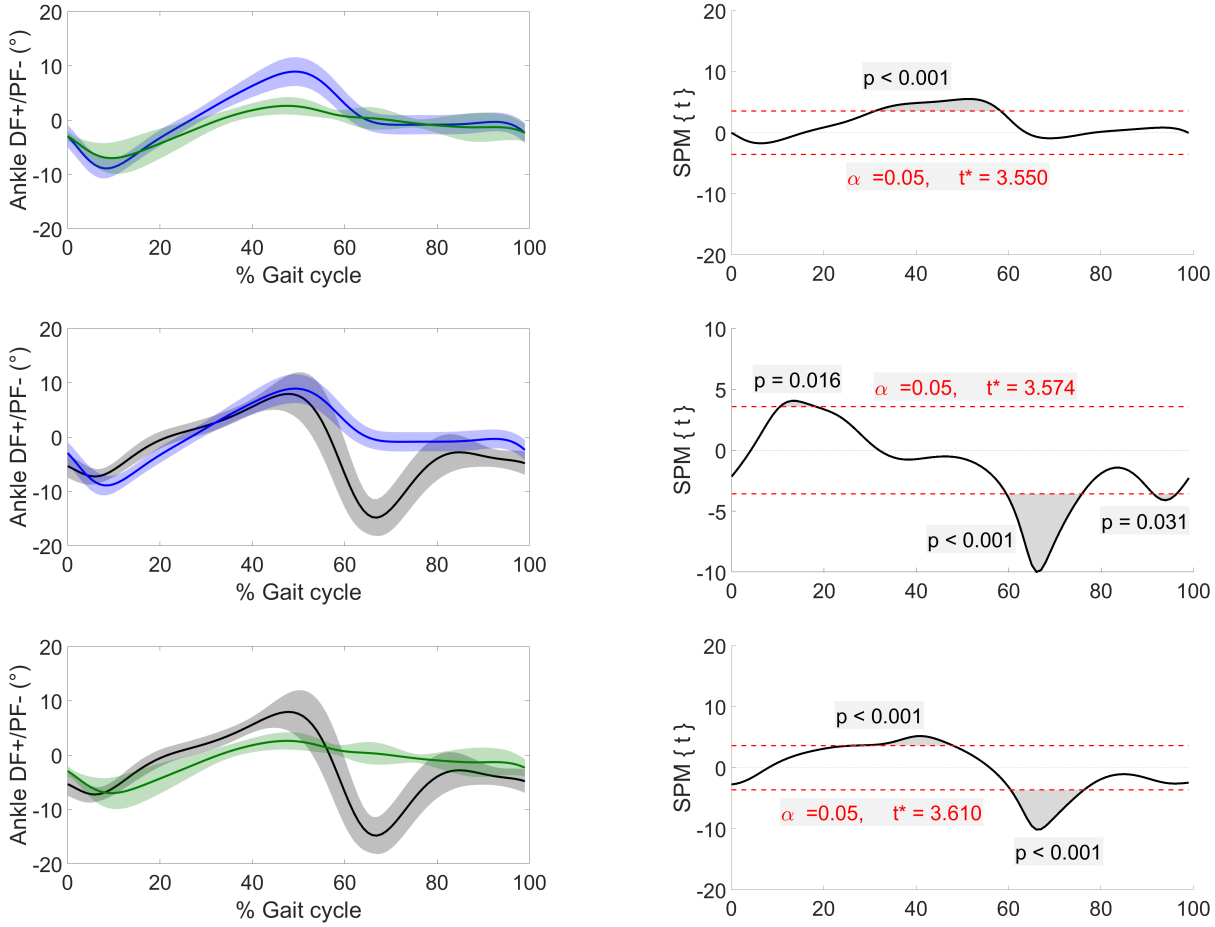


Figure 3.3: Left: Ankle dorsiflexion (DF)/plantar flexion (PF) angles. Right: Statistical parametric mapping results. BTF Sidekicks - green. BTF Genium - blue. AB - black.

Biomechanical parameter	BTF Sidekicks Mean ± SD	BTF Genium Mean ± SD	AB Mean ± SD
Peak ankle dorsiflexion (°)	3.61 ± 1.24 ***p=.001** ****p=.002**	9.14 ± 2.57	8.68 ± 3.57
Peak ankle plantar flexion (°)	7.95 ± 1.72 ***p<.001**	9.07 ± 1.80 ****p<.001**	15.81 ± 3.26
Ankle dorsiflexion/ plantar flexion ROM (°)	11.10 ± 1.89 ***p<.001** ****p<.001**	18.19 ± 2.47 ****p=.003**	24.49 ± 4.29

Table 3.5: Sagittal plane ankle kinematics.
ROM, range of motion. *Statistically significant differences from BTF Genium ($p<.05$).
**Statistically significant differences from AB controls ($p<.05$).

Figures 3.4 shows the hip joint angles in the coronal plane. BTF Genium adducted the hip more in swing than AB (p=.021). The hip abduction angles were larger for BTF Genium and BTF Sidekicks in stance than AB (p<.001). Whilst no significant differences were identified in stance, BTF Sidekicks had a significantly higher degree of hip abduction in swing than BTF Genium (p=.003). There were no differences in the peak hip coronal plane angles throughout the full gait cycle between cohorts (Table 3.6).

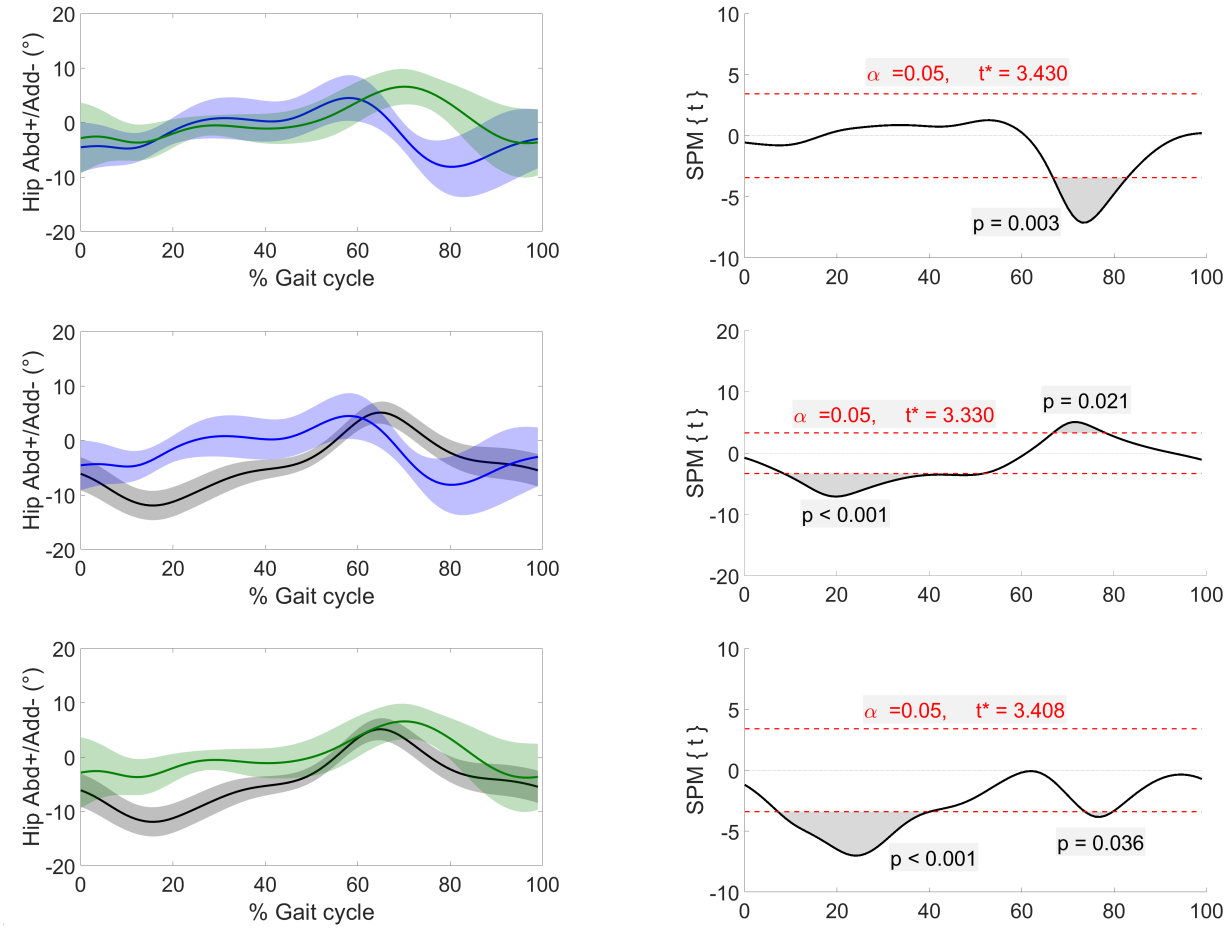


Figure 3.4: Left: Hip joint abduction (Abd)/adduction (Add) angles. Right: Statistical parametric mapping results. BTF Sidekicks - green. BTF Genium - blue. AB - black.

Biomechanical parameter	BTF Sidekicks Mean ± SD	BTF Genium Mean ± SD	AB Mean ± SD
Peak hip adduction (°)	7.70 ± 3.53	8.99 ± 5.53	11.99 ± 2.72
Peak hip abduction (°)	8.58 ± 2.62	5.22 ± 3.51	5.24 ± 1.96
Hip adduction/abduction ROM (°)	16.28 ± 5.51	14.21 ± 8.09	17.23 ± 3.45

Table 3.6: Coronal plane hip kinematics.
ROM, range of motion.

Figure 3.5 presents the hip joint angles in the sagittal plane. SPM reported larger hip extension angles for BTF Genium in late stance than BTF Sidekicks (p=.006) and AB (p=.022). When comparing discrete points in Table 3.7, BTF Sidekicks showed lower peak hip extension angles by 11.4° than 24.4° for BTF Genium (p<.001).

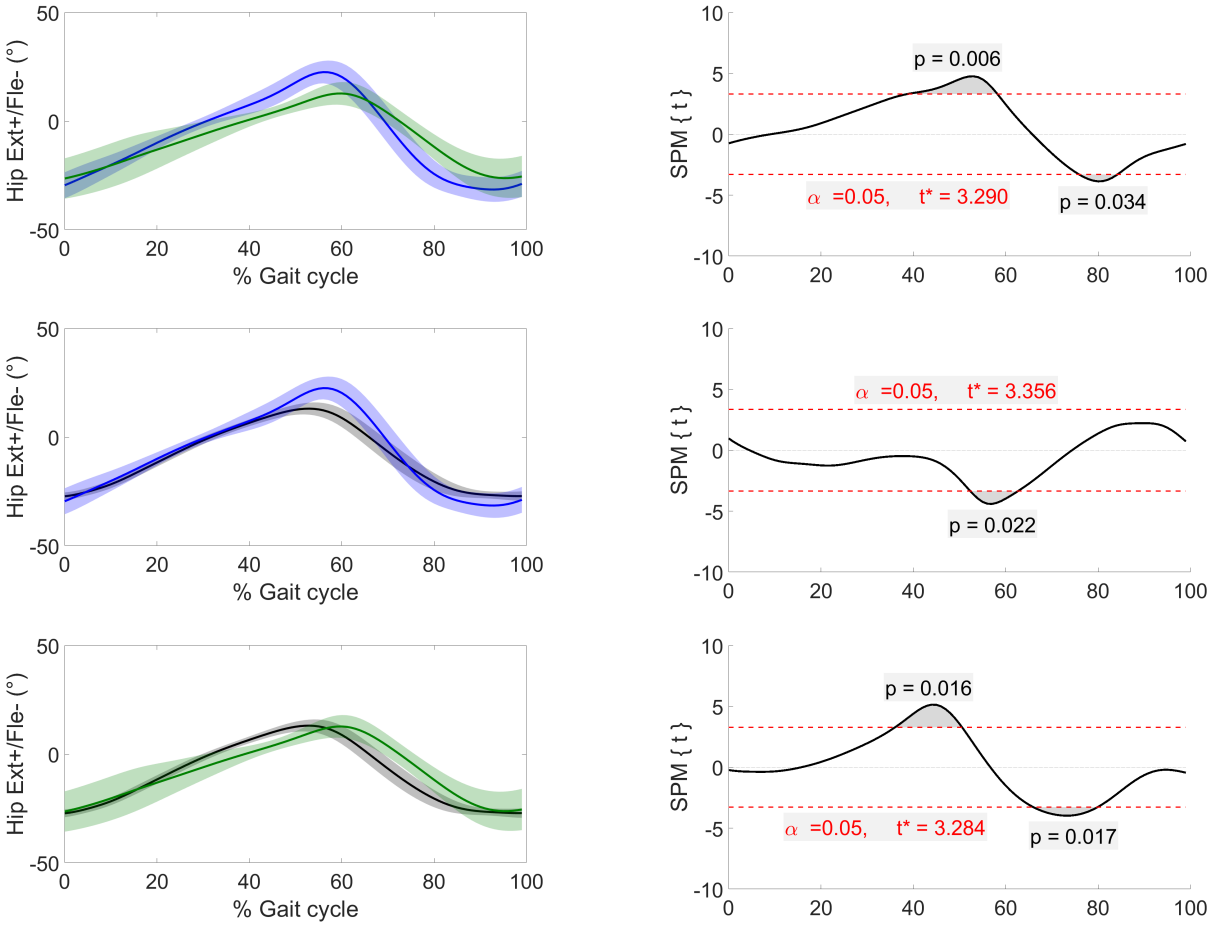


Figure 3.5: Left: Hip joint extension (Ext)/flexion (Fle) angles. Right: Statistical parametric mapping results. BTF Sidekicks - green. BTF Genium - blue. AB - black.

Biomechanical parameter	BTF Sidekicks Mean ± SD	BTF Genium Mean ± SD	AB Mean ± SD
Peak hip extension (°)	13.04 ± 5.09 ***p<.001**	24.43 ± 5.04 ****p<.001**	13.35 ± 2.67
Peak hip flexion (°)	27.79 ± 9.45	32.31 ± 5.79	28.29 ± 1.55
Hip extension/ flexion ROM (°)	27.79 ± 9.45	32.31 ± 5.79	28.89 ± 1.55

Table 3.7: Sagittal plane hip kinematics.
ROM, range of motion. *Statistically significant differences from BTF Genium (p<.05). **Statistically significant differences from AB (p<.05).

Figure 3.6 and Table 3.8 show the hip joint angles in the transverse plane. SPM reported higher hip internal rotation for BTF Genium than AB in swing (p=.014). The hip internal/external rotation range of motion was larger for BTF Genium by 6.8° than AB (p=.023).

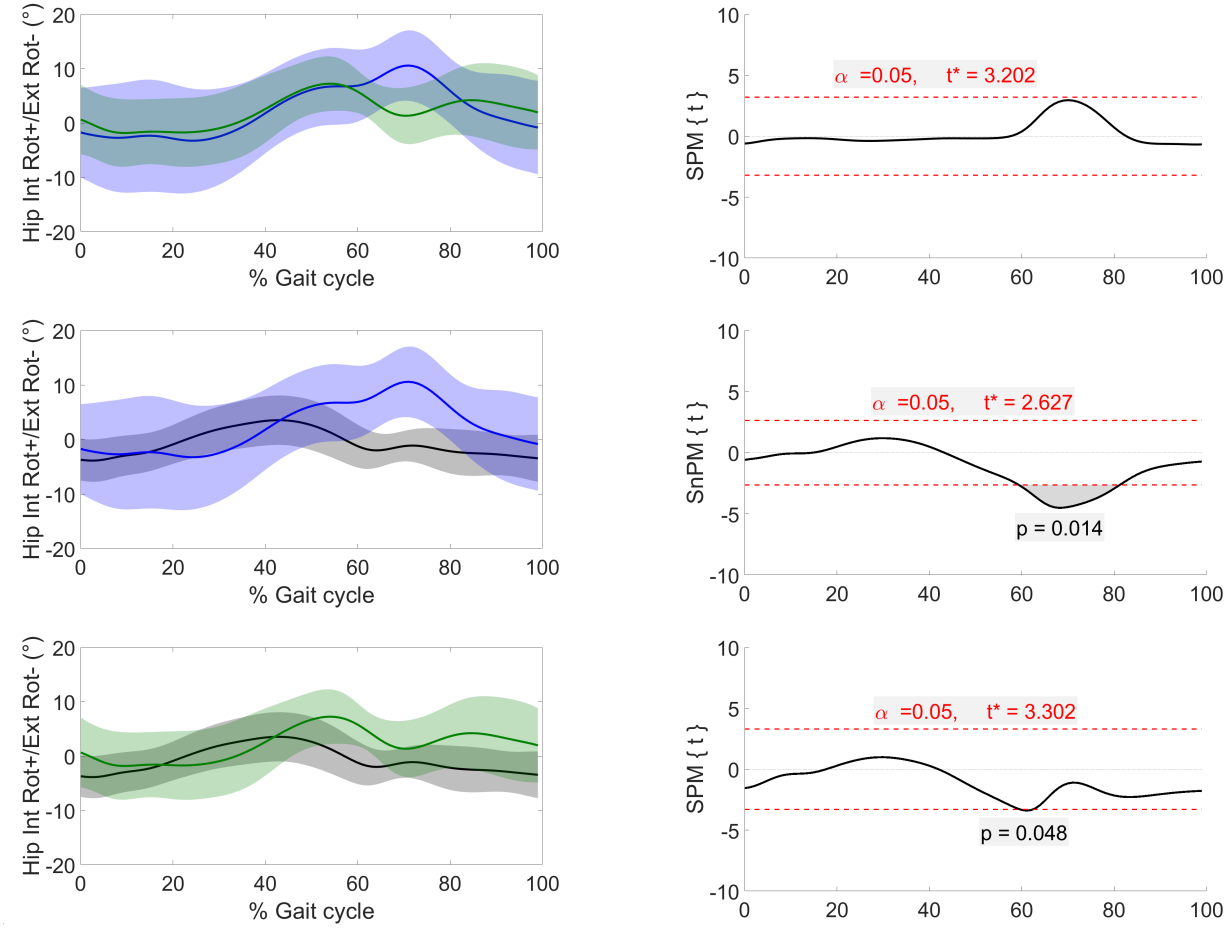


Figure 3.6: Left: Hip internal (Int)/external (Ext) rotation (Rot) angles. Right: Statistical parametric mapping results. BTF Sidekicks - green. BTF Genium - blue. AB - black.

Biomechanical parameter	BTF Sidekicks Mean ± SD	BTF Genium Mean ± SD	AB Mean ± SD
Hip internal/ external rotation ROM (°)	15.67 ± 4.19	17.41 ± 5.22 **p=.023	10.62 ± 3.25

Table 3.8: Transverse plane hip kinematics.
ROM, range of motion. **Statistically significant differences from AB (p<.05).

Figure 3.7, 3.8 and 3.9 show the pelvic tilt, obliquity and rotation angles over the course of the gait cycle, and Tables 3.9, 3.10 and 3.11 present the calculated peak-to-peak (P2P) values. SPM presented significantly larger pelvic obliquity, rotation and anterior pelvic tilt for both amputee cohorts than AB. BTF Genium presented similar pelvic obliquity profiles to BTF Sidekicks. BTF Sidekicks showed larger P2P pelvic rotation angles by 8.9° compared to 14.1° for BTF Genium (p<.001).

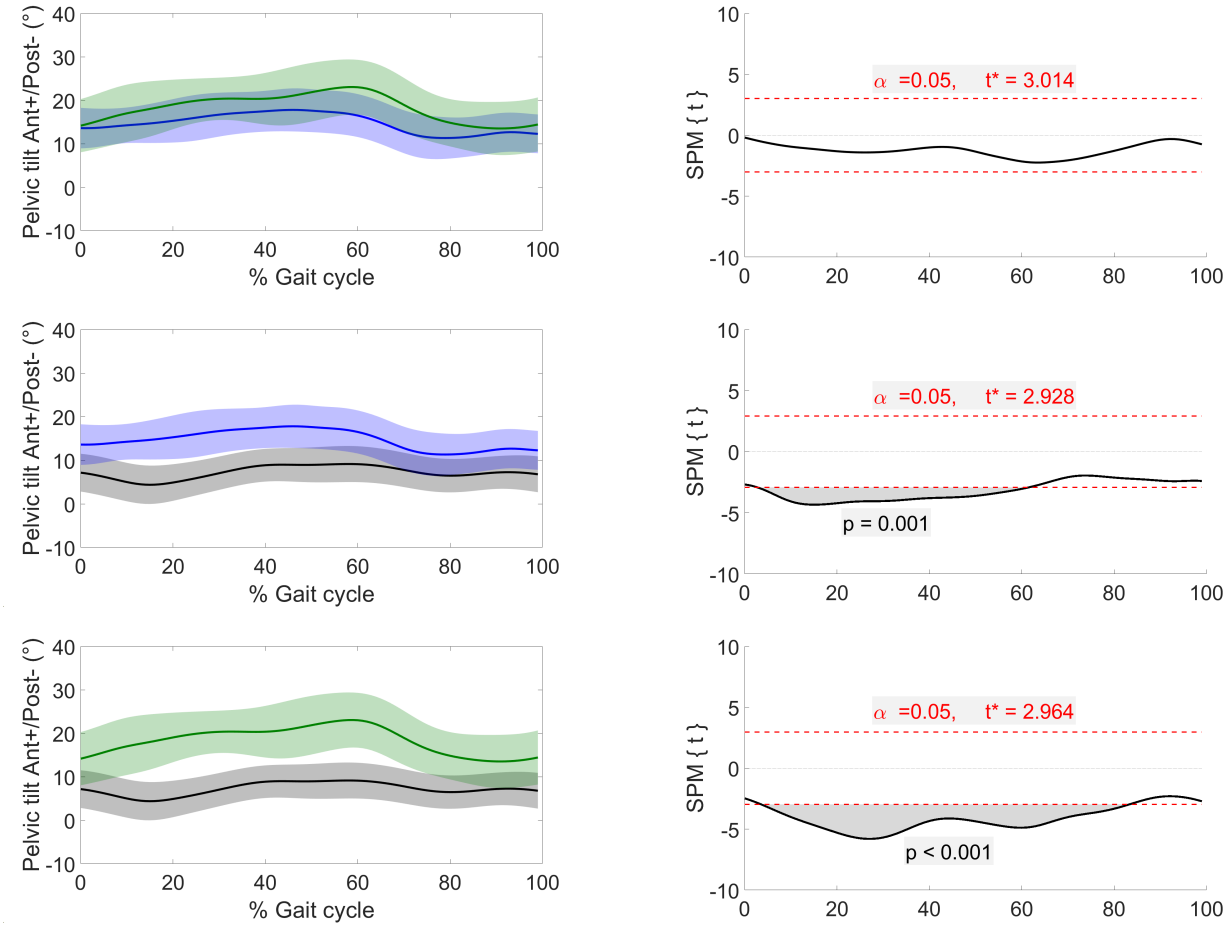


Figure 3.7: Left: Pelvic anterior (Ant)/posterior (Post) tilt angles. Right: Statistical parametric mapping results. BTF Sidekicks - green. BTF Genium - blue. AB - black.

Biomechanical parameter	BTF Sidekicks Mean ± SD	BTF Genium Mean ± SD	AB Mean ± SD
P2P pelvic tilt (°)	11.77 ± 6.23 **p=.016	8.35 ± 1.42	5.51 ± 1.43

Table 3.9: Sagittal plane pelvic kinematics.
P2P, peak-to-peak. **Statistically significant differences from AB (p<.05).

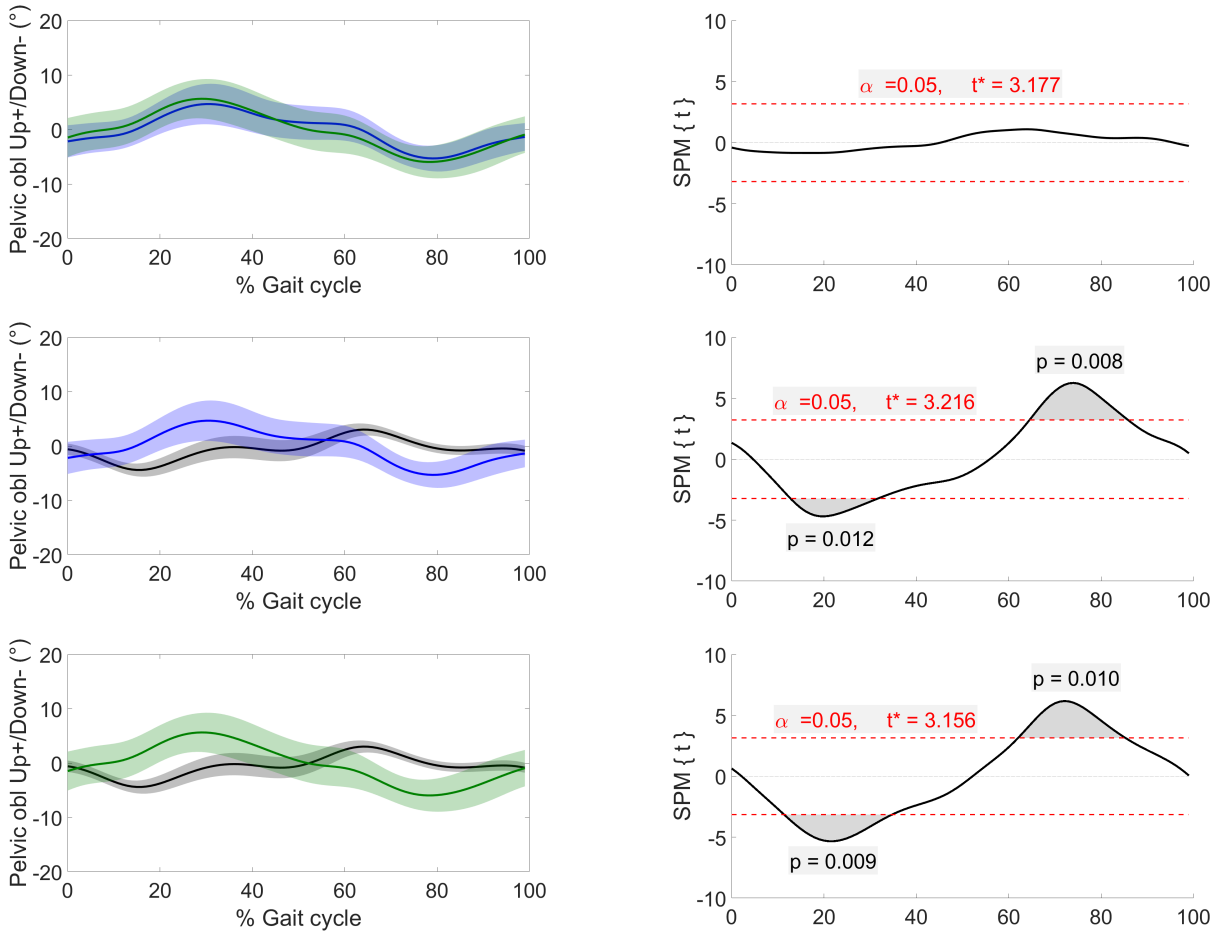


Figure 3.8: Left: Pelvic obliquity angles. Positive angles describe an increase in the vertical height of the contralateral hip. Right: Statistical parametric mapping results. BTF Sidekicks - green. BTF Genium - blue. AB - black.

Biomechanical parameter	BTF Sidekicks Mean ± SD	BTF Genium Mean ± SD	AB Mean ± SD
P2P pelvic obliquity (°)	12.16 ± 2.57 **p=.023	10.47 ± 4.06	7.71 ± 0.85

Table 3.10: Coronal plane pelvic kinematics.
P2P, peak-to-peak. **Statistically significant differences from AB (p<.05).

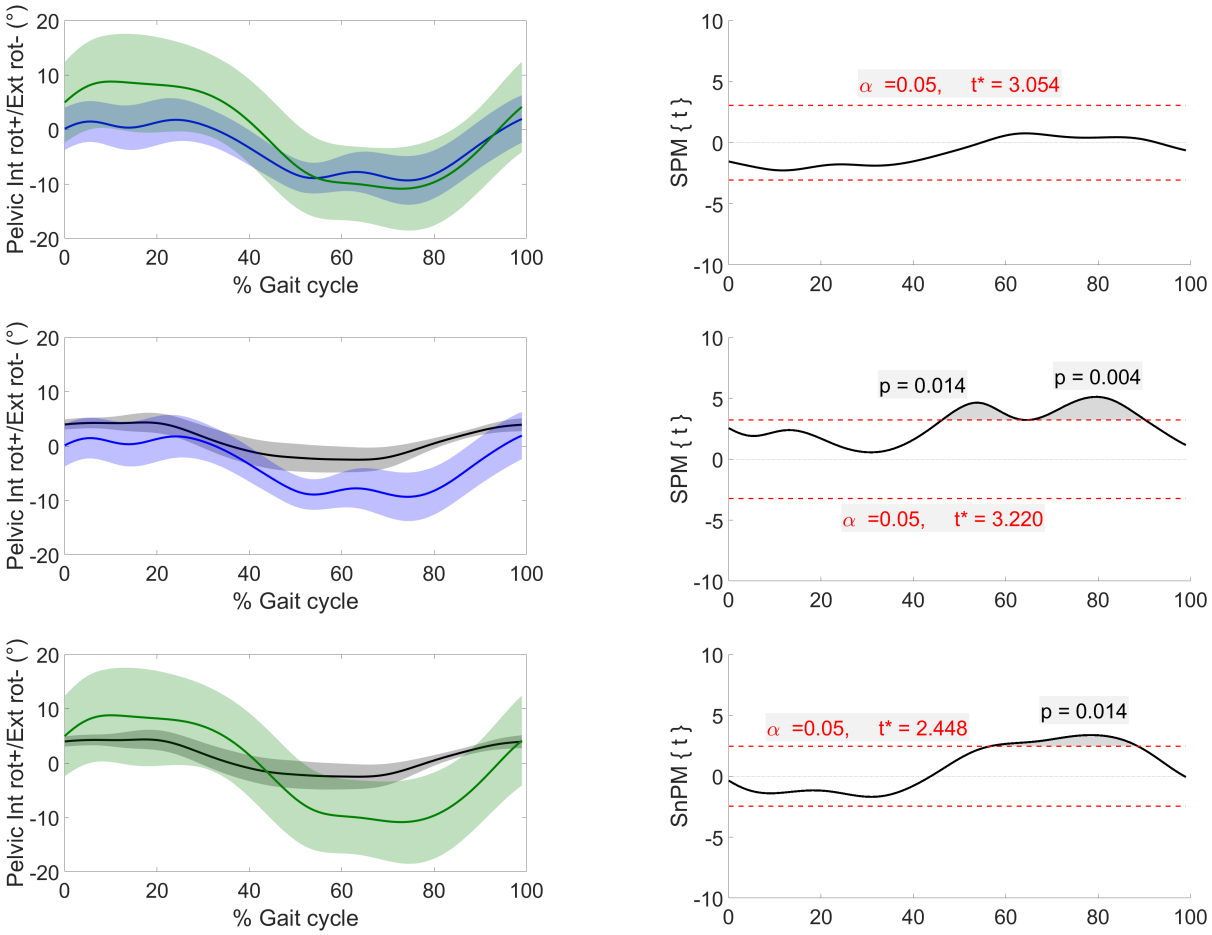


Figure 3.9: Left: Pelvic internal (Int)/external (Ext) rotation (Rot) angles. Right: Statistical parametric mapping results. BTF Sidekicks - green. BTF Genium - blue. AB - black.

Biomechanical parameter	BTF Sidekicks Mean ± SD	BTF Genium Mean ± SD	AB Mean ± SD
P2P pelvic rotation (°)	22.94 ± 4.93 ***p<.001** ****p<.001**	14.05 ± 3.52 ***p=.032**	8.59 ± 1.79

Table 3.11: Transverse plane pelvic kinematics.
P2P, peak-to-peak. *Statistically significant differences from BTF Genium (p<.05).
**Statistically significant differences from AB (p<.05).

Figure 3.10 shows the ground reaction force (GRF) profiles over the course of the gait cycle. Table 3.12 presents the peak GRF for each cohort. There were no significant differences in GRF between the amputee groups. SPM reported statistically significant differences between BTF Genium and AB in early stance (p=.030) and swing (p=.018). SPM also showed statistically significant differences between BTF Sidekicks and AB in early stance (p=.018, p=.025, p=.005).

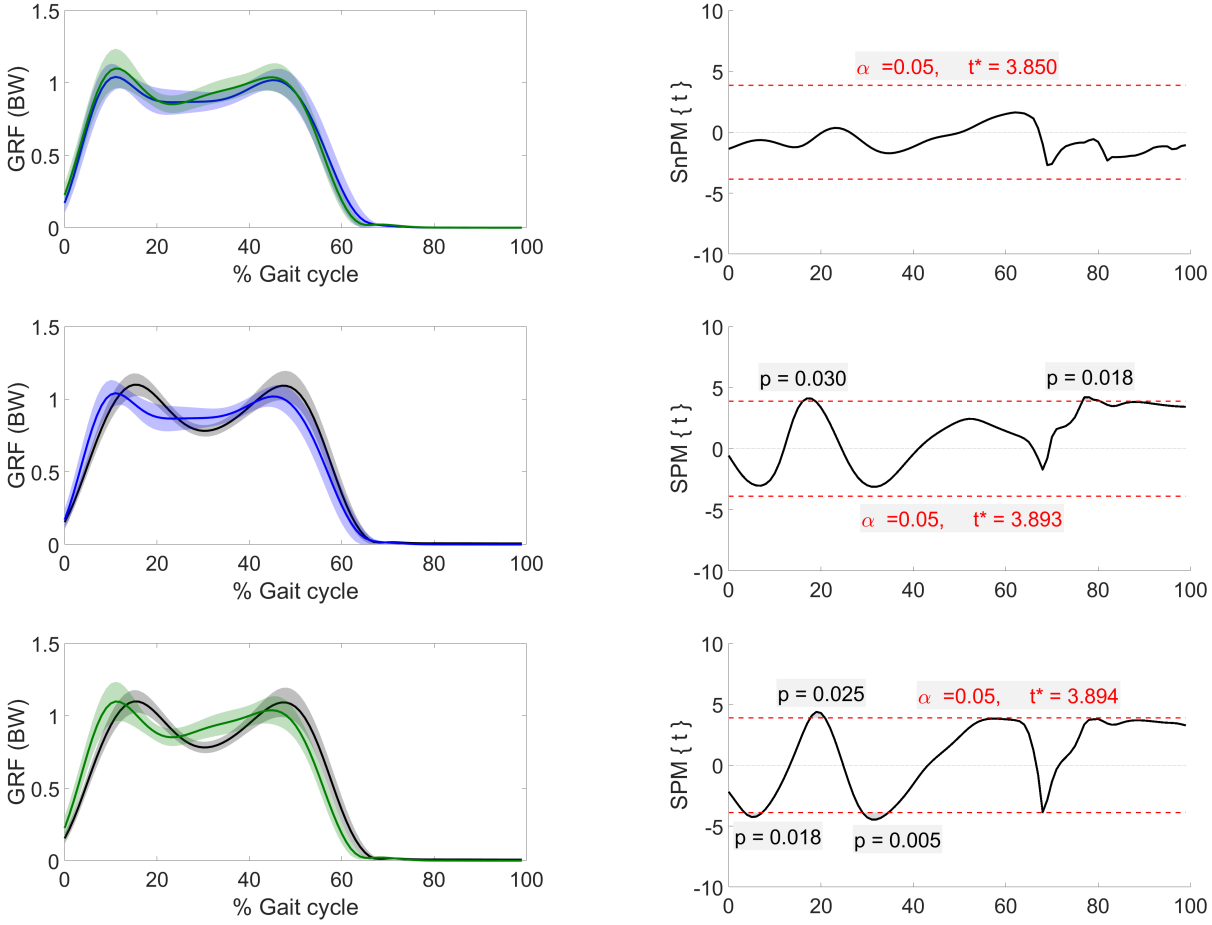


Figure 3.10: Left: Ground reaction forces (GRF). Right: Statistical parametric mapping results. BTF Sidekicks - green. BTF Genium - blue. AB - black.

Biomechanical parameter	BTF Sidekicks Mean ± SD	BTF Genium Mean ± SD	AB Mean ± SD
Peak GRF (BW)	1.14 ± 0.12	1.10 ± 0.07	1.14 ± 0.08

Table 3.12: Ground reaction forces (GRF).

Figure 3.11, Figure 3.12, Table 3.13 and Table 3.14 present the coronal and sagittal plane hip moments. SPM reported significantly larger hip abduction moments for BTF Sidekicks than BTF Genium in late stance (p=.002), and lower in swing (p=.004). The AB hip abduction moment was significantly larger than both amputee groups in stance (p<.001). BTF Genium showed larger hip flexion moments than BTF Sidekicks and AB (p=.009) at the push-off phase of the gait cycle. When comparing discrete points, BTF Genium showed higher peak hip flexion moments by 0.8 Nm/kg than BTF Sidekicks and AB (p<.001).

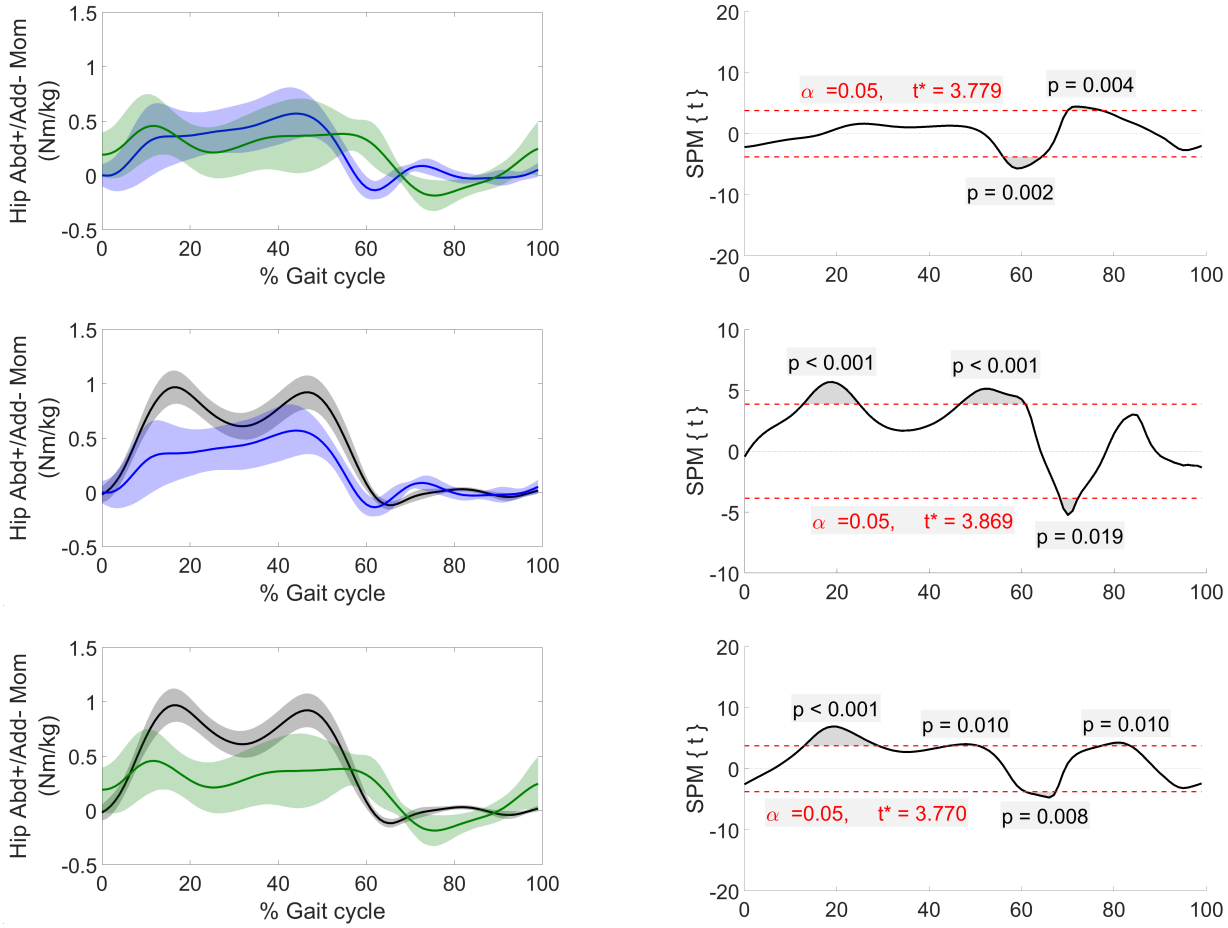


Figure 3.11: Left: Abduction (Abd)/adduction (Add) hip moments (Mom). Right: Statistical parametric mapping results. BTF Sidekicks - green. BTF Genium - blue. AB - black.

Biomechanical parameter	BTF Sidekicks Mean ± SD	BTF Genium Mean ± SD	AB Mean ± SD
Peak hip adduction moment (Nm/kg)	0.26 ± 0.16	0.19 ± 0.09	0.16 ± 0.05
Peak hip abduction moment (Nm/kg)	0.64 ± 0.23 ****p=.005**	0.63 ± 0.19 ****p=.004**	1.01 ± 0.15

Table 3.13: Coronal plane hip moments.
**Statistically significant differences from AB ($p<.05$).

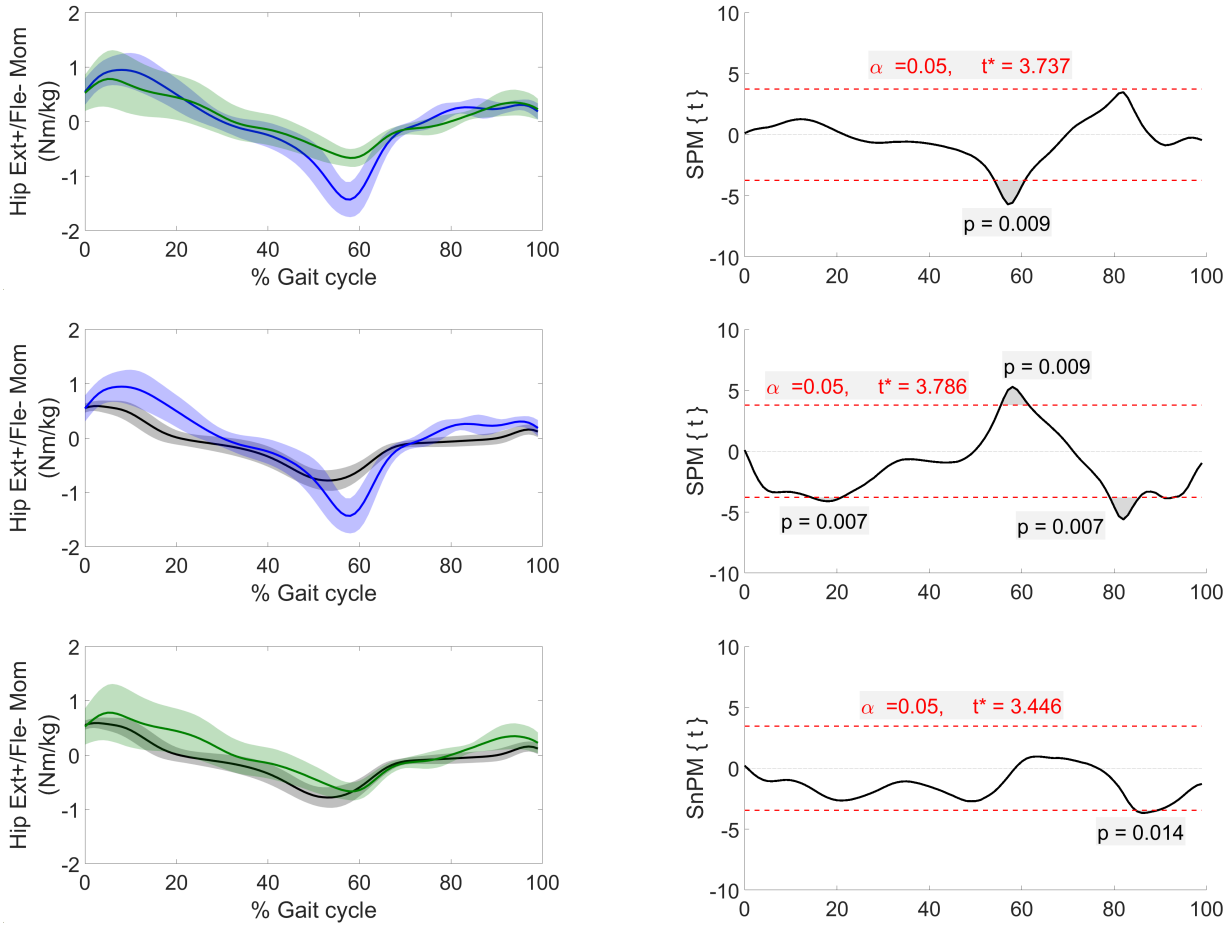


Figure 3.12: Left: Extension (Ext)/flexion (Fle) hip moments (Mom). Right: Statistical parametric mapping results. BTF Sidekicks - green. BTF Genium - blue. AB - black.

Biomechanical parameter	BTF Sidekicks Mean ± SD	BTF Genium Mean ± SD	AB Mean ± SD
Peak hip extension moment (Nm/kg)	0.87 ± 0.49	1.02 ± 0.31	0.63 ± 0.09
Peak hip flexion moment (Nm/kg)	0.76 ± 0.16 ***p<.001**	1.58 ± 0.30 ****p<.001**	0.82 ± 0.17

Table 3.14: Sagittal plane hip moments.
*Statistically significant differences from BTF Genium (p<.05). **Statistically significant differences from AB (p<.05).

Figure 3.13 shows the hip joint power over the course of the gait cycle. SPM reported significantly higher hip generated power in late stance for BTF Genium than BTF Sidekicks (p=.004) and AB (p=.003). Additionally, BTF Genium showed higher hip generated power than AB in early stance (p<.001). SPM reported higher hip absorbed power for BTF Genium than AB in stance (p=.002). When comparing discrete points in Ta-

ble 3.15, BTF Genium presented larger peak generated hip joint power by 1.9 W/kg compared to 1.2 W/kg for BTF Sidekicks and AB (p<.001).

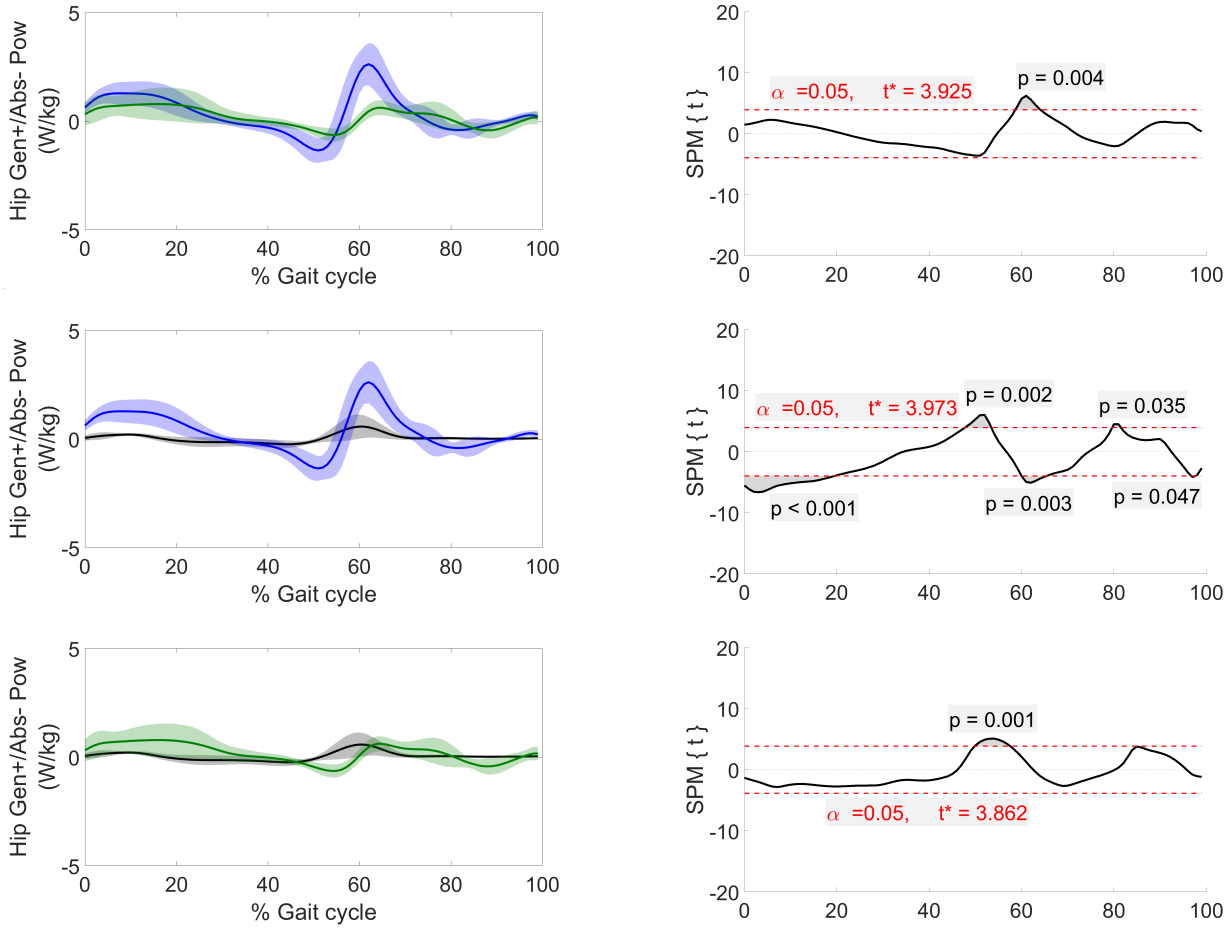


Figure 3.13: Left: Generated (Gen)/absorbed (Abs) hip joint power (Pow). Right: Statistical parametric mapping results. BTF Sidekicks - green. BTF Genium - blue. AB - black.

Biomechanical parameter	BTF Sidekicks Mean ± SD	BTF Genium Mean ± SD	AB Mean ± SD
Peak hip generation power (W/kg)	1.18 ± 0.68 ***p<.001**	3.12 ± 0.81 ****p<.001**	1.18 ± 0.46
Peak hip absorbed moment (Nm/kg)	0.79 ± 0.33 ***p<.001**	1.73 ± 0.41 ****p<.001**	0.85 ± 0.29

Table 3.15: Sagittal plane hip power.
*Statistically significant differences from BTF Genium (p<.05). **Statistically significant differences from AB (p<.05).

The hip joint contact force (HJCF) profiles and characteristics are shown in Figure 3.14 and Table 3.16. Whilst there was no significant difference in the magnitude of the first HJCF peak between the amputee cohorts, the second HJCF peak was 1.7 times larger for BTF Genium than BTF Sidekicks (p=.017). Additionally, SPM reported larger HJCF for BTF Genium than AB in late stance (p<.001). BTF Sidekicks and AB presented similar HJCF profiles during one gait cycle. However, the HJCF impulse normalised by walked distance was higher for BTF Sidekicks by 60.1 BW.s/m than AB (p=.017).

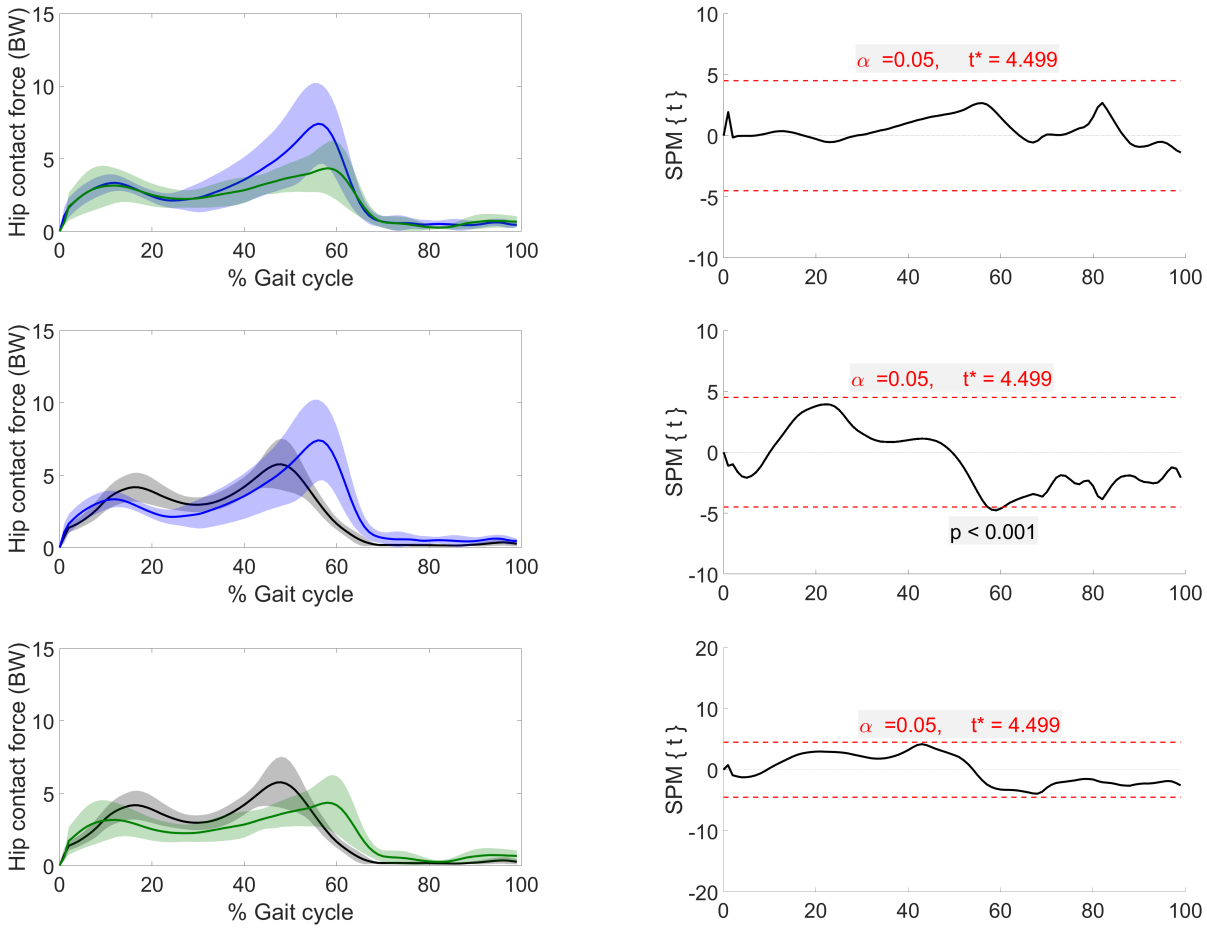


Figure 3.14: Left: Hip contact forces. Right: Statistical parametric mapping results. BTF Sidekicks - green. BTF Genium - blue. AB - black.

Biomechanical parameter	BTF Sidekicks Mean ± SD	BTF Genium Mean ± SD	AB Mean ± SD
First peak HJCF (BW)	3.46 ± 1.22	3.47 ± 0.58	4.31 ± 0.97
Second peak HJCF (BW)	4.91 ± 1.67 ***p=.017**	8.40 ± 2.75	5.88 ± 1.73
Normalised second peak HJCF (BW/(m/s))	5.67 ± 1.47	7.07 ± 1.87 ****p=.023**	4.66 ± 1.16
First peak HJCF SI (%)	85.56 ± 10.56	88.79 ± 5.67	92.24 ± 4.49
Second peak HJCF SI (%)	85.48 ± 4.20	87.20 ± 6.10	89.33 ± 6.70
HJCF impulse (BW.s)	267.95 ± 43.97	330.46 ± 70.90	292.15 ± 61.15
Normalised HJCF impulse (BW.s/m)	264.38 ± 27.07 ****p=.017**	232.02 ± 45.86	204.30 ± 34.25

Table 3.16: Hip joint contact forces (HJCF) and impulse.
SI, symmetry index, 100% indicates perfect symmetry. *Statistically significant differences from BTF Genium ($p<.05$). **Statistically significant differences from AB ($p<.05$).

Table 3.17 shows the calculated peak muscle forces, Table 3.18 shows the muscle force impulse and Table 3.19 shows the muscle force impulse normalised to walked distance. The peak adductor brevis ($p=.005$), adductor longus ($p=.002$) and pectineus ($p=.007$) muscle forces were larger for BTF Genium than BTF Sidekicks. Additionally, the adductor longus force impulse was larger for BTF Genium by 13.6 BW.s compared to 14.3 BW.s for BTF Sidekicks ($p=.020$). The muscle force impulse normalised by distance was not significantly different between the amputee groups.

Peak muscle force (BW)	BTF Sidekicks Mean ± SD *Median [95% CI]*	BTF Genium Mean ± SD *Median [95% CI]*
Adductor brevis	0.34 ± 0.20 ***p=.005**	0.72 ± 0.23
Adductor longus	0.53 ± 0.35 ***p=.002**	1.35 ± 0.47
Adductor magnus	0.21 ± 0.13	0.21 ± 0.12
Biceps femoris	0.34 ± 0.31	0.30 ± 0.14
Gluteus maximus	0.78 ± 0.34	0.80 ± 0.26
Gluteus medius	1.28 ± 0.58	1.97 ± 0.66
Gluteus minimus	0.28 ± 0.11	0.37 ± 0.14
Gracilis	*0.02 [0.01-0.04]*	*0.02 [0.01-0.16]*
Iliacus	0.92 ± 0.43	1.44 ± 0.68
Pectineus	0.12 ± 0.06 ***p=.007**	0.25 ± 0.10
Psoas	1.06 ± 0.51	1.65 ± 0.69
Rectus femoris	0.24 ± 0.12	0.34 ± 0.14
Sartorius	0.11 ± 0.06	0.17 ± 0.05
Tensor fascia latae	0.29 ± 0.16	0.37 ± 0.17

Table 3.17: Muscle forces.
CI, confidence interval. *Statistically significant differences from BTF Genium ($p<.05$).

Muscle force impulse (BW.s)	BTF Sidekicks Mean ± SD *Median [95% CI]*	BTF Genium Mean ± SD *Median [95% CI]*
Adductor brevis	11.11 ± 8.71	14.82 ± 5.48
Adductor longus	14.27 ± 8.94 ***p=.020**	27.88 ± 10.47
Adductor magnus	6.24 ± 4.34	6.20 ± 4.38
Biceps femoris	10.53 ± 9.98	8.98 ± 4.52
Gluteus maximus	22.42 ± 8.24	30.68 ± 11.08
Gluteus medius	60.61 ± 28.71	87.40 ± 28.34
Gluteus minimus	11.28 ± 3.85	13.27 ± 4.37
Gracilis	*0.57 [0.23-0.80]*	*0.44 [0.95-1.94]*
Iliacus	27.45 ± 12.67	33.92 ± 14.94
Pectineus	3.45 ± 1.86	5.67 ± 2.03
Psoas	32.58 ± 17.47	38.35 ± 13.45
Rectus femoris	7.10 ± 3.49	8.82 ± 3.61
Sartorius	2.14 ± 1.14	3.44 ± 1.27
Tensor fascia latae	9.71 ± 6.29	9.78 ± 4.31

Table 3.18: Muscle force impulse.
CI, confidence interval. *Statistically significant differences from BTF Genium ($p<.05$).

Normalised muscle force impulse (BW.s/m)	BTF Sidekicks Mean ± SD *Median [95% CI]*	BTF Genium Mean ± SD *Median [95% CI]*
Adductor brevis	10.89 ± 7.97	10.32 ± 3.37
Adductor longus	14.25 ± 8.84	19.46 ± 6.86
Adductor magnus	6.58 ± 5.03	4.48 ± 3.49
Biceps femoris	10.73 ± 10.40	6.39 ± 3.45
Gluteus maximus	22.58 ± 8.97	21.89 ± 8.79
Gluteus medius	58.90 ± 25.66	61.07 ± 19.24
Gluteus minimus	11.02 ± 3.45	9.25 ± 2.78
Gracilis	*0.52 [0.21-0.86]*	*0.31 [0.07-1.36]*
Iliacus	26.76 ± 11.89	23.63 ± 9.95
Pectineus	3.45 ± 1.84	3.99 ± 1.44
Psoas	31.55 ± 16.28	26.67 ± 8.41
Rectus femoris	6.81 ± 3.10	6.13 ± 2.36
Sartorius	2.05 ± 0.98	2.41 ± 0.89
Tensor fascia latae	9.35 ± 5.92	6.82 ± 2.87

Table 3.19: Normalised muscle force impulse.
CI, confidence interval.

Summary of key results for prosthesis type

- BTF Genium achieved similar stride lengths, walking speeds and cadence to AB.
- BTF Genium showed higher stride lengths by 0.4 m and higher walking speeds by 0.3 m/s than BTF Sidekicks.
- BTF Sidekicks and BTF Genium showed larger step widths by 0.2 m and 0.1 m, respectively, than AB.
- BTF Sidekicks showed larger hip abduction angles in swing than BTF Genium.
- BTF Genium showed larger hip extension angles by 11.4° than BTF Sidekicks and by 11.1° than AB.
- BTF Genium showed larger peak hip flexion moments at the push-off phase of the gait cycle by 0.8 Nm/kg than BTF Sidekicks and AB.
- BTF Genium showed larger hip power at the push-off phase of the gait cycle by 1.9 W/kg than BTF Sidekicks and AB.
- BTF Genium showed larger second peak of the hip joint contact force by 3.5 BW than BTF Sidekicks and by 2.5 BW than AB.
- BTF Sidekicks showed similar hip loading profiles to AB during one gait cycle.
- BTF Sidekicks presented larger hip impulse normalised to walked distance by 60.1 BW.s/m than AB.

3.4.2 Comparison between stubbies and full-length prostheses for amputees who could use both

This section compares the biomechanical data between Sidekicks and Genium for amputees who can walk with both types of prostheses. Cohort 1 (n=4) represents the study participants able to walk with both Genium and Sidekicks stubby prostheses. Cohort 1_Sidekicks indicates Cohort 1 when walking with Sidekicks stubbies, and Cohort 1_Genium indicates Cohort 1 when walking with Genium prosthetic knees.

Table 3.20 presents the leg length details for Cohort 1. The leg length of Cohort 1 was lower when fitted with Sidekicks by 0.3 m (p=.001) than full-length articulated prostheses.

Biomechanical parameter	Cohort 1_Sidekicks Mean ± SD	Cohort 1_Genium Mean ± SD
Leg length	0.61 ± 0.05 ***p=.001**	0.90 ± 0.04

Table 3.20: Leg length details of Cohort 1.
*Statistically significant differences between prostheses (p<.05).

Table 3.21 presents the calculated temporospatial parameters for Cohort 1 when walking with Sidekicks and Genium. The repeated trials showed lower stride lengths by 0.5 m (p=.001) with Sidekicks than Genium. Whilst the walking speed was lower by 0.3 m/s (1.1 km/h) with Sidekicks (p=.009), cadence was higher by 12.6 steps/min when walking with Sidekicks (p=.037).

Biomechanical parameter	Cohort 1_Sidekicks Mean ± SD	Cohort 1_Genium Mean ± SD
Step width (m)	0.23 ± 0.03	0.22 ± 0.03
Step length (m)	0.52 ± 0.05 ***p=.011**	0.72 ± 0.05
Stride length (m)	0.96 ± 0.13 ***p=.001**	1.46 ± 0.07
Cadence (steps/min)	114.74 ± 3.90 ***p=.037**	102.17 ± 2.48
Walking speed (m/s)	0.93 ± 0.10 ***p=.009**	1.22 ± 0.06
Gait SI (%)	97.85 ± 0.38	96.71 ± 2.03
Stance time (% cycle)	61.56 ± 1.19 ***p=.044**	64.35 ± 1.42

Table 3.21: Temporospatial measures of Cohort 1.
SI, symmetry index. *Statistically significant differences between prostheses (p<.05).

Figure 3.15 shows the ankle joint angles over the course of the gait cycle. The paired comparison showed higher ankle dorsiflexion angles when walking with Genium prosthetic knees (fitted with dynamic response feet) than Sidekicks. The peak ankle dorsiflexion angles were lower with stubbies by 6.9° from 9.9° with dynamic response prosthetic feet (p=.016, Table 3.22).

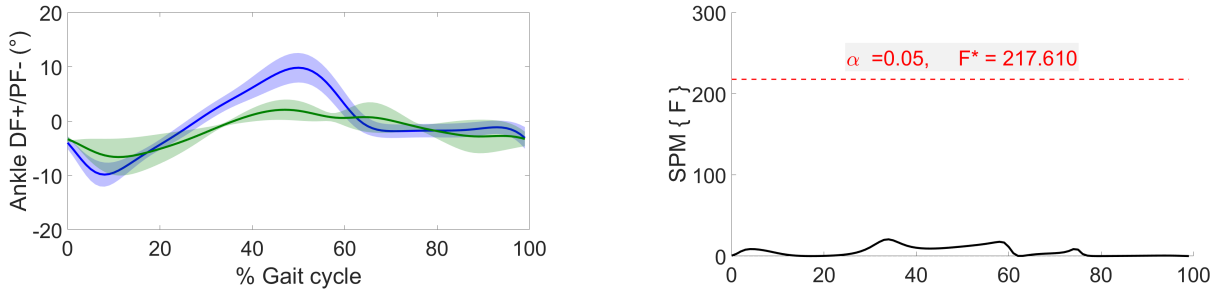


Figure 3.15: Left: Ankle dorsiflexion (DF)/plantar flexion (PF). Right: Statistical parametric mapping results. Cohort 1_Sidekicks - green. Cohort 1_Genium - blue.

Biomechanical parameter	Cohort 1_Sidekicks Mean ± SD	Cohort 1_Genium Mean ± SD
Peak ankle dorsiflexion (°)	3.03 ± 1.47 ***p=.016**	9.89 ± 2.68
Peak ankle plantar flexion (°)	8.22 ± 0.88	9.93 ± 2.22
Ankle dorsiflexion/ plantar flexion (ROM) °	11.26 ± 1.89 ***p=.020**	19.82 ± 1.54

Table 3.22: Sagittal plane ankle kinematics of Cohort 1.
ROM, range of motion. *Statistically significant differences between prostheses (p<.05).

Figure 3.16 and Table 3.23 show the hip joint angles in the coronal, sagittal and transverse plane over the course of the gait cycle. Cohort 1 showed higher hip abduction angles in swing when walking with Sidekicks compared to Genium. The peak hip extension angle was smaller at the end of stance by 10.1° with Sidekicks than Genium. The transverse plane hip rotation profiles were similar between prostheses.

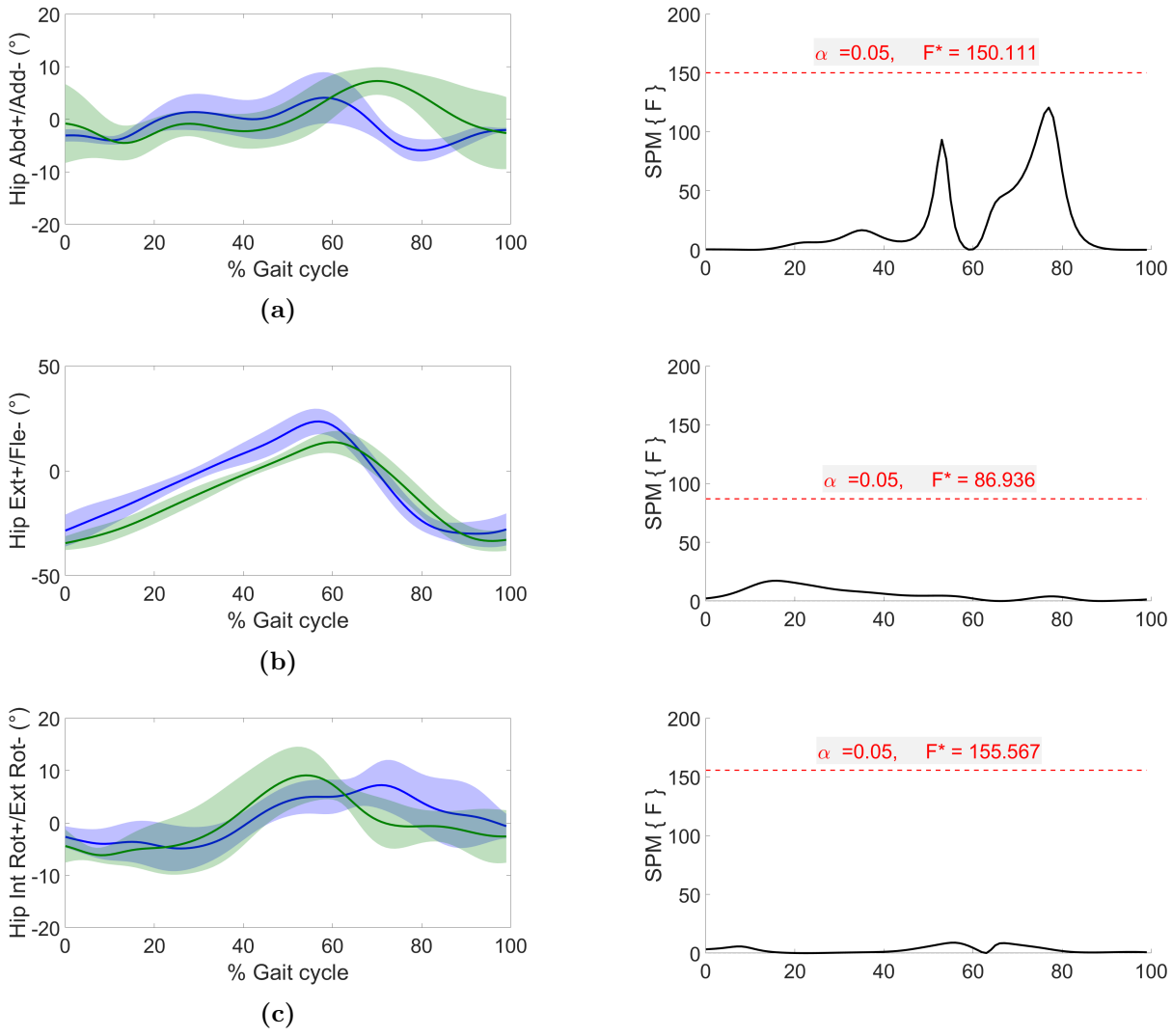


Figure 3.16: Left: Hip joint angles (a) Hip abduction (Abd)/adduction (Add). (b) Hip extension (Ext)/flexion (Fle). (c) Hip internal (Int)/external (Ext) rotation (Rot). Right: Statistical parametric mapping results. Cohort 1_Sidekicks - green. Cohort 1_Genium - blue.

Biomechanical parameter	Cohort 1_Sidekicks Mean ± SD *Median [95% CI]*	Cohort 1_Genium Mean (SD) *Median [95% CI]*
Peak hip adduction (°)	7.95 ± 2.76	6.79 ± 1.60
Peak hip abduction (°)	9.90 ± 1.63	5.11 ± 3.74
Hip adduction/ abduction ROM (°)	17.85 ± 4.13	11.90 ± 5.03
Peak hip extension (°)	13.81 ± 5.23	23.94 ± 5.92
Peak hip flexion (°)	*38.05 [28.70-43.11]*	*30.48 [19.24-42.95]*
Hip extension/flexion ROM (°)	49.71 ± 5.63	55.03 ± 5.83
Hip internal/external rotation ROM (°)	17.72 ± 3.90	16.49 ± 2.34

Table 3.23: Hip kinematics of Cohort 1.
CI, confidence interval. ROM, range of motion.

Figure 3.17 shows the pelvic orientations in the coronal, sagittal and transverse planes over the course of the gait cycle, and Table 3.24 shows the calculated P2P values. The repeated trials showed similar pelvic tilt and obliquity patterns between walking with Sidekicks and Genium. The transverse plane P2P pelvic rotation was larger when walking with Sidekicks by 8.2° compared to 13.3° when walking with Genium (p=.038).

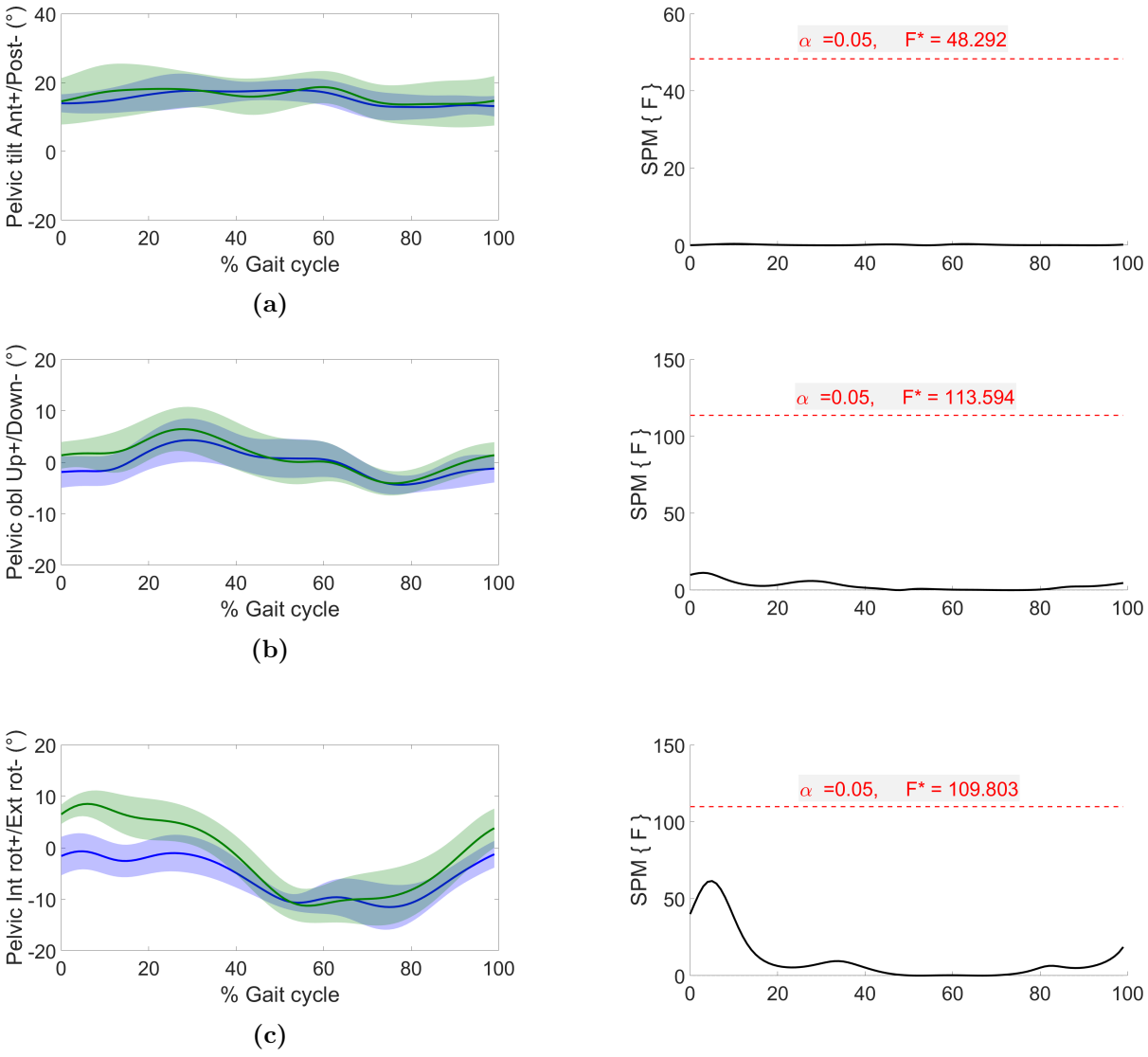


Figure 3.17: Left: Pelvic angles (a) Pelvic anterior (Ant)/posterior (Post) tilt. (b) Pelvic obliquity, where positive angles describe an increase in the vertical height of the contralateral hip. (c) Pelvic internal (Int)/external (Ext) rotation (Rot). Right: Statistical parametric mapping results. Cohort 1_Sidekicks - green. Cohort 1_Genium - blue.

Biomechanical parameter	Cohort 1_Sidekicks Mean ± SD	Cohort 1_Genium Mean ± SD
P2P pelvic tilt (°)	7.75 ± 1.88	7.56 ± 1.30
P2P pelvic obliquity (°)	10.84 ± 2.65	9.14 ± 3.17
P2P pelvic rotation (°)	21.49 ± 3.22 ***p=.038**	13.26 ± 3.51

Table 3.24: Pelvic kinematics of Cohort 1.
P2P, peak-to-peak. *Statistically significant differences between prostheses (p<.05).

Figure 3.18 and Table 3.25 show the ground reaction force (GRF) profiles, with no significant differences between prostheses.

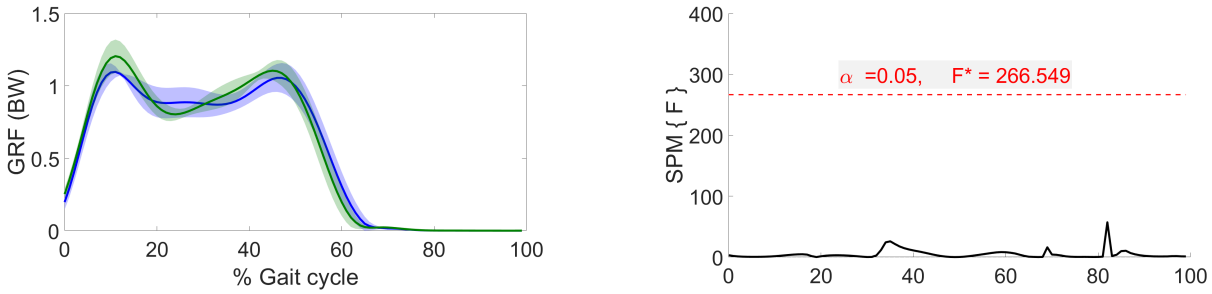


Figure 3.18: Left: Ground reaction forces (GRF). Right: Statistical parametric mapping results. Cohort 1_Sidekicks - green. Cohort 1_Genium - blue.

Biomechanical parameter	Cohort 1_Sidekicks Mean ± SD	Cohort 1_Genium Mean ± SD
Peak GRF (BW)	1.23 ± 0.09	1.15 ± 0.04

Table 3.25: Ground reaction forces (GRF) of Cohort 1.

Figure 3.19 and Table 3.26 show the coronal, sagittal plane hip joint moments and power. Cohort 1 showed larger peak hip flexion moments by 1.0 Nm/kg (p=.002) and larger peak generated hip joint power at push-off by 1.9 W/kg with Genium than Sidekicks. Additionally, the peak hip absorbed power was higher by 0.9 W/kg with Genium than Sidekicks (p=.005).

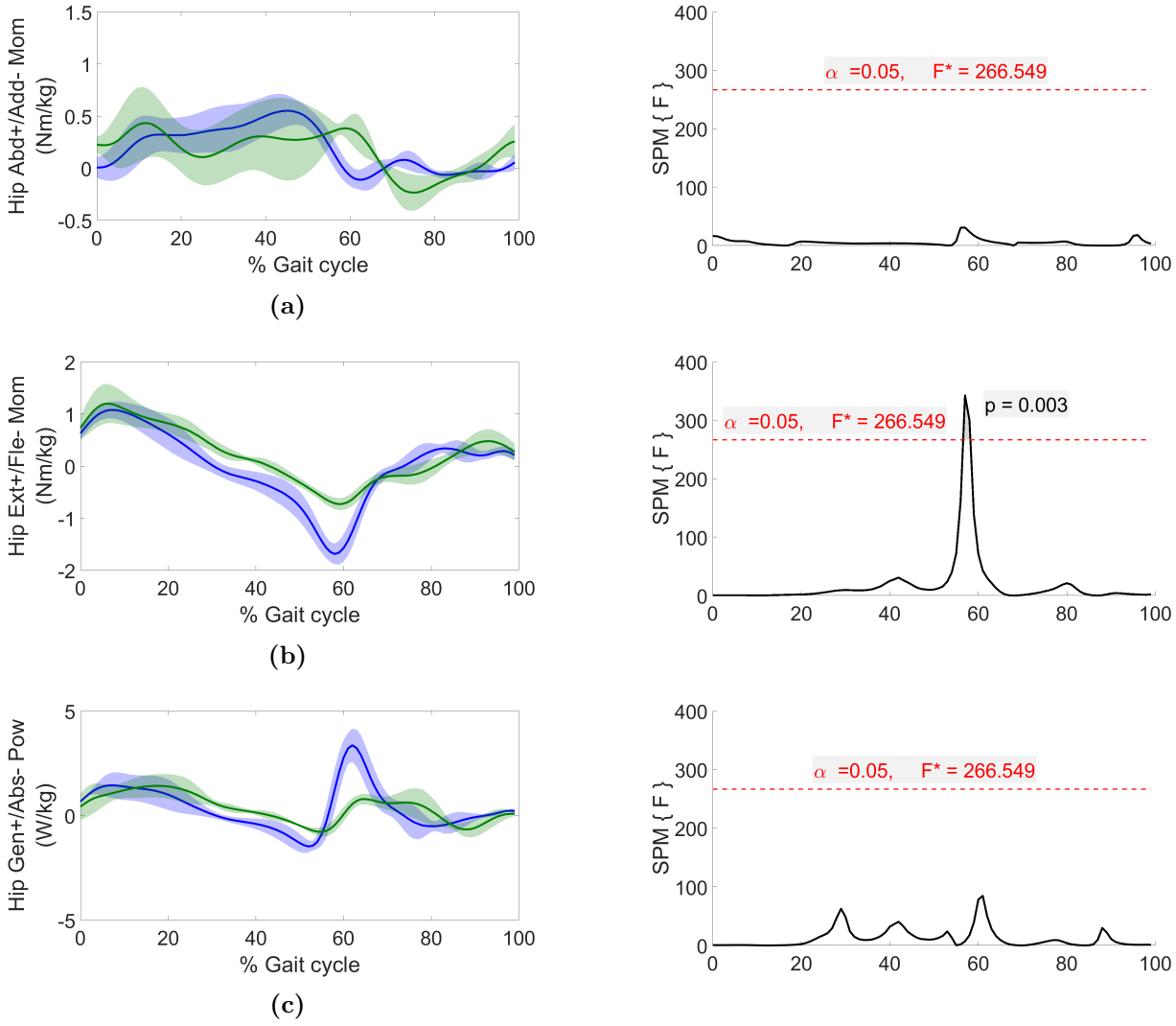


Figure 3.19: Left: Hip joint moments and power (a) Abduction (Abd)/ adduction (Add) hip moments (Mom). (b) Extension (Ext)/flexion (Fle) hip moments (Mom). (c) Generated (Gen)/absorbed (Abs) hip joint power (Pow). Right: Statistical parametric mapping results. Cohort 1_Sidekicks - green. Cohort 1_Genium - blue.

Biomechanical parameter	Cohort 1_Sidekicks Mean ± SD	Cohort 1_Genium Mean ± SD
Peak hip adduction moment (Nm/kg)	0.32 ± 0.21	0.16 ± 0.07
Peak hip abduction moment (Nm/kg)	0.65 ± 0.20	0.59 ± 0.13
Peak hip extension moment (Nm/kg)	1.24 ± 0.39	1.11 ± 0.17
Peak hip flexion moment (Nm/kg)	0.75 ± 0.12 ***p=.002**	1.78 ± 0.27
Peak hip generated power (W/kg)	1.69 ± 0.50	3.62 ± 0.83
Peak hip absorbed power (W/kg)	0.93 ± 0.30 ***p=.005**	1.79 ± 0.32

Table 3.26: Hip moments and power of Cohort 1.
*Statistically significant differences between prostheses (p<.05).

The hip joint contact force (HJCF) profiles of Cohort 1 with Sidekicks and Genium are shown in Figure 3.20. SPM reported lower HJCF at push-off and in swing with Sidekicks than Genium (p<.001). When comparing discrete values in Table 3.27, the HJCF second peak was lower with Sidekicks by 3.8 BW than Genium (9.1 BW, p=.011).

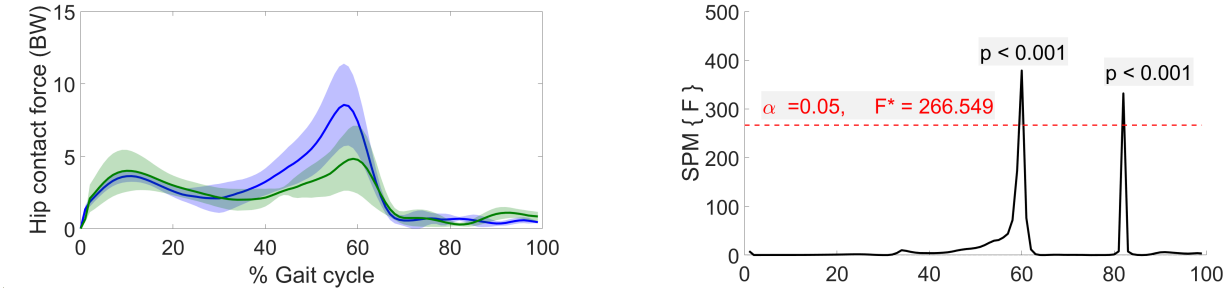


Figure 3.20: Left: Hip joint contact forces. Right: Statistical parametric mapping results. Cohort 1_Sidekicks - green. Cohort 1_Genium - blue.

Biomechanical parameter	Cohort 1_Sidekicks Mean ± SD	Cohort 1_Genium Mean ± SD
First peak HJCF (BW)	4.06 ± 1.45	3.67 ± 0.37
Second peak HJCF (BW)	5.25 ± 2.15 ***p=.011**	9.07 ± 2.87
Normalised second peak HJCF (BW/(m/s))	5.58 ± 1.98	7.35 ± 2.03
First peak HJCF SI (%)	81.11 ± 12.61	85.45 ± 5.79
Second peak HJCF SI (%)	83.11 ± 2.83	87.70 ± 3.30
HJCF impulse (BW.s)	263.68 ± 58.61	350.41 ± 61.43
Normalised HJCF impulse (BW.s/m)	272.63 ± 30.52	239.36 ± 34.70

Table 3.27: Hip joint contact forces (HJCF) and impulse of Cohort 1.
SI, symmetry index. *Statistically significant differences between prostheses (p<.05).

Tables 3.28, 3.29 and 3.30 show the calculated peak muscle forces, impulse and impulse normalised to distance, respectively, for Cohort 1 with Sidekicks and Genium. Compared to Sidekicks, walking with Genium showed larger peak muscle forces for adductor brevis (p=.003), adductor longus (p=.001), gluteus minimus (p=.037), iliacus (p=.040) and pectineus (p=.014). Additionally, walking with Genium showed larger muscle force impulse for adductor longus (p=.023), gluteus minimus (p=.031), iliacus (p=.022), pectineus (p=.012), psoas (p=.046), rectus femoris (p=.021), sartorius (p=.046) and tensor fascia latae (p=.026).

Peak muscle force (BW)	Cohort 1_Sidekicks Mean ± SD *Median [95% CI]*	Cohort 1_Genium Mean ± SD *Median [95% CI]*
Adductor brevis	0.34 ± 0.16 ***p=.003**	0.82 ± 0.23
Adductor longus	0.70 ± 0.32 ***p=.001**	1.50 ± 0.40
Adductor magnus	0.24 ± 0.06	0.17 ± 0.05
Biceps femoris	*0.25 [0.21-1.11]*	*0.32 [0.14-0.57]*
Gluteus maximus	0.89 ± 0.36	0.76 ± 0.22
Gluteus medius	*1.71 [0.43-2.55]*	*1.72 [1.07-2.93]*
Gluteus minimus	0.29 ± 0.15 ***p=.037**	0.41 ± 0.14
Gracilis	*0.02 [0.002-0.05]*	*0.02 [0.001-0.29]*
Iliacus	0.99 ± 0.57 ***p=.040**	1.59 ± 0.71
Pectineus	0.12 ± 0.07 ***p=.014**	0.25 ± 0.11
Psoas	1.03 ± 0.67	1.84 ± 0.86
Rectus femoris	0.25 ± 0.14	0.38 ± 0.14
Sartorius	0.11 ± 0.08	0.18 ± 0.04
Tensor fascia latae	0.28 ± 0.21	0.38 ± 0.19

Table 3.28: Muscle forces of Cohort 1.
CI, confidence interval. *Statistically significant differences between prostheses (p<.05).

Muscle force impulse (BW.s)	Cohort 1_Sidekicks Mean ± SD *Median [95% CI]*	Cohort 1_Genium Mean ± SD *Median [95% CI]*
Adductor brevis	*9.99 [3.62-15.13]*	*13.44 [5.61-27.78]*
Adductor longus	18.28 ± 7.68 ***p=.023**	30.79 ± 9.16
Adductor magnus	8.38 ± 3.21	5.26 ± 1.95
Biceps femoris	*10.88 [3.08-35.93]*	*11.02 [7.69-14.53]*
Gluteus maximus	26.33 ± 7.02	28.58 ± 10.20
Gluteus medius	63.69 ± 29.28	95.87 ± 15.49
Gluteus minimus	9.93 ± 3.74 ***p=.031**	15.32 ± 2.60
Gracilis	*0.80 [0.32-1.09]*	*0.44 [0.01-3.23]*
Iliacus	19.51 ± 11.14 ***p=.022**	35.71 ± 13.13
Pectineus	3.01 ± 1.90 ***p=.012**	5.31 ± 1.24
Psoas	19.60 ± 11.51 ***p=.046**	40.29 ± 15.15
Rectus femoris	4.49 ± 2.67 ***p=.021**	9.34 ± 3.14
Sartorius	1.54 ± 0.87 ***p=.046**	3.23 ± 0.27
Tensor fascia latae	5.14 ± 3.47 ***p=.026**	9.68 ± 4.25

Table 3.29: Muscle force impulse of Cohort 1.
CI, confidence interval. *Statistically significant differences between prostheses ($p<.05$).

Normalised muscle force impulse (BW.s/m)	Cohort 1_Sidekicks Mean ± SD *Median [95% CI]*	Cohort 1_Genium Mean ± SD *Median [95% CI]*
Adductor brevis	*11.38 [4.47-15.24]*	*9.31 [4.78-17.87]*
Adductor longus	*22.83 [5.69-32.74]*	*20.04 [10.86-31.10]*
Adductor magnus	9.32 ± 4.46	3.61 ± 1.36
Biceps femoris	*11.60 [2.69-37.13]*	*7.79 [4.95-10.33]*
Gluteus maximus	27.98 ± 7.43	19.77 ± 7.61
Gluteus medius	64.19 ± 25.00	65.63 ± 9.62
Gluteus minimus	10.11 ± 3.18	10.47 ± 1.52
Gracilis	*0.78 [0.24-1.32]*	*0.31 [0.07-2.23]*
Iliacus	19.80 ± 9.80	24.23 ± 7.92
Pectineus	3.23 ± 2.01	3.65 ± 0.87
Psoas	20.02 ± 11.23	27.28 ± 9.18
Rectus femoris	4.48 ± 2.27	6.34 ± 1.84
Sartorius	1.55 ± 0.81	2.22 ± 0.15
Tensor fascia latae	5.12 ± 3.18	6.55 ± 2.60

Table 3.30: Muscle force impulse normalised by walked distance of Cohort 1. CI, confidence interval.

Summary of key results for amputees who could use both prostheses

- The leg lengths were shorter with Sidekicks by 0.3 m than full-length articulated prostheses.
- The step length, stride length and walking speed were lower with Sidekicks by 0.2 m, 0.5 m and 0.3 m/s, respectively, than Genium.
- Cadence was higher with Sidekicks by 12.6 steps/min than Genium.
- The pelvic tilt and obliquity angles were similar between prostheses.
- The P2P pelvic internal/external rotation was larger with Sidekicks by 8.2° than Genium.
- The hip flexion moment at the push-off phase of the gait cycle was larger with Genium by 1.0 Nm/kg than Sidekicks.
- The second peak of the hip joint contact force was larger with Genium by 3.8 BW than Sidekicks.
- When walking with Genium, amputees showed larger muscle forces for adductor brevis (by 0.5 BW), adductor longus (by 0.8 BW), gluteus minimus (by 0.1 BW), iliacus (by 0.6 BW) and pectineus (by 0.1 BW) than Sidekicks.

- When walking with Genium, amputees showed larger muscle force impulse for adductor longus (by 12.5 BW.s), gluteus minimus (by 5.4 BW.s), iliacus (by 16.2 BW.s), pectineus (by 2.3 BW.s), psoas (by 20.7 BW.s), rectus femoris (by 4.9 BW.s), sartorius (by 1.7 BW.s) and tensor fascia latae (by 4.5 BW.s) than Sidekicks.

3.4.3 Stubby prostheses analysis

This section compares the biomechanical data with Sidekicks prostheses of amputees who can walk with both types of prostheses and amputees who can only walk with Sidekicks. Cohort 1_Sidekicks indicates Cohort 1 walking with Sidekicks (n=4), and Cohort 2 indicates Sidekicks-only users (n=4). The leg lengths of the study participants in Cohort 2 were larger than those of Cohort 1_Sidekicks by 0.25 m (p=.002, Table 3.32).

Biomechanical parameter	Cohort 1_Sidekicks Mean ± SD	Cohort 2 Mean ± SD
Leg length (m)	0.61 ± 0.05 ***p=.002**	0.86 ± 0.07

Table 3.31: Leg length details of stubby prostheses users.
*Statistically significant differences between cohorts (p<.05).

Table 3.32 presents the temporospatial parameters for stubbies users. The step and stride length were similar between groups. Cohort 2 walked with lower cadence by 23.5 steps/min than Cohort 1_Sidekicks (p=.007).

Biomechanical parameter	Cohort 1_Sidekicks Mean ± SD	Cohort 2 Mean ± SD
Step width (m)	0.23 ± 0.03	0.30 ± 0.06
Step length (m)	0.52 ± 0.05	0.54 ± 0.02
Stride length (m)	0.96 ± 0.13	1.07 ± 0.05
Cadence (steps/min)	114.74 ± 3.90 ***p=.007**	91.23 ± 9.33
Walking speed (m/s)	0.93 ± 0.10	0.79 ± 0.11

Table 3.32: Temporospatial characteristics of stubby prostheses users.
*Statistically significant differences between cohorts (p<.05).

Figure 3.21 and Table 3.33 show the ankle joint angles over the course of the gait cycle, with no significant differences between groups.

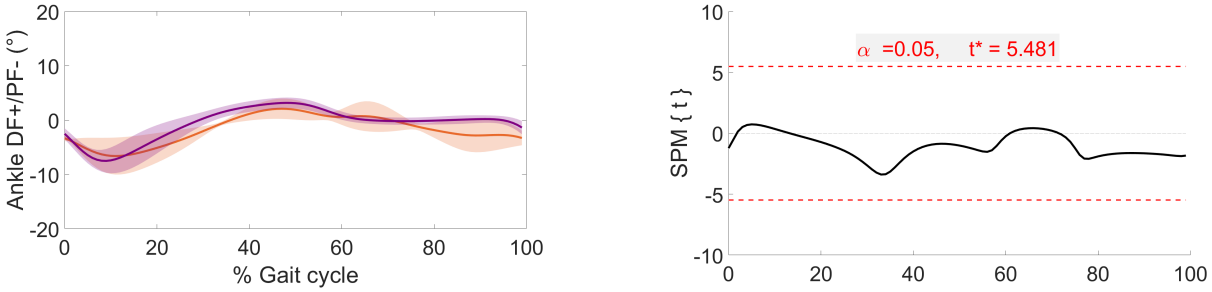


Figure 3.21: Left: Ankle dorsiflexion (DF)/plantar flexion (PF) angles. Right: Statistical parametric mapping results. Cohort 1_Sidekicks - orange. Cohort 2 - purple.

Biomechanical parameter	Cohort 1_Sidekicks Mean ± SD	Cohort 2 Mean ± SD
Peak ankle dorsiflexion (°)	3.03 ± 1.47	3.28 ± 0.93
Peak ankle plantar flexion (°)	8.22 ± 0.88	7.67 ± 2.23
Ankle dorsiflexion/ plantar flexion ROM (°)	11.26 ± 1.89	10.95 ± 1.88

Table 3.33: Sagittal plane ankle kinematics of stubby prostheses users. ROM, range of motion.

Figure 3.22 shows the hip joint angles over the course of the gait cycle. Cohort 1_Sidekicks and Cohort 2 showed similar hip movement profiles in the coronal plane. SPM reported lower hip flexion angles for Cohort 2 than Cohort 1_Sidekicks at the start and end of the gait cycle (p=.014). When comparing discrete values in Table 3.34, Cohort 2 presented lower peak hip flexion angles by 16.1° compared to 35.9° for Cohort 1_Sidekicks (p=.006).

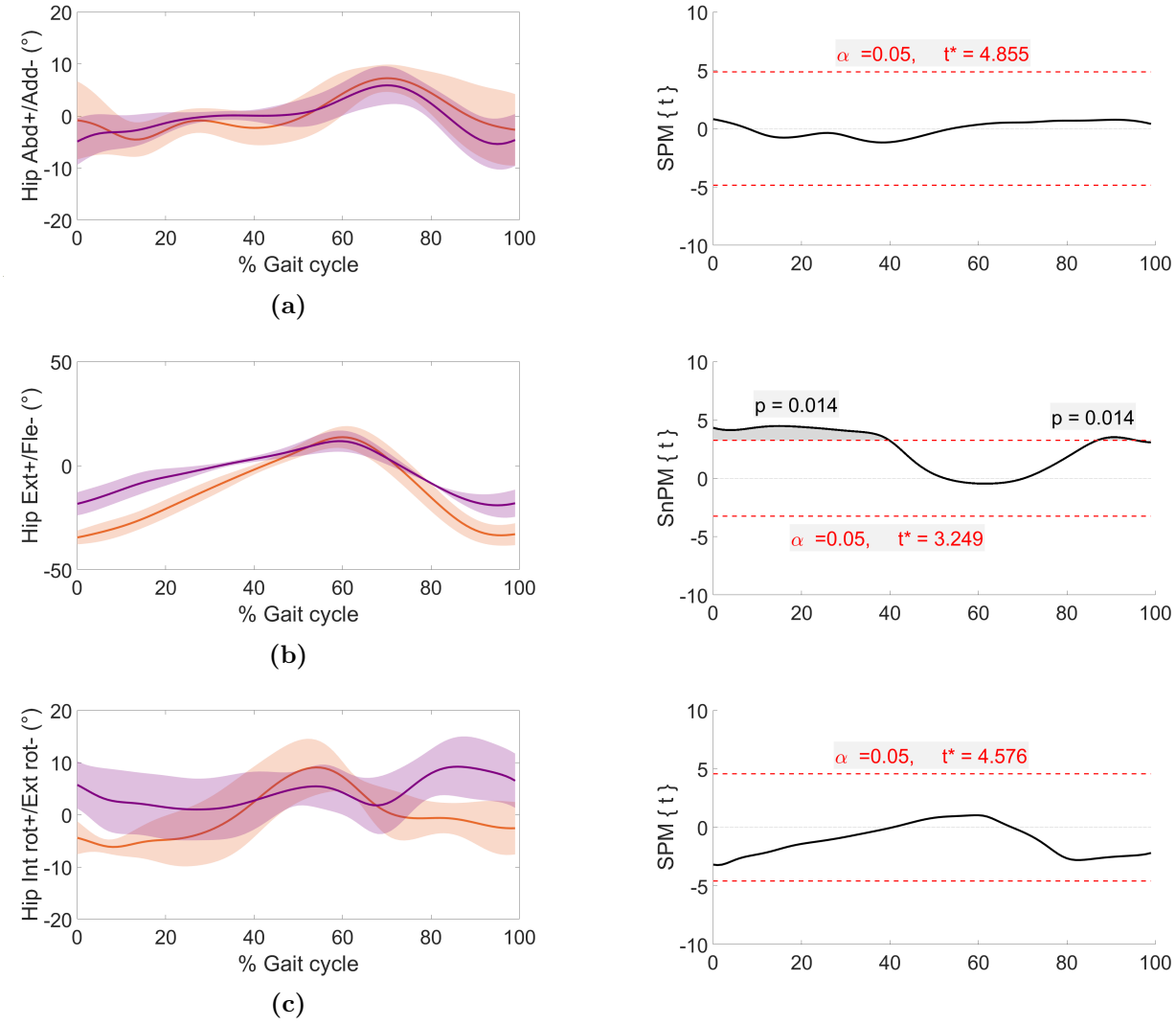


Figure 3.22: Left: Hip joint angles (a) Hip abduction (Abd)/adduction (Add). (b) Hip extension (Ext)/flexion (Fle). (c) Hip internal (Int)/external (Ext) rotation (Rot). Right: Statistical parametric mapping results. Cohort 1_Sidekicks - orange. Cohort 2 - purple.

Biomechanical parameter	Cohort 1_Sidekicks Mean ± SD *Median [95% CI]*	Cohort 2 Mean ± SD *Median [95% CI]*
Peak hip adduction (°)	*7.01 [2.87-13.03]*	*9.69 [0.14-15.06]*
Peak hip abduction (°)	9.90 ± 1.63	7.26 ± 2.76
Hip adduction/ abduction ROM (°)	17.85 ± 4.13	14.72 ± 6.22
Peak hip extension (°)	13.81 ± 5.23	12.28 ± 4.83
Peak hip flexion (°)	35.90 ± 3.92 ***p=.006**	19.86 ± 5.61
Hip extension/ flexion ROM (°)	49.71 ± 5.63 ***p=.039**	31.96 ± 10.19
Hip internal/ external rotation ROM (°)	17.72 ± 3.90	13.62 ± 3.40

Table 3.34: Hip kinematics of stubby prostheses users.
CI, confidence interval. ROM, range of motion. *Statistically significant differences between cohorts (p<.05).

Figure 3.23 and Table 3.35 present the pelvic angles over the course of the gait cycle. Cohort 2 showed larger P2P anterior pelvic tilt by 8.0° compared to 7.8° for Cohort 1_Sidekicks. SPM reported larger pelvic obliquity angles for Cohort 2 than Cohort 1_Sidekicks in early stance (p=.029) and swing (p=.014). There were no significant differences in the pelvic rotation angles between cohorts.

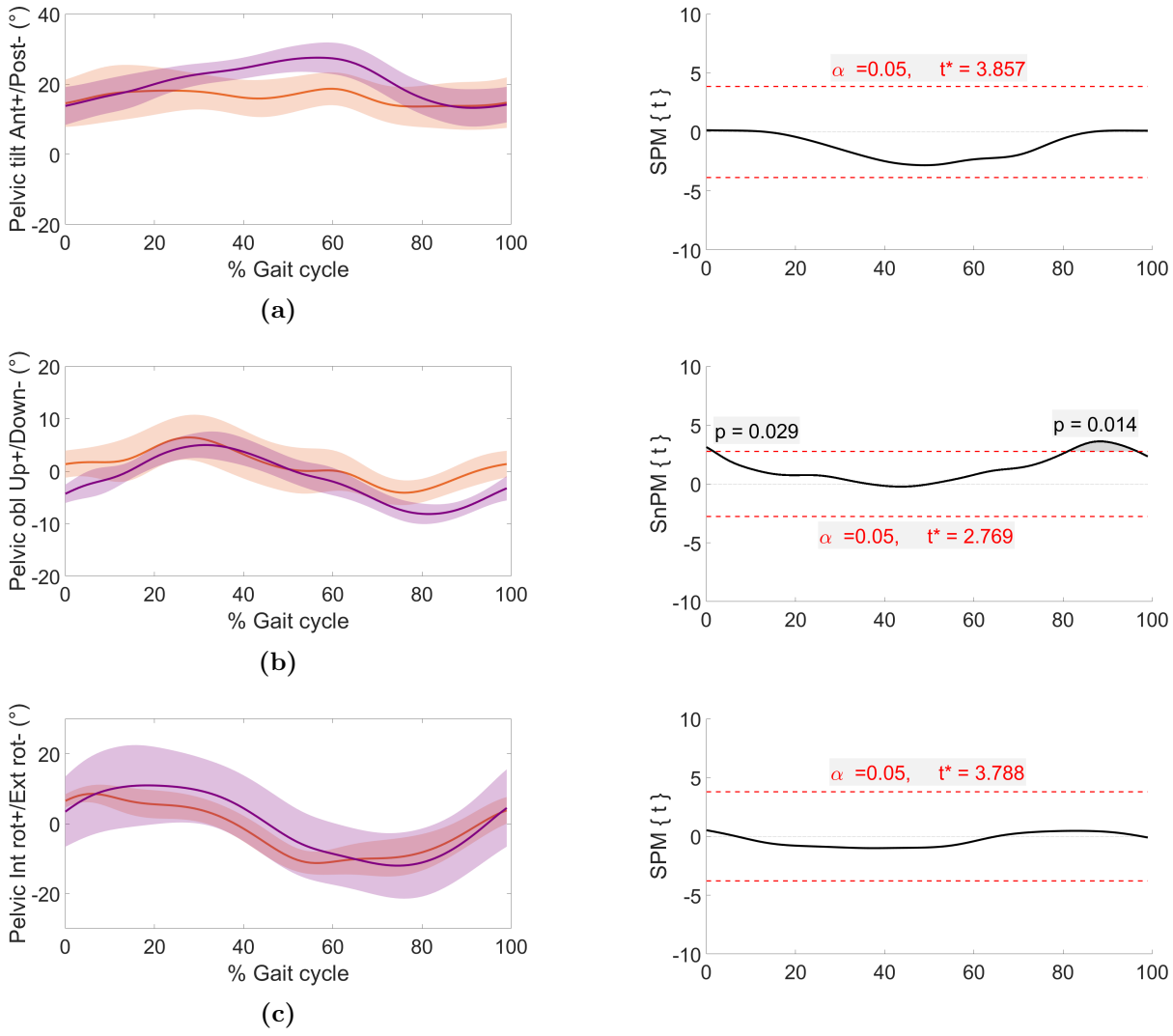


Figure 3.23: Left: Pelvic angles (a) Pelvic anterior (Ant)/posterior (Post) tilt angles. (b) Pelvic obliquity angles, where positive angles describe an increase in the vertical height of the contralateral hip. (c) Pelvic internal (Int)/external (Ext) rotation (Rot) angles. Right: Statistical parametric mapping results. Cohort 1_Sidekicks - orange. Cohort 2 - purple.

Biomechanical parameter	Cohort 1_Sidekicks Mean ± SD	Cohort 2 Mean ± SD
P2P pelvic tilt (°)	7.75 ± 1.88	15.79 ± 6.46
P2P pelvic obliquity (°)	10.84 ± 2.65	13.49 ± 1.63
P2P pelvic rotation (°)	21.49 ± 3.22	24.40 ± 5.84

Table 3.35: Pelvic kinematics of stubby prostheses users. P2P, peak-to-peak.

Figure 3.24 shows the ground reaction force (GRF) profiles over the course of the gait cycle. SPM did not report any significant differences between cohorts. When comparing discrete values in Table 3.36, Cohort 2 showed lower peak GRF by 0.2 BW than Cohort 1_Sidekicks (1.2 BW, p=.018).

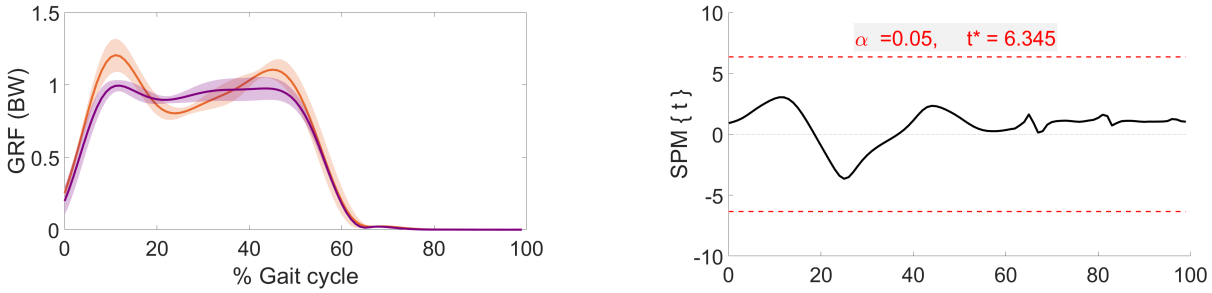


Figure 3.24: Left: Ground reaction forces (GRF). Right: Statistical parametric mapping results. Cohort 1_Sidekicks - orange. Cohort 2 - purple.

Biomechanical parameter	Cohort 1_Sidekicks Mean ± SD	Cohort 2 Mean ± SD
Peak GRF (BW)	1.23 ± 0.09 ***p=.018**	1.04 ± 0.06

Table 3.36: Ground reaction forces (GRF) of stubby prostheses users. *Statistically significant differences between cohorts (p<.05).

Figure 3.25 shows the coronal and sagittal plane hip joint moments and power. There were no significant differences in the coronal plane hip moments between cohorts. SPM reported lower hip extension moments (p=.014) and generated power (p=.005) in stance for Cohort 2 than Cohort 1_Sidekicks. When comparing discrete values in Table 3.37, Cohort 2 showed lower hip extension moments by 0.6 Nm/kg (p=.034) and hip joint generated power by 1.0 W/kg than Cohort 1_Sidekicks (p=.032).

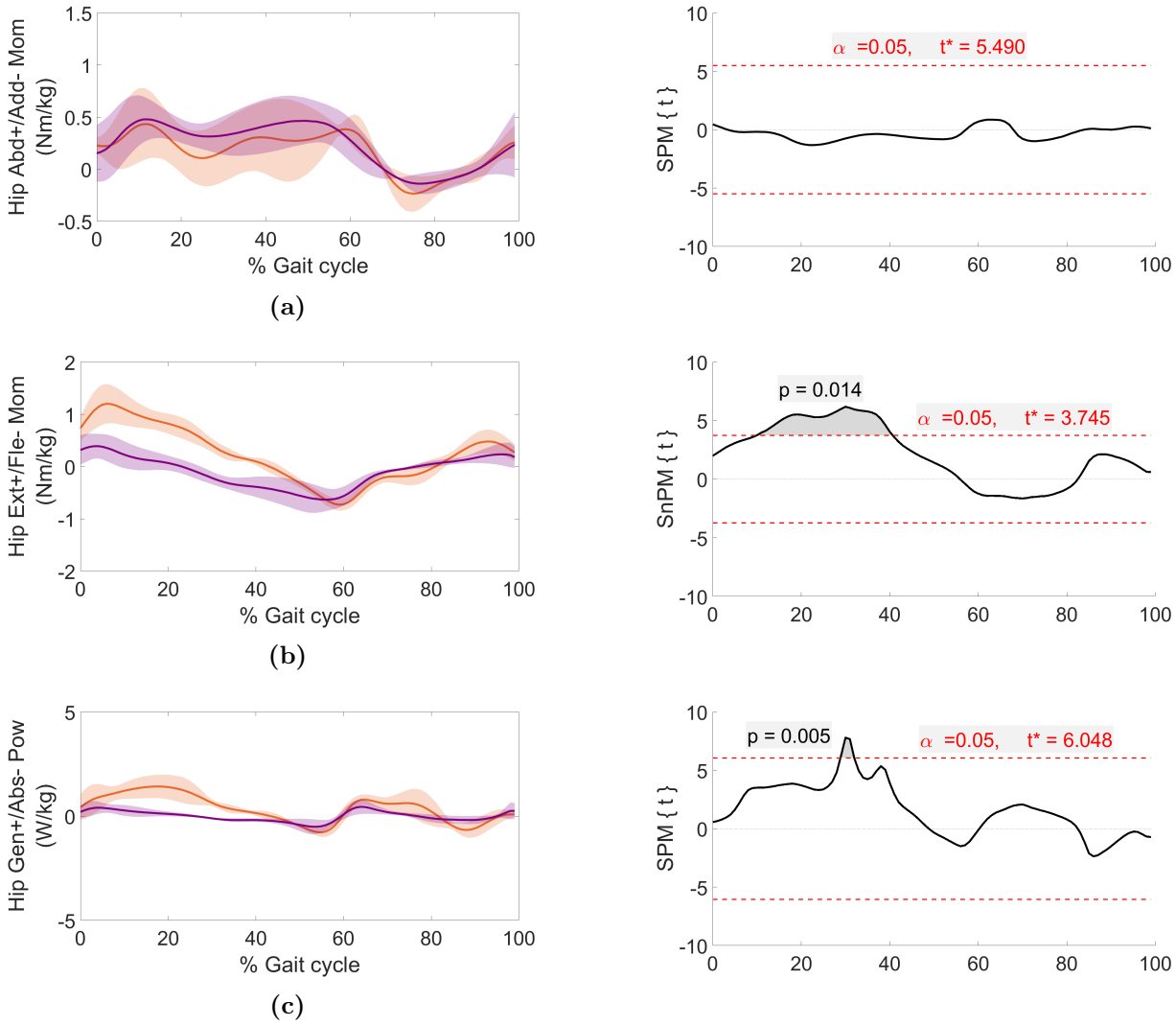


Figure 3.25: Left: Hip joint moments and power (a) Abduction (Abd)/ adduction (Add) hip moments (Mom). (b) Extension (Ext)/flexion (Fle) hip moments (Mom). (c) Generated (Gen)/absorbed (Abs) hip joint power (Pow). Right: Statistical parametric mapping results. Cohort 1_Sidekicks - orange. Cohort 2 - purple.

Biomechanical parameter	Cohort 1_Sidekicks Mean ± SD	Cohort 2 Mean ± SD
Peak hip adduction moment (Nm/kg)	0.32 ± 0.21	0.20 ± 0.06
Peak hip abduction moment (Nm/kg)	0.65 ± 0.20	0.62 ± 0.26
Peak hip extension moment (Nm/kg)	1.24 ± 0.39 ***p=.034**	0.62 ± 0.26
Peak hip flexion moment (Nm/kg)	0.75 ± 0.12	0.77 ± 0.20
Peak hip generated power (W/kg)	1.69 ± 0.50 ***p=.032**	0.68 ± 0.39
Peak hip absorbed power (W/kg)	0.93 ± 0.30	0.66 ± 0.30

Table 3.37: Hip moments and power of stubby prostheses users. *Statistically significant differences between cohorts (p<.05).

The hip joint contact force (HJCF) profiles and characteristics are shown in Figure 3.26 and Table 3.38, with no significant differences in hip loading between Cohort 1_Sidekicks and Cohort 2.

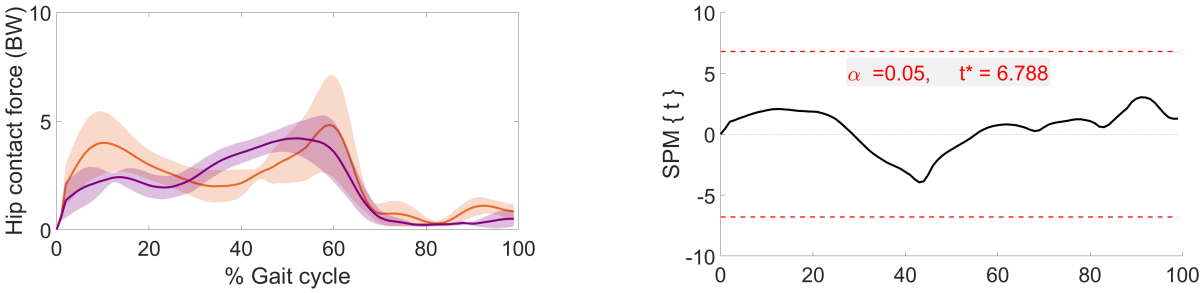


Figure 3.26: Left: Hip joint contact forces. Right: Statistical parametric mapping results. Cohort 1_Sidekicks - orange. Cohort 2 - purple.

Biomechanical parameter	Cohort 1_Sidekicks Mean ± SD	Cohort 2 Mean ± SD
First peak HJCF (BW)	4.06 ± 1.45	2.85 ± 0.38
Second peak HJCF (BW)	5.25 ± 2.15	4.57 ± 0.86
Normalised second peak HJCF (BW/(m/s))	5.58 ± 1.98	5.76 ± 0.60
First peak HJCF SI (%)	81.11 ± 12.61	90.02 ± 4.90
Second peak HJCF SI (%)	83.11 ± 2.83	87.86 ± 3.99
HJCF impulse (BW.s)	263.68 ± 58.61	272.22 ± 19.88
Normalised HJCF impulse (BW.s/m)	272.63 ± 30.52	256.13 ± 19.94

Table 3.38: Hip joint contact forces and impulse of stubby prostheses users. SI, symmetry index.

Tables 3.39, 3.40 and 3.41 show the calculated peak muscle forces, muscle force impulse and muscle force impulse normalised by walked distance. Compared to Cohort 1_Sidekicks, Cohort 2 showed larger muscle force impulse for psoas (p=.035), rectus femoris (p=.032) and tensor fascia latae (p=.041). Similarly, Cohort 2 presented larger psoas (p=.049), rectus femoris (p=.031) and tensor fascia latae (p=.047) normalised muscle force impulse than Cohort 1_Sidekicks. The biceps femoris normalised impulse was lower for Cohort 2 than Cohort 1_Sidekicks (p=.029).

Peak muscle force (BW)	Cohort 1_Sidekicks Mean ± SD *Median [95%]*	Cohort 2 Mean ± SD *Median [95%]*
Adductor brevis	0.34 ± 0.16	0.34 ± 0.23
Adductor longus	0.70 ± 0.32	0.35 ± 0.30
Adductor magnus	0.24 ± 0.06	0.18 ± 0.17
Biceps femoris	*0.25 [0.02-1.11]*	*0.22 [0.12-0.57]*
Gluteus maximus	0.89 ± 0.36	0.66 ± 0.28
Gluteus medius	1.49 ± 0.58	1.07 ± 0.50
Gluteus minimus	0.29 ± 0.15	0.27 ± 0.04
Gracilis	0.02 ± 0.01	0.02 ± 0.01
Iliacus	0.99 ± 0.57	0.84 ± 0.18
Pectineus	0.12 ± 0.07	0.12 ± 0.03
Psoas	1.03 ± 0.67	1.09 ± 0.26
Rectus femoris	0.25 ± 0.14	0.23 ± 0.09
Sartorius	0.11 ± 0.08	0.12 ± 0.05
Tensor fascia latae	0.28 ± 0.21	0.30 ± 0.09

Table 3.39: Muscle forces of stubby prostheses users.
CI, confidence interval.

Muscle force impulse (BW.s)	Cohort 1_Sidekicks Mean ± SD *Median [95% CI]*	Cohort 2 Mean ± SD *Median [95% CI]*
Adductor brevis	9.37 ± 3.13	12.85 ± 11.65
Adductor longus	18.28 ± 7.68	10.26 ± 8.28
Adductor magnus	*8.81 [2.48-14.28]*	*1.74 [1.04-11.96]*
Biceps femoris	*10.88 [3.08-35.93]*	*3.92 [2.96-12.23]*
Gluteus maximus	26.33 ± 7.02	18.51 ± 7.49
Gluteus medius	63.69 ± 29.28	57.54 ± 27.78
Gluteus minimus	9.93 ± 3.74	12.64 ± 3.47
Gracilis	0.71 ± 0.21	0.32 ± 0.30
Iliacus	19.51 ± 11.14	35.38 ± 8.44
Pectineus	3.01 ± 1.90	3.89 ± 1.71
Psoas	19.60 ± 11.51 ***p=.035**	45.55 ± 11.89
Rectus femoris	4.49 ± 2.67 ***p=.032**	9.72 ± 1.89
Sartorius	1.54 ± 0.87	2.74 ± 1.05
Tensor fascia latae	5.14 ± 3.47 ***p=.041**	14.29 ± 5.02

Table 3.40: Muscle force impulse of stubby prostheses users.
CI, confidence interval. *Statistically significant differences between cohorts (p<.05).

Normalised muscle force impulse (BW.s/m)	Cohort 1_Sidekicks Mean ± SD *Median [95% CI]*	Cohort 2 Mean ± SD *Median [95% CI]*
Adductor brevis	*11.38 [4.47-15.24]*	*8.46 [1.88-31.74]*
Adductor longus	*22.83 [5.69-32.74]*	*8.38 [4.06-22.62]*
Adductor magnus	9.32 ± 4.46	3.83 ± 3.96
Biceps femoris	*11.60 [2.69-37.13]* ***p=.029**	*3.48 [2.74-11.20]*
Gluteus maximus	27.98 ± 7.43	17.19 ± 6.89
Gluteus medius	64.19 ± 25.00	53.60 ± 25.22
Gluteus minimus	10.11 ± 3.18	11.94 ± 3.47
Gracilis	0.78 ± 0.29	0.29 ± 0.26
Iliacus	19.80 ± 9.80	33.71 ± 9.49
Pectineus	3.23 ± 2.01	3.66 ± 1.63
Psoas	20.02 ± 11.23 ***p=.049**	43.08 ± 11.77
Rectus femoris	4.48 ± 2.27 ***p=.031**	9.14 ± 1.77
Sartorius	1.55 ± 0.81	2.55 ± 0.87
Tensor fascia latae	5.12 ± 3.18 ***p=.047**	13.57 ± 4.92

Table 3.41: Muscle force impulse normalised by walked distance of stubby prostheses users. CI, confidence interval. *Statistically significant differences between cohorts ($p<.05$).

Figure 3.27 presents subject-specific hip flexor muscle parameters for three participants in Cohort 1 and three participants in Cohort 2. The rectus femoris muscle volume was 2.6 fold lower for Cohort 2 than Cohort 1 (p=.049). There were no significant differences in the iliacus, psoas major and sartorius characteristics between the groups.

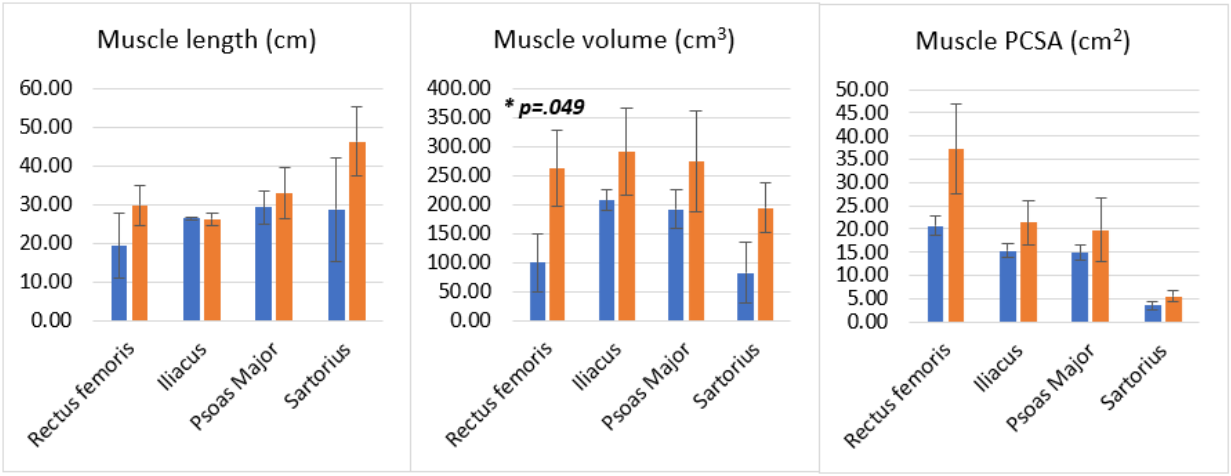


Figure 3.27: Subject-specific flexor muscle parameters (length, volume, PCSA). *Statistically significant differences between cohorts (p<.05). Cohort 1 - orange. Cohort 2 - blue.

Summary of key results for stubby prostheses users

- Cohort 2 (Sidekicks-only users) had longer legs by 0.3 m than Cohort 1_Sidekicks (amputees with Sidekicks who are also able to walk with full-length articulated prostheses).
- Cadence was lower for Cohort 2 by 23.5 steps/min than Cohort 1_Sidekicks.
- Cohort 2 showed lower peak hip flexion angles by 16.1° than Cohort 1_Sidekicks.
- The peak-to-peak pelvic tilt was higher for Cohort 2 by 8.0° than Cohort 1_Sidekicks.
- Cohort 2 presented lower ground reaction forces by 0.2 BW than Cohort 1_Sidekicks.
- The hip joint contact forces and impulse were similar between Cohort 1_Sidekicks and Cohort 2.
- Cohort 2 showed larger muscle force impulse for psoas by 23.1 BW.s/m, rectus femoris by 4.7 BW.s/m and tensor fascia latae by 8.5 BW.s/m than Cohort 1_Sidekicks.
- The rectus femoris muscle volume was 2.6 fold lower for Cohort 2 than Cohort 1.

3.5 Discussion

This is the first study to comprehensively investigate differences in function and loading of the BTF musculoskeletal system during level-ground walking with two different types of prostheses: foreshortened non-articulated Sidekicks stubbies and microprocessor-controlled Genium prosthetic knee units coupled with dynamic response feet. The amputee biomechanical data were then compared to that of persons without limb loss. The key findings of this chapter are presented in Table 3.42.

Key differences between amputees with different prostheses and able-bodied persons
1. Amputees with full-length prostheses showed step lengths, cadence and walking speeds similar to able-bodied persons.
2. Amputees with stubbies showed lower step lengths (by 0.2 m) and walking speeds (by 0.3 m/s) than amputees with Genium.
3. Amputees with Genium presented at the push-off phase of the gait cycle larger peak hip extension angle (by 11.4°), flexion moment (by 0.8 Nm/kg), generated power (by 1.9 W/kg) and contact force (by 3.5 BW) than amputees with Sidekicks.
4. Amputees with Genium presented at the push-off phase of the gait cycle larger peak hip extension angle (by 11.1°), flexion moment (by 0.8 Nm/kg), generated power (by 1.9 W/kg) and contact force (by 2.5 BW) than able-bodied persons.
5. Amputees with Sidekicks showed similar hip loading profiles to able-bodied persons during one gait cycle.
6. Amputees with Sidekicks presented larger hip joint impulse normalised to walked distance by 60.1 BW.s/m than able-bodied persons.
7. Amputees able to walk with both types of prostheses showed higher cadence with Sidekicks than Genium (by 12.6 steps/min) and able-bodied persons (by 9.7 steps/min).
8. Amputees able to walk with both types of prostheses showed with Genium larger muscle forces for adductor brevis (by 0.5 BW), adductor longus (by 0.8 BW), gluteus minimus (by 0.1 BW), iliacus (by 0.6 BW) and pectineus (by 0.1 BW) muscle forces than Sidekicks.
Key differences between stubby prostheses users
1. Sidekicks-only users used longer pylons by 0.3 m than other amputees with stubbies, but who are also able to walk with Genium.
2. Sidekicks-only users showed lower cadence by 23.5 steps/min than other amputees walking with stubbies.
3. Sidekicks-only users showed lower hip flexion angles by 16.1° and larger anterior pelvic tilt angles by 8.0° than other amputees walking with stubbies.
4. Sidekicks-only users showed larger psoas muscle force impulse by 23.1 BW.s/m than other amputees with stubbies.
5. Sidekicks-only users showed 2.6 fold lower rectus femoris muscle volume than amputees who are able to walk with both types of prostheses.

Table 3.42: Key findings of the biomechanical effect of full-length articulated and non-articulated stubby prostheses for BTF.

Albeit severely injured, the BTF Genium cohort demonstrated stride lengths, cadence and walking speeds similar to those of able-bodied persons (AB), as previously seen in the literature (Jarvis et al. 2017). Conversely, BTF Sidekicks showed lower walking speeds by 0.31 m/s than BTF Genium. As this difference is higher than the minimal clinically important difference in walking speed for individuals with lower limb amputation (0.21 m/s (Carse et al. 2021)), the lower walking speed demonstrates lower functional abilities with stubbies. Cadence did not significantly differ between the amputee cohorts, as

previously seen in a study with participants who did not test both prostheses (Carroll et al. 2018). However, Cohort 1 showed higher cadence with stubbies than prosthetic knees and AB. This may indicate an attempt to maintain similar walking speeds to those achieved with prosthetic knees by increasing cadence (Fiodorenko-Dumas et al. 2021), which was not sufficient given the lower stride lengths with stubbies. However, unlike BTF Sidekicks, BTF Genium needed to adopt larger stride lengths to be able to swing the full-length prosthesis back from a larger hip extension position. This created higher hip flexion moments, hip flexor muscle forces and ultimately higher hip joint contact forces during the late stance phase of the gait cycle. Faster walking speeds increase the whole-body angular momentum and necessitate larger hip and trunk stabilization moments, which may contribute to lower back injuries (Kulkarni et al. 2005, Hendershot et al. 2018). The higher muscular effort is demonstrated in this chapter by the larger adductor brevis, adductor longus, gluteus minimus, iliacus and pectineus muscle forces of Cohort 1 with Genium than Sidekicks, as well as larger iliacus, psoas, rectus femoris and sartorius muscle force impulse.

In contrast to able-body baseline, muscular activation changes after amputation as required by anatomical factors, prosthetic requirements and adopted biomechanics. Although BTF Genium were able to achieve similar functional levels to persons without limb loss, they experienced significantly larger hip joint contact forces. Conversely, the hip loading profile of BTF Sidekicks was comparable to that of AB controls. BTF Genium had a second HJCF peak that was nearly double than that observed for BTF Sidekicks, indicating that the maximum hip joint loading occurs in the double support phase at push-off. This is supported by the significantly larger hip generated power at push-off of BTF Genium than BTF Sidekicks. However, walking speed has a direct effect on the second HJCF peak (Giarmatzis et al. 2015), and BTF Sidekicks walked at slower speeds than BTF Genium. The larger walking speed of BTF with prosthetic knees, as well as the higher centre of gravity from the ground, may have required higher muscle co-contraction, which in turn increased the hip joint loading magnitude. However, muscle co-contraction is not represented in static-optimization based musculoskeletal models, and the effect of this limitation could be investigated.

The mechanics of osteoarthritis development in the BTF amputee population has not been investigated. However, the risk of osteoarthritis for unilateral transfemoral and transtibial amputees has been linked to abnormal joint loading (Felson 2013, Ding et al. 2020, Gailey et al. 2008, Morgenroth et al. 2012, Norvell et al. 2005). Although walking speed with stubbies reduced the magnitude of the maximum force at the hip during one gait cycle, the hip joint force impulse (loading dose) normalised by walked distance was significantly higher than AB. Stubby prostheses may introduce similar hip loading profiles to those of persons without limb loss only if they are used for walking short distances, training and use around the house. The results suggest that high-functioning BTF amputees with full-length articulated prostheses may be more susceptible to hip osteoarthritis onset than BTF fitted with non-articulated prostheses.

All amputee participants walked with larger step widths than AB, in accordance with

previous literature on BTF gait with prosthetic knees (Jarvis et al. 2017). Increasing the step width reduces the hip adduction moment at full hip extension to better mechanically recruit the abductor muscles, and increases stability and power production capabilities (Chang et al. 2011). Stability with stubbies was also ensured by the larger hip abduction angles during swing, as well as larger pelvic obliquity angles than able-bodied people (results in accordance with a previous study (Gitter et al. 2002)), adopted to create clearance needed for the prosthetic toe (Gard 2006). Metabolic cost has been suggested to be strongly correlated to the base-of-support (Weinert-Aplin et al. 2017). Therefore, based on this parameter, this study may suggest that use of stubbies may increase metabolic energy expenditure and reduce efficiency if used for walking long distances and periods of time, as seen in a previous case study (Perry et al. 2004). Anecdotal evidence shows that amputees sometimes prefer stubbies over articulated prostheses for short use at home or when they feel tired. Future could investigate factors related to fatigue.

Cohort 2 (Sidekicks-only users) presented lower cadence than Cohort 1_Sidekicks, indicating lower functional capabilities. Despite the longer legs and larger stride lengths, Cohort 2 presented lower hip flexion angles and larger anterior pelvic tilt than Cohort 1_Sidekicks. The lordotic posture and restriction in the hip range of motion may indicate hip flexor weakness and atrophy (progressive degeneration of muscle tissue). Rectus femoris in Cohort 2 was characterized by lower muscle length (by 55%), volume (by 164%) and PCSA (by 81%) compared to Cohort 1. Tight rectus femoris reattachments might have also caused the observed lordotic posture. In the able-bodied population, rectus femoris is a biarticular muscle that maintains postural stability by controlling both the hip and knee joints in response to angular momentum changes of the upper body (Schumacher et al. 2019). As this function is disrupted in above-knee amputations, amputees adopt a more anterior tilt of the pelvis to be able to increase stability. However, this might lead to higher compressive loading of the lumbar spine (Devan et al. 2017, Day et al. 1984, Hendershot & Wolf 2014) and contribute to low back pain, as suggested in this study by the larger psoas muscle force impulse in Cohort 2 compared to Cohort 1_Sidekicks. Prolonged wheelchair use might have amplified the degree of rectus femoris atrophy observed in Cohort 2. Nonetheless, walking with full-length articulated prostheses promotes constant natural stretching of the flexor muscles, thus limiting muscle atrophy. Therefore, it is not simple to conclude whether the lower muscle volume was a cause or an effect of walking with stubby prostheses only. Future work could investigate this. Finally, three out of four study participants in Cohort 2 had short residual limbs, affecting the ability to stabilize and successfully ambulate with full-length articulated prostheses, as the larger weight may cause the socket to come off a short residuum.

3.6 Limitations

There are a number of limitations to this study. The small cohort limits the use of these results to a wider amputee population and variations in height, body mass, gender, rehabilitation pathway, activity levels, reason of amputation and level of amputation could be considered in future studies. However, the number of study participants was as large as

could be achieved. Moreover, four musculoskeletal models were not subject-specific, and linear scaling may have introduced errors in force predictions. However, customization of musculoskeletal models is time and computationally intensive, and scaling to a model with similar anthropometry has been shown in Chapter 2 to introduce minimal errors for above/through-knee amputee models. Finally, scaling of muscle PCSAs should be integrated in the musculoskeletal model to account for muscle atrophy and hypertrophy to better represent the anatomical variability seen in the BTF amputee population. Other modelling limitations are detailed in Chapter 2.

3.7 Conclusion

This chapter highlights differences in musculoskeletal function and loading for bilateral above/through-knee amputees with non-articulated Sidekicks stubbies and full-length articulated prostheses (microprocessor-controlled Genium knees coupled with dynamic response feet) during level-ground walking. Stubby prostheses present lower functional abilities (as determined by walking speed), higher energy cost for long-term use (as determined by hip joint impulse) and poor cosmetic appearance. Conversely, advanced microprocessor knees and dynamic response feet improve appearance, functional abilities (as determined by walking speed), yet may introduce detrimental hip joint loading, increasing osteoarthritis risk. Hip flexor weakness (through atrophy or residuum length) might be a factor limiting the use of full-length articulated prostheses.

There is no simple answer to the question of which prosthesis to choose as this chapter did not take into account other factors such as prosthesis control and user satisfaction. However, based on the findings of this chapter, it can be concluded that the choice of adequate prosthesis should be based on musculoskeletal health factors, subject activity levels, goals and cosmesis preference. The balance between these varies per individual.

The modelling pipeline and analytical methods presented in this chapter can be applied to lower limb amputees with any type of amputation in order to thoroughly investigate the biomechanical effect of prosthetic design and propose mitigation strategies to reduce the risk of post-amputation musculoskeletal complications. The following chapters will focus on understanding the unilateral above/through-knee traumatic amputee musculoskeletal system function and loading with various prosthetic designs.

Chapter 4

Understanding the musculoskeletal function and loading of unilateral transfemoral amputees

This chapter investigates the musculoskeletal function and loading of unilateral above/through-knee traumatic amputees (UTF) and explains the high rates of osteoarthritis in the knee of the intact limb. Seven UTF and seven able-bodied matched controls underwent gait analysis. Musculoskeletal modelling was used to quantify joint contact forces for both cohorts. The results of this chapter allow for the development of mitigation strategies to improve long-term musculoskeletal health in this patient group.

4.1 Introduction

The 2020 Global Burden of Disease estimated that there were 28.9 million unilateral lower limb traumatic amputees (Mcdonald et al. 2020). In particular, the 2003 - 2014 Afghanistan conflict has resulted in 153 United Kingdom military casualties who sustained transfemoral amputations, primarily caused by improvised explosive devices, mines, gunshots, grenades and arms fire (Edwards et al. 2015). Among the civilian population, road traffic accidents, falls and cancer were common causes of traumatic or medically-induced amputations (Mcdonald et al. 2020). Regardless of the injury mechanism, the post-amputation disruption of the musculoskeletal system can have a profound impact the amputee's locomotion and quality of life.

Return to movement is achieved through rehabilitation and use of prosthetic devices. Commercially available prosthetic knees for unilateral above/through-knee amputees (UTF) are microprocessor-controlled (MPK) units such as Genium (Ottobock, Germany), C-leg (Ottobock, Germany), Rheo XC (Ossur, Iceland) and Orion 3 (Blatchford, United Kingdom). MPK units have the most advanced prosthetic design, as they are able to reproduce the physiological knee joint absorption power (Czerniecki 1996) and the eccentric function of the quadriceps and hamstrings. Additionally, the in-built sensors enable MPK units to adjust the resistance to the prosthetic user's bodyweight, allowing for variable walking speeds. MPK units are commonly fitted with dynamic response prosthetic feet, which absorb energy during the stance phase of the gait cycle and release it at push-off. Examples of dynamic response feet include Triton (Ottobock, Germany), Echelon (Blatchford, United Kingdom), Freedom Innovations (Proteor, United States) and Re-Flex Rotate (Ossur, Iceland). Different from the other mentioned types of prosthetic feet, Re-Flex Rotate offers high-levels of vertical and rotational shock absorption. Its integrated titanium coil absorbs and generates dynamic energy, reducing impact to the body.

Prostheses can be fixed to the residual limb using prosthetic sockets or osseointegration (direct skeletal fixation). The two main types of prosthetic sockets for transfemoral amputees are the quadrilateral and ischial containment sockets, which achieve weight bearing primarily through the gluteus muscles and ischium bone. For some amputees, a socket-suspended prosthesis is impossible to fit due to soft tissue issues, pain, or discomfort, which can cause amputees to be wheelchair bound (Hanspal & Sullivan 2021). This is a problem especially for blast injury patients who develop heterotropic ossification and have delicate skin grafts on their stumps, which break down with traditional sockets (Potter et al. 2006, Melcer et al. 2011). The direct skeletal fixation method involves the insertion of a titanium implant into the bone, eliminating the need for traditional socket-based prosthetic technology. As the prosthesis is anchored directly to the bone, it offers greater freedom from the limitations and complications (e.g. skin lesions) commonly associated with socket-based prosthetic systems. Although it is believed that osseointegration has the potential to improve clinical outcomes (McMenemy et al. 2020), it is not yet commonly performed.

Although locomotion can be restored through the use of prostheses, amputees need to

adopt muscular adaptations to successfully complete movement tasks. However, these might produce deleterious effects on the amputee musculoskeletal system. Comorbid conditions associated with lower limb amputation include osteoarthritis (Burke et al. 1978, Norvell et al. 2005), osteopenia (Rush et al. 1994) and low back pain (Ephraim et al. 2005). This chapter will focus on osteoarthritis due to its known association with biomechanical factors and, as such, is conducive to the approach used in this thesis.

The high rates of knee osteoarthritis in the unilateral amputee population (Norvell et al. 2005, Gailey et al. 2008, Kulkarni & Adams 1998) may be explained by the larger functional demands of the sound limb. UTF compensate for the limb loss by increasing the reliance on the intact limb for propulsion. Specifically, UTF spend a longer time in the stance phase of the intact side gait cycle than the prosthetic one (Jaegers et al. 1995, Mâaref et al. 2010). Due to the hypothesized inability of the femoral remnant to bear axial loads and pain or insecurity with the prosthesis, UTF shift a greater bodyweight percentage to the intact limb during ambulation than the prosthetic limb. Therefore, this amputee population presents larger ground reaction forces (Castro et al. 2014, Nolan et al. 2003), net sagittal plane joint moments and power (Nolan & Lees 2000) of the sound limb than unilateral transtibial amputees (UTT) and able-bodied persons. Abnormal loading of the joints (as determined by larger external knee moments, loading rates and contact forces) is thought to be linked to osteoarthritis development and progression (Ding et al. 2020, Felson 2013, Morgenroth et al. 2012, Crossley et al. 2012, Manal et al. 2015).

The knee is subdivided into the medial, lateral and patellofemoral compartments, where healthy articular cartilage allows bones to glide over each other with minimal friction (Buckwalter 1992). In the case of repetitive high loading, tissue degeneration might occur (Ewers et al. 2001, Kerin et al. 2003) in one or more compartments of the knee. Previous studies have demonstrated lower peak external knee adduction moments and higher ground reaction loading rates for military UTF compared to matched able-bodied service members (Russell Esposito et al. 2015, Pruziner et al. 2014), where high loading rates may place the articular cartilage and tissue of the UTF sound limb at risk of degeneration. However, given the lower knee adduction moments, it has been suggested that the damage might not be localized to the medial compartment of the knee (Russell Esposito et al. 2015). The contact forces in the medial and lateral compartments of the intact knee have not been previously investigated in the UTF population.

Abnormal joint contact forces are a consequence of the post-amputation altered muscle activation patterns created by the newly adopted movement strategies. Vaulting is a compensatory movement adopted by UTF, which is characterized by excessive sound ankle plantar flexion (Drevelle et al. 2014), and used to create ground clearance needed for the prosthetic toe in mid-swing to prevent falls (Riveras et al. 2020). Previous literature demonstrated that UTF excessively plantar flex the sound ankle during level-ground walking (Jarvis et al. 2020), thus increasing the functional demand of the plantar flexor muscles. The main plantar flexors are the medial and lateral heads of the gastrocnemius muscle, which originate from the medial and lateral femoral condyles. The distal end of

the gastrocnemius heads forms the Achilles tendon, which inserts on the calcaneus. As the gastrocnemius muscle spans both the knee and ankle joints, its larger forces may lead to abnormal ankle and knee contact forces.

Osteopenia is characterized by bone mineral density (BMD) reduction, thought to be primarily caused by disuse atrophy (Rush et al. 1994, Kulkarni & Adams 1998) and insufficient loading of the amputated limb. Osteopenia is more prevalent in the UTF than UTT population (Kulkarni & Adams 1998, Sherk et al. 2008), placing UTF at higher risks of fragility fractures. Specifically, the UTF amputated side presents significantly lower femoral neck BMD than the intact side (Rush et al. 1994, Kulkarni & Adams 1998). This outcome might be the result of different factors. Firstly, available prosthetic sockets for UTF minimize axial load transmission through the distal end of the residual femur, thus reducing femoral neck BMD. Due to loss of joints and muscle volume, transfemoral amputees rely on the hip spanning muscles for propulsion of the amputated limb. However, it has been suggested that the loading the residual muscles may not sufficient to sustain physiologically normal BMD levels in the femoral neck (Sherk et al. 2008). Although potentially significant for UTF, this chapter focuses mainly on osteoarthritis, yet the results will be discussed also in the context of unloading osteopenia.

Low back pain is another comorbid condition that is of concern for persons with lower limb loss (Sivapuratharasu et al. 2019). The higher prevalence in the UTF population than persons without limb loss (Smith et al. 1999) has been demonstrated to have detrimental effects on functional performance and quality of life (Ehde et al. 2001, Taghipour et al. 2009). The causation of low back pain has been attributed to spine overload (Adams et al. 2007), leg length discrepancy and muscle weakness (Kulkarni et al. 2005). UTF often present asymmetric trunk motion (Hendershot & Wolf 2014) in order to increase equilibrium and stability. However, trunk asymmetry and anterior pelvic tilt angles may lead to higher spine compression and low back pain than able-bodied persons (Shojaei et al. 2016, Devan et al. 2017, Day et al. 1984, Adams et al. 2007, Christie et al. 1995). Like osteoporosis, low back pain is not the primary focus of this chapter, yet the discussion will consider this chapter's results in this context as well.

The aforementioned mechanically driven comorbidies have a strong negative impact on the musculoskeletal capacity to support locomotion, and so, management of these conditions is essential for optimal rehabilitation. Biomechanics can be used to identify abnormal loading of the musculoskeletal system and understand the causation of secondary musculoskeletal disorders. Whilst joint moments and loading rates have been associated with osteoarthritis development (Crossley et al. 2012, Manal et al. 2015), there is a need for the quantification of joint contact forces to provide comprehensive descriptions of the musculoskeletal system loading in the UTF population. Musculoskeletal modelling is a widely used tool that quantifies muscle and joint contact forces (Ding et al. 2019, Cleather & Bull 2015), and allows for the differentiation between the loading of the medial and lateral compartments of the knee during activities of daily living (Ding et al. 2020).

The aim of this chapter is to investigate the function and joint loading profiles of trau-

matic UTF fitted with MPK units, dynamic response feet and prosthetic sockets. It is hypothesized that the loading of the UTF intact limb is higher than healthy able-bodied persons, placing UTF at higher risks of joint degeneration. This work allows for the development of mitigation strategies to improve long-term musculoskeletal health of UTF traumatic amputees.

4.2 Methods

4.2.1 Data acquisition and processing

Ethical approval was obtained from the Joint Research Compliance Office and the Imperial College Research Ethics Committee (Reference 20IC6268). Signed informed consent was obtained from all study participants, whose details are presented in Table 4.1. Data were collected from seven (two civilian, five ex-military) unilateral above/through-knee amputees (UTF) with no known secondary conditions. Military amputees had undergone rehabilitation at the Defence Medical Rehabilitation Centre, UK. All participants had a K3 activity level (ability or potential for ambulation with variable speed (Balk et al. 2018)) or higher, and had been prosthesis users for a minimum of two years. Through-knee amputees were fitted with quadrilateral prosthetic sockets. Above-knee amputees were fitted with ischial containment sockets.

One female and six male civilian able-bodied controls (AB) were group matched to the UTF cohort by sex, height and adjusted mass for amputation. The adjusted mass was calculated using Equation 2.6 presented in Chapter 2. There were no significant differences between groups in adjusted mass (p=.710), height (p=.165) and age (p=.259). This was checked with a Mann-Whitney test with a .05 significance level. The control dataset is a subgroup of a previous dataset (Long et al. 2017).

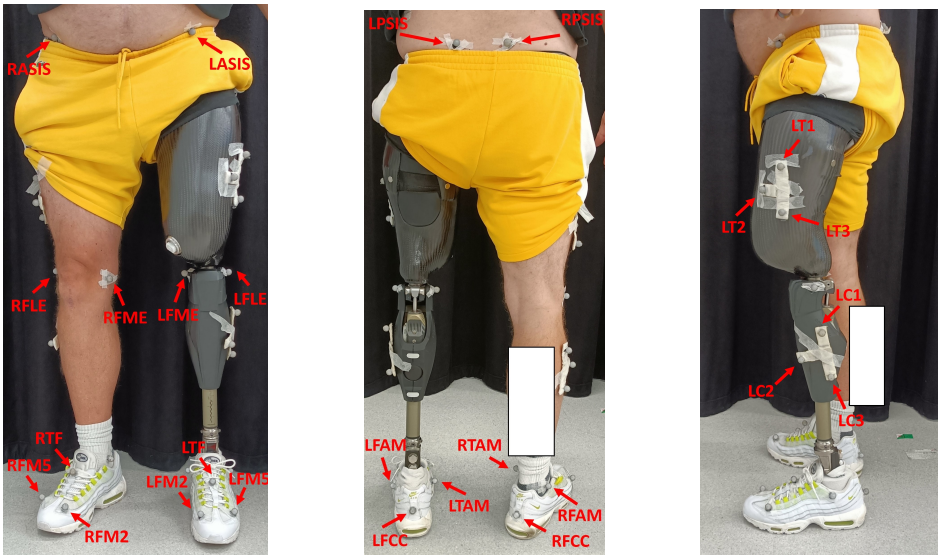
Part. No. (Gender)	Cause of amp.	Age (y)	Adj. mass (kg)	Height (m)	Amp. level	Prosth. knee	Prosth. foot
UTF 1 (Male)	IED	33	81	1.78	TF	Rheo XC	Re-Flex Rotate
UTF 2 (Male)	Motorcycle accident	41	77	1.78	TK	Genium X3	Freedom Innovations Low Profile
UTF 3 (Male)	Motorcycle accident	66	69	1.73	TF	Orion3	Echelon VT
UTF 4 (Male)	Cancer	57	73	1.65	TF	Orion3	Echelon
UTF 5 (Female)	Leg injury	55	102	1.72	TK	Genium X3	Triton Low Profile
UTF 6 (Male)	IED	47	95	1.76	TF	Genium X3	Triton 1C64 Heavy Duty
UTF 7 (Male)	Leg injury	57	94	1.76	TF	C-leg	Triton
Mean ± SD		51 ± 10	84 ± 12	1.74 ± 0.04			
Control (n=7) Mean ± SD		45 ± 13	85 ± 8	1.79 ± 0.06			

Table 4.1: Study participant details.
IED, improvised explosive device. TF, transfemoral. TK, through-knee.

Gait data were collected using a 10-camera VICON optoelectronic based motion capture analysis system (VICON 2.10.3, Oxford Metrics Group, UK) with two force plates (Kistler Type 9286B, Kistler Instrumente AG, Winterthur, Switzerland). Retro-reflective markers were attached to anatomical landmarks of the lower body (Ding et al. 2019), as detailed in Table 4.2. In addition to the anatomical landmark markers, four clusters of three markers each were placed on the thigh and shank segments (Duffell et al. 2014). Figure 4.1 illustrates the marker positions for one representative unilateral above-knee amputee.

Marker name	Anatomical landmark
RASIS/LASIS	Right/Left anterior superior iliac spine
RPSIS/LPSIS	Right/Left posterior iliac spine
RFME/LFME	Right/Left medial femoral epicondyle prosthetic equivalent: medial side of the knee centre of rotation
RFLE/LFLE	Right/Left lateral femoral epicondyle prosthetic equivalent: lateral side of the knee centre of rotation
RFAM/LFAM	Right/Left lateral malleoli prosthetic equivalent: lateral side of the ankle centre of rotation
RTAM/LTAM	Right/Left medial malleoli prosthetic equivalent: medial side of the ankle centre of rotation
RFM2/LFM2	Right/Left second metatarsal head prosthetic equivalent: front edge of the foot above second toe
RFM5/LFM5	Right/Left fifth metatarsal head prosthetic equivalent: front edge of the foot above fifth toe
RFCC/LFCC	Right/Left posterior calcaneus prosthetic equivalent: heel at toe height
RTF/LTF	Right/Left midfoot superior prosthetic equivalent: top of the foot, anterior to the pylon base
R/L T1/T2/T3	Right/Left thigh segment cluster
R/L C1/C2/C3	Right/Left shank segment cluster

Table 4.2: Marker placement locations.



(a) **(b)** **(c)**

Figure 4.1: Marker placement for one representative unilateral above-knee amputee. The labels highlight the marker and cluster positions as listed in Table 4.2.

Each participant completed one static calibration and six walking trials at self-selected

speeds. The walking trials were performed with complete foot placement on the force plate. Trials were continued until sufficient complete foot placements were achieved. Therefore, targeting effects, which might occur when the participant is instructed to step on the force plates, were minimized. The motion data were processed in VICON Nexus (VICON 2.10.3, Oxford Metrics Group, UK). The gait cycle events (foot strike, toe off and consecutive foot strike) were identified for each limb using a 30 N force threshold. The retro-reflective markers were labeled, and the marker trajectories gaps filled using the rigid body gap filling algorithm. Marker trajectories and force plate data were filtered in MATLAB (The Mathworks Inc., Natick, MA, USA) using a zero phase-lag, fourth order Butterworth filter with 6 Hz cut-off frequency (Yu et al. 1999).

4.2.2 Anthropometry and body segment parameters

Accurate in-vivo measurements of body segment parameters are not possible. Various alternative techniques have been proposed, including anthropometric reference manuals (Lohman et al. 1988) and the mass and height based regression equations developed by DeLeva (De Leva 1996). The inertial parameters of the intact segments in this study were obtained using the DeLeva method (De Leva 1996) based on adjusted mass and height. However, prosthetic components are lighter than their biological counterparts, and DeLeva calculations are not able to account for the prosthesis. Therefore, the reaction board method with moment equilibrium was used to obtain the inertial parameters of the prosthetic components (Smith et al. 2014). As the full prosthesis unit was not disassembled in the current study, the inertial parameters of the prosthetic components were obtained based on similar limbs from a previous dataset (Henson 2020) used in Chapter 2. The total moment of inertia of the thigh segment was obtained through the addition of the moment of inertia of the stump to that of the prosthetic socket, liner and connectors using the Huygens-Steiner parallel axis theorem (Haas 1928).

4.2.3 Musculoskeletal modelling

Inverse kinematics, inverse dynamics and musculoskeletal modelling simulations were performed using Freebody v2.1 (Ding et al. 2016, Cleather & Bull 2015), a segment based musculoskeletal model adapted for both able-body and amputee use. The able-body Freebody v2.1 musculoskeletal model was validated for tibiofemoral joint contact forces from instrumented implant measurements (Ding et al. 2019). The above/through-knee amputee Freebody v2.1 musculoskeletal model was validated using electromyography recordings as presented in Chapter 2.

The UTF intact and amputated limbs were modeled separately. The UTF intact limbs and matched able-body models were simulated using the able-body version of Freebody v2.1, detailed in Chapter 3. The closest anatomical datasets were chosen based on similar mass, gender and limb length to pelvis width ratio in order to predict ankle, knee and hip joint contact forces with minimal errors (Ding et al. 2019). The UTF amputated limb models were simulated using the above/through-knee version of Freebody v2.1, as detailed in Chapter 2. The closest amputee models were chosen using the anatomical atlas

and regression models developed in Chapter 2. In order to accurately predict muscle and hip joint contact forces, the models were chosen based on similar pelvis width, adjusted body mass index (Tzamaloukas et al. 1994) and stump length to pelvis width ratio.

4.2.4 Data analysis

Statistical analysis of walking characteristics was performed using IBM SPSS Statistics 27.0.0 (IBM Corp. Armonk, NY). Parametric data were compared between groups by independent t-tests. Non-parametric data were compared using Mann-Whitney U tests. Data normality was checked using the Shapiro-Wilk statistical test. Normally distributed data are presented as Mean ± SD and non-normally distributed data are presented as Median [95% Confidence Interval].

The computed whole-time data series were expressed as a gait cycle percentage from 0% at heel strike to 100% at the consecutive heel strike in intervals of 1% and averaged over 3 trials. Statistical parametric mapping (SPM) (Friston et al. 2007, Papi et al. 2020, Pataky et al. 2013) was used to compare the whole time-series data between cohorts. Depending on data normality, parametric or non-parametric two-tailed independent sample t-tests were performed to identify biomechanical differences between cohorts. p values of less than .05 were considered to indicate statistical significance. The key statistically and clinically significant results (differences of 10% or higher) are then summarised.

4.3 Results

4.3.1 Temporal and spatial gait characteristics

Table 4.3 presents the temporal and spatial gait characteristics of AB, UTF intact and prosthetic limbs. UTF walked at similar speeds and cadence as AB. The UTF intact side step length was lower by 0.06 m than the prosthetic side step length (p=.029). The percentage time spent in the stance phase of the UTF intact limb gait cycle was larger by 6.0% than the UTF prosthetic limb (p<.001) and by 3.2% than AB (p=.002). UTF showed larger step widths by 0.05 m than AB (p=.018).

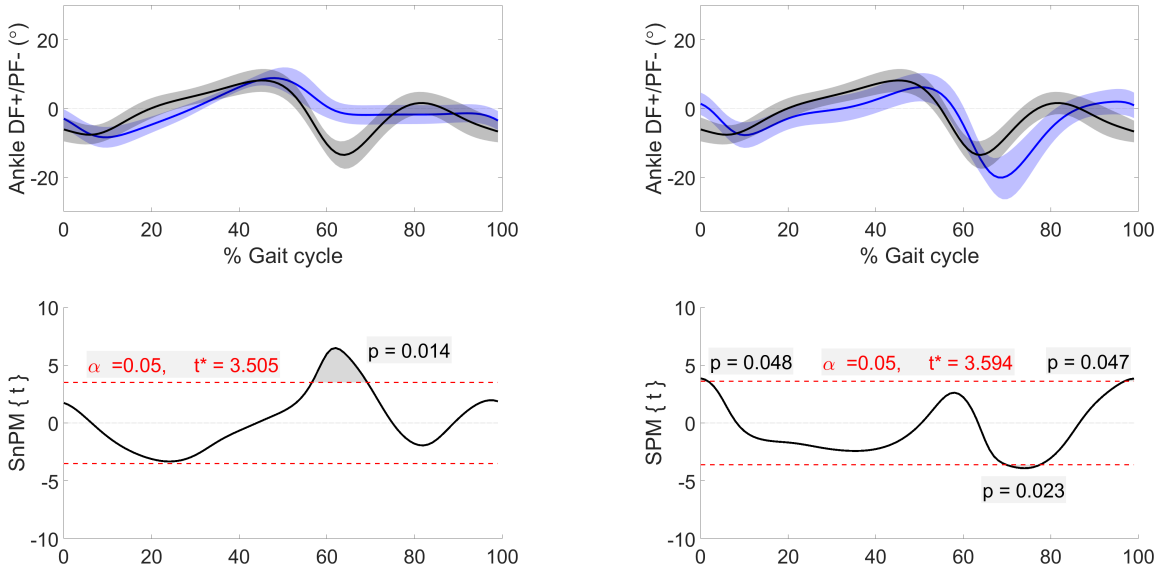
	Unilateral transfemoral		
Biomechanical parameter	Prosthetic side Mean ± SD *Median [95% CI]*	Intact side Mean ± SD *Median [95% CI]*	Able-bodied controls Mean ± SD *Median [95% CI]*
Walking speed (m/s)	*1.10 [1.05-1.20]*		*1.17 [1.04-1.26]*
Cadence (steps/min)	*98.02 [94.94-106.54]*		*106.00 [95.68-110.11]*
Step width (m)	0.16 ± 0.04 ***p=.018**		0.11 ± 0.02
Step length (m)	0.70 ± 0.05 ***p=.042** ****p=.029**	0.64 ± 0.03	0.64 ± 0.03
Stride length (m)	1.35 ± 0.06	1.35 ± 0.07	1.34 ± 0.07
Stance time (% gait cycle)	60.76 ± 2.33 ***p=.020** ****p<.001**	66.76 ± 1.80 ***p=.002**	63.52 ± 0.96

Table 4.3: Temporal and spatial parameters characteristics.
CI, confidence interval. *Statistically significant differences from able-bodied controls (p<.05).
**Statistically significant differences between UTF limbs (p<.05).

4.3.2 Kinematics

The whole-time data are presented over the course of the gait cycle from heel strike to the consecutive heel strike. SPM results are presented for identification of significant differences between UTF and AB . Grey threshold clusters indicate statistically significant differences and red dashed lines represent critical thresholds.

Figure 4.2 presents the sagittal plane ankle kinematics. SPM reported lower plantar flexion angles for the UTF prosthetic ankle than AB in late stance (p=.014). SPM showed higher plantar flexion angles for the UTF intact ankle than AB in late stance (p=.023). When comparing discrete values in Table 4.4, the prosthetic ankle showed lower plantar flexion angles by 12.4° than the UTF intact side (21.1°, p<.001) and by 5.1° than AB (13.7°, p=.026). UTF presented larger intact ankle peak plantar flexion angles by 7.4° than AB (p=.030).



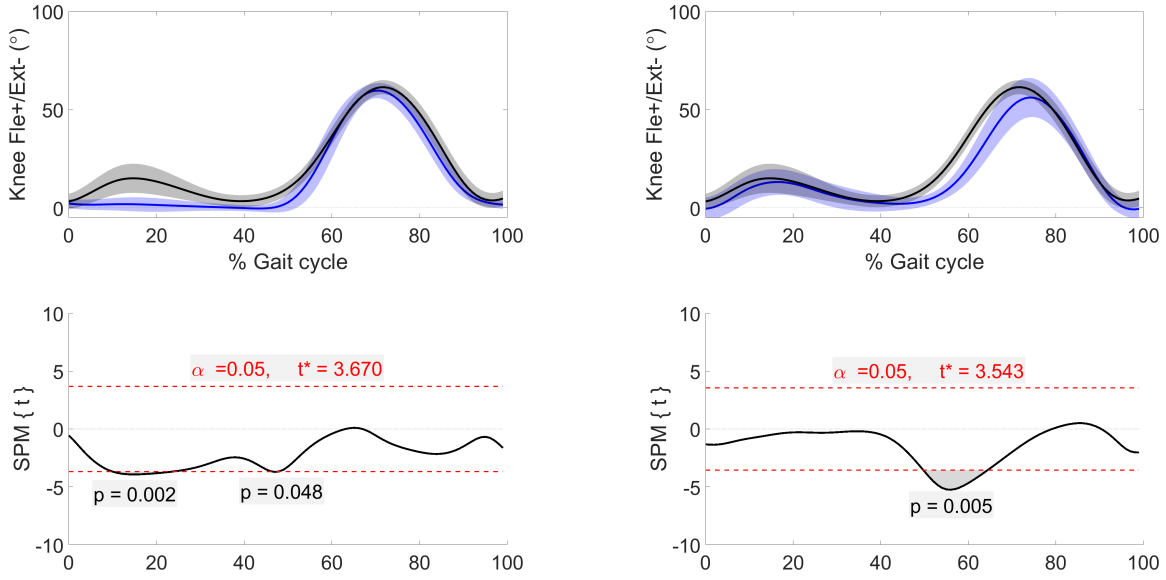
(a) Prosthetic side **(b)** Intact side

Figure 4.2: Top: Ankle dorsiflexion (DF)/plantar flexion (PF) angles of UTF (blue) and AB (black). Bottom: Statistical parametric mapping results.

	Unilateral transfemoral		
Biomechanical parameter	Prosthetic side Mean ± SD	Intact side Mean ± SD	Able-bodied controls Mean ± SD
Peak ankle dorsiflexion (°)	9.47 ± 2.18	7.85 ± 2.30	8.42 ± 3.23
Peak ankle plantar flexion (°)	8.65 ± 2.94 ***p=.026** ****p<.001**	21.07 ± 6.16 ***p=.030**	13.71 ± 3.91
Ankle dorsiflexion/ plantar flexion ROM (°)	18.12 ± 3.38 ****p=.004**	28.92 ± 6.53 ***p=.040**	22.13 ± 3.05

Table 4.4: Sagittal plane ankle kinematics.
ROM, range of motion. *Statistically significant differences from able-bodied controls (p<.05). **Statistically significant differences between UTF limbs (p<.05).

Figure 4.3 presents the sagittal plane knee joint angles. SPM reported lower UTF prosthetic knee flexion angles than AB in stance (p=.002, p=.048). There was a timing difference between the UTF intact knee flexion angles and AB in terminal stance (p=.005). When comparing discrete values in Table 4.5, the peak prosthetic knee flexion in early stance was lower than the intact side (p=.005) and AB (p=.001).



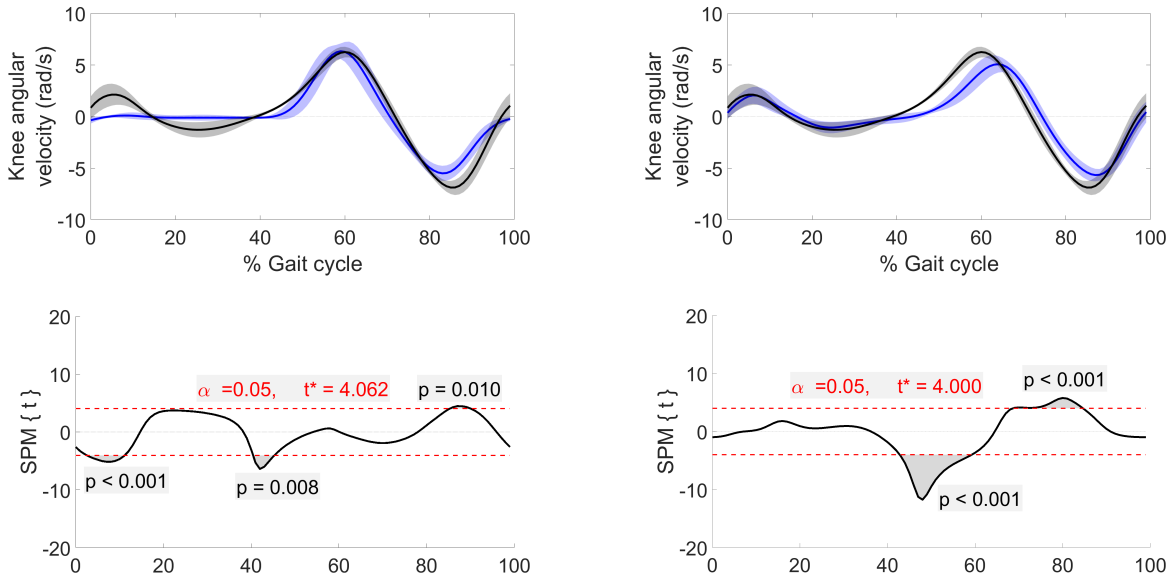
(a) Prosthetic side **(b)** Intact side

Figure 4.3: Top: Knee flexion (Fle)/extension (Ext) angles of UTF (blue) and AB (black). Bottom: Statistical parametric mapping results.

	Unilateral transfemoral		
Biomechanical parameter	Prosthetic side Mean ± SD	Intact side Mean ± SD	Able-bodied controls Mean ± SD
Peak knee flexion (°)	60.27 ± 3.84	56.67 ± 10.01	61.87 ± 3.77
Peak knee flexion early stance (°)	3.02 ± 3.41 ***p=.001** ****p=.005**	13.72 ± 6.90	15.56 ± 6.67

Table 4.5: Sagittal plane knee kinematics.
*Statistically significant differences from able-bodied controls (p<.05). **Statistically significant differences between UTF limbs (p<.05).

Figure 4.4 presents the sagittal plane knee angular velocity. SPM reported statistically significant differences between the UTF prosthetic and AB knee angular velocity in stance (p<.001, p=.008) and swing (p=.010). SPM also showed significant timing differences between the UTF intact and AB knee angular velocity (p<.001). When comparing discrete values in Table 4.6, the UTF peak intact knee angular velocity in terminal stance was lower by 1.1 rad/s than AB (6.3 rad/s, p=.014). There were no significant differences in the peak knee angular velocity in terminal stance between the prosthetic limb and AB.



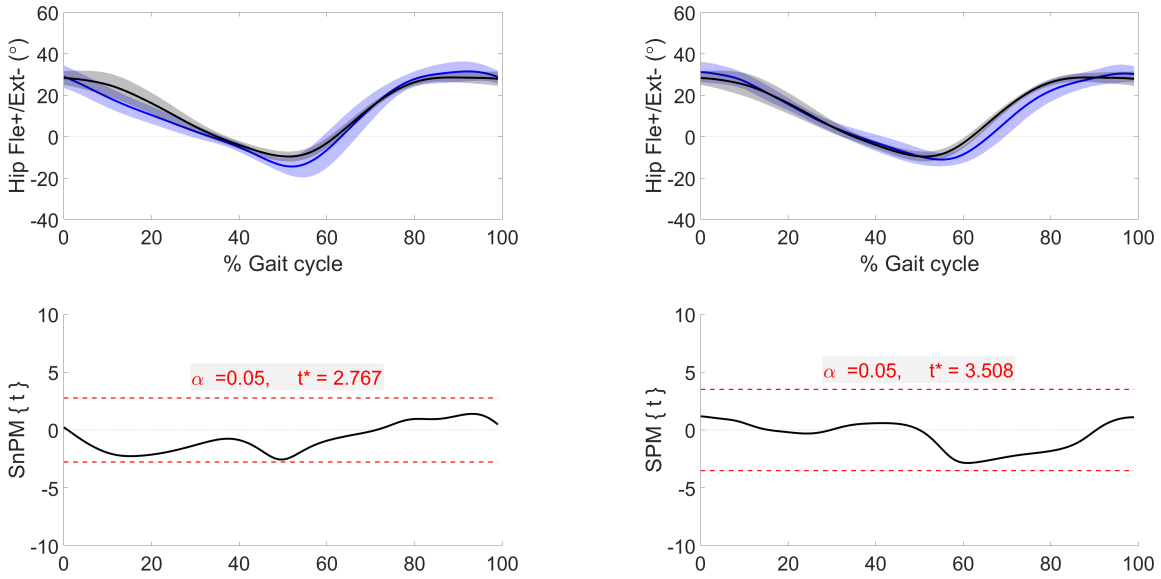
(a) Prosthetic side **(b)** Intact side

Figure 4.4: Top: Knee angular velocity of UTF (blue) and AB (black). Bottom: Statistical parametric mapping results.

	Unilateral transfemoral		
Biomechanical parameter	Prosthetic side Mean ± SD	Intact side Mean ± SD	Able-bodied controls Mean ± SD
Peak knee angular velocity (rad/s)	6.82 ± 0.73 ****p=.003**	5.21 ± 0.76 ***p=.014**	6.26 ± 0.49

Table 4.6: Peak sagittal plane knee angular velocity in terminal stance. *Statistically significant differences from able-bodied controls (p<.05). **Statistically significant differences between UTF limbs (p<.05).

Figure 4.5 and Table 4.7 present the sagittal plane hip angles. The peak prosthetic side hip extension was larger by 6.0° than AB (9.6°, p=.028). No significant differences were identified in the sagittal plane hip kinematics between the UTF intact side and AB.



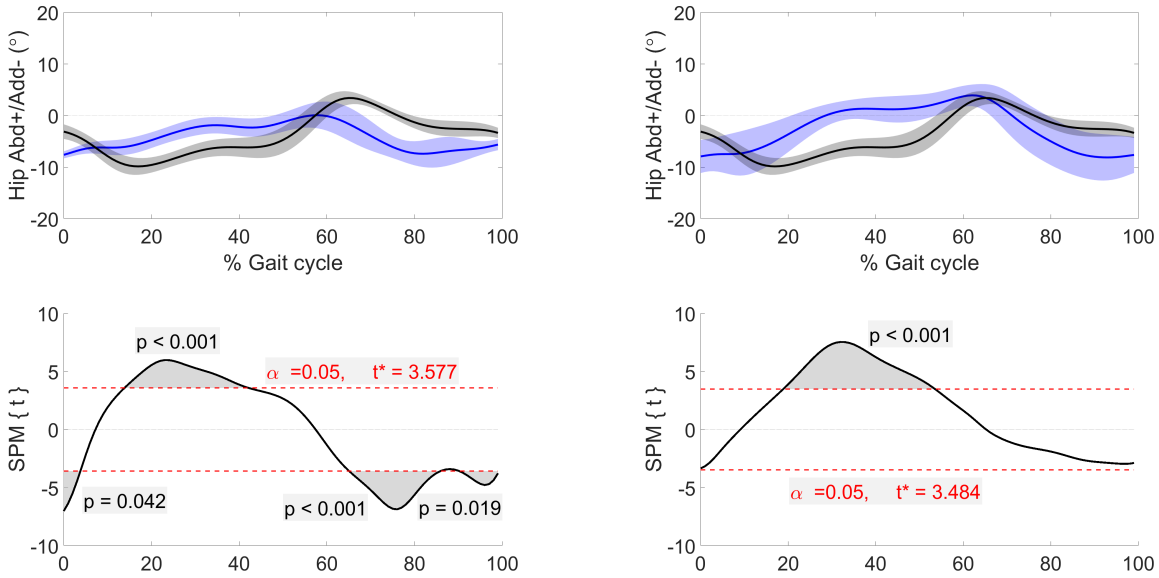
(a) Prosthetic side **(b)** Intact side

Figure 4.5: Top: Hip flexion (Fle)/extension (Ext) angles of UTF (blue) and AB (black). Bottom: Statistical parametric mapping results.

	Unilateral transfemoral		
Biomechanical parameter	Prosthetic side Mean ± SD	Intact side Mean ± SD	Able-bodied controls Mean ± SD
Peak hip flexion (°)	31.98 ± 4.85	32.40 ± 4.44	29.61 ± 3.09
Peak hip extension (°)	15.60 ± 5.54 ***p=.028**	11.76 ± 2.65	9.58 ± 2.12
Hip flexion/ extension ROM (°)	47.56 ± 9.75	44.16 ± 4.45	39.18 ± 3.67

Table 4.7: Sagittal plane hip kinematics.
ROM, range of motion. *Statistically significant differences from able-bodied controls (p<.05).

Figure 4.6 presents the coronal plane hip angles. SPM showed that whilst AB adducted the hip in stance, UTF abducted both the prosthetic and intact side hips at this stage of the gait cycle (p<.001). SPM reported larger prosthetic side hip adduction angles than AB in swing (p<.001). When comparing discrete values in Table 4.8, the UTF prosthetic side hip showed lower peak hip abduction angles by 3.8° than the UTF intact side hip (p=.008) and by 2.7° than AB (p=.018).



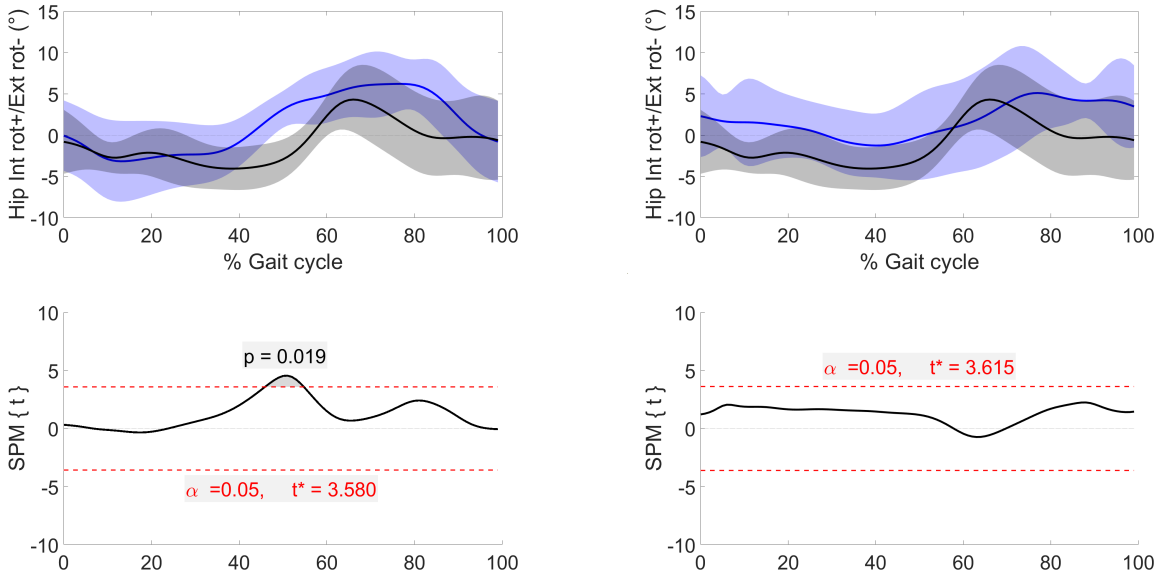
(a) Prosthetic side **(b)** Intact side

Figure 4.6: Top: Hip abduction (Abd)/adduction (Add) angles of UTF (blue) and AB (black). Bottom: Statistical parametric mapping results.

	Unilateral transfemoral		
Biomechanical parameter	Prosthetic side Mean ± SD	Intact side Mean ± SD	Able-bodied controls Mean ± SD
Peak hip abduction (°)	0.82 ± 2.10 ***p=.018** ****p=.008**	4.65 ± 2.09	3.53 ± 1.18
Peak hip adduction (°)	8.85 ± 1.59	10.38 ± 3.90	9.76 ± 1.56
Hip abduction/ adduction ROM (°)	9.68 ± 2.50 ***p=.008** ****p=.012**	14.91 ± 3.56	13.29 ± 1.21

Table 4.8: Coronal plane hip kinematics.
ROM, range of motion. *Statistically significant differences from able-bodied controls (p<.05). **Statistically significant differences between UTF limbs (p<.05).

Figure 4.7 and Table 4.9 present the transverse plane hip angles. SPM reported larger prosthetic side hip internal rotation angles than AB at 50% in the gait cycle (p=.019). No significant differences were identified in the transverse plane hip angles between the UTF intact side and AB.



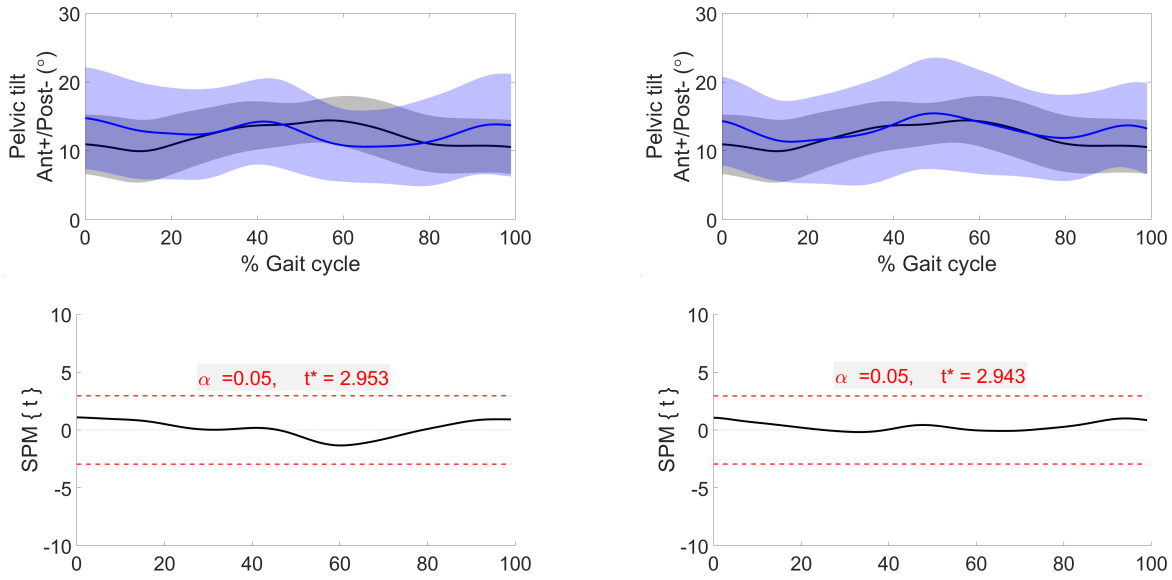
(a) Prosthetic side **(b)** Intact side

Figure 4.7: Top: Hip internal (Int)/external (Ext) rotation (Rot) angles of UTF (blue) and AB (black). Bottom: Statistical parametric mapping results.

	Unilateral transfemoral		
Biomechanical parameter	Prosthetic side Mean ± SD	Intact side Mean ± SD	Able-bodied controls Mean ± SD
Hip internal rotation/ external rotation ROM (°)	13.59 ± 5.23	14.46 ± 4.00	10.70 ± 2.70

Table 4.9: Transverse plane hip kinematics.
ROM, range of motion.

Figure 4.8 presents the sagittal plane pelvic angles over the course of the gait cycle, with no significant differences identified in the SPM results. When comparing the peak-to-peak (P2P) amplitudes in Table 4.10, UTF showed larger P2P pelvic tilt angles by 2.3° than AB (5.5°, p=.026).



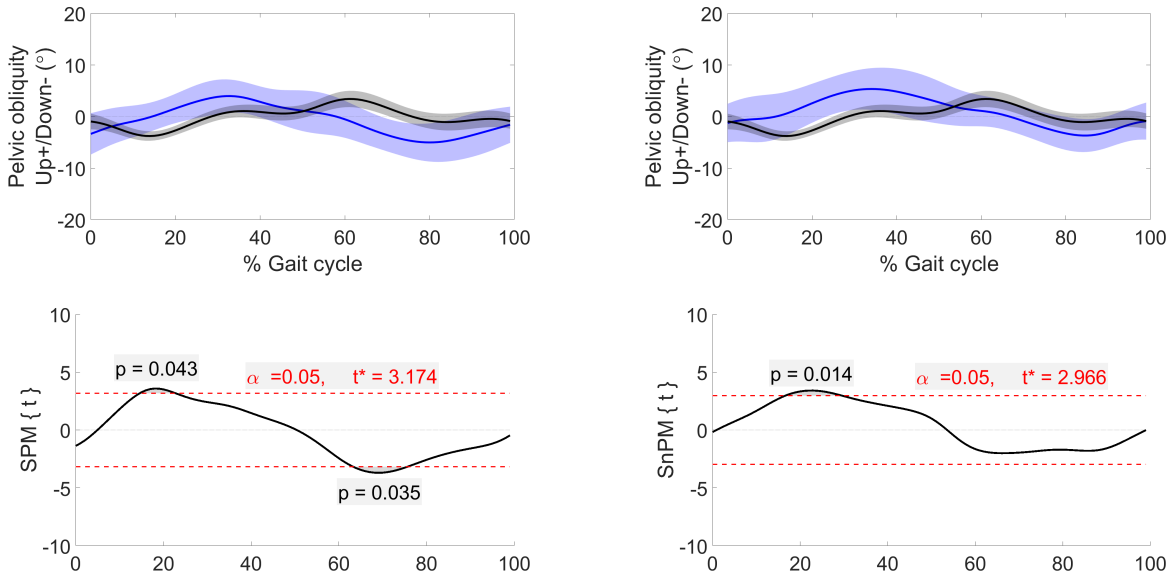
(a) Prosthetic side **(b)** Intact side

Figure 4.8: Top: Pelvic anterior (Ant)/posterior (Post) tilt angles of UTF (blue) and AB (black). Bottom: Statistical parametric mapping results.

	Unilateral transfemoral		
Biomechanical parameter	Prosthetic side Mean ± SD	Intact side Mean ± SD	Able-bodied controls Mean ± SD
P2P pelvic tilt (°)	7.82 ± 1.86 ***p=.026**	7.28 ± 2.31	5.51 ± 1.24

Table 4.10: Sagittal plane pelvic kinematics.
P2P, peak-to-peak. *Statistically significant differences from able-bodied controls (p<.05).

Figure 4.9 and Table 4.11 present the coronal plane pelvic angles (pelvic obliquity) over the course of the gait cycle. SPM reported larger vertical height of the UTF prosthetic side hip during the intact limb stance phase than AB (p=.014). The P2P pelvic obliquity during the intact limb gait cycle was larger for UTF by 2.5° than AB (7.0°, p=.029).



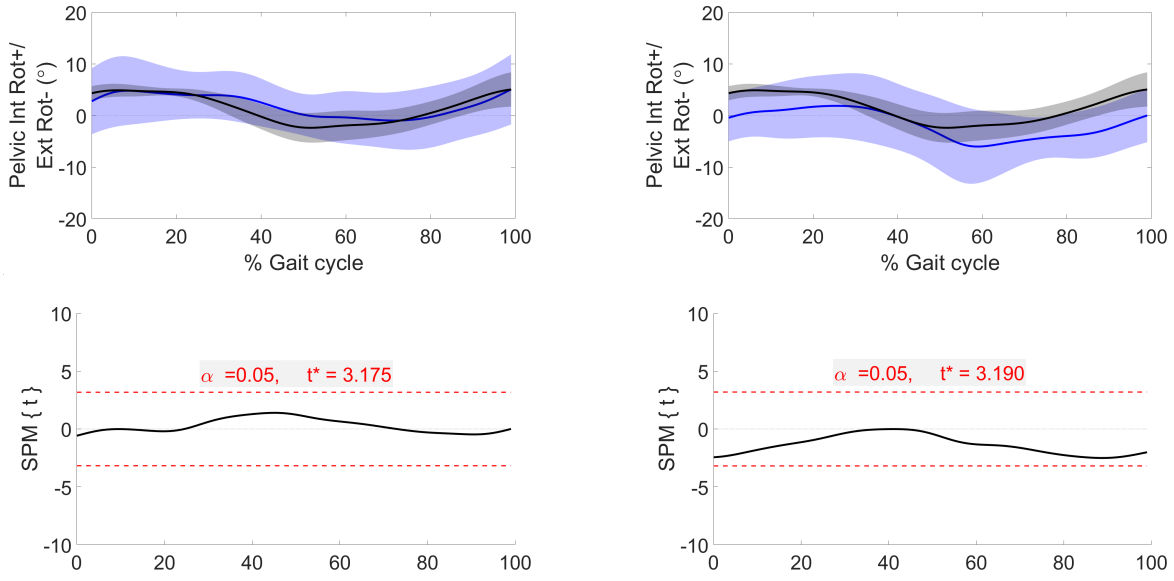
(a) Prosthetic side **(b)** Intact side

Figure 4.9: Top: Pelvic obliquity angles of UTF (blue) and AB (black). Positive angles describe an increase in the vertical height of the contralateral hip. Bottom: Statistical parametric mapping results.

	Unilateral transfemoral		
Biomechanical parameter	Prosthetic side Mean ± SD	Intact side Mean ± SD	Able-bodied controls Mean ± SD
P2P pelvic obliquity (°)	9.48 ± 1.97 ***p=.027**	9.50 ± 2.05 ***p=.029**	7.05 ± 1.29

Table 4.11: Coronal plane pelvic kinematics.
P2P, peak-to-peak. *Statistically significant differences from able-bodied controls (p<.05).

Figure 4.10 and Table 4.12 present the transverse plane pelvic angles, with no significant differences between cohorts.



(a) Prosthetic side **(b)** Intact side

Figure 4.10: Top: Pelvic internal (Int)/external (Ext) rotation (Rot) angles of UTF (blue) and AB (black). Bottom: Statistical parametric mapping results.

	Unilateral transfemoral		
Biomechanical parameter	Prosthetic side Mean ± SD	Intact side Mean ± SD	Able-bodied controls Mean ± SD
P2P pelvic rotation (°)	9.95 ± 3.70	11.50 ± 4.60	8.81 ± 2.66

Table 4.12: Transverse plane pelvic kinematics. P2P, peak-to-peak.

Figure 4.11 shows the AB (one limb only) and UTF body orientations in the stance phase of the intact limb gait cycle. To summarize the intact limb kinematics results in stance, certain patterns are different between UTF and AB. Specifically, the pelvis is tilted more upwards, the intact side hip is more abducted and the intact ankle is more plantar flexed in stance for UTF than AB.

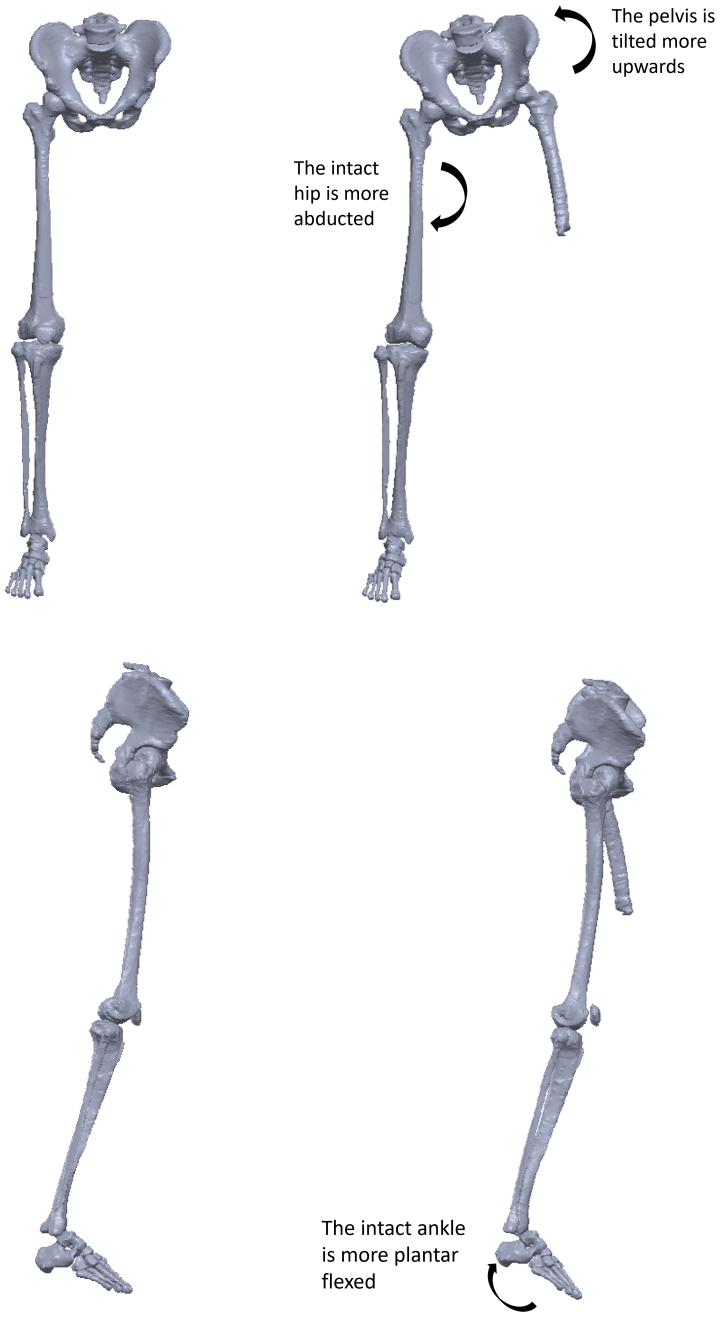
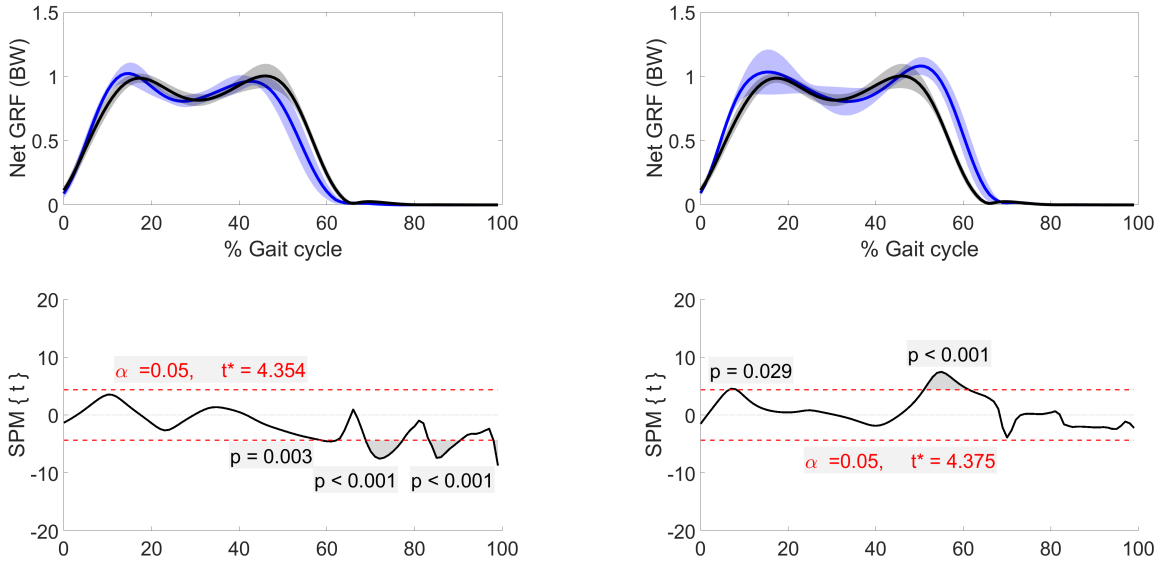


Figure 4.11: AB (left) and UTF (right) body orientations in the intact limb stance phase. Top: Front view. Bottom: Lateral view.

4.3.3 Kinetics

Figure 4.12 presents the ground reaction forces (GRF). SPM reported significant GRF differences between the prosthetic limb and AB in late stance (p=.003) and swing (p<.001). SPM also showed significant GRF differences between the UTF intact limb and AB in late stance (p<.001). When comparing discrete values in Table 4.13, the second peak of the UTF intact limb GRF was larger by 0.1 BW than the prosthetic limb (1.0 BW, p=.014).



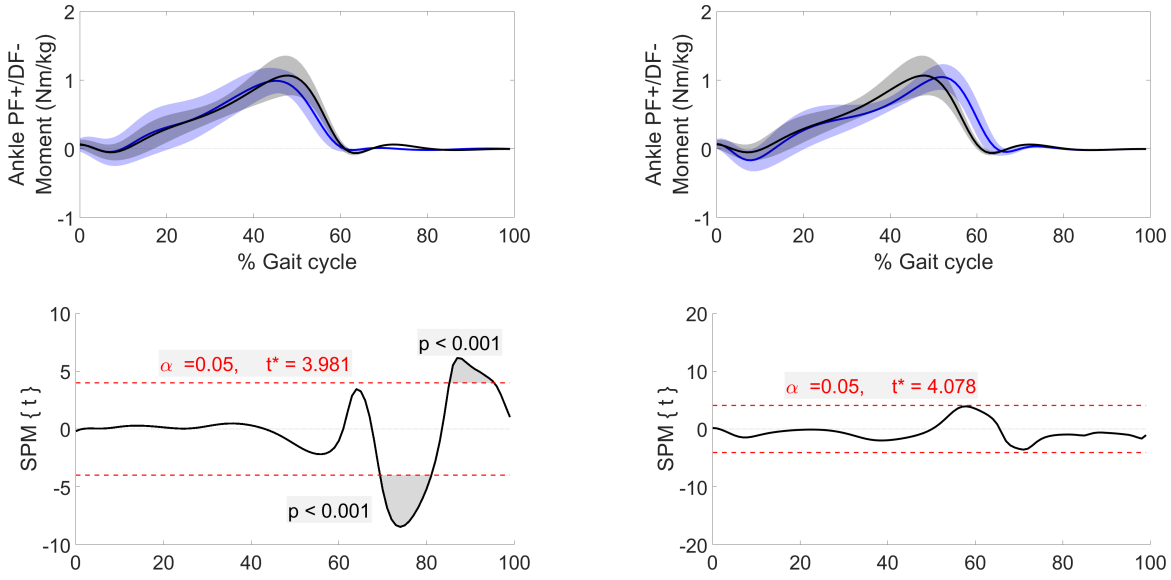
(a) Prosthetic side **(b)** Intact side

Figure 4.12: Top: Net ground reaction forces (GRF) of UTF (blue) and AB (black). Bottom: Statistical parametric mapping results.

	Unilateral transfemoral		
Biomechanical parameter	Prosthetic side Mean ± SD	Intact side Mean ± SD	Able-bodied controls Mean ± SD
First peak GRF (BW)	1.03 ± 0.08	1.06 ± 0.16	0.98 ± 0.05
Second peak GRF (BW)	0.99 ± 0.05 ****p=.014**	1.09 ± 0.07	1.01 ± 0.08

Table 4.13: Ground reaction forces (GRF).
**Statistically significant differences between UTF limbs (p<.05).

Figure 4.13 and Table 4.14 present the sagittal plane ankle moments during gait. SPM reported significant differences in the sagittal plane moments between the UTF prosthetic ankle and AB in swing (p<.001). There were no significant differences in the peak sagittal plane ankle moments between cohorts.



(a) Prosthetic side **(b)** Intact side

Figure 4.13: Top: Ankle plantar flexion (PF)/dorsiflexion (DF) moments of UTF (blue) and AB (black). Bottom: Statistical parametric mapping results.

	Unilateral transfemoral		
Biomechanical parameter	Prosthetic side Mean ± SD *Median [95% CI]*	Intact side Mean ± SD *Median [95% CI]*	Able-bodied controls Mean ± SD *Median [95% CI]*
Peak ankle dorsiflexion moment (Nm/kg)	*0.07 [0.01-0.29]*	*0.17 [0.08-0.32]*	*0.10 [0.05-0.20]*
Peak ankle plantar flexion moment (Nm/kg)	1.02 ± 0.17	1.06 ± 0.19	1.07 ± 0.28

Table 4.14: Sagittal plane ankle moments.
CI, confidence interval.

Figure 4.14 and Table 4.15 present the coronal plane intact knee moments over the course of the gait cycle, with no significant differences in the peak adduction moments between the UTF intact knee and AB. The loading rate of the UTF intact knee was larger by 1.4 Nm/(kg.s) than AB (3.4 Nm/(kg.s), p=.045).

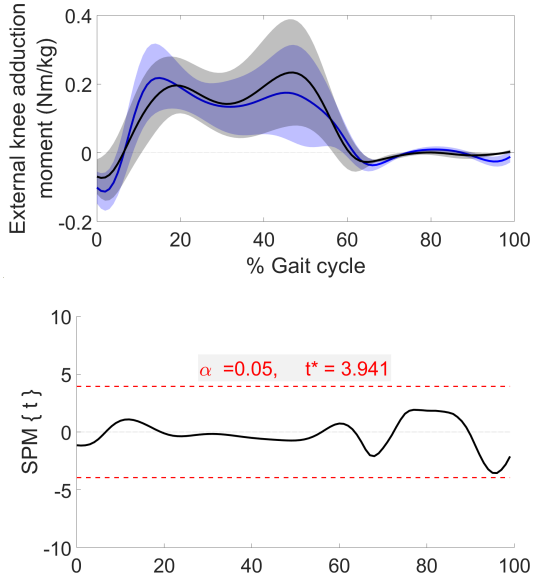
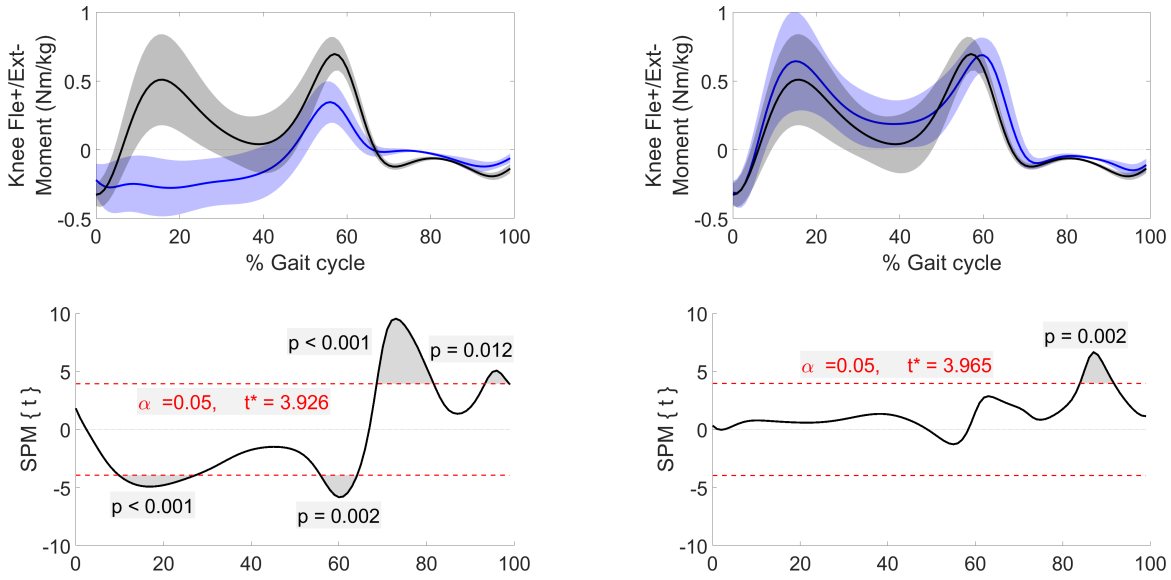


Figure 4.14: Top: Intact knee external adduction moment of UTF (blue) and AB (black). Bottom: Statistical parametric mapping results.

Biomechanical parameter	Unilateral transfemoral Mean ± SD	Able-bodied controls Mean ± SD
Peak knee adduction moment (Nm/kg)	0.28 ± 0.10	0.27 ± 0.11
Knee loading rate (Nm/(kg.s))	4.82 ± 1.75 ***p=.045**	3.44 ± 0.56

Table 4.15: Coronal plane intact knee moments and loading rate. *Statistically significant differences from able-bodied controls (p<.05).

Figure 4.15 presents the sagittal plane knee moments over the course of the gait cycle. SPM reported higher intact knee flexion moments than AB in swing (p=.002). SPM also reported lower prosthetic knee flexion moments than AB in stance (p<.001, p=.002). When comparing discrete values in Table 4.16, the prosthetic knee peak sagittal plane moments were lower by 0.5 Nm/kg than the intact limb (p<.001) and by 0.4 Nm/kg than AB (p<.001).



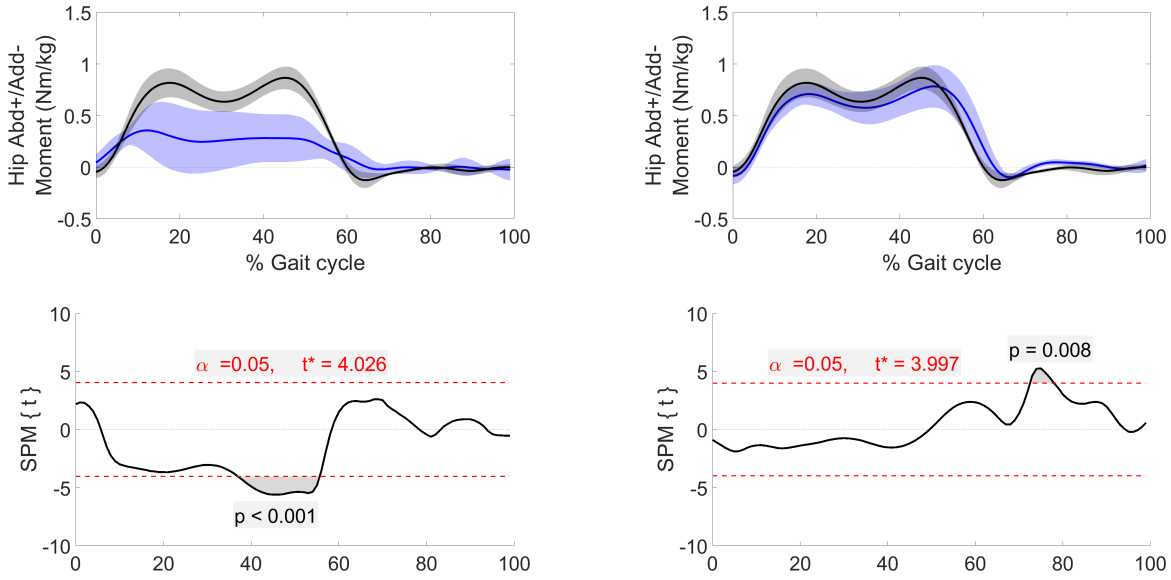
(a) Prosthetic side **(b)** Intact side

Figure 4.15: Top: Knee external flexion (Fle)/extension (Ext) moments of UTF (blue) and AB (black). Bottom: Statistical parametric mapping results.

	Unilateral transfemoral		
Biomechanical parameter	Prosthetic side Mean ± SD	Intact side Mean ± SD	Able-bodied controls Mean ± SD
Peak knee flexion moment (Nm/kg)	0.41 ± 0.11 ***p<.001** ****p<.001**	0.86 ± 0.19	0.79 ± 0.09
Peak knee extension moment (Nm/kg)	0.39 ± 0.16	0.33 ± 0.08	0.35 ± 0.10

Table 4.16: Sagittal plane knee moments.
*Statistically significant differences from able-bodied controls (p<.05). **Statistically significant differences between UTF limbs (p<.05).

Figure 4.16 presents the coronal plane hip moments over the course of the gait cycle. SPM reported lower hip abduction moments for the UTF prosthetic side than AB in stance (p<.001). The intact side hip moments were higher than AB in swing (p=.008). When comparing discrete values in Table 4.17, the prosthetic side hip abduction moments were lower by 0.5 Nm/kg than the intact side hip (p=.008) and by 0.5 Nm/kg than AB (p=.017).



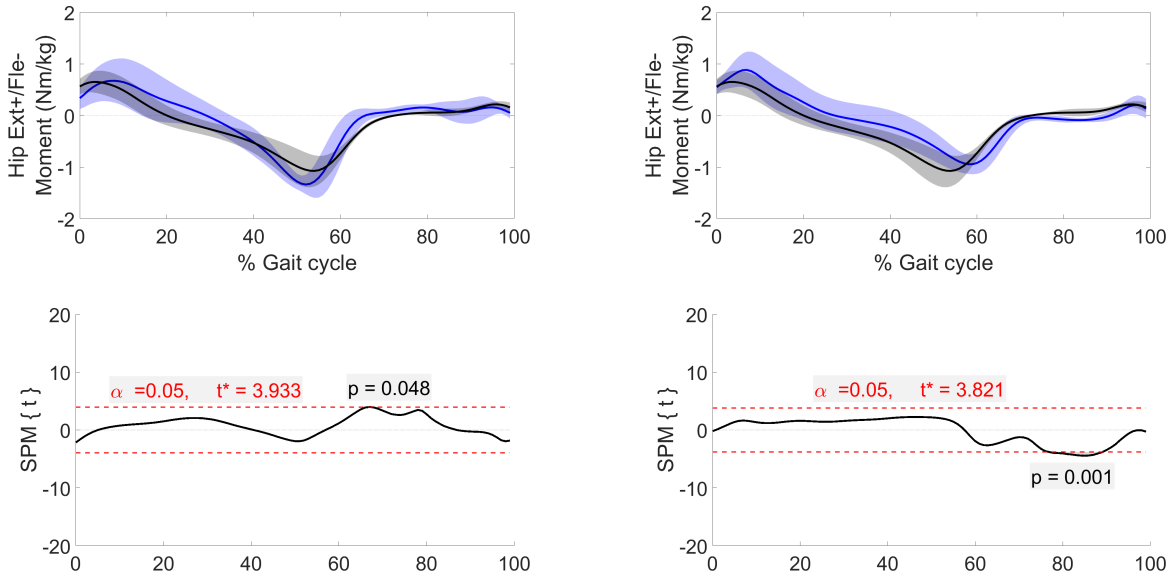
(a) Prosthetic side **(b)** Intact side

Figure 4.16: Top: Hip abduction (Abd)/adduction (Add) moments of UTF (blue) and AB (black). Bottom: Statistical parametric mapping results.

	Unilateral transfemoral		
Biomechanical parameter	Prosthetic side *Median [95% CI]*	Intact side *Median [95% CI]*	Able-bodied controls *Median [95% CI]*
Peak hip abduction moment (Nm/kg)	*0.37 [0.23-0.70]* ***p=.017** ****p=.008**	*0.84 [0.67-1.02]*	*0.89 [0.80-1.01]*
Peak hip adduction moment (Nm/kg)	*0.10 [0.04-0.17]*	*0.14 [0.09-0.19]*	*0.12 [0.07-0.21]*

Table 4.17: Coronal plane hip moments.
CI, confidence interval. *Statistically significant differences from able-bodied controls (p<.05). **Statistically significant differences between UTF limbs (p<.05).

Figure 4.17 presents the hip flexion moments over the course of the gait cycle. SPM reported different sagittal plane moments between the UTF prosthetic side hip and AB in late stance (p=.048). SPM also reported different sagittal plane moments between the UTF intact side hip and AB in swing (p=.001). When comparing discrete values in Table 4.18, the prosthetic side hip showed larger peak flexion moments by 0.5 Nm/kg than the UTF intact side (1.0 Nm/kg, p<.001), and by 0.4 Nm/kg than AB (1.1 Nm/kg, p=.017)



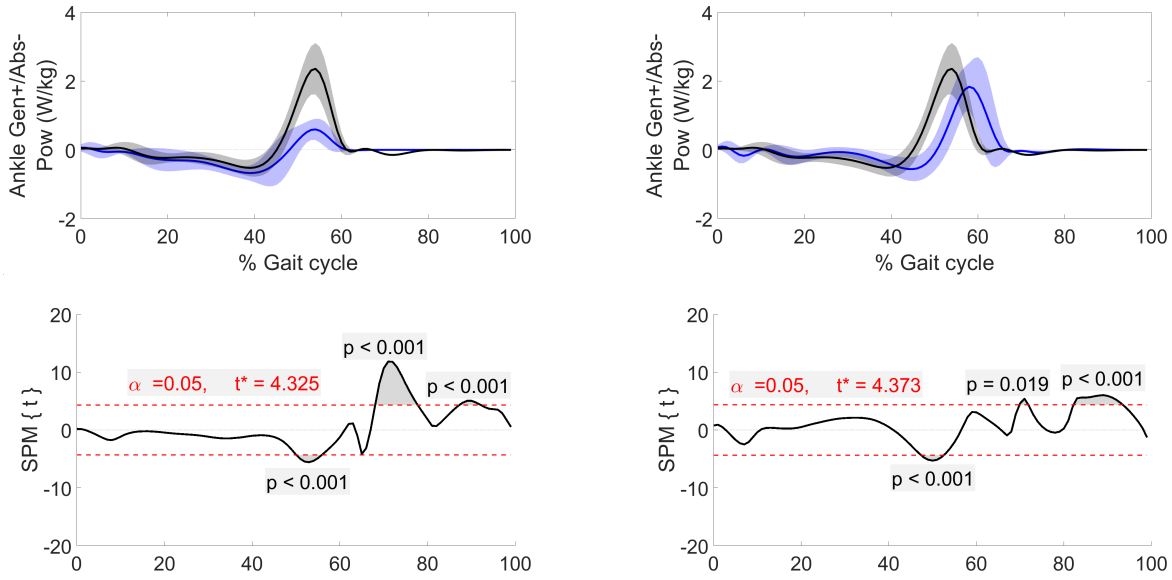
(a) Prosthetic side **(b)** Intact side

Figure 4.17: Top: Hip flexion (Fle)/extension (Ext) moments of UTF (blue) and AB (black). Bottom: Statistical parametric mapping results.

	Unilateral transfemoral		
Biomechanical parameter	Prosthetic side Mean ± SD	Intact side Mean ± SD	Able-bodied controls Mean ± SD
Peak hip flexion moment (Nm/kg)	1.49 ± 0.17 ***p=.017** ****p<.001**	0.99 ± 0.20	1.10 ± 0.32
Peak hip extension moment (Nm/kg)	0.75 ± 0.37	0.92 ± 0.31	0.66 ± 0.20

Table 4.18: Sagittal plane hip moments.
*Statistically significant differences from able-bodied controls (p<.05). **Statistically significant differences between UTF limbs (p<.05).

Figure 4.18 presents the sagittal plane ankle power. SPM reported significantly lower prosthetic ankle generated power at push-off than AB (p<.001). SPM also reported timing differences in the ankle power between the UTF intact side and AB (p<.001). When comparing discrete values in Table 4.19, the peak UTF prosthetic ankle generated power was lower by 1.4 W/kg than the UTF intact ankle (2.1 W/kg, p=.003). There were no significant differences between the peak UTF intact ankle power and AB.



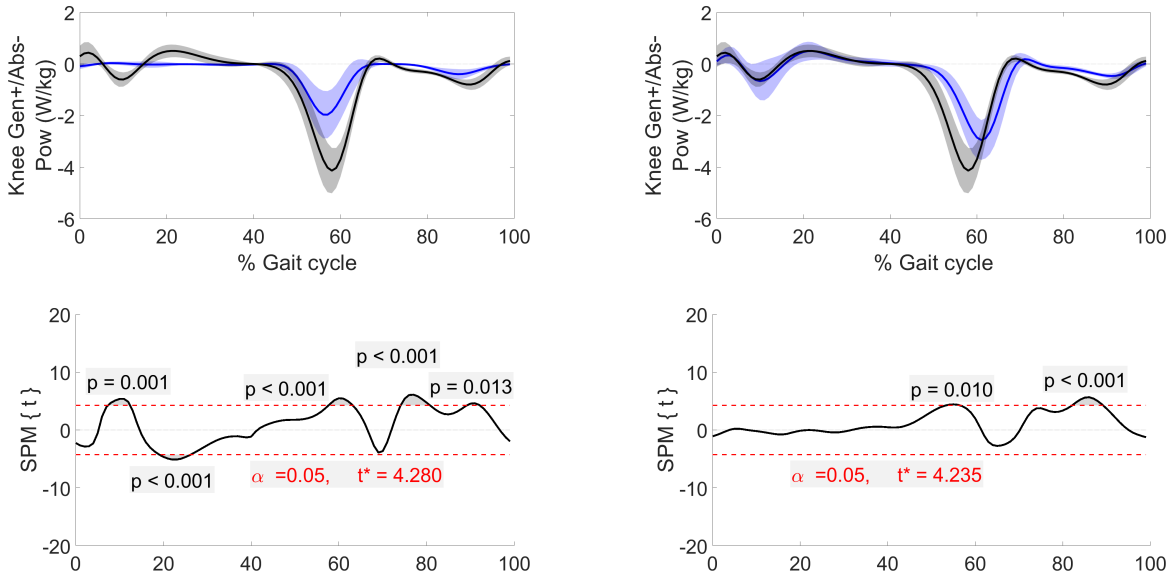
(a) Prosthetic side **(b)** Intact side

Figure 4.18: Top: Ankle generated (Gen)/absorbed (Abs) power (Pow) of UTF (blue) and AB (black). Bottom: Statistical parametric mapping results.

	Unilateral transfemoral		
Biomechanical parameter	Prosthetic side Mean ± SD *Median [95% CI]*	Intact side Mean ± SD *Median [95% CI]*	Able-bodied controls Mean ± SD *Median [95% CI]*
Peak ankle generated power (W/kg)	*0.68 [0.54-1.15]* ***p<.001** ****p=.003**	*2.05 [1.38-3.18]*	*2.28 [1.75-3.18]*
Peak ankle absorbed power (W/kg)	*0.71 [0.50-1.10]*	*0.56 [0.38-0.96]*	*0.49 [0.38-0.85]*

Table 4.19: Sagittal plane ankle power.
CI, confidence interval. *Statistically significant differences from able-bodied controls (p<.05). **Statistically significant differences between UTF limbs (p<.05).

Figure 4.19 presents the sagittal plane knee power over the course of the gait cycle. SPM reported lower prosthetic knee power than AB in stance (p=.001, p<.001) and swing (p=.013). SPM also reported lower UTF intact knee absorbed power than AB in late stance (p=.010) and swing (p<.001). When comparing discrete values in Table 4.20, the peak UTF intact knee absorbed power was lower by 1.0 W/kg than AB (4.2 W/kg, p=.045). Similarly, the UTF prosthetic knee showed lower absorbed power by 1.7 W/kg than AB (4.2 W/kg, p=.001).



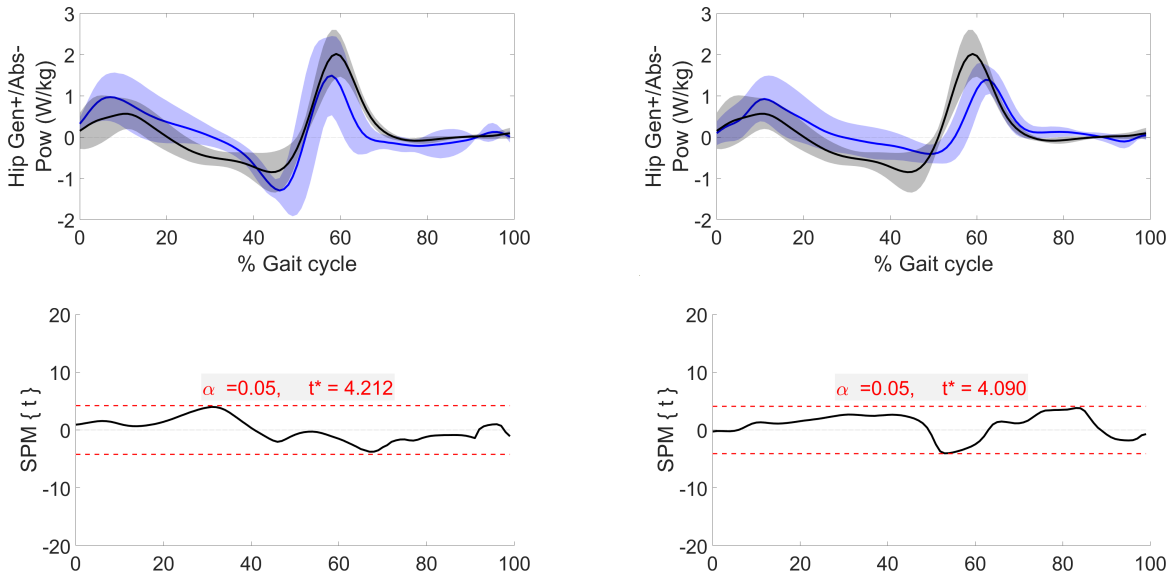
(a) Prosthetic side **(b)** Intact side

Figure 4.19: Top: Knee generated (Gen)/absorbed (Abs) power (Pow) of UTF (blue) and AB (black). Bottom: Statistical parametric mapping results.

	Unilateral transfemoral		
Biomechanical parameter	Prosthetic side Mean ± SD	Intact side Mean ± SD	Able-bodied controls Mean ± SD
Peak knee generated power (W/kg)	0.15 ± 0.08 ***p<.001** ****p<.001**	0.74 ± 0.24	0.78 ± 0.22
Peak knee absorbed power (W/kg)	2.51 ± 0.54 ***p=.001**	3.21 ± 0.67 ***p=.045**	4.22 ± 0.87

Table 4.20: Sagittal plane knee power.
*Statistically significant differences from able-bodied controls (p<.05). **Statistically significant differences between UTF limbs (p<.05).

Figure 4.20 and Table 4.21 present the sagittal plane hip power over the course of the gait cycle, with no significant differences between UTF intact side and AB. The prosthetic side hip peak absorbed power was higher by 0.9 W/kg than the UTF intact side (0.5 W/kg, p=.003) and by 0.7 W/kg than AB (0.8 W/kg, p=.017).



(a) Prosthetic side **(b)** Intact side

Figure 4.20: Top: Hip generated (Gen)/absorbed (Abs) power (Pow) of UTF (blue) and AB (black). Bottom: Statistical parametric mapping results.

	Unilateral transfemoral		
Biomechanical parameter	Prosthetic side Mean ± SD *Median [95% CI]*	Intact side Mean ± SD *Median [95% CI]*	Able-bodied controls Mean ± SD *Median [95% CI]*
Peak hip generated power (W/kg)	2.19 ± 0.71	1.68 ± 0.27	2.06 ± 0.58
Peak hip absorbed power (W/kg)	*1.44 [1.02-2.34]* ***p=.017** ****p=.003**	*0.50 [0.23-0.89]*	*0.79 [0.48-1.39]*

Table 4.21: Sagittal plane hip power.
CI, confidence interval. *Statistically significant differences from able-bodied controls (p<.05). **Statistically significant differences between UTF limbs (p<.05).

4.3.4 Joint contact forces

Figure 4.21 and Table 4.22 present the intact ankle joint contact forces over the course of the gait cycle, with no significant differences between cohorts.

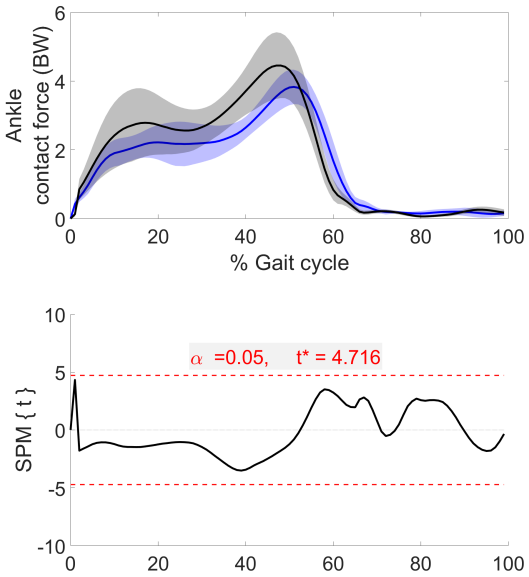


Figure 4.21: Top: Intact ankle joint contact forces of UTF (blue) and AB (black). Bottom: Statistical parametric mapping results.

Biomechanical parameter	Unilateral transfemoral Mean ± SD	Able-bodied controls Mean ± SD
First peak ankle contact force (BW)	2.48 ± 0.37	2.88 ± 0.98
Second peak ankle contact force (BW)	3.87 ± 0.47	4.53 ± 0.94
Ankle impulse (BW.s)	153.56 ± 13.75	175.92 ± 31.75
Normalised ankle impulse (BW.s/m)	115.01 ± 6.97	131.36 ± 21.54

Table 4.22: Intact ankle joint contact forces and impulse.

Figure 4.22 and Table 4.23 present the medial compartment of the intact knee joint contact forces, with no significant differences between cohorts.

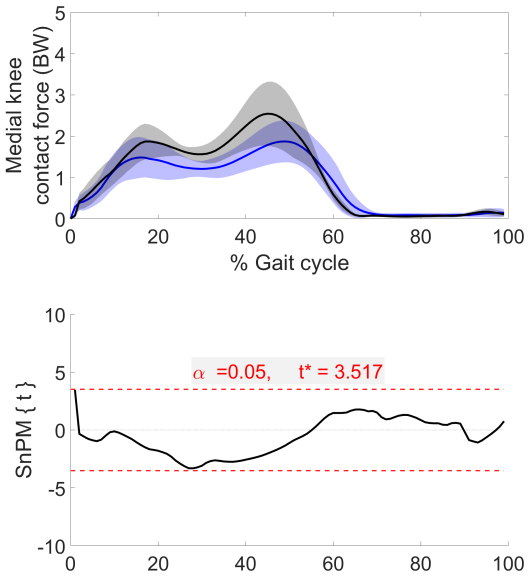


Figure 4.22: Top: Medial intact knee joint contact forces of UTF (blue) and AB (black). Bottom: Statistical parametric mapping results.

Biomechanical parameter	Unilateral transfemoral Mean ± SD	Able-bodied controls Mean ± SD
First peak medial knee contact force (BW)	1.55 ± 0.52	1.95 ± 0.42
Second peak medial knee contact force (BW)	1.97 ± 0.51	2.57 ± 0.75
Medial knee impulse (BW.s)	84.84 ± 18.48	101.63 ± 16.38
Normalised medial knee impulse (BW.s/m)	63.71 ± 13.83	72.77 ± 14.73

Table 4.23: Medial compartment of the intact knee contact forces and impulse.

Figure 4.23 and Table 4.24 present the lateral compartment of the intact knee contact forces and impulse. The UTF lateral compartment of the knee presented higher loading than AB. Specifically, the first peak of the UTF lateral compartment contact force was larger by 0.6 BW than AB (1.6 BW, p=.024), and the second peak was larger by 0.7 BW than AB. Additionally, the UTF lateral compartment impulse was larger by 27.7 BW.s than AB (103.5 BW.s, p=.038). The UTF lateral compartment normalised impulse was larger by 21.4 BW.s/m than AB (77.1 BW.s/m, p=.029).

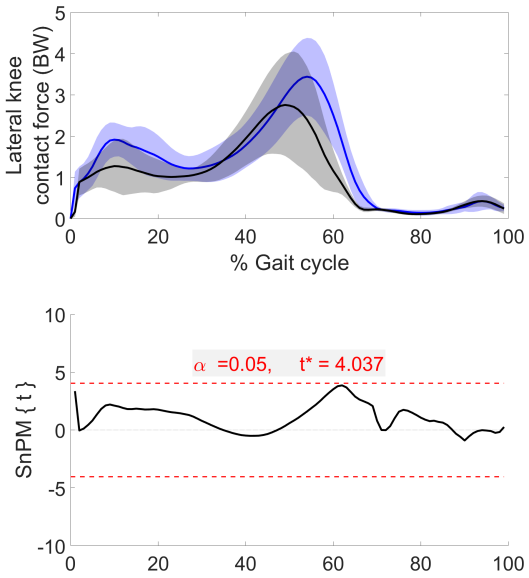


Figure 4.23: Top: Lateral intact knee joint contact forces of UTF (blue) and AB (black). Bottom: Statistical parametric mapping results.

Biomechanical parameter	Unilateral transfemoral Mean (SD)	Able-bodied controls Mean (SD)
First peak lateral knee contact force (BW)	2.10 (0.40) ***p=.024**	1.55 (0.47)
Second peak lateral knee contact force (BW)	3.51 (0.97)	2.84 (1.27)
Lateral knee impulse (BW.s)	131.22 (23.08) ***p=.038**	103.50 (26.40)
Normalised lateral knee impulse (BW.s/m)	98.45 (17.00) ***p=.029**	77.07 (18.28)

Table 4.24: Lateral compartment of the intact knee contact forces and impulse. *Statistically significant differences from able-bodied controls (p<.05).

The ratio of medial to lateral intact knee impulse in the UTF cohort was larger by 0.3 than AB (p=.001, Table 4.25).

Biomechanical parameter	Unilateral transfemoral Mean ± SD	Able-bodied controls Mean ± SD
Ratio medial knee impulse / lateral knee impulse	0.66 ± 0.13 ***p=.001**	1.01 ± 0.14

Table 4.25: Medial intact knee impulse to lateral intact knee impulse ratio. *Statistically significant differences from able-bodied controls (p<.05).

Figure 4.24 and Table 4.26 present the total intact knee joint contact forces and impulse, with no significant differences identified between cohorts.

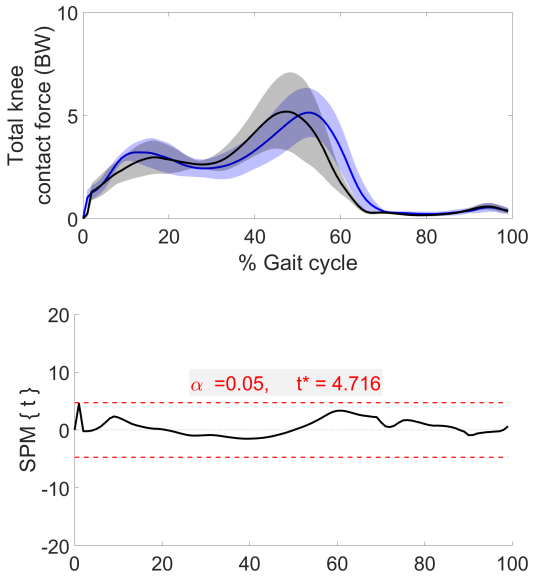
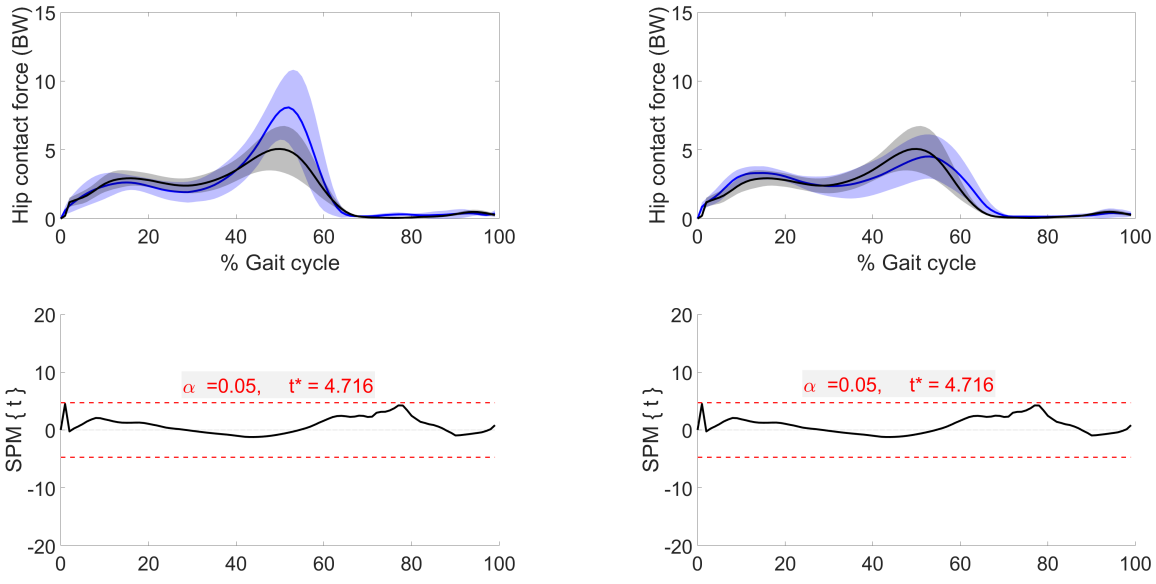


Figure 4.24: Top: Total intact knee joint contact forces of UTF (blue) and AB (black). Bottom: Statistical parametric mapping results.

Biomechanical parameter	Unilateral transfemoral Mean ± SD	Able-bodied controls Mean ± SD
First peak total knee contact force (BW)	3.65 ± 0.47	3.50 ± 0.80
Second peak total knee contact force (BW)	5.48 ± 1.30	5.41 ± 1.96
Total knee impulse (BW.s)	216.06 ± 36.59	205.13 ± 40.80
Normalised total knee impulse (BW.s/m)	162.15 ± 27.14	152.97 ± 27.20

Table 4.26: Total intact knee contact forces and impulse.

Figure 4.25 and Table 4.27 present the hip joint contact forces and impulse. The second peak of the prosthetic side hip joint contact force was larger by 3.1 BW than the intact side hip (4.6 BW, p=.003) and by 3.3 BW than AB (4.5 BW, p=.007).



(a) Prosthetic side **(b)** Intact side

Figure 4.25: Top: Hip joint contact forces of UTF (blue) and AB (black). Bottom: Statistical parametric mapping results.

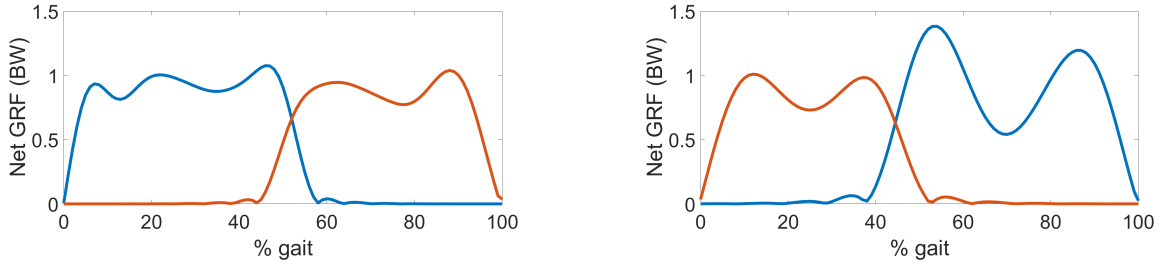
	Unilateral transfemoral		
Biomechanical parameter	Prosthetic side Mean ± SD *Median [95% CI]*	Intact side Mean ± SD *Median [95% CI]*	Able-bodied controls Mean ± SD *Median [95% CI]*
First peak HJCF (BW)	*2.82 [2.39-3.47]*	*3.59 [3.13-3.89]*	*2.94 [2.52-3.58]*
Second peak HJCF (BW)	*7.76 [6.62-10.71]* ***p=.007** ****p=.003**	*4.62 [3.14-6.29]*	*4.49 [3.45-6.87]*
HJCF impulse (BW.s)	218.87 ± 40.00	201.75 ± 45.03	194.80 ± 35.26
Normalised HJCF impulse (BW.s/m)	162.42 ± 25.10	151.01 ± 31.63	146.44 ± 26.91

Table 4.27: Hip joint contact forces and impulse.
CI, confidence interval. *Statistically significant differences from able-bodied controls (p<.05). **Statistically significant differences between UTF limbs (p<.05).

4.3.5 Case study

This section presents the functional performance results for participants UTF 1 and UTF 6. These two case studies were chosen from the available UTF cohort due to the similarity in injury type (IED), rehabilitation pathway (military), amputation level (above-knee) and prosthetic socket type (ischial containment). UTF 1 was fitted with the Rheo XC prosthetic knee and Re-Flex Rotate prosthetic foot, and UTF 6 was fitted with the Genium X3 knee and Triton prosthetic foot.

Figure 4.26 and Table 4.28 demonstrate different ground reaction forces (GRF) profiles between the two subjects. Compared to UTF 1, UTF 6 showed larger GRF asymmetry between the intact and prosthetic limbs by 9.9% for the first peak and 7.5% for the second peak GRF. UTF 6 showed larger intact side first peak GRF by 0.4 BW and larger intact side second peak GRF by 0.1 BW than UTF 1. Moreover, UTF 6 spent a larger percentage time in the intact limb stance by 4.2% than UTF 1. Finally, whilst UTF 6 showed larger intact side first peak GRF than the prosthetic side, UTF 1 presented similar first peak GRF values between the two limbs.



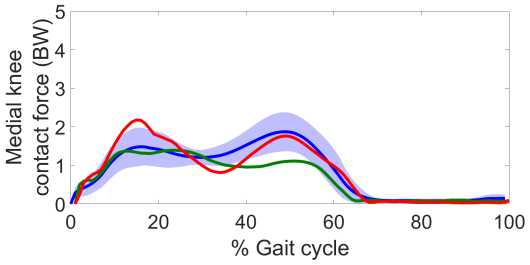
(a) UTF 1 **(b)** UTF 6

Figure 4.26: Case study GRF subjects UTF 1 and UTF 6 over the course of one complete intact and prosthetic side gait cycle. Intact side - blue. Prosthetic side - orange.

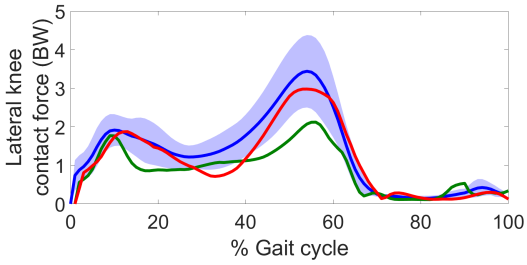
Biomechanical parameter	UTF 1	UTF 6	Percentage difference (%)
Intact side stance time (% gait cycle)	64.33	69.52	4.2
Intact side first peak GRF (BW)	0.90	1.32	46.4
Prosthetic side first peak GRF (BW)	0.99	0.98	-1.7
First GRF peak symmetry (%)	95.05	85.16	-9.9
Intact side second peak GRF (BW)	1.04	1.12	7.0
Prosthetic side second peak GRF (BW)	1.02	0.94	-7.9
Second GRF peak symmetry (%)	98.86	91.36	-7.5

Table 4.28: Case study biomechanical results.
Positive differences in intact limb characteristics and negative differences in prosthetic limb characteristics and symmetry indicate higher intact limb loading for UTF 6 than UTF 1.

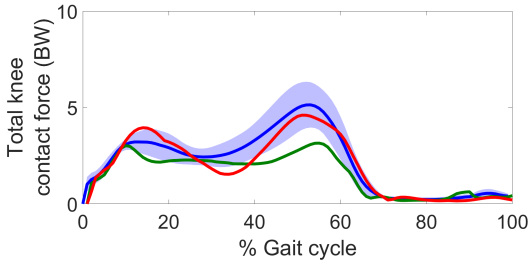
Figure 4.27 and Table 4.29 present the intact knee contact forces and impulse for subjects UTF 1 and UTF 6. UTF 1 presented lower medial, lateral and total knee contact forces and impulse than UTF 6. Additionally, UTF 1 presented the lowest lateral knee contact forces and impulse in this study's UTF cohort.



(a) Medial knee contact force



(b) Lateral knee contact force



(c) Total knee contact force

Figure 4.27: Case study results comparing UTF 1 (green) and UTF 6 (red) to the UTF cohort results (blue).

Biomechanical parameter	UTF 1	UTF 6	Percentage difference (%)
First peak medial knee contact force (BW)	1.43	2.19	53.3
Second peak medial knee contact force (BW)	1.23	1.76	43.8
Medial knee impulse (BW.s)	67.79	84.95	25.3
Normalised medial knee impulse (BW.s/m)	48.76	66.45	36.3
First peak lateral knee contact force (BW)	1.79	1.88	5.0
Second peak lateral knee contact force (BW)	2.15	2.98	38.7
Lateral knee impulse (BW.s)	87.32	113.72	30.2
Normalised lateral knee impulse (BW.s/m)	62.83	88.91	41.5
First peak total knee contact force (BW)	3.22	4.07	26.4
Second peak total knee contact force (BW)	3.38	4.74	40.6
Total knee impulse (BW.s)	155.12	198.68	28.1
Normalised total knee impulse (BW.s/m)	111.60	155.37	39.2

Table 4.29: Case study joint loading results.
Positive differences indicate higher intact knee loading for UTF 6 than UTF 1.

4.4 Discussion

This study provides an in-depth biomechanical analysis of unilateral above/through-knee amputee (UTF) musculoskeletal system function and loading during level-ground walking with microprocessor-controlled prosthetic knees (MPK), dynamic response feet and prosthetic sockets compared to able-bodied persons (AB). Musculoskeletal modelling was used to understand the high incidence of osteoarthritis reported for this amputee population (Burke et al. 1978, Norvell et al. 2005). The key findings of this chapter are presented in Table 4.30.

1. UTF showed similar walking speeds and cadence to AB.
2. UTF showed larger step widths by 0.05 m than AB.
3. UTF showed larger intact ankle plantar flexion by 7.4° than AB.
4. Microprocessor prosthetic knees showed lower knee flexion angles in early stance by 12.5° than AB.
5. UTF showed larger pelvic obliquity by 2.5° than AB.
6. UTF abducted both hips more than AB in stance.
7. The UTF intact limb step lengths were shorter by 0.1 m than the prosthetic limb step lengths.
8. UTF showed longer stance time (by 6.0%) and higher ground reaction forces (by 0.1 BW) on the intact limb than the prosthetic limb.
9. UTF showed higher intact knee loading rate by 1.4 Nm/(kg.s) than AB.
10. The UTF intact knee absorbed power was lower by 1.0 W/kg than AB.
11. The UTF lateral compartment of the knee joint presented higher first peak (by 0.6 BW), second peak (by 0.7 BW), impulse (by 27.7 BW.s) and normalised impulse (by 21.4 BW.s/m) than AB.
12. Prosthetic feet with shock absorbing components improve ground reaction force symmetry (by 9.9%) and intact knee contact forces (by 0.8 BW) and impulse (by 26.4 BW.s).
13. The UTF prosthetic side hip showed higher second peak contact force by 3.3 BW than AB.

Table 4.30: Key findings of the UTF musculoskeletal function and loading.

UTF presented similar functional abilities to AB, as determined by the similar walking speeds and cadence between cohorts. This demonstrates the ability of active traumatic lower limb amputees to achieve high levels of function, close to the pre-injury ones. However, compensatory strategies were required for successful task completion. Firstly, as previously seen in the literature, UTF adopted larger step widths in order to better mechanically recruit the abductor muscles, and improve stability and power production during gait (Jarvis et al. 2017, Chang et al. 2011). This is in agreement with this study's findings, which showed that whilst AB adducted the hip during stance, UTF abducted both the prosthetic and intact side hips at this stage of the gait cycle. However, the step width parameter has been shown to be a strong predictor of metabolic cost during level-ground walking (Weinert-Aplin et al. 2017). Therefore, the observed larger step

widths came at the cost of higher metabolic cost than AB, in concordance with previous literature (Jarvis et al. 2017).

Despite its advanced design, the full prosthesis system, consisting of the prosthetic knee, foot and socket, is not able to fully replicate the complex functions of its biological counterpart. The MPK unit presents functional limitations, as observed in this study's results, where the MPK unit allowed for a minimal degree of knee flexion in early stance. Additionally, the peak prosthetic knee absorbed power was lower by 41% than the biological knee due to the lower prosthetic knee sagittal plane moments. Similarly, although the dynamic response foot is considered to be at the high-end of the spectrum of prosthetic feet designs, it is still not able to offer the same function as the AB foot, as demonstrated in this study by the lower prosthetic ankle plantar flexion angles by 37% and maximum generated power by 66% than AB, as seen in the literature (Jarvis et al. 2020). This limitation can be overcome by improved passive joint designs or by using powered prostheses, which have been shown to provide greater power production capabilities, close to those of persons without limb loss (Grimmer et al. 2016). However, this type of prosthetic devices is not yet commonly prescribed. Interestingly, the UTF peak intact knee absorbed power was lower than AB. As the sagittal plane moments were similar between the UTF intact knee and AB, the lower absorbed power was a consequence of the lower intact knee angular velocity in late stance, which occurs in the early stance phase of the prosthetic limb gait cycle. This gait pattern might be due to lack of proprioception in the prosthetic limb, which caused UTF to slow down the intact knee sagittal plane motion in the beginning of the prosthetic limb gait cycle to ensure stability by having the prosthetic foot in full contact with the ground. As the intact limb has proprioceptive mechanisms, this gait pattern was not adopted on the prosthetic side, where the knee showed similar angular velocity to AB. The lack of proprioception can be overcome by use of osseointegrated prostheses, and future work could investigate this.

Prostheses were anchored to the residuum through the use of prosthetic sockets, which do not allow for the direct transmission of axial loads through the femur, and instead distribute the force to the ischium bone or gluteus muscles for stability (Muller 2016). Although stable, this weight distribution may contribute to socket discomfort (Fatone et al. 2021) and pain. If the prosthetic socket and liner fit is not optimal, the amputee might face difficulty in stabilizing the stump in the prosthetic socket, therefore being unable to make full use of the advanced function of MPK units and dynamic feet. Due to the limited functionality of the prosthetic components, insecurity with the prosthesis, pain or socket discomfort, UTF increased the reliance on the intact limb for successful ambulation. This is supported by the findings of this study. Firstly, the percentage time spent in the stance phase of the intact limb gait cycle was larger than the prosthetic limb and persons without limb loss. Secondly, UTF walked with shorter intact side step lengths than the prosthetic side. The uneven step lengths were adopted so that participants could transfer the bodyweight quickly from the prosthetic to the sound limb for stability.

Stability during ambulation is dependent on the prosthetic design. The high incidence of

falls (commonly caused by trips (Chen et al. 1991)) in the UTF population is larger than the unilateral transtibial amputee (UTT) population by 43% (Gauthier-Gagnon et al. 1999), and has been associated with low prosthetic toe clearance (Riveras et al. 2020). It is known that single-axis microprocessor knees provide lower toe clearance than the biological knee and polycentric knees (Gard et al. 1996), which allow for shank shortening (Bellmann et al. 2020). In order to create clearance needed for the prosthetic toe, this study's UTF cohort simultaneously adopted two different movement strategies: greater vaulting and pelvic obliquity in the swing phase of the prosthetic limb gait cycle. Vaulting is defined by higher body elevation, and characterized by excessive plantar flexion angles of the sound ankle (Drevelle et al. 2014). The current UTF cohort presented significantly larger intact ankle plantar flexion angles at the push-off phase of the gait cycle by 54% than AB. This observation demonstrated that UTF elevated their body during swing.

In addition to vaulting, UTF showed higher vertical height of the prosthetic side hip in the prosthetic side swing phase, which occurred when the contralateral limb was in stance. The ability to reduce pelvic obliquity (coronal plane pelvic motion) relies on the ability to flex the hip whilst concurrently flexing the knee and plantar flexing the ankle in swing (Whittle 2006). However, as MPK units and dynamic feet constrained the ability to achieve this coupling mechanism, UTF presented larger peak-to-peak pelvic obliquity by 35% than AB to further increase toe clearance for enhanced stability. Whilst larger pelvic motions allow for the ability to successfully ambulate with prostheses, they might contribute to spine muscle overload and low back pain (Hendershot & Wolf 2014, Davis & Marras 2000). Future work could investigate the upper body compensatory mechanism to comprehensively understand the loading of the lumbar spine and its effect on low back pain in the UTF population.

The higher vertical height of the prosthetic side hip, together with the excessive plantar flexion of the sound ankle, shifted the centre of mass laterally towards the intact limb in stance. This movement strategy led to lower prosthetic limb ground reaction forces than AB, which in turn led to higher intact limb loading, as previously seen in the literature (Pruziner et al. 2014). The asymmetry and higher loading of the sound limb is supported by the larger second peak of the ground reaction forces by 11% than the prosthetic limb.

Unilateral lower limb amputees are at high risks of intact knee osteoarthritis (Norvell et al. 2005, Burke et al. 1978), and the external knee adduction moments and loading rates have been suggested to be indicators of knee osteoarthritis presence (Crossley et al. 2012, Manal et al. 2015) and progression (Miyazaki et al. 2002). Therefore, high intact knee adduction moments were expected. However, whilst the UTF intact knee loading rate was larger by 40% than AB, there were no significant differences in the peak external knee adduction moments between cohorts. Conversely, a previous study identified lower knee adduction moments for military UTF than military AB matched controls (Russell Esposito et al. 2015). Nonetheless, the biomechanics of AB military personnel might differ from that of the civilian population due to the higher activity levels and functional demands, and future work could investigate these differences.

Ground reaction forces and joint moments may not be sufficient for the in-depth analysis of joint loading as these measures do not account for muscle forces. Muscular activation, which contributes to joint contact forces, changes post-amputation due to the newly adopted compensatory strategies needed to meet prosthetic and anatomical requirements. Therefore, musculoskeletal modelling was required to analyse joint contact forces. Expectedly, this study's UTF cohort showed higher knee contact forces than AB controls. The excessive plantar flexion of the intact ankle increased the recruitment of the main plantar flexor muscles (soleus, gastrocnemius). As the gastrocnemius originates on the femoral epicondyles, its increased activation inevitably contributed to higher loading of the knee joint. Whilst there were no significant differences in the loading of medial compartment of the knee between UTF and AB, the first and second peaks of the lateral knee contact forces was larger for the UTF cohort by 0.6 BW (from 1.6 BW for AB) and 0.7 BW (from 2.8 BW for AB), respectively. Moreover, the UTF lateral knee impulse (loading dose) was larger by 28% than AB. The medial to lateral knee loading dose ratio was significantly lower for UTF than AB, showing that the higher knee loading was localized to the lateral compartment. The high and repetitive loading might lead to knee joint degeneration in the long term (Ewers et al. 2001, Kerin et al. 2003). A previous study demonstrated that higher knee adduction moment impulse, and not peak knee adduction moment, is linked to greater cartilage loss in the knee over time (Bennell et al. 2011). As joint contact loading has not been previously investigated in the UTF population, it is yet not clear whether the maximum joint contact force or loading impulse has a larger effect on joint health. Direct causal links between mechanical loading and biological changes in the cartilage are not well understood. Nonetheless, the larger knee loading rate and lateral knee contact forces and impulse indicate that UTF might be more susceptible to lateral knee osteoarthritis, as opposed to UTT who are susceptible to medial knee osteoarthritis (Ding et al. 2020). Future work could provide a detailed comparison of UTT and UTF walking patterns and joint loading profiles in order to understand the incidence of knee osteoarthritis in the two amputee populations.

Finally, in order to achieve the required larger prosthetic step lengths for stability, UTF increased the prosthetic side hip extension angles at the end of stance. The created larger hip flexion moment on the prosthetic side required larger effort from the hip muscles. Future work could investigate muscle forces and identify overworked muscles in the UTF population. The sole reliance on the muscles spanning the prosthetic side hip for propulsion, without the neural capability to control the prosthesis, led to larger second peak of the hip joint contact force by 68% than AB. The mechanism of hip osteoarthritis development is not known for lower limb amputees. Nonetheless, high mechanical forces may create damage to the joint and contribute to the development of mechanically driven osteoarthritis (Felson 2013). However, when ischial containment sockets are used, the load might be transferred through the ischium, thus explaining the prevalence of osteopenia in the UTF population (Kulkarni & Adams 1998, Sherk et al. 2008). Bone mineral density cannot be quantified using the biomechanical tools presented in this thesis, and future work could use dual energy x-ray absorptiometry to assess the femoral neck bone health in the UTF amputee population.

4.4.1 Case study discussion

The case study results showed very different loading profiles for two participants with similar amputation type and reason, rehabilitation pathway and prosthetic socket type. However, the prosthetic knees and feet were different between subjects. UTF 6 was fitted with the microprocessor Genium X3 prosthetic knee and Triton dynamic response foot. UTF 1 was fitted with the microprocessor Rheo XC knee and Re-Flex Rotate prosthetic foot. The primary difference between the two subjects concerns the loading distribution between the prosthetic and intact limbs. Subject UTF 6 showed higher intact limb ground reaction forces than the prosthetic limb, as opposed to UTF 1 who showed improved loading symmetry between limbs. The symmetry was achieved through an improved reliance on the prosthetic limb during gait, with lower time spent in the intact limb stance phase. The difference may be attributed to the prosthetic foot UTF 1 was fitted with: Re-Flex Rotate is a high-performance prosthetic foot that protects the amputated limb by dampening rotational and vertical forces. The ability to absorb high-levels of rotational and vertical shock inevitably resulted in improved reliance on the prosthetic limb and minimisation of intact limb loading, which in turn led to lower medial, lateral and total intact knee contact forces and impulse. As the Triton prosthetic foot does not possess these features, UTF 6 presented loading asymmetry and higher intact knee joint loading than UTF 1. This finding demonstrates the importance of the type of prosthetic foot design for transfemoral amputees, and that prosthetic feet with in-built shock absorbing components might enhance comfort and long-term musculoskeletal health for high-functioning lower limb amputees.

4.5 Limitations

This study has a number of limitations. Firstly, the small number of participants may limit the use of these findings to a wider amputee population, and a greater sample size is required to reach strong statistical power. However, the cohort size was as large as could be achieved. Secondly, whilst five study participants were former military personnel, two study participants were part of the civilian population, and the study did not discriminate between the two populations or reasons of amputation. The different rehabilitation protocols and prior exercise history in the two populations might have had an effect on the observed functional outcomes. Nonetheless, all participants sustained traumatic amputations and had an activity level of K3 or higher. Additionally, the study did not discriminate between levels of amputations, and there might be biomechanical differences between above- and through-knee amputees. The end load bearing capabilities of through-knee amputees might improve the reliance on the prosthetic limb and so, improve symmetry during gait. Through-knee amputations have been shown to improve performance and quality of life compared to above-knee amputations (Penn-Barwell 2011). Future work could investigate the differences in musculoskeletal function and loading between traumatic unilateral through- and above-knee amputees.

There are also limitations to the modelling methods of this study. The anatomical datasets used in the musculoskeletal modelling pipeline were not based on their own

anatomy. The articular joint geometry and muscle parameters of the intact limb were obtained through linear scaling to able-bodied models (Ding et al. 2019). Similarly, the anatomical information of the amputated limb was obtained through linear scaling to a limb from the bilateral above/through-knee (BTF) anatomical dataset developed in Chapter 2. However, the higher functional demands of the UTF intact limb might lead to muscular volume adaptations and different muscle parameters from able-bodied persons. Although this has been demonstrated for UTT and BTF amputees (Henson et al. 2021), UTF muscular adaptations have not been investigated. Future work could build an anatomical dataset of subject-specific UTF models. A sensitivity analysis of the musculoskeletal model was not performed; future work could investigate the dependency of the input parameters on the output variables. Other musculoskeletal modelling limitations are presented in Chapter 2 and Chapter 3.

4.6 Conclusion

Although high-functioning traumatic UTF amputees achieved similar activity levels to those of persons without limb loss, compensatory movement strategies were required for successful task completion. UTF showed higher functional demand of the intact limb during gait. The observed asymmetry in this amputee population and the repetitive nature of walking may increase the risk of lateral knee osteoarthritis. Mitigation strategies need to be proposed to improve long-term musculoskeletal health, whilst maintaining optimal functional levels. The type of prosthetic design may have an influence on the amputee musculoskeletal function and loading, and the following chapters will investigate this.

Chapter 5

Biomechanical differences between high- and low-cost prostheses for transfemoral amputees

Whilst amputees in high-income countries have access to state-of-the art high-cost microprocessor prosthetic knees, amputees in low-to-middle-income countries lack the financial resources to cover the cost of these. The International Committee of the Red Cross (ICRC) developed a low-cost polycentric prosthetic knee for use in resource-limited environments. However, the ICRC knee has not been evaluated based on performance metrics of gait. This chapter investigates functional abilities and loading of unilateral above/through-knee traumatic amputees walking with microprocessor and ICRC prostheses, and identifies the design features that should be considered in the development of passive prosthetic knees. Addressing the hypothesis introduced in Chapter 4, the results demonstrate that prosthetic design choices influence amputee functional abilities and musculoskeletal system loading. The findings form the basis of the work done in the later chapters.

5.1 Introduction

The 2020 Global Burden of Disease estimated that there were 28.9 million unilateral lower limb traumatic amputees, with the highest prevalence recorded in East and South Asia, followed by Western Europe (Mcdonald et al. 2020). Reasons of amputations included road traffic accidents, war conflicts and falls (Mcdonald et al. 2020, Edwards et al. 2015). Return to movement after limb loss is achieved through intensive rehabilitation and use of prosthetic devices. As detailed in Chapter 4, compensatory strategies required for successful task completion may introduce detrimental functional demands of the intact limb of unilateral above/through-knee amputees (UTF). Common musculoskeletal disorders in this amputee population include osteoarthritis (Burke et al. 1978, Norvell et al. 2005), osteopenia (Rush et al. 1994) and low-back pain (Ephraim et al. 2005).

Appropriate prosthesis prescription may ensure optimal musculoskeletal function and health. Amputees in high-income countries have satisfactory access to prosthetic devices and rehabilitation services. Specifically, British military amputees undergo comprehensive rehabilitation at the Defence Medical Rehabilitation Centre UK, with access to the most advanced prostheses. Conversely, over 75% low-to-middle-income countries (LMICs) have no prosthetics and orthotics (P&O) training programmes (Gupta et al. 2011), and face systematic challenges arising from high demand and low supply of prosthetic devices. It is estimated that 29 million people require P&O services in LMICs (Ikeda et al. 2014), the need being over four times higher than high-income countries. However, the World Health Organization estimates that only 5-15% amputees receive prosthetic devices (ATscale 2020).

Prosthetic technology for above- and through-knee amputees has seen considerable developments, with a wide range of commercially available prosthetic knees. At the high end of the spectrum, the high-cost monocentric microprocessor prosthetic knees (MPK) can reproduce the eccentric function of the quadriceps at heel strike and hamstrings in terminal swing, as well as the power absorption phases of able-bodied gait (Czerniecki 1996). MPK units allow for variable walking speeds by adjusting the knee damping to the amputee's gait. The most advanced MPK unit design is Genium X3 (Ottobock, Germany), which costs £50,000. MPK units are commonly fitted with dynamic response feet such as the high-cost Triton Low Profile (Ottobock, Germany), Talio (Ottobock, Germany) and Echelon (Blatchford, UK). Dynamic response feet provide energy return capabilities, optimal flexibility and rollover function that meet the demands of highly active prosthetic users. These are generally preferred over low-cost solid-ankle-cushioned-heel (SACH) feet, which present limited dorsiflexion capabilities and push-off power. SACH feet do not allow for variable cadence and walking speeds, and are suitable for amputees who ambulate at low to medium impact levels (Steeper Group 2022). SACH feet are commonly used in resource-limited environments as the manufacturing process can be completed using local materials (Meanley 1995). However, the robustness of these prosthetic feet may not be appropriate for the requirements of highly active users. A previous study showed that common SACH feet used in developing countries failed the strictest International Organization for Standardization (ISO) tests for safety and strength (ISO10328),

where the failure was due to permanent forefoot deformations (Jensen & Treichl 2007).

Previous research focused on the analysis of lower limb amputee function with high-cost microprocessor and mechanically-controlled prosthetic knees (Jarvis et al. 2017, 2020, Eberly et al. 2014, Uchytil et al. 2014). The selection of MPK units and dynamic response feet over non-computerised knees and SACH feet is recommended for UTF in order to be able to achieve faster walking speeds on level ground and uneven terrains, metabolic efficiency and confidence with the prosthesis (Stevens & Wurdeman 2019). Additionally, previous studies have demonstrated that microprocessor knees introduce more natural gait patterns (Eberly et al. 2014, Uchytil et al. 2014) and improve gait symmetry (Kaufman et al. 2012) compared to simpler mechanical prosthetic knee designs. Whilst amputees in high-income countries have access to high-cost state of the art monocentric MPK, amputees in LMICs lack financial resources to cover the cost of these prosthetic devices. Moreover, the design development of prosthetic devices is concentrated in European, North American and East Asian countries, and evaluated against the specifications and requirements in developed areas. This is despite the fact that the vast majority of traumatic amputees are in limited resources environments. High-cost prosthetic knees are generally not appropriate for an LMIC environment, as they often present limited range of motion, need regular charging, and may not be waterproof or dustproof.

As a solution, the International Committee of the Red Cross (ICRC) has developed an affordable prosthetic knee for transfemoral amputees and provided 1015 prostheses in 2020 in Cambodia, where landmines and explosive remnants of war often lead to amputations (Physical Rehabilitation Programme 2020). The ICRC knee is a mechanical four-bar polycentric knee joint whose instantaneous center of rotation is positioned more posteriorly and superiorly than the mechanical axes when the knee is in the fully extended position. This feature improves stability in stance and the ability to efficiently control the residual muscles, with less effort than a knee with a simple hinge mechanism (Radcliffe 1994, 1977). Polycentric knees provide shank shortening and higher toe clearance in mid-swing compared to monocentric prosthetic knees (Bellmann et al. 2020). This is beneficial as low critical toe clearance values have been associated with risks of tripping (Riveras et al. 2020) due to the small distance between the ground and toe. The ICRC knee uses a conventional extension assist mechanism that links one of the bars to the body of the prosthesis. This design feature introduces a singularity in the delivery of the spring action: past a certain knee flexion angle, the spring pushes towards flexion. The low-cost ICRC polycentric knee joint has not been evaluated based on performance metrics of gait.

The aim of this chapter is to compare the effect of walking with high-cost prostheses (MPK units with dynamic response feet) and low-cost prostheses (ICRC polycentric knees with SACH feet) on amputee function and loading. This is primarily a descriptive study that provides baseline data for comparison. In addition, it is hypothesized that high-cost prostheses improve gait performance, minimize gait deviations and improve intact limb loading.

5.2 Methods

5.2.1 Data acquisition and processing

Ethical approval was obtained from the Joint Research Compliance Office and the Imperial College Research Ethics Committee (Reference 20IC6268). Two civilian and five ex-military UTF traumatic amputees (Table 5.1) took part in the study. Military amputees underwent rehabilitation at the Defence Medical Rehabilitation Centre, United Kingdom. All participants had been prosthesis users for a minimum of two years. Through-knee amputees were fitted with quadrilateral prosthetic sockets. Above-knee amputees were fitted with ischial containment sockets.

Part. No. (Gender)	Cause of amp.	Age (y)	Adj. mass (kg)	Height (m)	Amp. level	Prosth. knee	Prosth. foot
1 (Male)	IED	33	81	1.78	TF	Rheo XC	Vari-Flex
2 (Male)	Motorcycle accident	41	77	1.78	TK	Genium X3	Freedom Innovations Low Profile
3 (Male)	Motorcycle accident	66	69	1.73	TF	Orion3	Echelon VT
4 (Male)	Cancer surgery	57	73	1.65	TF	Orion3	Echelon
5 (Female)	Knee injury	55	102	1.72	TK	Genium X3	Triton Low Profile
6 (Male)	IED	47	95	1.76	TF	Genium X3	Triton 1C64 Heavy Duty
7 (Male)	Leg injury	57	94	1.76	TF	C-leg	Triton
Mean ± SD		51 ± 10	84 ± 12	1.74 ± 0.04			

Table 5.1: UTF study participants details.
IED, improvised explosive device. TF, transfemoral. TK, through-knee.

The protocol was conducted in two stages. Firstly, all study participants completed gait trials with their own prostheses, consisting of prosthetic sockets, liners, microprocessor-controlled knees (MPK) and dynamic response feet. Retro-reflective markers were placed on lower limb anatomical landmarks following the locations presented in Table 4.2, Chapter 4. Gait data were collected using a 10-camera VICON optoelectronic based motion capture system (VICON 2.10.3, Oxford Metrics Group, UK) with two force plates (Kistler Type 9286B, Kistler Instrumente AG, Winterthur, Switzerland). Each participant completed one static calibration and six level-ground walking trials at self-selected and fast speeds. The speeds were chosen by the participant. The self-selected speed walking trials were performed with complete foot placement on the force plate. Targeting effects were

minimized through the continuation of the trial until sufficient complete foot placements were achieved.

Following data collection with the participant's own prosthesis, participants were fitted with the ICRC prosthesis (ICRC knee, SACH foot, participant's prosthetic socket and liner). The ICRC prosthesis alignment was the same as that of the participant's own prosthesis. Prior to removing any prosthetic components, the position of the participant's own prosthetic knee alignment was marked on the spherical part of the proximal knee pyramid. Whilst the participant was seated, only two adjoining pyramid screws were removed to ensure the prosthetic alignment was not affected. Whilst the prosthetic socket was not changed between trials, the complete shank-foot unit was removed, without disassembling the foot from the participant's knee. The unit was swapped for the ICRC prosthesis, which used a pylon cut at the same length as the participant's prosthesis. The ICRC knee was fitted with a SACH foot of the same size as the participant's own prosthetic foot. The alignment of the SACH foot was adjusted copying the participant's own setup. Small ankle adjustments were made when the participant was in a standing position. Torques were checked with a torque wrench. Figure 5.1 presents one representative study participant fitted with the two trialled prostheses.

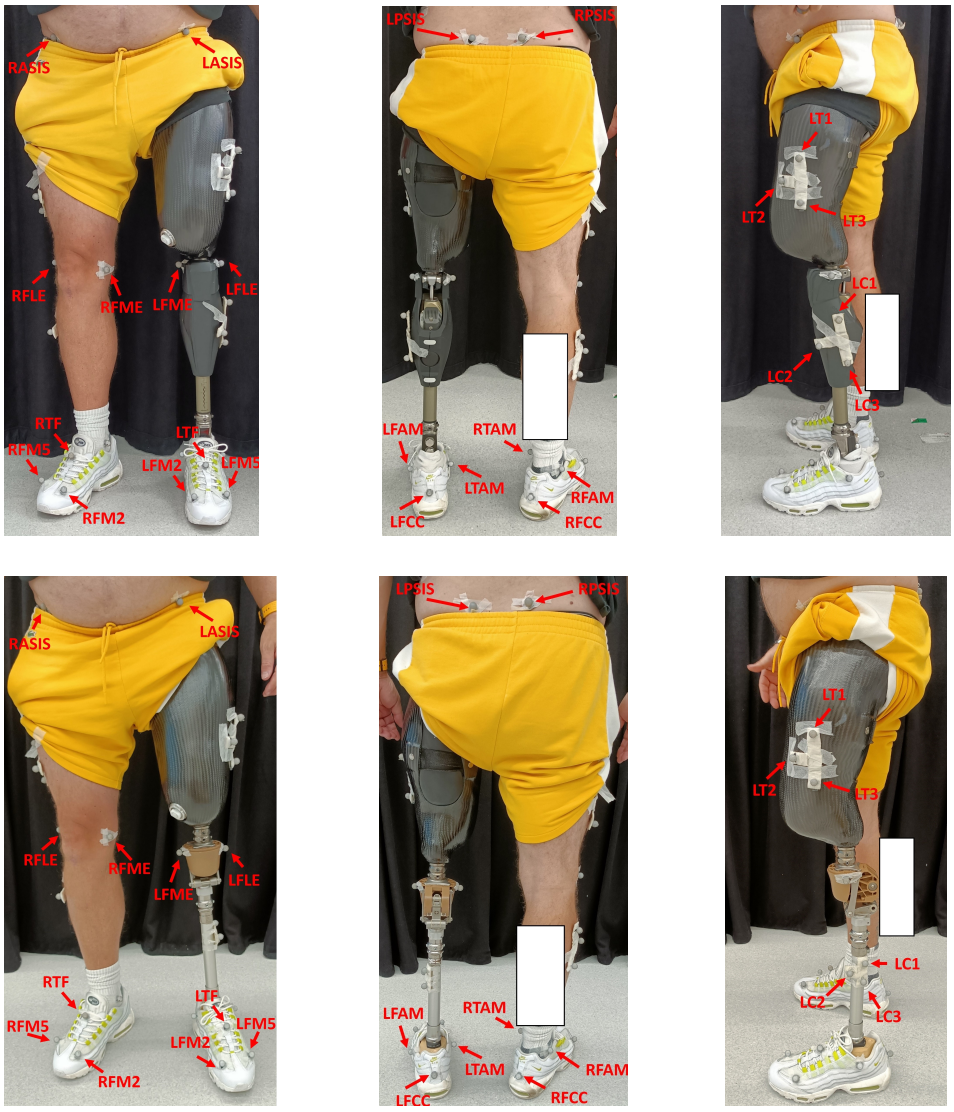


Figure 5.1: UTF study participant. The labels highlight the marker and cluster positions as listed in Table 4.2, Chapter 4. Top: MPK unit and dynamic response foot. Bottom: ICRC knee and SACH foot.

The fitting process was then followed by a familiarization period in the laboratory, where the participant was given as long as they required to walk with the prosthesis using parallel walking bars. Data collection started once the participant was comfortable walking with the ICRC prosthesis. After completing the trials, the ICRC prosthesis was removed by unscrewing the two previously specified adjoining screws, and the participant's own prosthesis was fitted back by tightening only these two screws to the manufacturer's recommended torque using a torque wrench. The alignment was double-checked with the marking made at the beginning of the trial.

The motion data were processed in VICON Nexus (VICON 2.10.3, Oxford Metrics Group, UK), as detailed in Chapter 4. Briefly, the foot strike, toe off and ipsilateral foot strike events were identified for each limb. The retro-reflective markers were labelled and the

marker trajectory gaps were filled using the rigid body filling algorithm. MATLAB (The Mathworks Inc., Natick, MA, USA) was used to filter the marker trajectory and force plate data with a zero phase-lag, fourth order Butterworth filter with 6 Hz cut-off frequency (Yu et al. 1999).

5.2.2 Anthropometry and body segment parameters

The inertial parameters of the intact segments (mass, length, centre of mass, moment of inertia) were obtained using DeLeva calculations (De Leva 1996). The inertial parameters of the MPK units and dynamic feet were obtained based on similar limbs from the dataset (Henson 2020) presented in Chapter 3. The reaction board method with moment equilibrium (Smith et al. 2014) was used to obtain the inertial parameters of the prosthetic socket, ICRC knee and SACH foot (Figure 5.2). The thigh segment consisted of the upper component of the ICRC knee that moves with the thigh, connectors, socket, liner and residual limb. The shank segment consisted of the ICRC knee part that moves with the shank, pylon and connector. The total moment of inertia of each segment was obtained by adding the moment of inertia of each component in the respective segment using the Huygens-Steiner parallel axis theorem (Haas 1928).

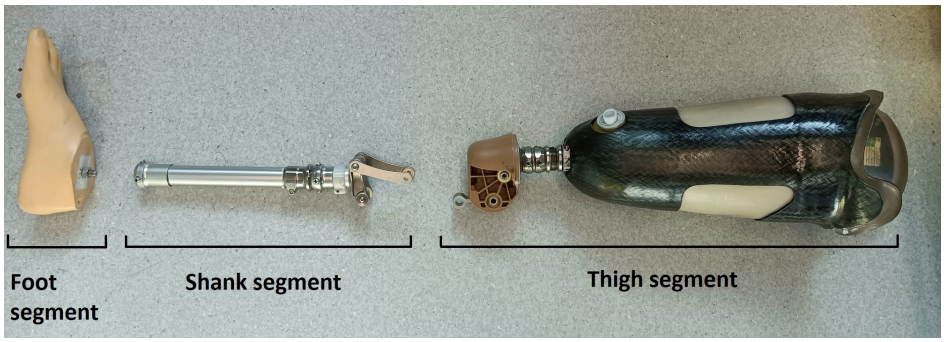


Figure 5.2: ICRC prosthesis system.

5.2.3 Musculoskeletal modelling

The musculoskeletal modelling process was performed as detailed in Chapter 4 for each prosthesis fitting case. Briefly, inverse kinematics, inverse dynamics and musculoskeletal modelling simulations were performed for the two self-selected speeds using Freebody v2.1 (Ding et al. 2016, Cleather & Bull 2015). Muscle and joint contact forces were computed using a one-step static load sharing optimisation algorithm that minimizes the sum of cubed muscle activations (Crowninshield & Brand 1981). The left and right limbs of each participant were analysed separately. The musculoskeletal model anatomical information was obtained from linear scaling to anatomical datasets available in an open-source repository (https://www.msksoftware.org.uk). The closest anatomical datasets for the intact limb models were chosen based on similar mass, gender and limb length to pelvis width ratio in order to predict ankle, knee and hip joint contact forces with minimal errors (Ding et al. 2019). Similarly, the UTF amputee models were linearly scaled to the anatomical datasets developed in Chapter 3. The closest amputee datasets were chosen

based on the most similar pelvis width, estimated intact body mass index (calculated according to literature (Tzamaloukas et al. 1994)) and stump length to pelvis width ratio to accurately predict muscle and hip joint contact forces. The same anatomical dataset was used for each model in the two prosthesis fitting conditions.

5.2.4 Data analysis

The whole-time data series for kinematics, kinetics and joint contact forces were expressed as a gait cycle percentage from 0% at heel strike to 100% at the consecutive ipsilateral heel strike, in intervals of 1% and averaged over three trials. Comparison analyses were performed between the two fitting conditions, where study participants walking with their prostheses acted as their own controls using a repeated measures design. Statistical parametric mapping (SPM) was used to statistically compare the whole time-series data (Friston et al. 2007, Papi et al. 2020, Pataky et al. 2013) between prosthesis fitting conditions. IBM SPSS Statistics 27.0.0 (IBM Corp. Armonk, NY) was used to statistically compare single-valued gait characteristics. Data normality was checked using the Shapiro-Wilk statistical test. Parametric data were compared between conditions by one-way ANOVA with repeated measures, and non-parametric data were compared using Friedman with Wilcoxon tests. p values of less than .05 were considered to indicate statistical significance.

5.3 Results

All biomechanical results are reported for the self-selected speed (with the exception of the calculated fast speed). Normally distributed data are presented as Mean ± SD and non-normally distributed data are presented as Median [95% Confidence Interval]. The whole-time data are presented over the course of the gait cycle. SPM results are presented for identification of significant differences between prosthesis fitting conditions, where grey threshold clusters indicate statistically significant differences, and red dashed lines represent critical thresholds. The gait characteristics of the prosthetic and intact limbs were statistically compared between the MPK and ICRC prosthesis fitting conditions. The MPK prosthesis consists of the participant's prosthetic socket, MPK and dynamic response foot. The ICRC prosthesis consists of the participant's prosthetic socket, ICRC knee and SACH foot. The key statistically and clinically significant results (differences of 10% or higher) are then summarised.

5.3.1 Prosthetic components parameters

Table 5.2 present the mass of prosthetic components. The ICRC prosthesis was lighter by 0.9 kg than the full MPK prosthesis (4.8 kg, $p<.001$). SACH feet were lighter by 0.5 kg than dynamic feet (1.1 kg, $p=.028$). The ICRC shank segment was lighter by 1.3 kg than MPK (1.9 kg, $p=.018$). The thigh segment was 0.7 kg heavier with ICRC than MPK (12.8 kg, $p<.001$), where the composite thigh includes the residual thigh, socket, liner, connector (and upper component of the ICRC prosthetic knee).

Parameter	MPK Mean ± SD *Median [95% CI]*	ICRC Mean ± SD *Median [95% CI]*
Full prosthesis mass (kg)	4.75 ± 0.75 ***p<.001**	3.86 ± 0.61
Foot segment mass (kg)	*1.09 [0.70-1.21]* ***p=.028**	*0.62 [0.56-0.63]*
Shank segment mass (kg)	*1.95 [1.75-2.02]* ***p=.018**	*0.64 [0.59-0.66]*
Composite thigh segment mass (kg)	12.77 ± 2.51 ***p<.001**	13.50 ± 2.51

Table 5.2: Prosthetic components masses.
CI, confidence interval. *Statistically significant differences between prostheses (p<.05).

5.3.2 Temporal and spatial gait characteristics

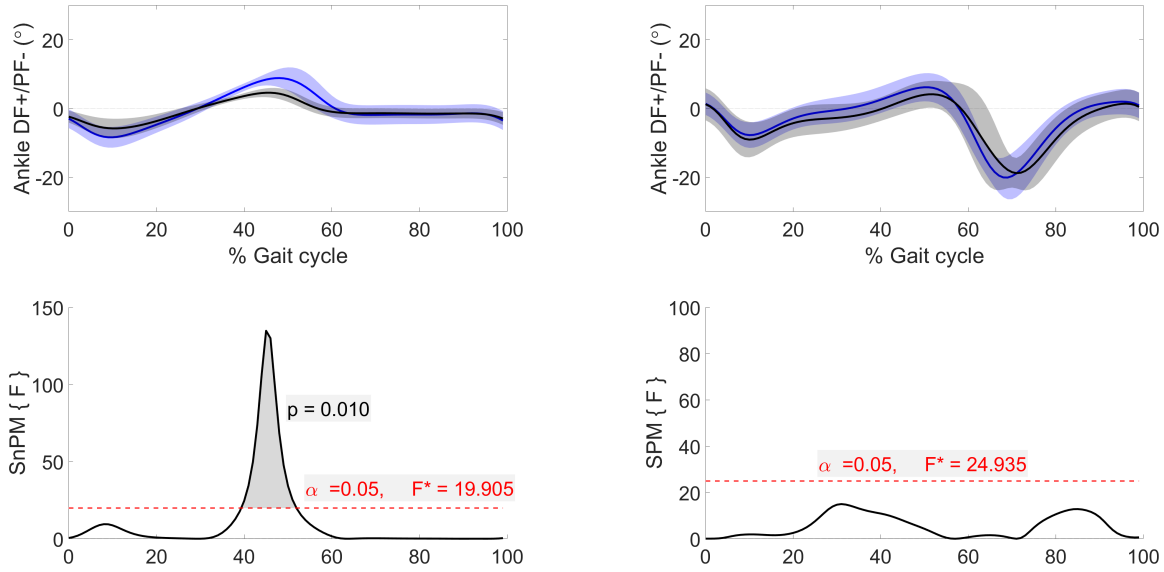
Table 5.3 presents the calculated temporal and spatial parameters of UTF walking with MPK and ICRC prostheses. The self-selected speed was lower with ICRC by 0.1 m/s than MPK (1.1 m/s, p=.032). Cadence was lower with ICRC by 7.4 steps/min than MPK (98.0 steps/min, p=.018). The gait cycle percentage spent in the ICRC prosthetic limb stance was lower by 3.6% than MPK (60.8%, p=.004). Participants walked with similar step lengths between prosthesis fitting cases. Finally, fast speeds were lower with ICRC by 0.2 m/s than MPK (1.4 m/s, p=.002). One study participant was not able to walk at fast speeds with the ICRC prosthesis.

	MPK Mean ± SD *Median [95% CI]*		ICRC Mean ± SD *Median [95% CI]*	
Biomechanical parameter	Prosthetic side	Intact side	Prosthetic side	Intact side
Step length (m)	0.70 ± 0.05	0.64 ± 0.03	0.68 ± 0.12	0.61 ± 0.05
Stride length (m)	1.35 ± 0.06	1.35 ± 0.07	1.30 ± 0.15	1.30 ± 0.15
Stance time (% gait cycle)	60.76 ± 2.33 ***p=.004**	66.76 ± 1.80 ***p=.031**	57.18 ± 2.51	69.30 ± 3.17
Self-selected speed (m/s)	1.12 ± 0.08 ***p=.032**		1.00 ± 0.13	
Cadence (steps/min)	*98.02 [94.94-106.54]* ***p=.018**		*90.62 [88.54-96.47]*	
Step width (m)	0.16 ± 0.04		0.17 ± 0.04	
Gait SI (%)	94.25 ± 3.30		92.37 ± 5.31	
Fast speed (m/s)	1.37 ± 0.19 ***p=.002**		1.16 ± 0.18	

Table 5.3: Spatial and temporal characteristics (n=7, except for fast speed, where n=6). CI, confidence interval. *Statistically significant differences between prosthesis fitting cases (p<.05).

5.3.3 Kinematics

Figure 5.3 shows the sagittal plane ankle kinematics. SPM reported lower dorsiflexion angles for SACH than dynamic response feet in terminal stance (p=.010). When comparing discrete values in Table 5.4, SACH feet showed lower peak dorsiflexion by 4.7° than dynamic feet (9.5°, p<.001). Moreover, the peak SACH plantar flexion angles were lower by 4.1° than dynamic feet (8.7°, p=.028). There were no differences in the intact ankle sagittal plane angles between prosthesis fitting cases.



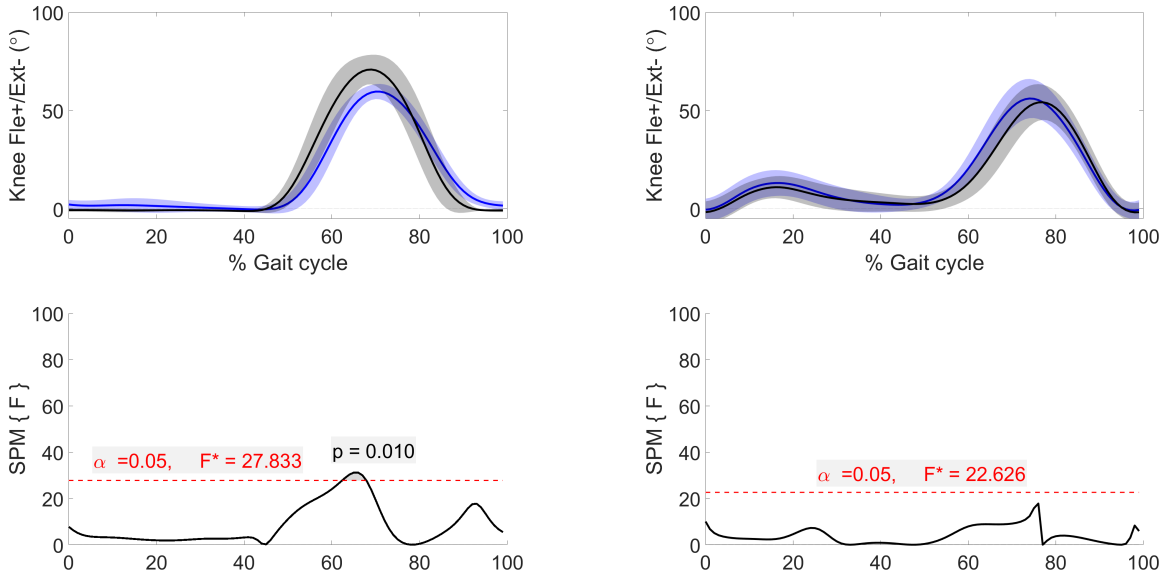
(a) Prosthetic side **(b)** Intact side

Figure 5.3: Top: Ankle dorsiflexion (DF)/plantar flexion (PF) angles of UTF with MPK (blue) and ICRC (black) prostheses. Bottom: Statistical parametric mapping results.

	MPK Mean ± SD *Median [95% CI]*		ICRC Mean ± SD *Median [95% CI]*	
Biomechanical parameter	Prosthetic side	Intact side	Prosthetic side	Intact side
Peak ankle dorsiflexion (°)	9.47 ± 2.18 ***p<.001**	7.85 ± 2.30	4.74 ± 1.31	6.56 ± 3.80
Peak ankle plantar flexion (°)	*8.71 [7.72-11.59]* ***p=.028**	21.07 ± 6.16	*4.64 [3.01-8.63]*	22.68 ± 5.35
Ankle dorsiflexion/plantar flexion ROM (°)	18.12 ± 3.38 ***p<.001**	28.92 ± 6.53	10.56 ± 3.00	29.24 ± 6.71

Table 5.4: Sagittal plane ankle kinematics.
CI, confidence interval. ROM, range of motion. *Statistically significant prosthetic side differences between prosthesis fitting cases (p<.05).

Figure 5.4 shows the sagittal plane knee angles with MPK and ICRC prostheses. SPM reported higher flexion angles of the ICRC knee than MPK in early swing (p=.010). When comparing discrete values in Table 5.5, the peak ICRC prosthetic knee flexion was larger by 12.7° than MPK (60.3°, p=.001). No significant differences in the intact knee sagittal plane kinematics were identified between prosthesis fitting cases.



(a) Prosthetic side **(b)** Intact side

Figure 5.4: Top: Knee flexion (Fle)/extension (Ext) angles of UTF with MPK (blue) and ICRC (black) prostheses. Bottom: Statistical parametric mapping results.

	MPK Mean ± SD		ICRC Mean ± SD	
Biomechanical parameter	Prosthetic side	Intact side	Prosthetic side	Intact side
Peak knee flexion (°)	60.27 ± 3.84 ***p=.001**	56.57 ± 10.01	72.95 ± 6.42	55.65 ± 9.01
Peak knee flexion early stance (°)	3.02 ± 3.41	13.72 ± 6.90	0.42 ± 0.14	11.56 ± 5.77

Table 5.5: Sagittal plane knee kinematics.
*Statistically significant prosthetic side differences between prosthesis fitting cases (p<.05).

Figure 5.5 shows the prosthetic knee angular velocity and acceleration over the course of the gait cycle. SPM reported higher ICRC knee angular velocity than MPK in swing (p=.030). When comparing discrete values in Table 5.6, the peak ICRC knee angular velocity in was larger by 2.3 rad/s than MPK (5.6 rad/s, p<.001). Similarly, the peak ICRC knee angular acceleration was larger in swing by 36.6 rad/s^2 than MPK (52.3 rad/s^2, p<.001).

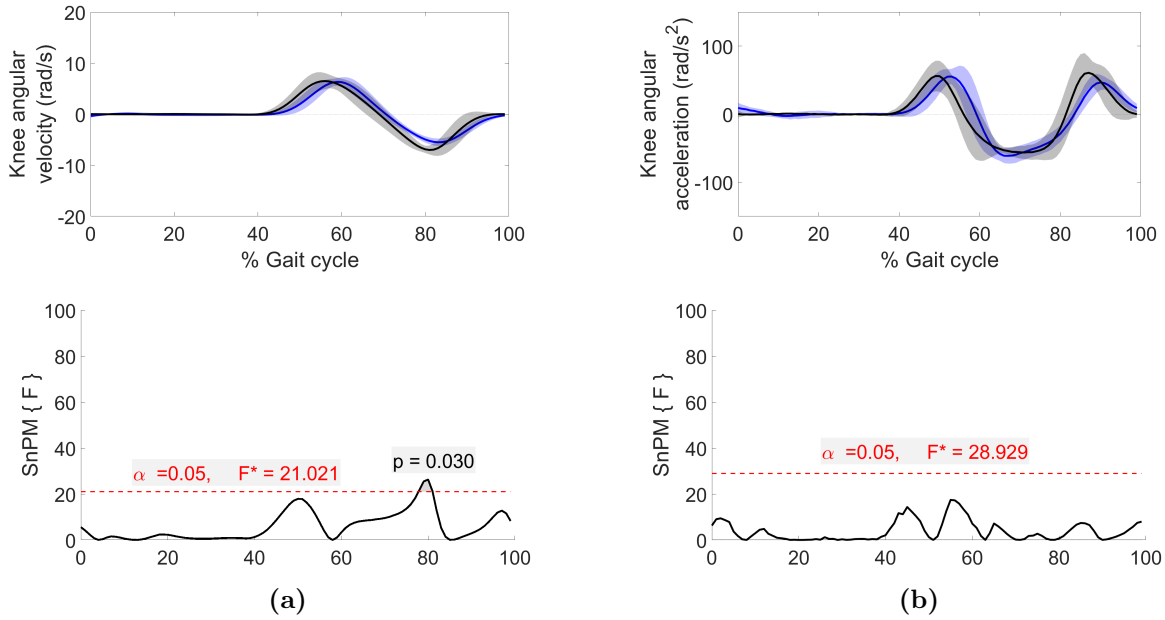
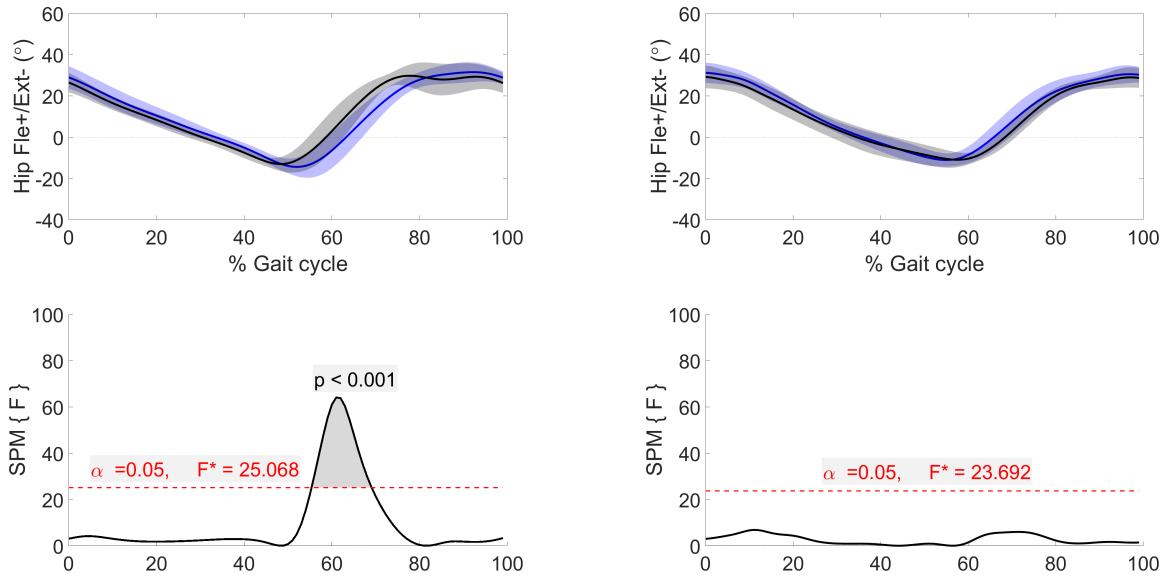


Figure 5.5: Top: Prosthetic knee angular velocity and acceleration of UTF with MPK (blue) and ICRC (black) prostheses. Bottom: Statistical parametric mapping results.

Biomechanical parameter	MPK Mean ± SD	ICRC Mean ± SD
Peak knee angular velocity swing (rad/s)	5.61 ± 0.74 ***p<.001**	7.88 ± 0.67
Peak knee angular acceleration swing (rad/s^2)	52.28 ± 10.43 ***p<.001**	88.85 ± 9.91

Table 5.6: Peak sagittal plane prosthetic knee angular velocity and acceleration in swing. *Statistically significant differences between prosthesis fitting cases (p<.05).

Figure 5.6 and Table 5.7 show the sagittal plane hip angles over the course of the gait cycle, with no significant differences in the peak hip angles between prosthesis fitting cases. SPM reported timing differences between ICRC and MPK when bringing the prosthetic side hip back towards flexion ($p<.001$).



(a) Prosthetic side **(b)** Intact side

Figure 5.6: Top: Hip flexion (Fle)/extension (Ext) angles of UTF with MPK (blue) and ICRC (black) prostheses. Bottom: Statistical parametric mapping results.

	MPK Mean ± SD		ICRC Mean ± SD	
Biomechanical parameter	Prosthetic side	Intact side	Prosthetic side	Intact side
Peak hip extension (°)	15.60 ± 5.54	11.76 ± 2.65	15.23 ± 3.94	11.79 ± 3.11
Peak hip flexion (°)	31.98 ± 4.85	32.40 ± 4.44	32.20 ± 6.06	30.63 ± 4.34
Hip extension / flexion ROM (°)	47.56 ± 9.75	44.16 ± 4.45	47.43 ± 9.32	42.42 ± 5.45

Table 5.7: Sagittal plane hip kinematics.
ROM, range of motion.

Figure 5.7 shows the sagittal plane prosthetic side hip angular velocity and acceleration. SPM reported lower prosthetic side hip angular velocity with ICRC than MPK in mid swing (p<.001). SPM also showed timing differences in the prosthetic side hip angular acceleration profiles between ICRC and MPK (p=.006). When comparing discrete values in Table 5.8, the prosthetic side hip angular acceleration was larger by 23.5 rad/s^2 with ICRC than MPK (p<.001) in late swing.

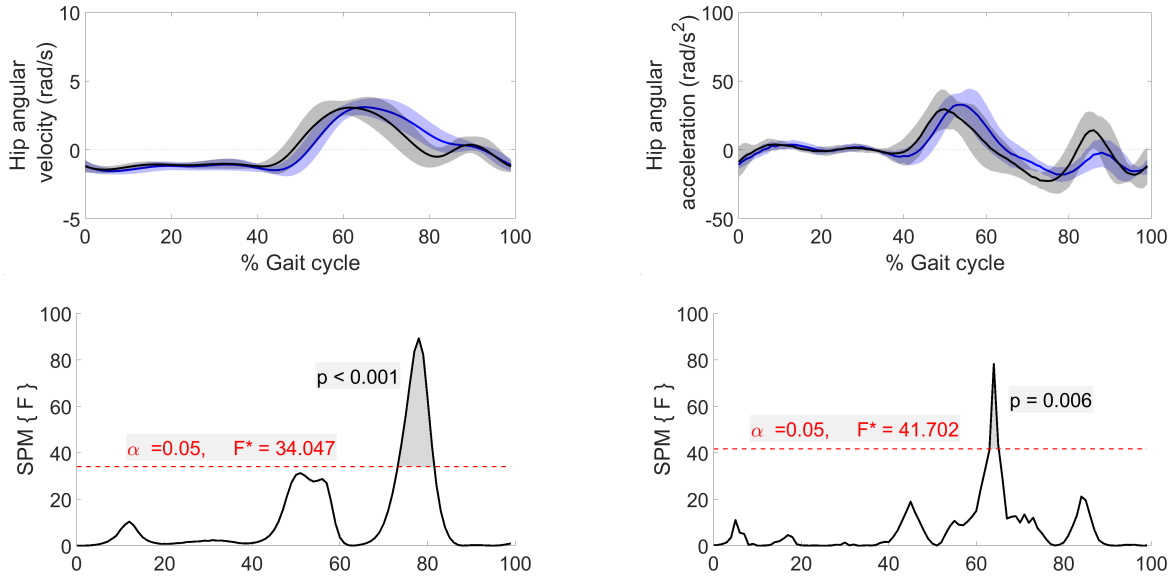
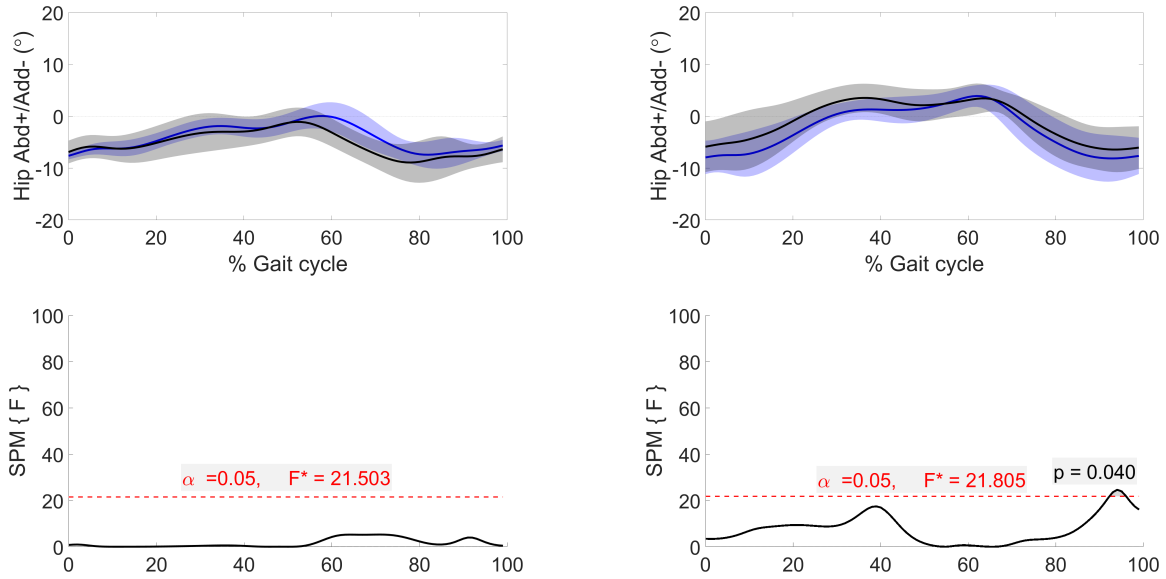


Figure 5.7: Top: Prosthetic side hip angular velocity and acceleration of UTF with MPK (blue) and ICRC (black) prostheses. Bottom: Statistical parametric mapping results.

Biomechanical parameter	MPK Mean ± SD	ICRC Mean ± SD
Peak hip angular velocity swing (rad/s)	0.04 ± 0.14 ***p=.015**	0.70 ± 0.41
Peak hip angular acceleration swing (rad/s^2)	3.29 ± 7.21 ***p<.001**	26.74 ± 8.53

Table 5.8: Peak prosthetic side hip angular velocity and acceleration in late swing. *Statistically significant prosthetic side differences between prosthesis fitting cases (p<.05).

Figure 5.8 and Table 5.9 show the coronal plane hip joint kinematics. SPM reported higher intact side hip adduction angles with MPK than ICRC in late swing (p=.040).



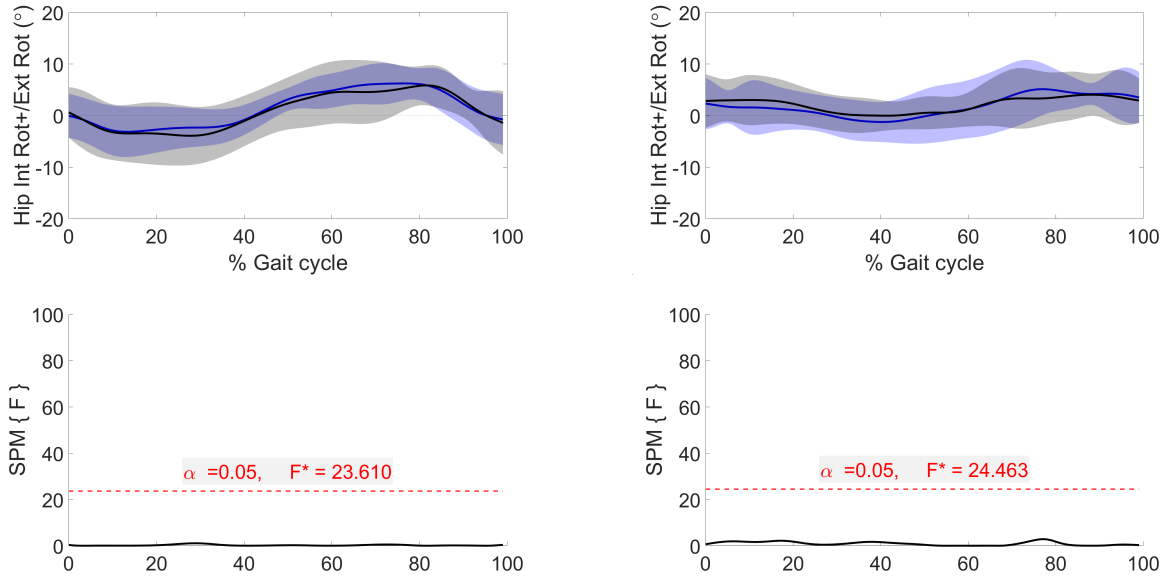
(a) Prosthetic side **(b)** Intact side

Figure 5.8: Top: Hip Abduction (Abd)/Adduction (Add) angles of UTF with MPK (blue) and ICRC (black) prostheses. Bottom: Statistical parametric mapping results.

	MPK Mean ± SD		ICRC Mean ± SD	
Biomechanical parameter	Prosthetic side	Intact side	Prosthetic side	Intact side
Peak hip abduction (°)	0.82 ± 2.10	4.65 ± 2.09	1.21 ± 4.27	5.46 ± 1.84
Peak hip adduction (°)	8.85 ± 1.59	10.38 ± 3.90	8.20 ± 5.24	8.40 ± 5.34
Hip abduction/ adduction ROM (°)	9.68 ± 2.50	14.91 ± 3.56	9.41 ± 1.78	13.86 ± 5.22

Table 5.9: Coronal plane hip kinematics.
ROM, range of motion.

Figure 5.9 and Table 5.10 show the transverse plane hip joint kinematics, with no significant differences between prosthesis fitting cases.



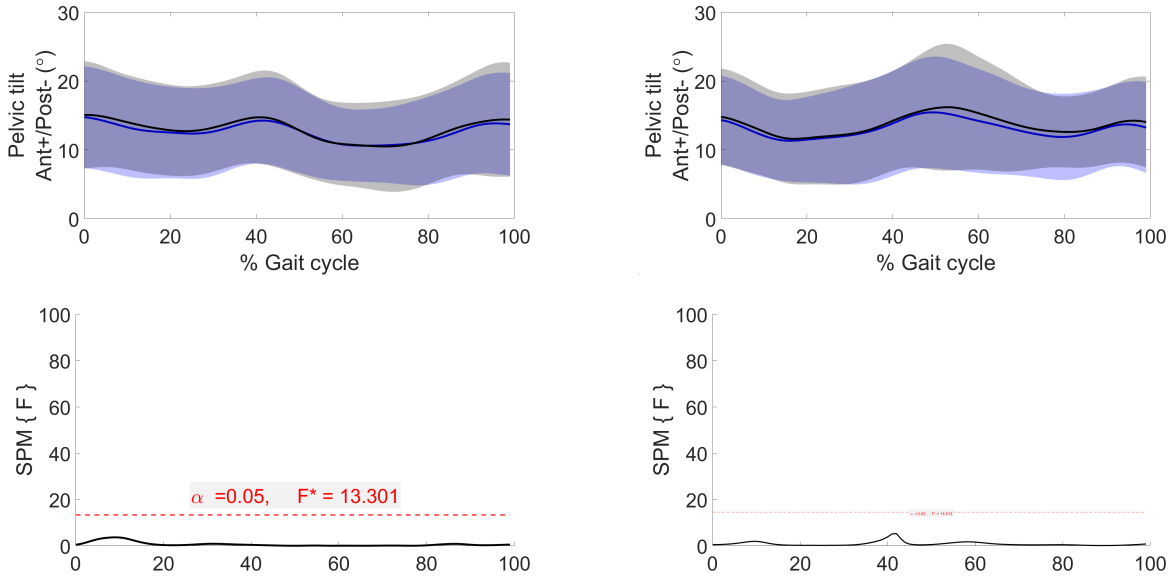
(a) Prosthetic side **(b)** Intact side

Figure 5.9: Top: Hip Internal (Int)/External (Ext) Rotation (Rot) angles of UTF with MPK (blue) and ICRC (black) prostheses. Bottom: Statistical parametric mapping results.

	MPK Mean ± SD *Median [95% CI]*		ICRC Mean ± SD *Median [95% CI]*	
Biomechanical parameter	Prosthetic side	Intact side	Prosthetic side	Intact side
Hip internal/external rotation ROM (°)	13.59 ± 5.23	*13.35 [10.46-18.45]*	14.85 ± 4.80	*12.25 [10.38-15.68]*

Table 5.10: Transverse plane hip kinematics.
ROM, range of motion.

Figure 5.10 and Table 5.11 present the pelvic tilt angles over the course of the gait cycle, with no significant differences between prosthesis fitting cases.



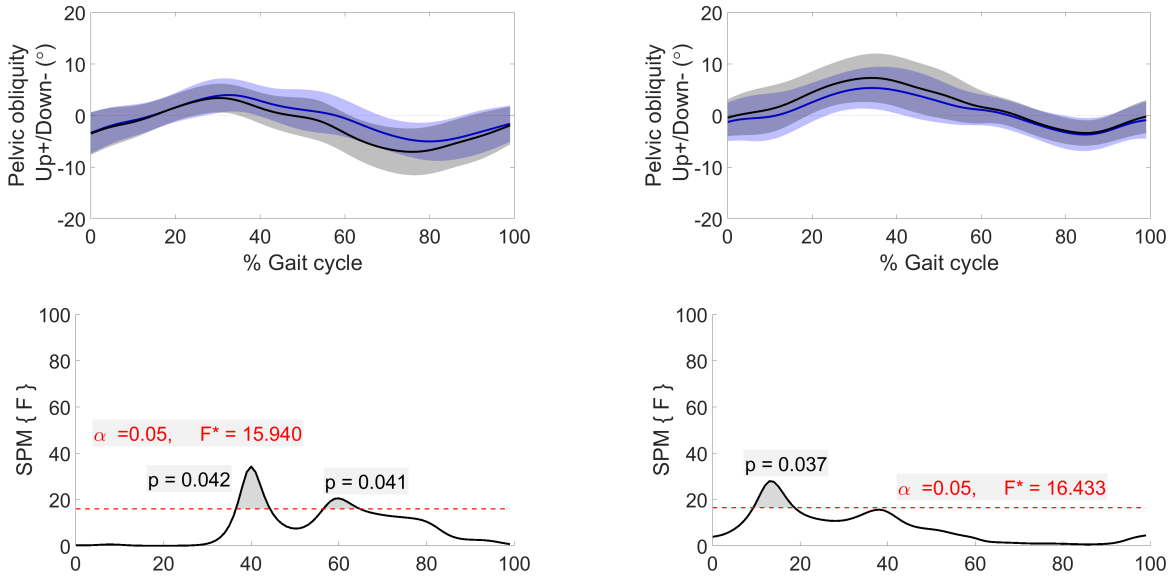
(a) Prosthetic side **(b)** Intact side

Figure 5.10: Top: Pelvic Anterior (Ant)/Posterior (Post) tilt angles of UTF with MPK (blue) and ICRC (black) prostheses. Bottom: Statistical parametric mapping results.

	MPK Mean ± SD		ICRC Mean ± SD	
Biomechanical parameter	Prosthetic side	Intact side	Prosthetic side	Intact side
P2P pelvic tilt (°)	7.82 ± 1.86	7.28 ± 2.31	8.01 ± 2.83	7.34 ± 2.11

Table 5.11: Sagittal plane pelvic kinematics.
P2P, peak-to-peak.

Figure 5.11 and Table 5.12 show the pelvic obliquity angles over the course of the gait cycle. SPM reported larger vertical height of the prosthetic side hip with ICRC than MPK (p=.037) in the early stance phase of the intact limb gait cycle.



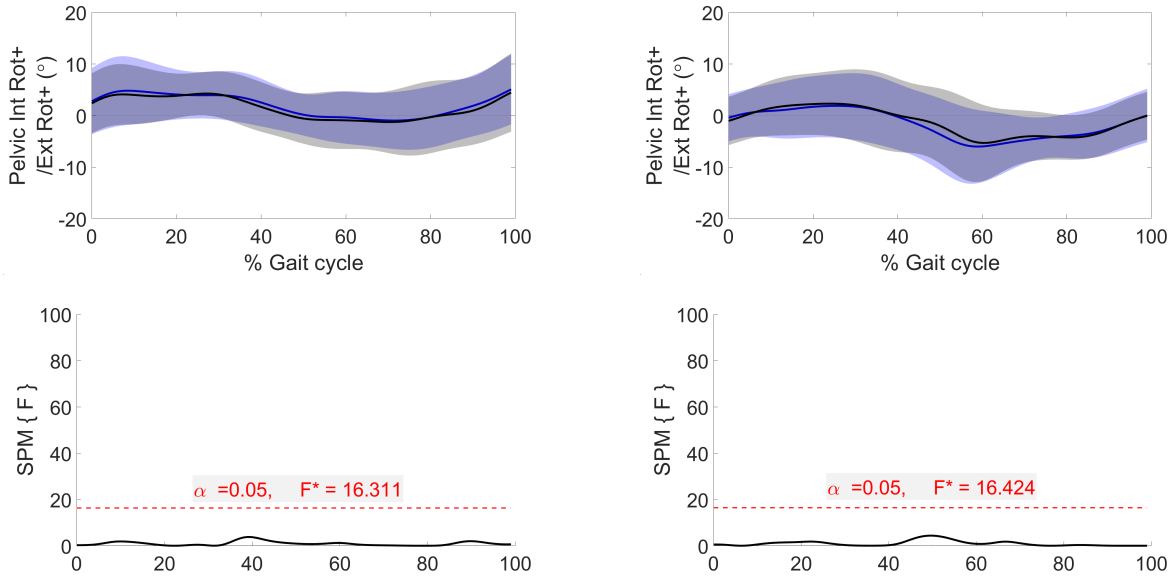
(a) Prosthetic side **(b)** Intact side

Figure 5.11: Top: Pelvic obliquity angles of UTF with MPK (blue) and ICRC (black) prostheses. Positive angles describe an increase in the vertical height of the contralateral hip. Bottom: Statistical parametric mapping results.

	MPK *Median [95% CI]*		ICRC *Median [95% CI]*	
Biomechanical parameter	Prosthetic side	Intact side	Prosthetic side	Intact side
P2P pelvic obliquity (°)	*9.22 [7.50-11.45]*	*9.79 [7.45-11.54]*	*11.82 [7.78-13.70]*	*12.43 [8.13-14.13]*

Table 5.12: Coronal plane pelvic kinematics. CI, confidence interval. P2P, peak-to-peak.

Figure 5.12 and Table 5.13 show the pelvic angles in the transverse plane, with no significant differences between prosthesis fitting cases.



(a) Prosthetic side **(b)** Intact side

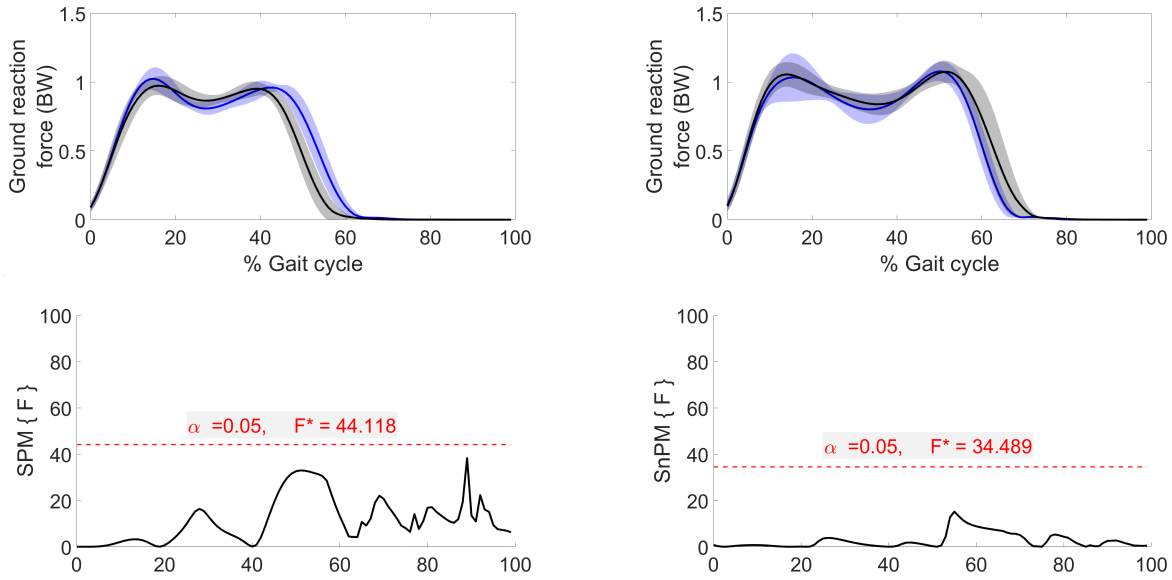
Figure 5.12: Top: Pelvic Internal (Int)/External (Ext) Rotation (Rot) angles of UTF with MPK (blue) and ICRC (black) prostheses. Bottom: Statistical parametric mapping results.

	MPK Mean ± SD		ICRC Mean ± SD	
Biomechanical parameter	Prosthetic side	Intact side	Prosthetic side	Intact side
P2P pelvic rotation (°)	9.95 ± 3.70	11.15 ± 4.60	11.33 ± 2.89	11.93 ± 3.81

Table 5.13: Transverse plane pelvic kinematics.
P2P, peak-to-peak.

5.3.4 Kinetics

Figure 5.13 and Table 5.14 show the ground reaction forces (GRF) over the course of the gait cycle. The second peak of the intact limb GRF was larger with ICRC by 0.02 BW than MPK (1.09 BW, p=.027). No significant differences in the prosthetic limb GRF were identified between prosthesis fitting cases.



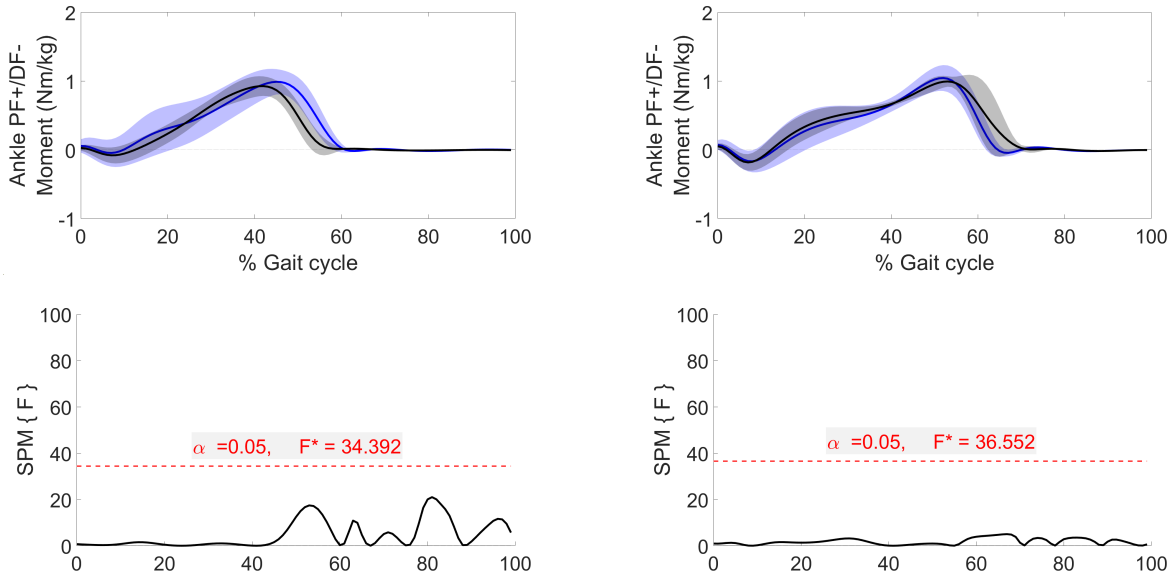
(a) Prosthetic side **(b)** Intact side

Figure 5.13: Top: Ground reaction forces of UTF with MPK (blue) and ICRC (black) prostheses. Bottom: Statistical parametric mapping results.

	MPK Mean ± SD		ICRC Mean ± SD	
Biomechanical parameter	Prosthetic side	Intact side	Prosthetic side	Intact side
First peak GRF (BW)	1.03 ± 0.08	1.06 ± 0.16	1.01 ± 0.07	1.10 ± 0.07
Second peak GRF (BW)	0.99 ± 0.05	1.09 ± 0.07 ****p=.027**	0.96 ± 0.04	1.11 ± 0.07

Table 5.14: Ground reaction forces (GRF).
**Statistically significant intact side differences between prosthesis fitting cases (p<.05).

Figure 5.14 and Table 5.15 show the sagittal plane ankle moments over the course of the gait cycle, with no significant differences between prosthesis fitting cases.



(a) Prosthetic side **(b)** Intact side

Figure 5.14: Top: Ankle Plantar flexion (PF)/Dorsiflexion (DF) Moments of UTF with MPK (blue) and ICRC (black) prostheses. Bottom: Statistical parametric mapping results.

	MPK Mean ± SD *Median [95% CI]*		ICRC Mean ± SD *Median [95% CI]*	
Biomechanical parameter	Prosthetic side	Intact side	Prosthetic side	Intact side
Peak ankle plantar flexion moment (Nm/kg)	1.02 ± 0.17	1.06 ± 0.19	0.95 ± 0.14	1.06 ± 0.11
Peak ankle dorsiflexion moment (Nm/kg)	*0.07 [0.01-0.29]*	0.20 ± 0.11	*0.10 [0.03-0.19]*	0.20 ± 0.10

Table 5.15: Sagittal plane ankle moments.
CI, confidence interval.

Figure 5.15 and Table 5.16 present the sagittal plane intact knee moments, with no significant differences in the flexion moments between prosthesis fitting cases. The peak intact knee extension moment was higher by 0.1 Nm/kg with MPK than ICRC (0.3 Nm/kg, p=.036).

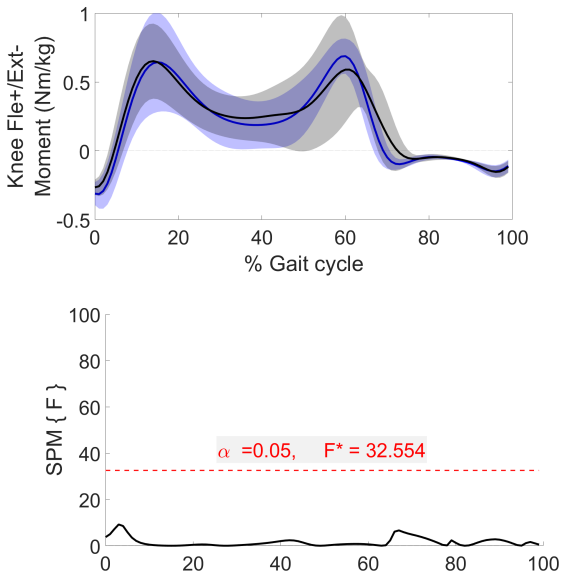


Figure 5.15: Top: Intact knee Extension (Ext)/Flexion (Fle) Moments of UTF with MPK (blue) and ICRC (black) prostheses. Bottom: Statistical parametric mapping results.

Biomechanical parameter	MPK Mean ± SD	ICRC Mean ± SD
Peak knee flexion moment (Nm/kg)	0.86 ± 0.19	0.80 ± 0.24
Peak knee extension moment (Nm/kg)	0.33 ± 0.08 ****p=.036**	0.27 ± 0.06

Table 5.16: Sagittal plane intact knee moments.
**Statistically significant intact side differences between prosthesis fitting cases (p<.05).

Figure 5.16 and Table 5.17 present the coronal plane intact knee moments and loading rate, with no significant differences between prosthesis fitting cases.

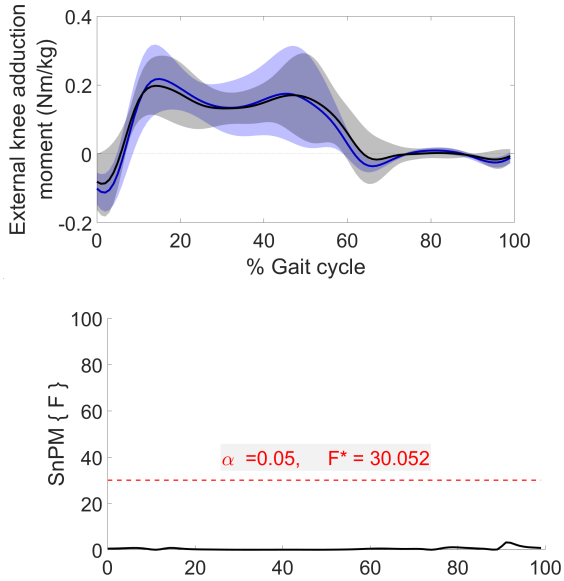
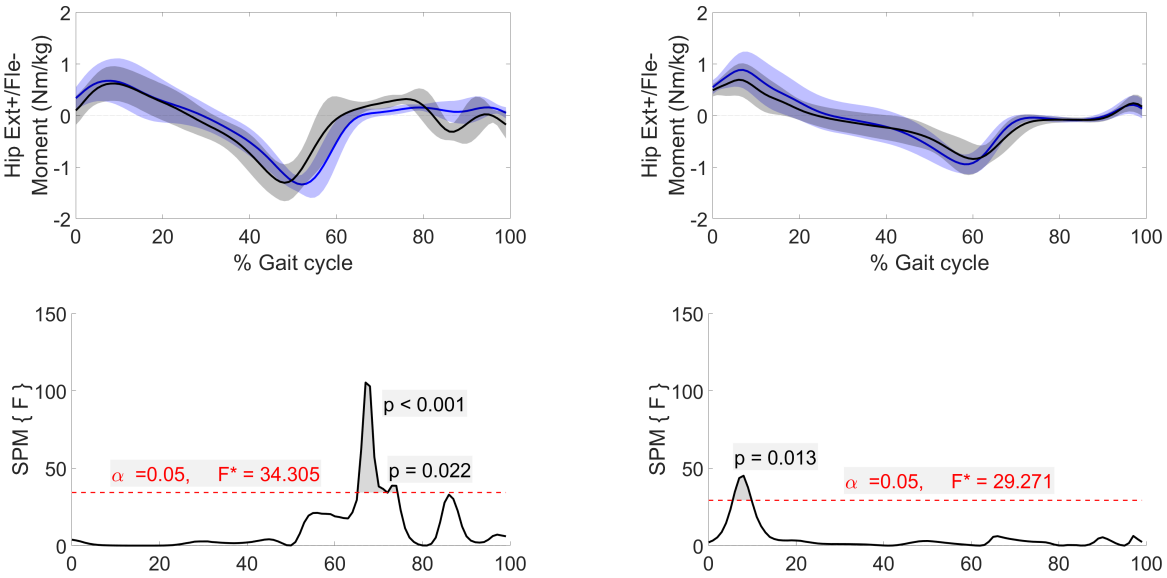


Figure 5.16: Top: External intact knee adduction moments of UTF with MPK (blue) and ICRC (black) prostheses. Bottom: Statistical parametric mapping results.

Biomechanical parameter	MPK Mean ± SD *Median [95% CI]*	ICRC Mean ± SD *Median [95% CI]*
Peak knee adduction moment (Nm/kg)	*0.29 [0.18-0.38]*	*0.18 [0.14-0.34]*
Peak knee loading rate (Nm/kg.s)	4.82 ± 1.75	3.29 ± 0.91

Table 5.17: Coronal plane intact knee moments and loading rate.

Figure 5.17 shows the sagittal plane hip moments over the course of the gait cycle. SPM reported lower prosthetic side hip sagittal plane moments with MPK than ICRC in early swing (p<.001, p=.022). SPM also showed lower intact side hip extension moments with ICRC than MPK in early stance (p=.013). When comparing discrete values in Table 5.18, the intact side hip peak extension moment was lower with ICRC by 0.2 Nm/kg than MPK (0.9 Nm/kg, p=.002).



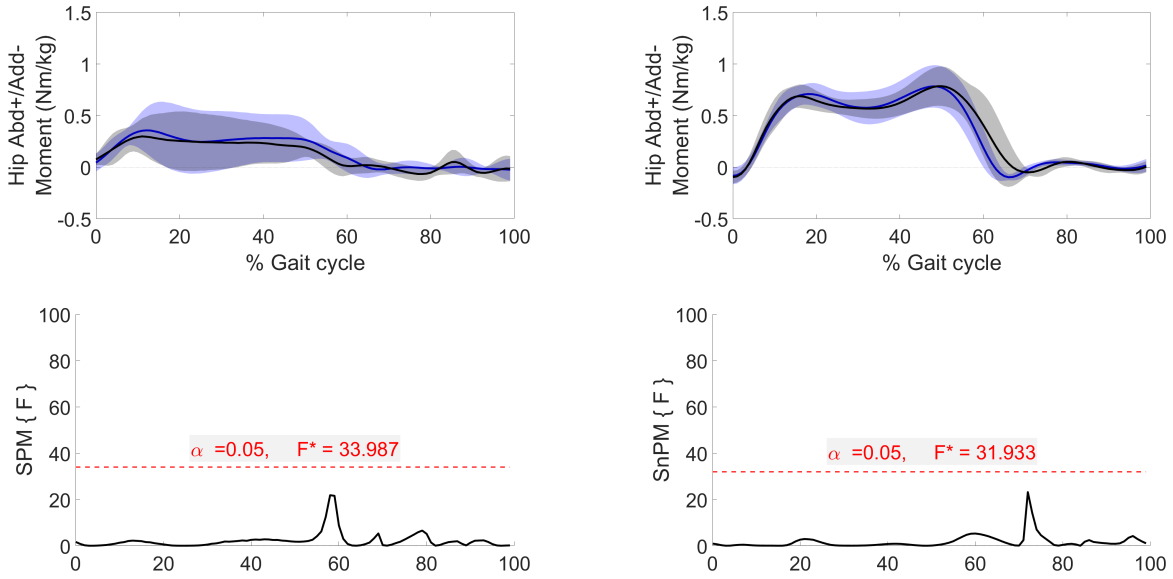
(a) Prosthetic side **(b)** Intact side

Figure 5.17: Top: Hip Extension (Ext)/Flexion (Fle) Moments of UTF with MPK (blue) and ICRC (black) prostheses. Bottom: Statistical parametric mapping results.

	MPK Mean ± SD		ICRC Mean ± SD	
Biomechanical parameter	Prosthetic side	Intact side	Prosthetic side	Intact side
Peak hip extension moment (Nm/kg)	0.75 ± 0.37	0.92 ± 0.31 ****p=.002**	0.71 ± 0.29	0.74 ± 0.28
Peak hip flexion moment (Nm/kg)	1.49 ± 0.17	0.99 ± 0.20	1.57 ± 0.25	0.95 ± 0.26

Table 5.18: Sagittal plane hip moments.
**Statistically significant intact side differences between prosthesis fitting cases (p<.05).

Figure 5.18 and Table 5.19 present the coronal plane hip moments, with no significant differences between prosthesis fitting cases.



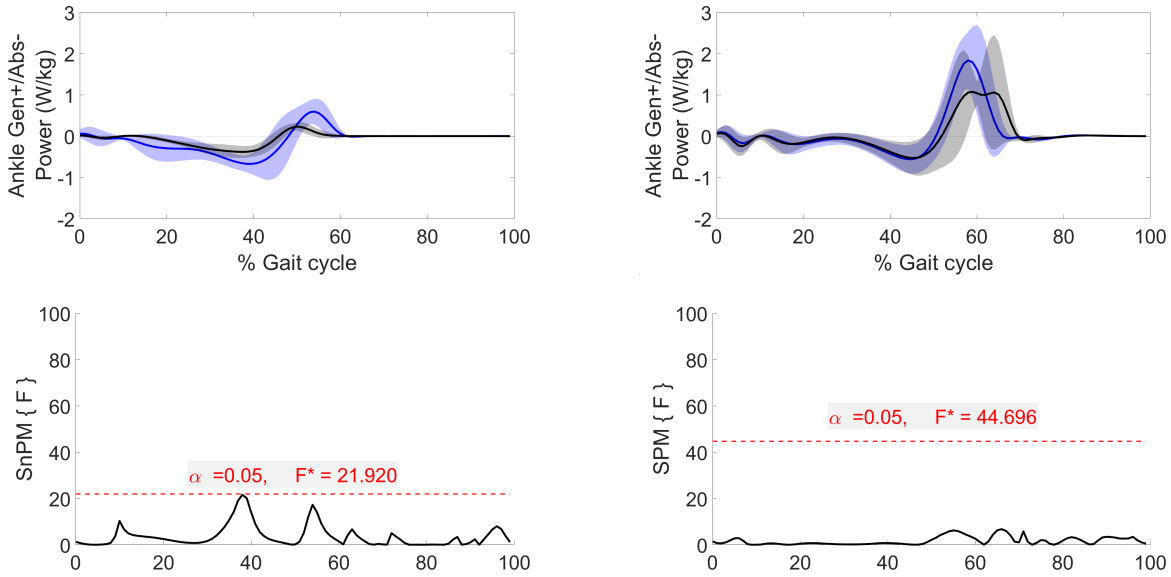
(a) Prosthetic side **(b)** Intact side

Figure 5.18: Top: Hip Abduction (Abd)/Adduction (Add) Moments of UTF with MPK (blue) and ICRC (black) prostheses. Bottom: Statistical parametric mapping results.

	MPK Mean ± SD *Median [95% CI]*		ICRC Mean ± SD *Median [95% CI]*	
Biomechanical parameter	Prosthetic side	Intact side	Prosthetic side	Intact side
Peak hip abduction moment (Nm/kg)	*0.37 [0.23-0.70]*	0.84 ± 0.17	*0.32 [0.22-0.62]*	0.82 ± 0.18
Peak hip adduction moment (Nm/kg)	0.10 ± 0.06	0.14 ± 0.05	0.12 ± 0.06	0.14 ± 0.03

Table 5.19: Coronal plane hip moments.
CI, confidence interval.

Figure 5.19 and Table 5.20 show the sagittal plane ankle power over the course of the gait cycle. The SACH peak generated power at the push-off phase of the gait cycle was lower by 0.5 W/kg than dynamic feet (0.9 W/kg, p=.005). SACH showed lower peak absorbed power by 0.4 W/kg than dynamic feet (0.8 W/kg, p=.004). No significant differences in the intact ankle power were identified between prosthesis fitting cases.



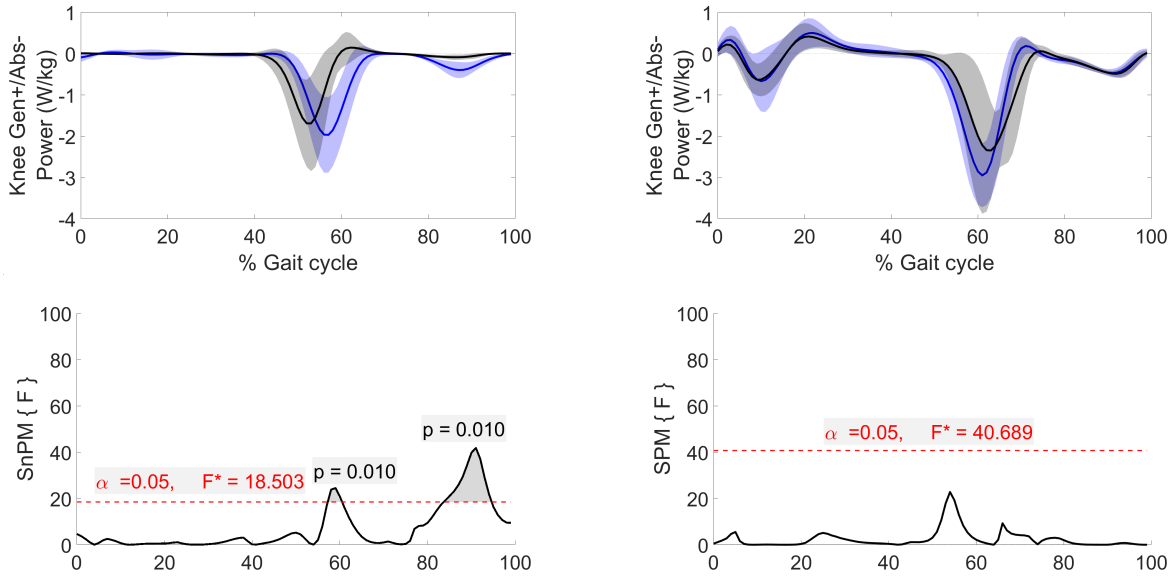
(a) Prosthetic side **(b)** Intact side

Figure 5.19: Top: Ankle Generated (Gen)/Absorbed (Abs) Power of UTF with MPK (blue) and ICRC (black) prostheses. Bottom: Statistical parametric mapping results.

	MPK Mean ± SD *Median [95% CI]*		ICRC Mean ± SD *Median [95% CI]*	
Biomechanical parameter	Prosthetic side	Intact side	Prosthetic side	Intact side
Peak ankle generated power (W/kg)	0.85 ± 0.31 ***p=.005**	2.28 ± 0.90	0.31 ± 0.07	2.17 ± 0.80
Peak ankle absorbed power (W/kg)	0.80 ± 0.30 ***p=.004**	*0.56* *[0.38-0.96]*	0.42 ± 0.15	*0.65* *[0.31-1.07]*

Table 5.20: Sagittal plane ankle power.
CI, confidence interval. *Statistically significant prosthetic side differences between prosthesis fitting cases (p<.05).

Figure 5.20 shows the sagittal plane knee power. SPM reported higher prosthetic knee absorbed power for MPK than ICRC in late stance (p=.010) and late swing (p=.010). When comparing discrete values in Table 5.21, the ICRC knee peak generated power was higher by 0.2 W/kg than MPK (0.2 W/kg, p=.006). No significant differences in the intact knee power were identified between prosthesis fitting cases.



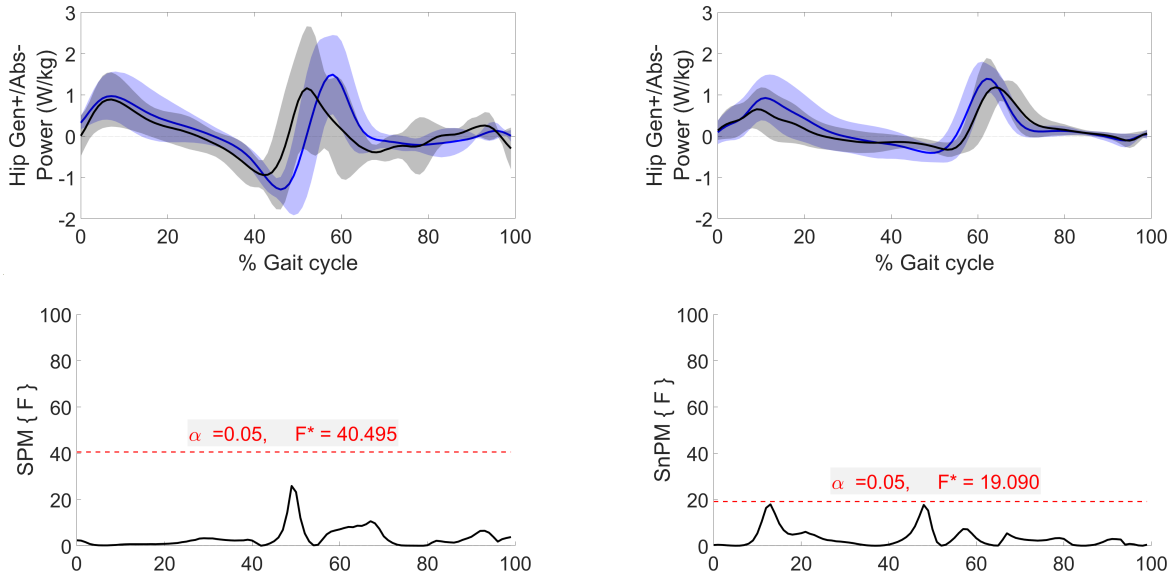
(a) Prosthetic side **(b)** Intact side

Figure 5.20: Top: Knee Generated (Gen)/Absorbed (Abs) Power of UTF with MPK (blue) and ICRC (black) prostheses. Bottom: Statistical parametric mapping results.

	MPK Mean ± SD		ICRC Mean ± SD	
Biomechanical parameter	Prosthetic side	Intact side	Prosthetic side	Intact side
Peak knee generated power (W/kg)	0.15 ± 0.08 ***p=.006**	0.74 ± 0.24	0.34 ± 0.15	0.65 ± 0.18
Peak knee absorbed power (W/kg)	2.51 ± 0.54	3.21 ± 0.67	2.11 ± 1.03	3.14 ± 1.01

Table 5.21: Sagittal plane knee power.
*Statistically significant prosthetic side differences between prosthesis fitting cases (p<.05).

Figure 5.21 and Table 5.22 show the hip power profiles over the course of the gait cycle, with no significant differences between prosthesis fitting cases.



(a) Prosthetic side **(b)** Intact side

Figure 5.21: Top: Hip Generated (Gen)/Absorbed (Abs) Power of UTF with MPK (blue) and ICRC (black) prostheses. Bottom: Statistical parametric mapping results.

	MPK Mean ± SD		ICRC Mean ± SD	
Biomechanical parameter	Prosthetic side	Intact side	Prosthetic side	Intact side
Peak hip generated power (W/kg)	2.19 ± 0.71	1.68 ± 0.27	2.34 ± 0.78	1.57 ± 0.40
Peak hip absorbed power (W/kg)	1.68 ± 0.66	0.56 ± 0.34	1.62 ± 0.44	0.46 ± 0.27

Table 5.22: Sagittal plane hip power.

Figure 5.22 and Table 5.23 show the intact ankle joint contact forces and impulse over the course of the gait cycle. The intact ankle contact force impulse normalised to walked distance was higher with ICRC by 24.1 BW.s/m than MPK (115.0 BW.s/m, p=.048).

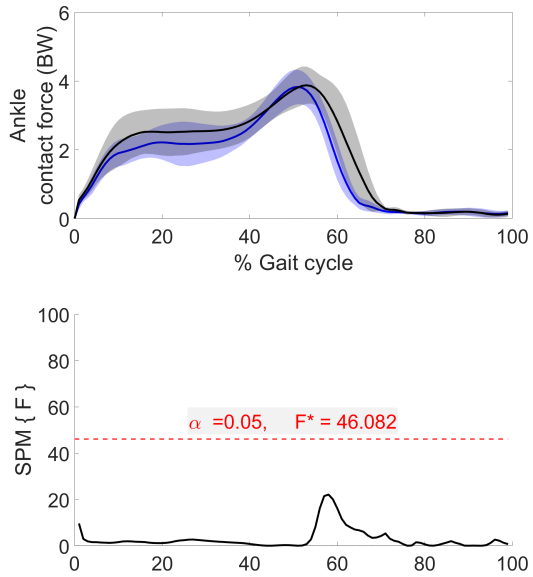


Figure 5.22: Top: Intact side intact ankle joint contact forces of UTF with MPK (blue) and ICRC (black) prostheses. Bottom: Statistical parametric mapping results.

Biomechanical parameter	MPK Mean ± SD	ICRC Mean ± SD
First peak ankle contact force (BW)	2.48 ± 0.37	2.83 ± 0.56
Second peak ankle contact force (BW)	3.87 ± 0.47	4.08 ± 0.51
Ankle contact force impulse (BW.s)	153.56 ± 13.75	177.81 ± 20.66
Normalised ankle contact force impulse (BW.s/m)	115.01 ± 6.97 **p=.048	139.07 ± 22.00

Table 5.23: Intact ankle joint contact forces and impulse.
**Statistically significant intact side differences between prosthesis fitting cases (p<.05).

Figure 5.23 and Table 5.24 show the medial compartment of the intact knee contact forces and impulse, with no significant differences between prosthesis fitting cases.

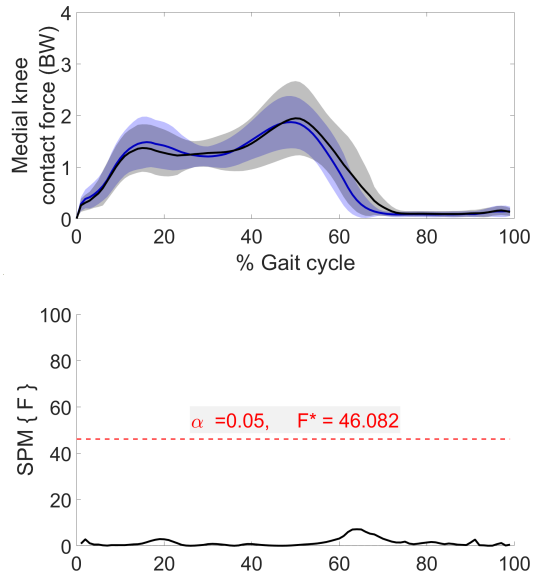


Figure 5.23: Top: Intact side medial knee joint contact forces of UTF with MPK (blue) and ICRC (black) prostheses. Bottom: Statistical parametric mapping results.

Biomechanical parameter	MPK Mean ± SD	ICRC Mean ± SD
First peak medial knee contact force (BW)	1.55 ± 0.51	1.46 ± 0.47
Second peak medial knee contact force (BW)	1.97 ± 0.51	1.98 ± 0.72
Medial knee contact force impulse (BW.s)	84.84 ± 18.48	87.03 ± 20.80
Normalised medial knee contact force impulse (BW.s/m)	63.71 ± 13.83	67.82 ± 16.18

Table 5.24: Medial compartment of the intact knee contact forces and impulse.

Figure 5.24 and Table 5.25 show the lateral compartment of the intact knee contact forces and impulse. The lateral compartment of the intact knee normalised impulse was larger when walking with ICRC by 14.9 BW.s/m than MPK (98.5 BW.s/m, p=.038).

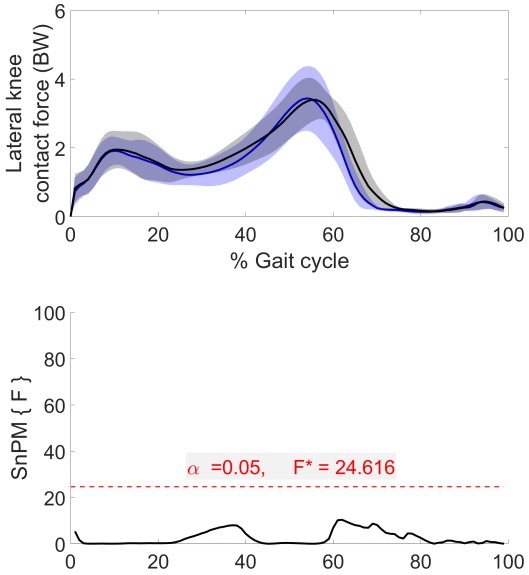


Figure 5.24: Top: Intact side lateral knee joint contact forces of UTF with MPK (blue) and ICRC (black) prostheses. Bottom: Statistical parametric mapping results.

Biomechanical parameter	MPK Mean ± SD	ICRC Mean ± SD
First peak lateral knee contact force (BW)	2.10 ± 0.40	2.13 ± 0.51
Second peak lateral knee contact force (BW)	3.51 ± 0.97	3.58 ± 0.56
Lateral knee contact force impulse (BW.s)	131.22 ± 23.08	143.22 ± 14.30
Normalised lateral knee contact force impulse (BW.s/m)	98.45 ± 17.00 ****p=.038**	112.40 ± 13.56

Table 5.25: Lateral compartment of the intact knee contact forces and impulse. **Statistically significant intact side differences between prosthesis fitting cases (p<.05).

Figure 5.25 and Table 5.26 present the total intact knee contact forces and impulse. The total intact knee normalised impulse was larger with ICRC by 18.1 BW.s/m than MPK (162.2 BW.s/m, p=.020).

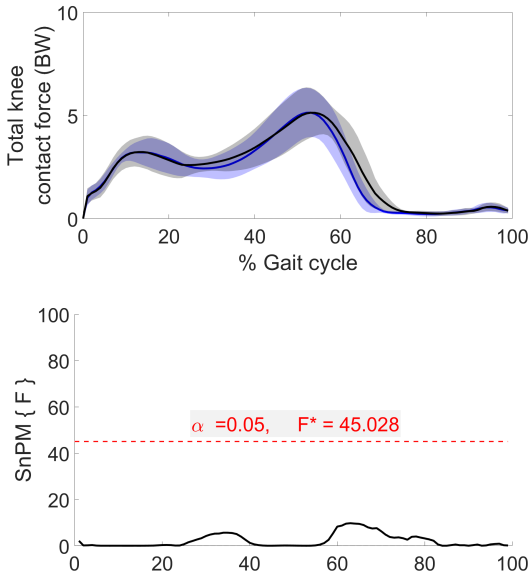
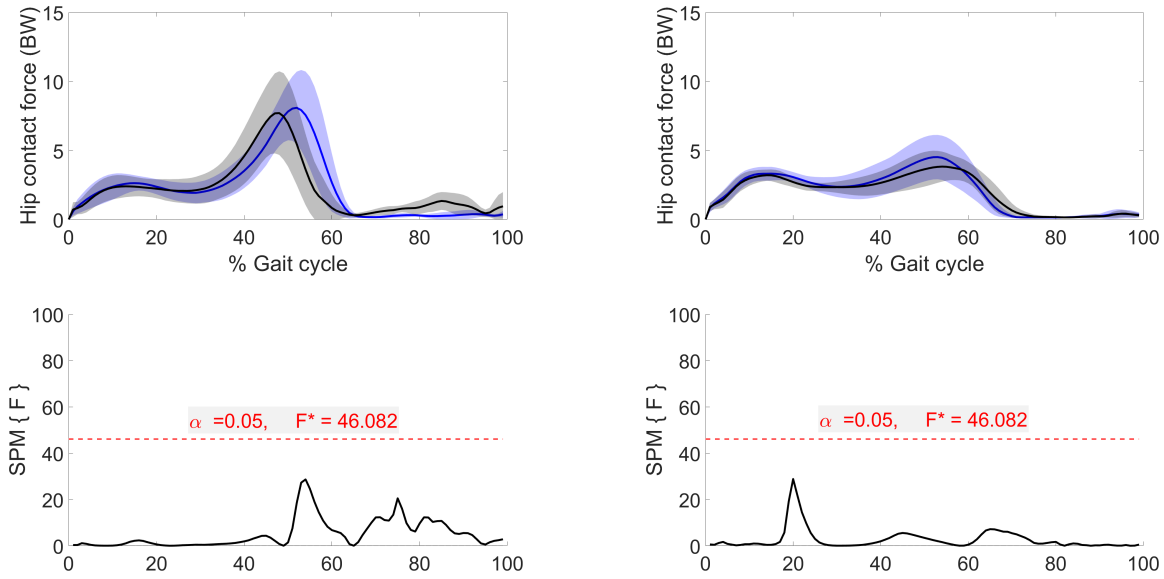


Figure 5.25: Top: Intact side total knee joint contact forces of UTF with MPK (blue) and ICRC (black) prostheses. Bottom: Statistical parametric mapping results.

Biomechanical parameter	MPK Mean ± SD	ICRC Mean ± SD
First peak total knee contact force (BW)	3.65 ± 0.47	3.60 ± 0.63
Second peak total knee contact force (BW)	5.48 ± 1.30	5.56 ± 1.15
Total knee contact force impulse (BW.s)	216.06 ± 36.59	230.25 ± 32.30
Normalised total knee contact force impulse (BW.s/m)	162.15 ± 27.14 ****p=.020**	180.22 ± 28.31

Table 5.26: Total intact knee contact forces and impulse.
**Statistically significant intact side differences between prosthesis fitting cases (p<.05).

Figure 5.26 and Table 5.27 show the hip joint contact forces and impulse over the course of the gait cycle. No significant differences were identified in the hip joint loading magnitude between prosthesis fitting cases.



(a) Prosthetic side **(b)** Intact side

Figure 5.26: Top: Hip joint contact forces of UTF with MPK (blue) and ICRC (black) prostheses. Bottom: Statistical parametric mapping results.

	MPK Mean ± SD *Median [95% CI]*		ICRC Mean ± SD *Median [95% CI]*	
Biomechanical parameter	Prosthetic side Mean (SD)	Intact side Mean (SD)	Prosthetic side Mean (SD)	Intact side Mean (SD)
First peak hip contact force (BW)	*2.82 [2.39-3.47]*	3.51 ± 0.38	*3.05 [2.02-3.48]*	3.36 ± 0.42
Second peak hip contact force (BW)	8.66 ± 2.05	4.66 ± 1.64	8.88 ± 2.76	4.10 ± 1.05
Second peak hip contact force normalised by speed (BW/(m/s))	7.64 ± 1.62	4.23 ± 1.60	8.75 ± 2.23	4.17 ± 0.87
Hip contact force impulse (BW.s)	218.87 ± 40.00	201.75 ± 45.03	220.86 ± 49.56	192.91 ± 33.21
Normalised hip contact force impulse (BW.s/m)	162.42 ± 25.10	151.01 ± 31.63	169.13 ± 30.02	150.27 ± 26.73

Table 5.27: Hip joint contact forces and impulse.
CI, confidence interval.

5.4 Discussion

The mechanical polycentric ICRC knee coupled with a SACH prosthetic foot is an affordable prosthesis for amputees living in resource-limited environments. At the other end of the spectrum, the most commonly used lower limb prosthesis in high-income countries consists of the high-cost advanced MPK unit and dynamic response prosthetic foot. This study identified differences in amputee musculoskeletal system function and loading during level-ground walking with low- and high-cost lower limb prostheses. The key biomechanical findings of this chapter are presented in Table 5.28.

1. Amputees showed lower walking speeds by 0.2 m/s with ICRC than MPK.
2. The prosthetic ankle sagittal plane range of motion was lower by 7.6° for SACH than dynamic feet.
3. The ICRC knee flexion angles were higher by 12.7° than MPK.
4. The ICRC knee angular velocity and acceleration in swing were higher by 2.3 rad/s and by 36.6 rad/s^2, respectively, than MPK.
5. The prosthetic side hip angular acceleration in terminal swing was larger by 23.5 rad/s^2 with ICRC than MPK.
6. Amputees spent a longer time in the stance phase of the intact limb gait cycle by 2.5% with ICRC than MPK.
7. The intact ankle impulse was larger by 24.1 BW.s/m with ICRC than MPK.
8. The intact lateral knee impulse was larger by 24.0 BW.s/m with ICRC than MPK.
9. The intact total knee impulse was larger by 18.1 BW.s/m with ICRC than MPK.

Table 5.28: Key differences between the biomechanical effects of MPK and ICRC prostheses on UTF function and loading.

It was observed that UTF walked with lower cadence and walking speeds with the ICRC prosthesis than MPK, where the difference in walking speeds was statistically and clinically significant. The ability to walk faster was directly influenced by the prosthetic design. The mechanical ICRC knee uses a conventional extension assist which introduces a singularity in the function of the spring mechanism. Once the knee reaches a certain angle, the spring pushes the knee into flexion, and due to this design feature, the ICRC knee presented larger peak knee flexion angles in swing than MPK. As a result, participants needed to wait for the ICRC knee to return from a position of higher flexion. Moreover, participants reported instability with the prosthesis when attempting to walk at faster speeds. Improvements of the extension assist mechanism may be able to prevent excessive knee flexion. The ICRC knee returned to the extended position in swing with higher angular acceleration than MPK. The faster forward kick was a consequence of the mechanical control of the ICRC knee, which has no components that can slow down the knee motion. Contrarily, the MPK unit's in-built sensors slowed down knee flexion, and adjusted the knee angular velocity and acceleration according to the participant's speed and activity level. Additionally, the SACH foot did not allow for variable cadence, further reducing walking speed when walking with ICRC. The limited duration of the familiarization period with the ICRC knee might have affected the ability to walk fast.

Expectedly, it was observed that the intact side step length was lower than that of the prosthetic limb with both MPK and ICRC prostheses. In addition to the uneven step lengths, another movement strategy adopted by the current UTF cohort was characterized by a larger percentage of the gait cycle spent in the intact limb stance phase compared to the prosthetic limb, in concordance with previous literature (Jaegers et al. 1995, Mâaref et al. 2010). When walking with ICRC, the percentage stance time spent on the intact limb was higher than MPK. The higher reliance on the intact limb when walking with the ICRC prosthesis was caused by different factors. Firstly, the ICRC knee was fitted with a SACH foot, which is more rigid than a dynamic response foot (SACH presented lower sagittal plane range of motion during gait by 41% than the dynamic foot). Given the inability to sufficiently flex the ankle joint, UTF lifted the prosthetic SACH foot off the ground earlier than the intact foot. The higher asymmetry when walking with ICRC may also be explained by insecurity with the prosthesis, causing UTF to transfer the body weight quickly from the prosthetic to the intact limb (Bowker & Michael 1992).

The aforementioned compensatory strategies, required for successful ambulation with the prosthesis, may reduce walking efficiency, and lead to high risks of musculoskeletal disorders. The intact limb of unilateral amputees has been shown to be at a high risk of osteoarthritis, which is thought to be linked to abnormal loading of the joint (Norvell et al. 2005, Felson 2013, Ding et al. 2020, Gailey et al. 2008, Morgenroth et al. 2012). The intact knee external adduction moment has been suggested to be a strong predictor of the presence of osteoarthritis (Manal et al. 2015) and its progression (Bennell et al. 2011) in the medial compartment of the knee. However, this UTF cohort did not demonstrate significant differences in the intact knee adduction moments between prosthesis fitting conditions. The knee adduction moment is influenced by the step width, which was similar between prostheses. As the study participants had been using their prosthesis for a minimum of two years, they would have become accustomed to a comfortable and efficient step width, and might have aimed to replicate it with the ICRC prosthesis. Chapter 4 demonstrated higher loading of the lateral compartment of the intact knee in the UTF population than persons without limb loss. The type of prosthetic device has a direct effect on the loading of the intact knee, as observed in the current study. The longer intact limb stance time when walking with the ICRC prosthesis led to larger lateral knee loading dose by 14% than MPK. Additionally, the intact ankle loading dose was larger by 21% with ICRC than MPK. These findings indicate that walking with a prosthesis consisting of a mechanical polycentric knee with a conventional extension assist and a SACH prosthetic foot may increase the risk of knee and ankle joint degeneration in the UTF population. The intact and prosthetic side hip joint contact forces were similar between prosthesis fitting cases. Given the sole reliance on the hip-spanning muscles for propulsion, the prosthetic side hip joint contact forces were significantly larger than the intact side hip joint contact forces in both fitting cases. Although hip osteoarthritis has not been investigated in the amputee population, high and repetitive loading of the joint might lead to tissue degeneration (Ewers et al. 2001, Kerin et al. 2003).

Whilst the amputated side hip showed similar magnitudes of sagittal plane kinematics

between prosthesis fitting cases in stance, walking with ICRC introduced a frequency effect in the hip angles in terminal swing. At this point in the gait cycle, the pulses experienced by the hip might have been caused by the knee reaching the full extension position, and larger hip angular acceleration was needed to bring the limb safely to the heel strike position. Additionally, UTF started to bring the prosthetic side hip towards flexion earlier than in the MPK fitting case, indicating that a greater effort might have been needed to swing the ICRC prosthesis back to heel strike. Heel strike is considered to be the most unstable phase of the transfemoral amputee gait cycle (Bowker & Michael 1992). The instability may be caused by an instantaneously created torque that tends to rotate the shin forward, and flex the knee (Bowker & Michael 1992).

The incidence of falling in the transfemoral amputee population is 43% higher than transtibial amputees (Gauthier-Gagnon et al. 1999) and trips are a common cause of this (Chen et al. 1991). The risk of tripping is influenced by the critical toe clearance, which occurs when the distance between the ground and toe reaches local minimum, approximately in the mid-swing phase of the gait cycle (Riveras et al. 2020). Polycentric knees are designed such that the leg shortens when the knee bends, thus providing larger toe clearance in swing (Bellmann et al. 2020) than monocentric knees (Gard et al. 1996). Therefore, the polycentric ICRC knee provided more toe clearance than the monocentric MPK. However, excessively increasing toe clearance may lead to gait abnormalities, including hip hiking and vaulting, which are used as safety measures to minimize the risk of tripping. Unexpectedly, this cohort showed higher vertical height of the prosthetic side hip during the intact limb gait cycle with ICRC than MPK, even though the ICRC polycentric knee provided higher toe clearance than the monocentric MPK unit. This might indicate that the lack of confidence with the ICRC prosthesis caused amputees to further increase toe clearance by increasing pelvic obliquity to minimize the risk of tripping. However, large pelvic motions may contribute to low back pain (Hendershot & Wolf 2014, Davis & Marras 2000). Vaulting has been characterized by intact ankle excessive plantar flexion (Drevelle et al. 2014). However, the two prosthesis fitting cases did not present any differences in the intact ankle kinematics. Newly developed prosthetic components should provide optimal toe clearance, whilst minimizing gait deviations.

This study's results showed similar prosthetic ankle joint moments between dynamic response and SACH feet. However, these results are only representative of normal gait at self-selected speeds, and active traumatic amputees may show unique loading conditions during highly strenuous activities. Future work could analyse differences in loading profiles of prosthetic feet for various activities performed over different terrains. In addition to this, bench testing could be used to simulate the strictest static and cyclic loading conditions and identify reasons for failure of prosthetic feet. This work could highlight possible limitations of the current ISO10328 standards (which only simulate idealized gait) and provide valuable information on prosthetic design requirement, allowing for improved standards for strength of lower limb prostheses to be proposed.

5.5 Limitations

There are a number of limitations in this study. Prior to data collection, participants walked with the low-cost prosthesis in the laboratory for as long as they required for familiarization. However, it is believed that prolonged prosthetic use allows amputees to further improve and adjust their gait accordingly. Therefore, comparing a new prosthetic device to their own prosthesis, that they have been using for more than two years, may not be equitable. Additional time with the ICRC prosthesis may have been needed to ensure study participants concluded the learning process. However, the experimental protocol was as appropriate as could be practically attained, as giving the low-cost prosthesis for continuous use at home without a prosthetist's professional help was not considered safe.

The small participant sample size may limit the generalization of these results to the wider transfemoral amputee population. A larger sample size would allow for stronger statistical power and understanding of the musculoskeletal system loading with the ICRC knee and SACH foot. However, the sample size was as large as could be practically achieved. A sensitivity analysis of the musculoskeletal model was not performed; future work could investigate the dependency of the input parameters of the output variables. Limitations of the musculoskeletal modelling process were discussed in previous chapters.

5.6 Conclusion

This chapter investigated the biomechanical effect of high-cost (MPK units with dynamic response feet) and low-cost prostheses (mechanical ICRC polycentric knees with SACH feet) on the musculoskeletal function and loading of lower-limb unilateral above/through-knee amputees. MPK units presented several benefits over the ICRC prostheses. Firstly, amputees with MPK were able to walk faster than with ICRC. The conventional extension assist used by the ICRC knee limited the ability to reach faster walking speeds, and prosthetic design development should focus on the improvement of this design feature. Secondly, MPK units minimized gait deviations and improved the loading of the intact ankle and knee joints. Although MPK units may have the ability to improve functional abilities and musculoskeletal health, they are not affordable for persons with limb loss in LMICs. Adequate prosthetic knees and feet for LMICs should be designed and tested by considering functionality (walking speeds, cadence, kneeling, squatting), musculoskeletal health (intact joint loading) and cost (affordable for amputees in limited-resource environments).

Chapter 6

The effect of spring extension assist mechanisms in polycentric prosthetic knees

Extension assist mechanisms in passive prosthetic knees improve the swing phase of gait. In conventional polycentric knees using a four-bar linkage, such as the ICRC knee presented in Chapter 5, the extension assist links one of the bars to the body of the prosthesis, causing the spring to push towards flexion when the knee reaches a certain flexion angle. A novel low-cost polycentric knee design has been created that pushes the knee towards extension throughout the knee full range of motion. This chapter presents the effect of the different extension assist mechanisms on the transfemoral amputee musculoskeletal function, loading and satisfaction with the prosthesis.

6.1 Introduction

It is estimated that 65 million amputees live in low-to-middle income countries (LMICs) and represent 64% of the world amputee population (ATscale 2020). Resource limited countries face systematic challenges arising from high demand and low supply of assistive technologies for mobility, with only 5-15% amputees being equipped with a prosthesis (ATscale 2020). The International Committee of the Red Cross (ICRC) physical rehabilitation programme has been distributing affordable monocentric and polycentric prosthetic knee units in LMICs since 1979. Specifically, ICRC provided 1015 prostheses in 2020 in Cambodia, where landmines and explosive remnants of war often lead to amputations (Physical Rehabilitation Programme 2020). Although the ICRC polycentric prosthetic knee is cost-effective, Chapter 5 demonstrated that it presents limited functional abilities (as determined by cadence and walking speed). The ICRC knee's extension assist mechanism links the rear bar to the body of the prosthesis. This design introduces a singularity in the delivery of the spring action, and past a certain knee flexion angle, the spring pushes towards flexion. As detailed in Chapter 5, this design feature creates excessive knee flexion angles in early swing, which require participants to wait for the knee to come back to the heel strike position, limiting the ability to walk fast.

Another limitation of the ICRC prosthesis is durability. The polypropylene material used in the ICRC system may deteriorate with time and start cracking. Additionally, the load acts through the bushings and links during stance, and this might also cause durability issues. The repairing process requires costly professional services and well-equipped workshops. However, lack of financial resources and materials are considered barriers to the provision of appropriate professional services in LMICs. Moreover, the limited number of healthcare facilities are located in urban areas. As only 20% of the population lives in urban areas (Radcliffe et al. 2016), rurally-located amputees need to travel long and costly distances to clinics. Consequently, amputees may not attend the clinic and are likely to rely on wheelchair and crutches for ambulation. This inevitably results in a severe and lifelong physical disability, which may cause stigmatisation and social and employment exclusion.

Through-knee amputees have reported improved performance and quality of life compared to above-knee amputees (Penn-Barwell 2011). Despite of this, through-knee surgeries are less common than above-knee amputations due to a lack of prosthetic components suitable for through-knee amputees. Given the long-term benefit of through-knee amputations and advancement in surgeries, there is a high demand for affordable polycentric prosthetic knees designed for persons with knee disarticulations. TaKeuP, a novel low-cost polycentric knee developed by researchers at Imperial College London (patent filing number 245-0004315541), can fit both above- and through-knee amputees. The TaKeuP knee consists of a patented four-bar linkage system which uses inexpensive bicycle parts, easily accessible in LMICs. The prosthesis fitting and service require low level skill, and can be completed by users. The bodyweight is carried by the main upper and lower parts of the prosthesis during stance, and not by the moving links as is the case with the ICRC knee, increasing the durability of the four-bar mechanism. Different from the

ICRC knee design, TaKeuP uses a spring extension mechanism that pushes the knee towards extension at all knee angles. Figure 6.1 shows the conventional extension assist mechanism used by ICRC, which links the rear bar to the top part of the knee, and the novel extension assist mechanism used by TaKeuP, which links the bottom to the top part of the knee.

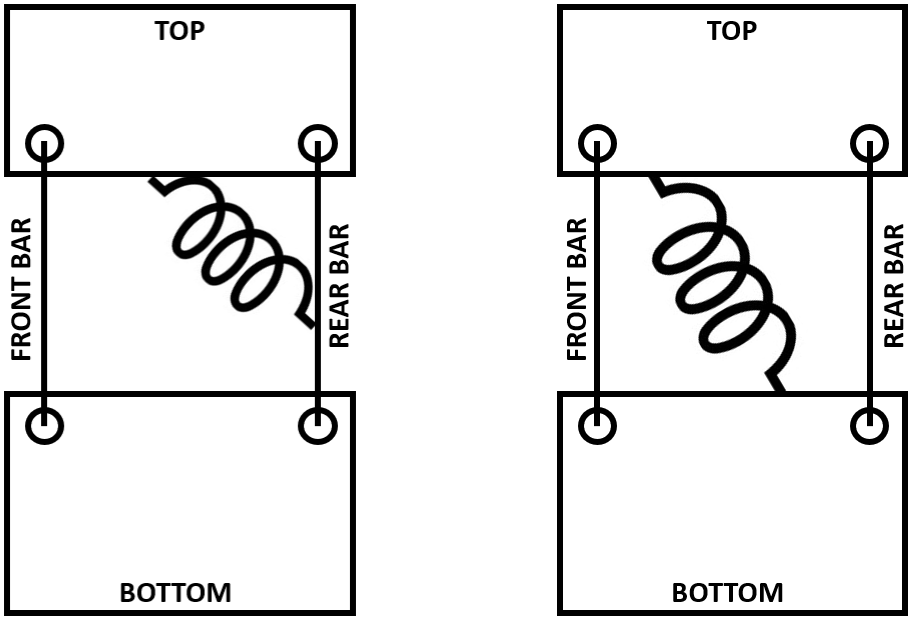


Figure 6.1: Prosthetic knee extension assist mechanisms. (a) Conventional extension assist that links the rear bar to the body of the prosthesis. (b) Novel extension assist that links the top and bottom knee parts.

The impact of the TaKeuP prosthetic knee on the amputee function, loading and satisfaction with the prosthesis has not been previously investigated. This chapter aims to investigate the effect of different spring extension assist mechanisms in polycentric prosthetic knees (ICRC and TaKeuP) on the walking capacity and prosthesis satisfaction of unilateral above/through-knee traumatic amputees. It is hypothesized that the novel extension mechanism of the TaKeuP knee improves functional abilities and user satisfaction compared to the conventional extension assist mechanism used in the ICRC polycentric prosthetic knee.

6.2 Methods

6.2.1 Data acquisition and processing

Ethical approval was obtained from the Joint Research Compliance Office and the Imperial College Research Ethics Committee (Reference 20IC6268). Eight UTF healthy amputees (two civilian, six ex-military) took part in this study. The participant details are presented in Table 6.1. Signed informed consent was obtained from all study participants. All participants had been prosthesis users for a minimum of two years and had a K3 activity level (ability or potential for ambulation with variable speed (Balk et al. 2018)) or higher. Through-knee amputees were fitted with quadrilateral prosthetic sockets and above-knee amputees were fitted with ischial containment sockets.

Part. No. (Gender)	Cause of amp.	Age (y)	Adj. mass (kg)	Height (m)	Amp. level	Own prosth. knee	Own prosth. foot
1 (Male)	IED	33	81	1.78	TF	Rheo XC	Vari-Flex
2 (Male)	Motorcycle accident	41	77	1.78	TK	Genium X3	Freedom Innovations Low Profile
3 (Male)	Motorcycle accident	66	69	1.73	TF	Orion3	Echelon VT
4 (Male)	Cancer surgery	57	73	1.65	TF	Orion3	Echelon
5 (Female)	Knee injury	55	102	1.72	TK	Genium X3	Triton Low Profile
6 (Male)	IED	47	95	1.76	TF	Genium X3	Triton 1C64 Heavy Duty
7 (Male)	Leg injury	57	94	1.76	TF	C-leg	Triton
8 (Male)	Gunshot	34	101	1.80	TK	KX06	SACH
Mean ± SD		49 ± 11	86 ± 12	1.75 ± 0.04			

Table 6.1: UTF study participant details.
IED, improvised explosive device. TF, transfemoral. TK, through-knee.

Study participants completed walking trials in two different fitting cases: ICRC knee with a solid-ankle-cushioned-heel (SACH) foot and the participant's own socket; and TaKeuP knee with SACH foot and participant's own socket. The order of fitting cases was randomised across participants. The prosthetic alignment was ensured following the process detailed in Chapter 5. The prosthetic socket was not changed between trials. The ICRC and TaKeuP knees were fitted with the same SACH foot for each participant. The alignment of the SACH foot was adjusted copying the participant's own prosthetic set-up. All

participants completed a familiarization period in the laboratory, where they walked with the prostheses using parallel walking bars for as long as they required. Retro-reflective markers were placed on lower limb anatomical and prosthetic landmarks following the locations presented in Table 4.2, Chapter 4. Figure 6.2 presents one representative UTF study participant in the two fitting cases.

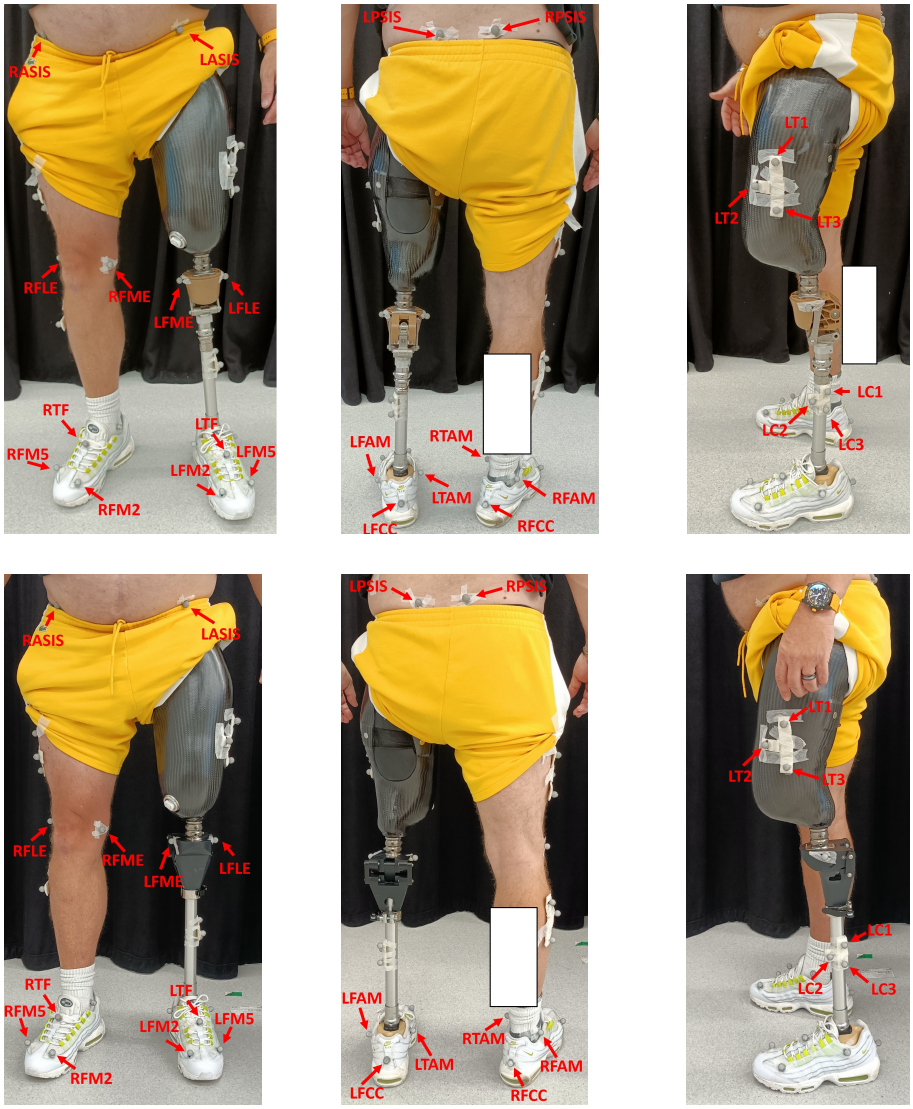


Figure 6.2: UTF study participant. The labels highlight the marker and cluster positions in Table 4.2, Chapter 4. Top: ICRC knee and SACH foot. Bottom: TaKeuP knee and SACH foot.

Static, self-selected and fast speed gait data were collected using a 10-camera VICON optoelectronic based motion capture analysis system (VICON 2.10.3, Oxford Metrics Group, UK). The self-selected speed walking trials were performed with complete foot placement on force plates (Kistler Type 9286B, Kistler Instrumente AG, Winterthur, Switzerland). Targeting effects were minimized through the continuation of the trial until sufficient complete foot placements were achieved.

After completing the motion trials, participants completed the validated SAT-PRO prosthesis satisfaction questionnaire (Bilodeau et al. 1999) for each trialled prosthesis. The SAT-PRO questionnaire, presented in Appendix C, consists of 15 questions (see Table 6.2) with four possible answers, which were assigned the following scores:

- Totally agree = 3
- Rather agree = 2
- Rather disagree = 1
- Totally disagree = 0

A minimum of 11 answered questions were required to consider the questionnaire valid. Questions 6 and 14 were assigned reversed scores (totally agree = 0, rather agree = 1, rather disagree = 2, totally disagree = 3), as recommended in the SAT-PRO questionnaire validation study (Bilodeau et al. 1999), because they refer to negative aspects of the prosthesis. The total satisfaction level for each individual was obtained by dividing the total number of scored points in the questionnaire by the maximum number of points, which was dependent on the number of answered questions. Finally, the scores were averaged across participants for each trialled prosthetic device. As the prosthetic knees were not trialled at home for a longer time, questions 3, 4, 8 and 9 (see Table 6.2) could not have been accurately answered based on the trial in the laboratory. The analysis will focus on the questions where the prosthetic knees were most likely to influence the participants' answers.

6.2.2 Anthropometry and body segment parameters

The intact and prosthetic segment inertial parameters were calculated as detailed in Chapter 5. Briefly, the DeLeva method was used to estimate the inertial parameters of the intact segments (De Leva 1996). The prosthetic inertial parameters were estimated using the reaction board method with moment equilibrium (Smith et al. 2014) as detailed in Chapter 3. The composite thigh moment of inertia was obtained by adding the moment of inertia of each component in the thigh segment using the Huygens-Steiner parallel axis theorem (Haas 1928). The ICRC system is illustrated in Figure 6.3. The ICRC composite thigh segment consisted of the residual limb, prosthetic liner, prosthetic socket, connectors, top component of the knee and rear bar. The ICRC shank segment consisted of the front bars and connecting pylon.

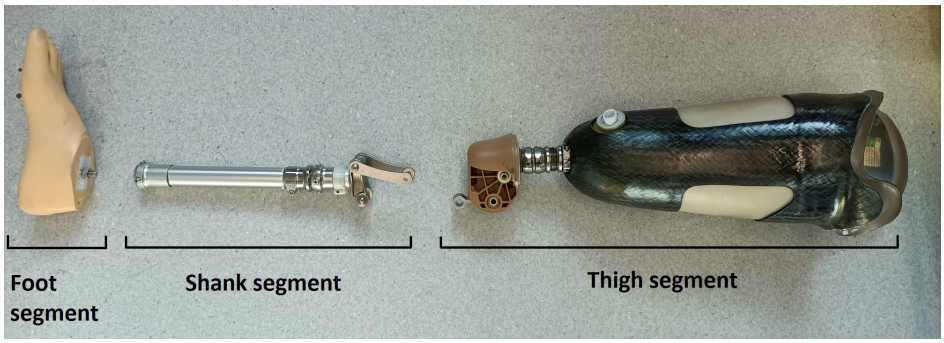


Figure 6.3: ICRC prosthesis system.

Figure 6.4 shows the TaKeuP system. The TaKeuP composite thigh segment consisted of the residual limb, prosthetic liner, socket, connector and top component of the knee with the external bars. The TaKeuP shank segment consisted of the pylon and bottom component of the knee.

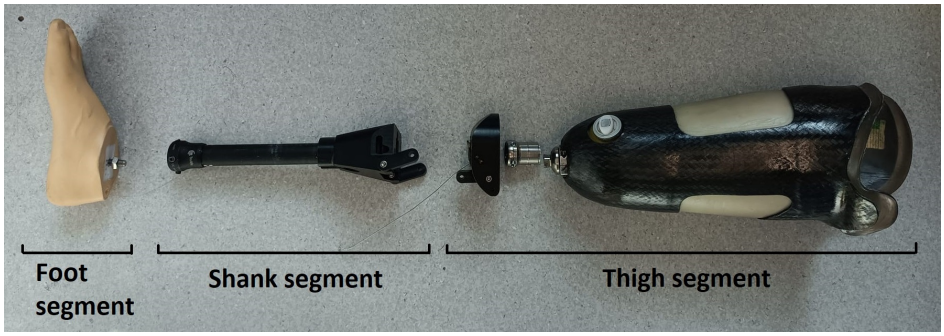


Figure 6.4: TaKeuP prosthesis system.

6.2.3 Musculoskeletal modelling

Musculoskeletal modelling was performed as detailed in Chapter 4 for each prosthesis. Briefly, Freebody v2.1 (Cleather & Bull 2015, Ding et al. 2016) was used to perform inverse kinematics, inverse dynamics and musculoskeletal modelling simulations of self-selected walking speed trials. Muscle and joint contact forces were estimated using a one-step static load sharing optimisation based on the minimization of muscle activations cubed (Crowninshield & Brand 1981). The anatomical information required for the UTF musculoskeletal models were obtained through linear scaling to able-bodied and above/through-knee anatomical datasets. The anatomical datasets for the intact limb models were chosen based on similar mass, gender and limb length to pelvis width ratio (Ding et al. 2019). The anatomical datasets and regression models developed in Chapter 2 were used for scaling the amputated limb models, and chosen based on similar pelvis width, adjusted body mass index (calculated according to literature (Tzamaloukas et al. 1994)) and stump length to pelvis width ratio. The same anatomical dataset was used for each model in the two prosthesis fitting conditions.

6.2.4 Data analysis

The whole-time data series for kinematics, kinetics and joint contact forces were expressed as a gait cycle percentage from 0% at heel strike to 100% at the consecutive heel strike, in intervals of 1% and averaged over three trials. Statistical parametric mapping (SPM) was used to compare the whole time-series data (Friston et al. 2007, Papi et al. 2020, Pataky et al. 2013) between prosthesis fitting conditions. Depending on data normality, one-way ANOVA with repeated measures or the Friedman test were used. IBM SPSS Statistics 27.0.0 (IBM Corp. Armonk, NY) was used to statistically compare single-valued gait characteristics. Data normality was checked using the Shapiro-Wilk statistical test. Parametric data were compared between conditions by one-way ANOVA with repeated measures, and non-parametric data were compared using Friedman with Wilcoxon tests. p values of less than .05 were considered to indicate statistical significance.

6.3 Results

The gait characteristics of the prosthetic and intact limbs were statistically compared between the ICRC and TaKeuP prosthesis fitting cases. All biomechanical parameters are reported for the self-selected speed. Normally distributed data are presented as Mean ± SD and non-normally distributed data are presented as Median [95% Confidence Interval]. The whole-time data are presented over the course of the gait cycle. Statistical parametric mapping results are presented for identification of significant differences between prostheses, where grey threshold clusters indicate statistically significant differences, and red dashed lines represent critical thresholds. The key statistically and clinically significant results (differences of 10% or higher) are summarised.

6.3.1 SAT-PRO questionnaires

Table 6.2 shows the results of the SAT-PRO questionnaire. Overall, participants reported levels of satisfaction of 83% with TaKeuP's new design, and of 80% with the conventional ICRC design, where a value of 0% indicates that the participant is very dissatisfied with the prosthesis, and a value of 100% represents the best possible satisfaction measured (Bilodeau et al. 1999). The results obtained from one study participant were excluded from the study as fewer questions than 11 were answered in the SAT-PRO questionnaires for both trialled knees. Analyzing the questions where the prosthetic knee was most likely to influence the questionnaire outcome, participants reported higher median scores for TaKeuP than ICRC for functionality and appearance. However, statistical significance was not reached. Participants found it equally easy to understand how to use the TaKeuP and ICRC prosthetic knees.

Question	ICRC *Median [95% CI]* (%)	TaKeuP *Median [95% CI]* (%)
1. My prosthesis is comfortable.	*67 [39-100]*	*67 [50-93]*
2. When I am in the presence of people other than my family, I am at ease wearing my prosthesis.	*67 [31-100]*	*100 [47-100]*
3. My prosthesis is easy to clean.	*67 [31-100]*	*67 [64-97]*
4. My prosthesis works well regardless of the weather.	*33 [17-87]*	*67 [44-99]*
5. My prosthesis is easy to put on.	*100 [69-100]*	*100 [61-100]*
6. There are chances that I will hurt myself with the prosthesis.	*33 [5-71]*	*33 [4-82]*
7. I find it easy to move with my prosthesis.	*67 [23-91]*	*83 [37-100]*
8. The repairs/adjustments to my prosthesis are done in reasonable time.	*67 [48-100]*	*83 [24-100]*
9. My prosthesis will last me a long time.	*67 [28-100]*	*67 [31-100]*
10. When I wear my prosthesis, I can accomplish more things than without it.	*100 [38-100]*	*100 [61-100]*
11. I am satisfied with the look of my prosthesis.	*67 [31-100]*	*67 [36-97]*
12. I find it easy to use my prosthesis with or without a walker/cane.	*100 [42-100]*	*67 [50-93]*
13. It was easy to understand how to use my prosthesis.	*100 [61-100]*	*100 [57-100]*
14. My prosthesis caused me physical pain or discomfort.	*67 [29-95]*	*67 [44-99]*
15. In general, I am satisfied with my prosthesis.	*67 [17-87]*	*67 [29-95]*
Total satisfaction	*80 [42-90]*	*83 [50-94]*

Table 6.2: SAT-PRO prosthesis satisfaction questionnaire scores.

6.3.2 Prosthetic inertial parameters

Table 6.3 presents the mass of prosthetic components. The full TaKeuP prosthesis was lighter by 0.1 kg than the ICRC prosthesis (3.7 kg, $p<.001$). The TaKeuP shank segment was heavier by 0.1 kg than the ICRC shank segment (0.6 kg, $p<.001$). The composite thigh segment was lighter with TaKeuP by 0.2 kg than ICRC (13.8 kg, $p<.001$). The composite thigh included the residual thigh, socket, liner, connector and upper component of the prosthetic knee.

Parameter	ICRC Mean ± SD	TaKeuP Mean ± SD
Full prosthesis mass (kg)	3.73 ± 0.68 ***p<.001**	3.61 ± 0.68
Foot segment mass (kg)	0.59 ± 0.03	0.59 ± 0.03
Shank segment mass (kg)	0.62 ± 0.04 ***p<.001**	0.75 ± 0.04
Composite thigh segment mass (kg)	13.79 ± 2.48 ***p<.001**	13.55 ± 2.48

Table 6.3: Prosthesis components masses.
*Statistically significant differences between prostheses (p<.05).

6.3.3 Temporal and spatial gait characteristics

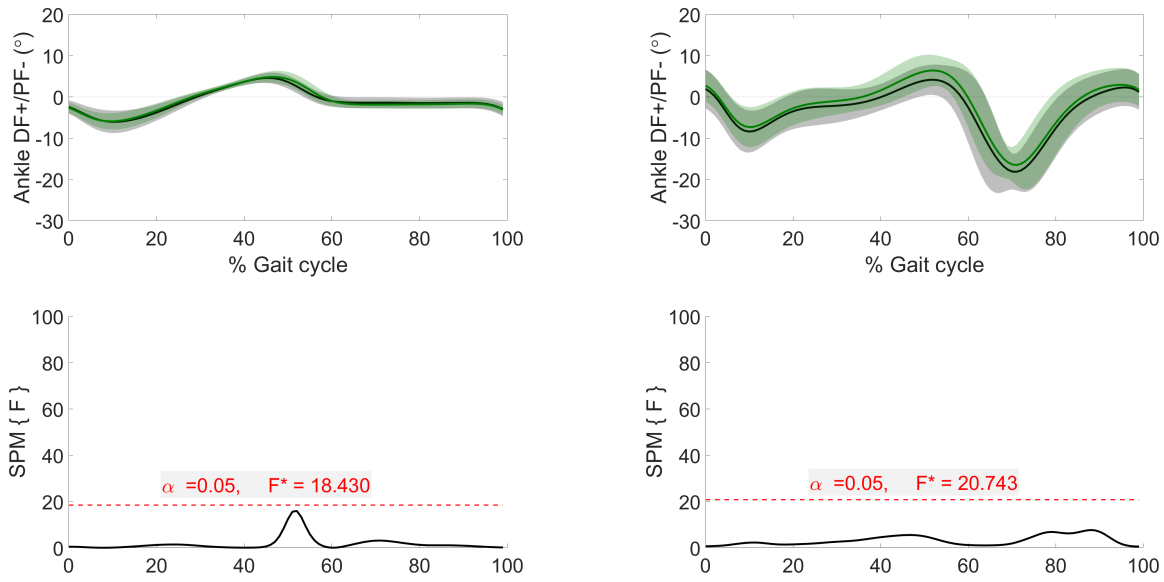
Table 6.4 presents the temporospatial parameters of UTF with ICRC and TaKeuP prostheses. When walking with TaKeuP, UTF spent a larger percentage of the prosthetic limb gait cycle in stance by 1.6% than ICRC (57.1%, p<.001). UTF walked faster with TaKeuP by 0.1 m/s than ICRC (1.2 m/s, p=.004). One participant was not able to walk at fast speeds with the ICRC and TaKeuP prostheses. There were no significant differences in the self-selected speeds, step length, gait symmetry index, stride length, cadence and step width between prosthesis fitting cases.

	ICRC Mean ± SD		TaKeuP Mean ± SD	
Biomechanical parameter	Prosthetic side	Intact side	Prosthetic side	Intact side
Step length (m)	0.69 ± 0.12	0.62 ± 0.05	0.71 ± 0.08	0.64 ± 0.04
Stride length (m)	1.33 ± 0.16	1.33 ± 0.16	1.36 ± 0.10	1.34 ± 0.12
Stance time (% gait cycle)	57.15 ± 2.35 ***p<.001**	69.16 ± 2.99	58.77 ± 2.14	68.91 ± 3.01
Self-selected speed (m/s)	1.03 ± 0.13		1.05 ± 0.13	
Cadence (steps/min)	92.74 ± 3.76		93.34 ± 8.24	
Step width (m)	0.17 ± 0.04		0.17 ± 0.03	
Gait SI (%)	92.27 ± 4.98		93.44 ± 3.22	
Fast speed (m/s)	1.19 ± 0.17 ***p=.004**		1.27 ± 0.21	

Table 6.4: Temporal and spatial gait characteristics.
(n=8, except for fast speed, where n=7). SI, symmetry index. *Statistically significant differences between prostheses (p<.05).

6.3.4 Kinematics

Figure 6.5 and Table 6.5 show the sagittal plane ankle angles over the course of the gait cycle, with no significant differences between prosthesis fitting cases.



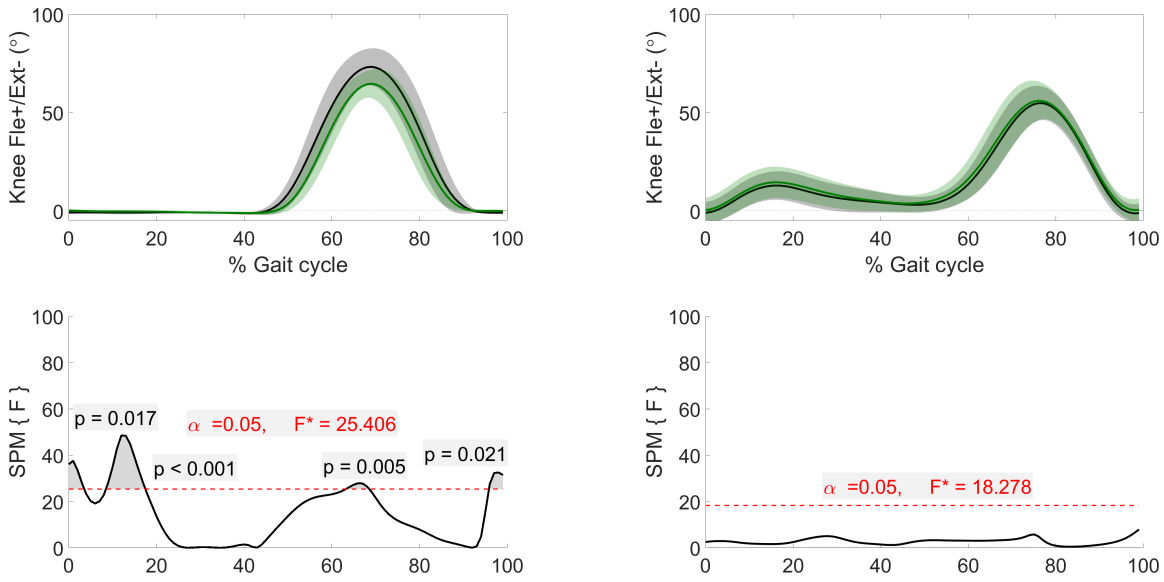
(a) Prosthetic side **(b)** Intact side

Figure 6.5: Top: Ankle DF (Dorsiflexion)/Plantar flexion (PF) angles with ICRC (black) and TaKeuP (green) prostheses. Bottom: Statistical parametric mapping results.

	ICRC Mean ± SD *Median [95% CI]*		TaKeuP Mean ± SD *Median [95% CI]*	
Biomechanical parameter	Prosthetic side	Intact side	Prosthetic side	Intact side
Peak ankle dorsiflexion (°)	4.71 ± 1.23	6.82 ± 3.62	4.92 ± 1.39	8.18 ± 3.89
Peak ankle plantar flexion (°)	*4.90 [3.64-8.50]*	21.91 ± 5.40	*5.53 [4.22-7.73]*	19.94 ± 4.62
Ankle dorsiflexion/plantar flexion ROM (°)	10.79 ± 2.87	28.73 ± 6.42	10.90 ± 2.28	28.12 ± 6.90

Table 6.5: Sagittal plane ankle kinematics.
CI, confidence interval. ROM, range of motion.

Figure 6.6 shows the sagittal plane knee angles. SPM reported different prosthetic knee flexion angles between ICRC and TaKeuP in stance (p=.017, p<.001) and swing (p=.005, p=.021). When comparing discrete values in Table 6.6, the peak TaKeuP knee flexion was lower by 8.8° than ICRC (75.1°, p<.001). There were no significant differences in the intact knee sagittal plane angles between prosthesis fitting cases. The symmetry between the prosthetic and intact knee flexion angles was higher for TaKeuP than ICRC (p=.007).



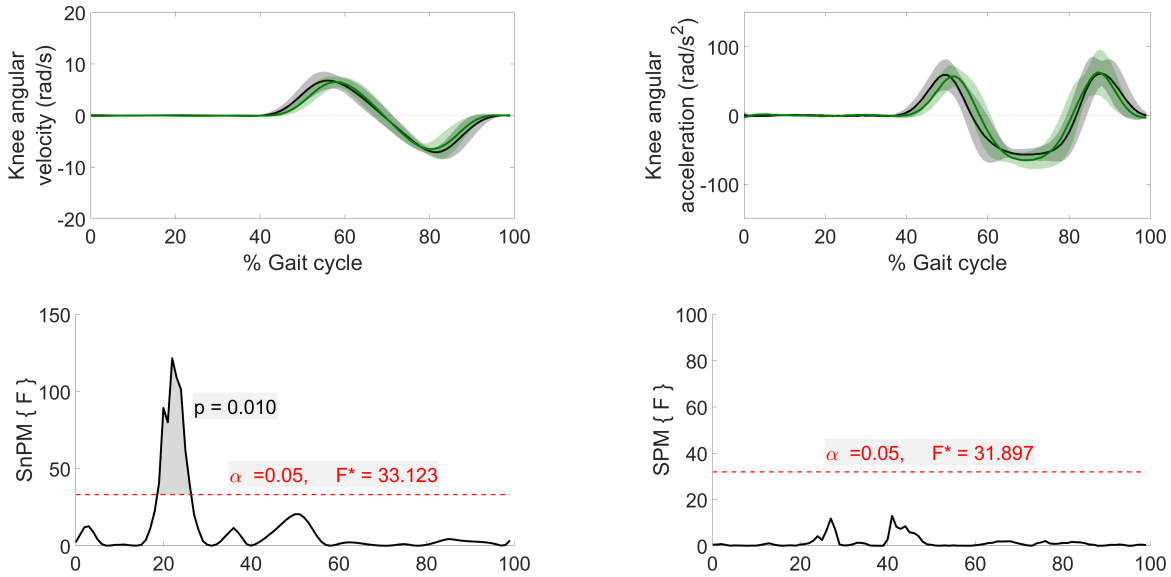
(a) Amputated side **(b)** Intact side

Figure 6.6: Top: Knee Flexion (Fle)/Extension (Ext) angles with ICRC (black) and TaKeuP (green) prostheses. Bottom: Statistical parametric mapping results.

	ICRC Mean ± SD		TaKeuP Mean ± SD	
Biomechanical parameter	Prosthetic side	Intact side	Prosthetic side	Intact side
Peak knee flexion (°)	75.08 ± 8.23 ***p<.001**	56.12 ± 8.52	66.31 ± 6.40	57.41 ± 9.37
Peak knee flexion early stance (°)	0.51 ± 0.26	13.72 ± 6.90	0.61 ± 0.37	11.56 ± 5.77
Prosthetic/intact knee flexion SI (%)	85.29 ± 8.74 ***p=.007**		90.74 ± 7.94	

Table 6.6: Sagittal plane knee kinematics.
SI, symmetry index. *Statistically significant prosthetic side differences between prosthesis fitting cases (p<.05).

Figure 6.7 shows the prosthetic knee angular velocity and acceleration over the course of the gait cycle. SPM reported different prosthetic knee angular velocities between ICRC and TaKeuP in stance (p=.010). When comparing discrete values in Table 6.7, the peak TaKeuP angular velocity in the swing phase of the gait cycle was lower by 0.7 rad/s than ICRC (8.0 rad/s, p=.008). No significant prosthetic knee angular acceleration differences were identified between prosthesis fitting cases.



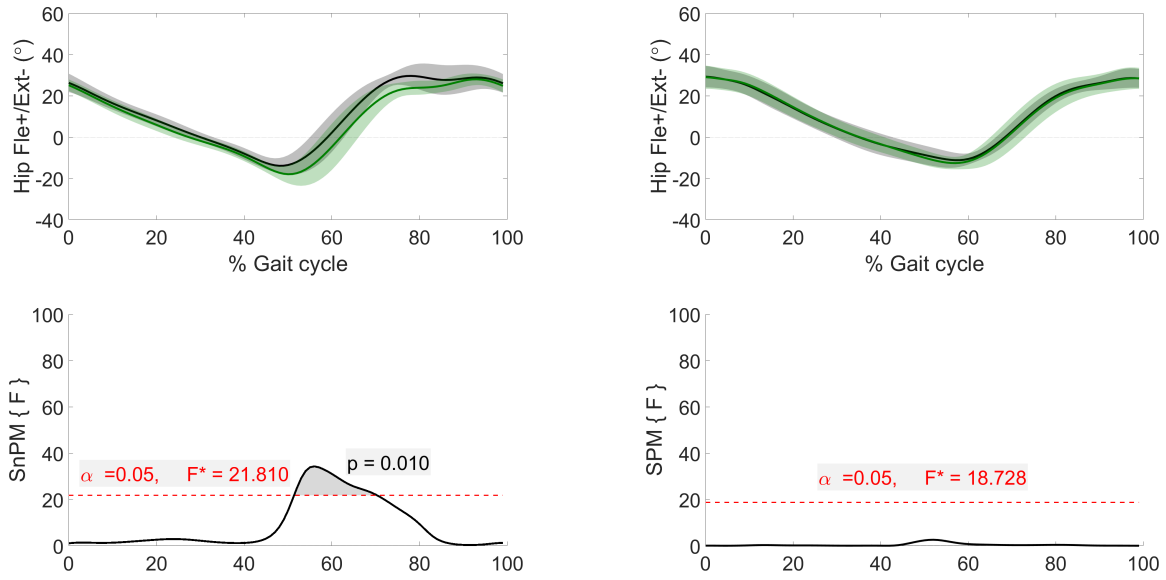
(a) Prosthetic side **(b)** Intact side

Figure 6.7: Top: Prosthetic knee angular velocity and acceleration with ICRC (black) and TaKeuP (green) prostheses. Bottom: Statistical parametric mapping results.

Biomechanical parameter	ICRC Mean ± SD	TaKeuP Mean ± SD
Peak knee angular velocity swing (rad/s)	8.02 ± 0.73 ***p=.008**	7.29 ± 0.92
Peak knee angular acceleration swing (rad/s^2)	90.50 ± 10.24	84.15 ± 11.56

Table 6.7: Peak prosthetic knee angular velocity and acceleration in late swing. *Statistically significant prosthetic side differences between prosthesis fitting cases (p<.05).

Figure 6.8 shows the sagittal plane hip angles over the course of the gait cycle. SPM reported higher prosthetic side hip extension angles with TaKeuP than ICRC in late stance (p=.010). When comparing discrete values in Table 6.8, the peak prosthetic side hip extension angles were larger with TaKeuP by 3.6° than ICRC (15.8°, p=.019).



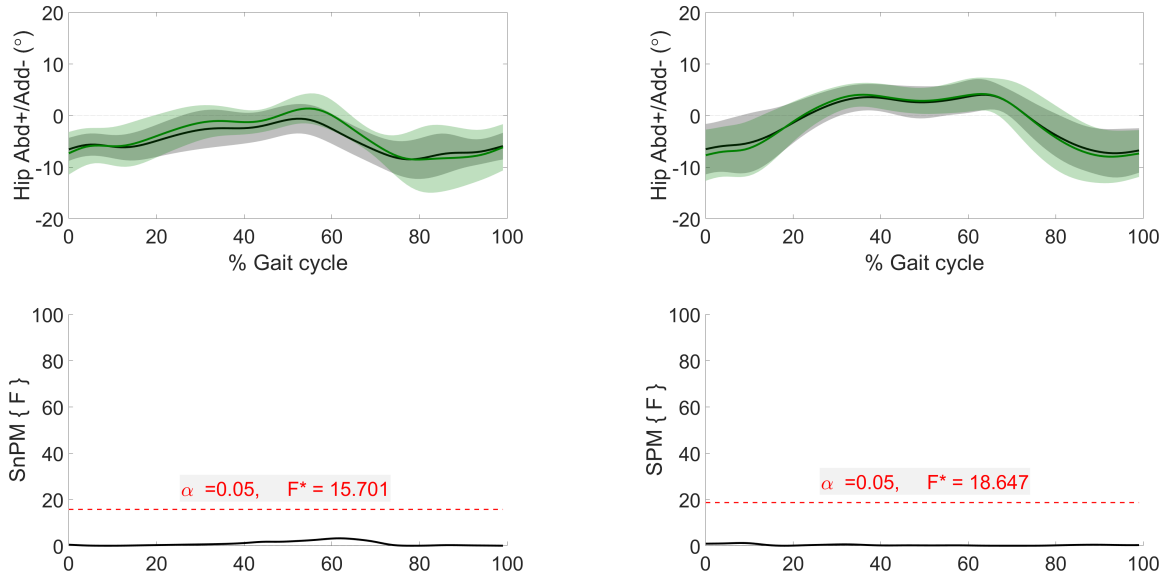
(a) Prosthetic side **(b)** Intact side

Figure 6.8: Top: Hip Flexion (Fle)/Extension (Ext) angles with ICRC (black) and TaKeuP (green) prostheses. Bottom: Statistical parametric mapping results.

	ICRC Mean ± SD *Median [95% CI]*		TaKeuP Mean ± SD *Median [95% CI]*	
Biomechanical parameter	Prosthetic side	Intact side	Prosthetic side	Intact side
Peak hip extension (°)	15.82 ± 4.00 ***p=.019**	11.90 ± 2.93	19.37 ± 6.04	13.67 ± 2.89
Peak hip flexion (°)	31.84 ± 5.75	30.73 ± 4.07	28.98 ± 2.87	30.40 ± 4.76
Hip extension/ flexion ROM (°)	47.66 ± 8.74	*44.29 [38.04-47.20]*	48.35 ± 7.40	*43.81 [40.59-47.56]*
Prosthetic/intact side hip extension SI (%)	81.10 ± 10.96		79.17 ± 9.30	

Table 6.8: Sagittal plane hip kinematics.
CI, confidence interval. ROM, range of motion. SI, symmetry index. *Statistically significant prosthetic side differences between prosthesis fitting cases (p<.05).

Figure 6.9 and Table 6.9 show the coronal plane hip angles over the course of the gait cycle, with no significant differences between prosthesis fitting cases.



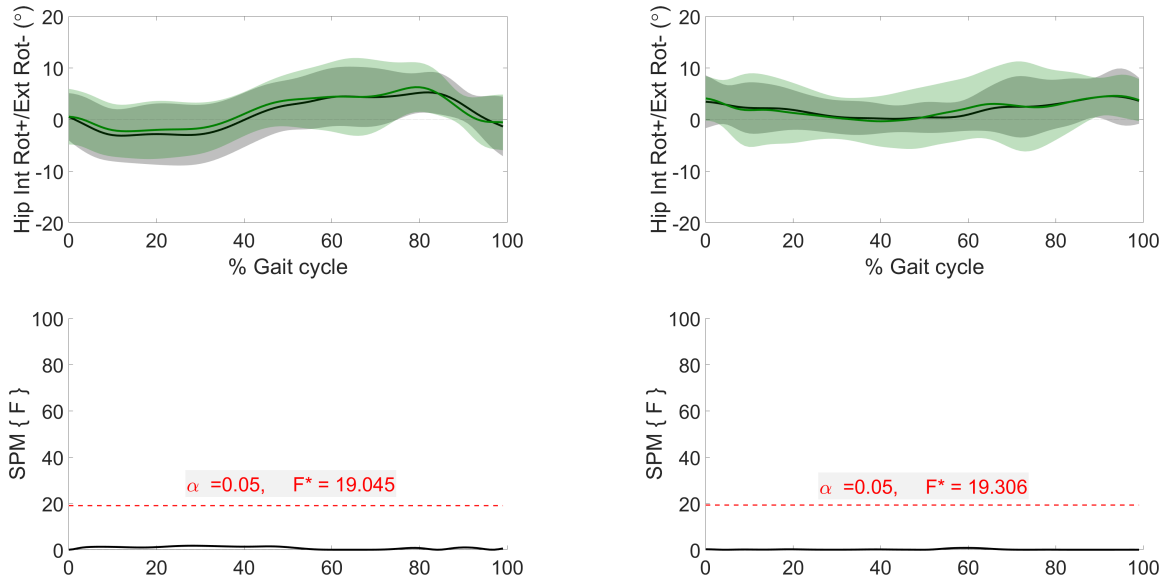
(a) Prosthetic side **(b)** Intact side

Figure 6.9: Top: Hip Abduction (Abd)/Adduction (Add) angles of UTF with ICRC (black) and TaKeuP (green) prostheses. Bottom: Statistical parametric mapping results.

	ICRC Mean ± SD *Median [95% CI]*		TaKeuP Mean ± SD *Median [95% CI]*	
Biomechanical parameter	Prosthetic side	Intact side	Prosthetic side	Intact side
Peak hip abduction (°)	1.40 ± 4.02	5.77 ± 1.91	2.32 ± 2.57	6.37 ± 1.76
Peak hip adduction (°)	*7.76* *[3.51-12.36]*	9.05 ± 5.28	*9.10* *[5.50-15.28]*	9.96 ± 5.53
Hip abduction / adduction ROM (°)	*9.04* *[7.84-10.84]*	14.82 ± 5.52	*10.88* *[6.76-18.65]*	16.33 ± 5.44

Table 6.9: Coronal plane hip kinematics.
CI, confidence interval. ROM, range of motion.

Figure 6.10 and Table 6.10 show the transverse plane hip joint kinematics over the course of the gait cycle, with no significant differences between prosthesis fitting cases.



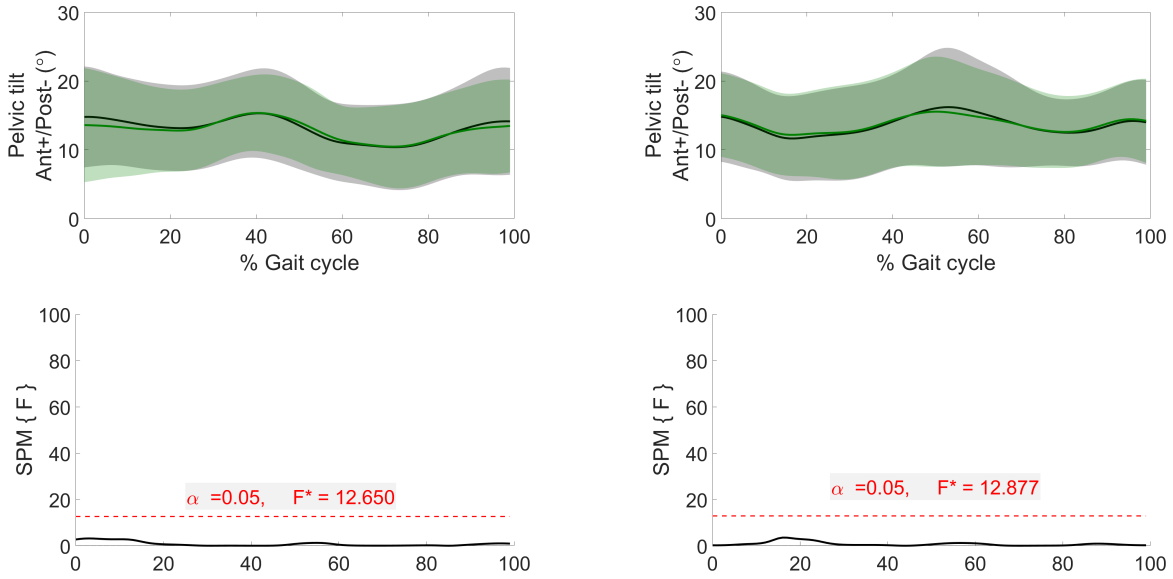
(a) Prosthetic side **(b)** Intact side

Figure 6.10: Top: Hip Internal (Int)/External (Ext) Rotation (Rot) angles with ICRC (black) and TaKeuP (green) prostheses. Bottom: Statistical parametric mapping results.

	ICRC Mean ± SD		TaKeuP Mean ± SD	
Biomechanical parameter	Prosthetic side	Intact side	Prosthetic side	Intact side
Hip internal/external rotation ROM (°)	14.23 ± 4.78	13.21 ± 2.52	14.29 ± 4.07	13.05 ± 2.38

Table 6.10: Transverse plane hip kinematics.
ROM, range of motion.

Figure 6.11 and Table 6.11 show the pelvic tilt angles over the course of the gait cycle, with no significant differences between prosthesis fitting cases.



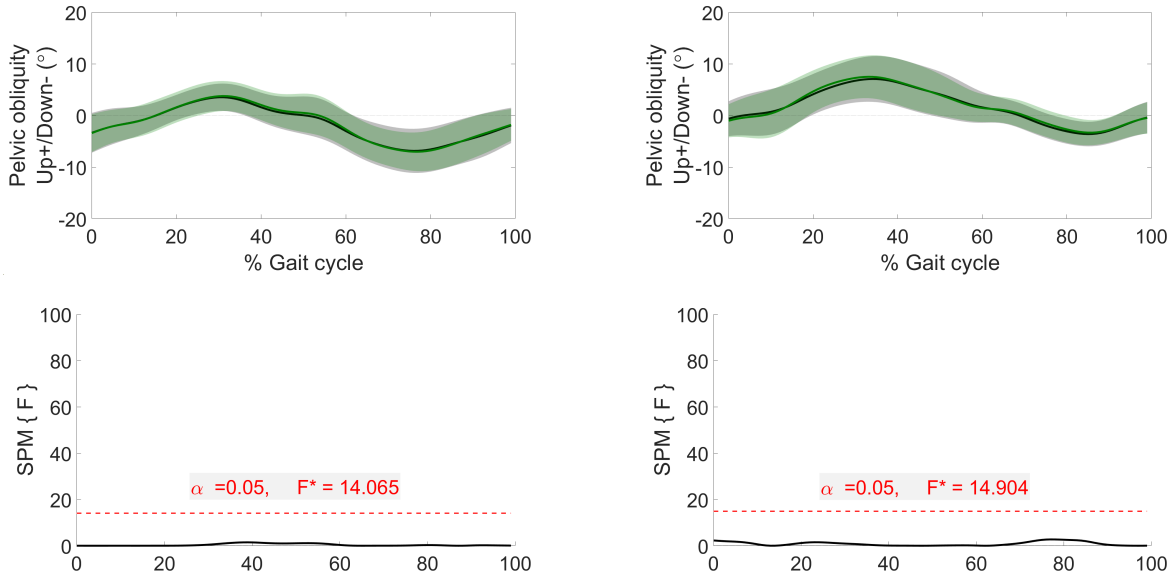
(a) Prosthetic side **(b)** Intact side

Figure 6.11: Top: Pelvic Anterior (Ant)/Posterior (Post) tilt angles with ICRC (black) and TaKeuP (green) prostheses. Bottom: Statistical parametric mapping results.

	ICRC Mean ± SD		TaKeuP Mean ± SD	
Biomechanical parameter	Prosthetic side	Intact side	Prosthetic side	Intact side
P2P pelvic tilt (°)	8.42 ± 2.86	7.03 ± 2.15	8.61 ± 2.21	6.47 ± 1.90

Table 6.11: Sagittal plane pelvic kinematics.
P2P, peak-to-peak.

Figure 6.12 and Table 6.12 show the pelvic obliquity angles over the course of the gait cycle, with no significant differences between prosthesis fitting cases.



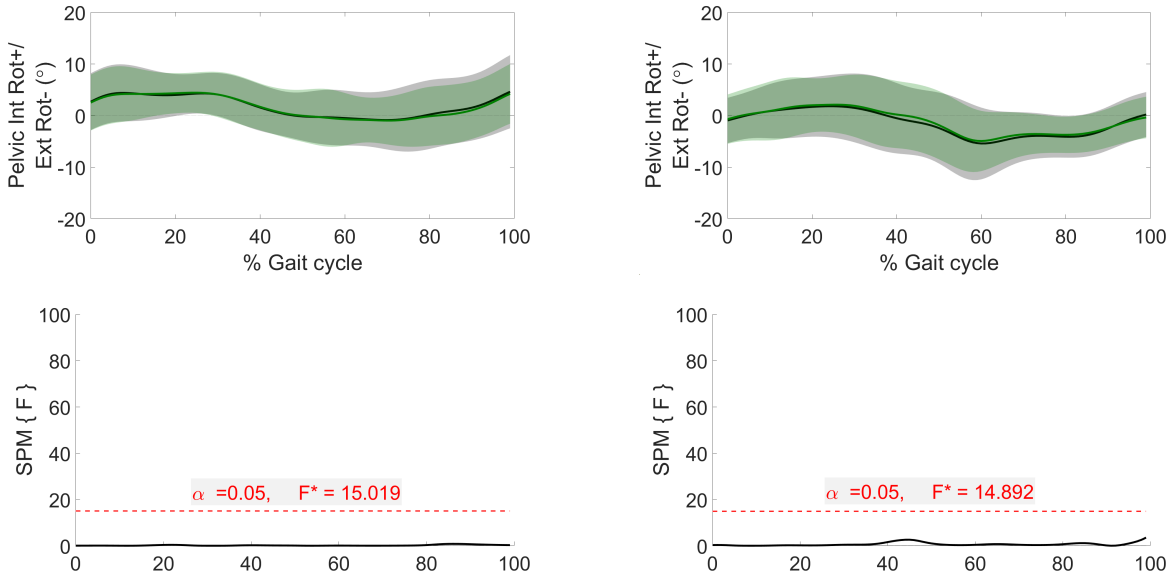
(a) Prosthetic side **(b)** Intact side

Figure 6.12: Top: Pelvic obliquity angles with ICRC (black) and TaKeuP (green) prostheses. Bottom: Statistical parametric mapping results.

	ICRC *Median [95% CI]*		TaKeuP *Median [95% CI]*	
Biomechanical parameter	Prosthetic side	Intact side	Prosthetic side	Intact side
P2P pelvic obliquity (°)	*11.34 [8.21-13.16]*	*11.88 [8.58-13.60]*	*11.58 [9.22-13.00]*	*11.85 [8.89-13.85]*

Table 6.12: Coronal plane pelvic kinematics.
CI, confidence interval. P2P, peak-to-peak.

Figure 6.13 and Table 6.13 shows the transverse plane pelvic rotation angles over the course of the gait cycle, with no significant differences between prosthesis fitting cases.



(a) Prosthetic side **(b)** Intact side

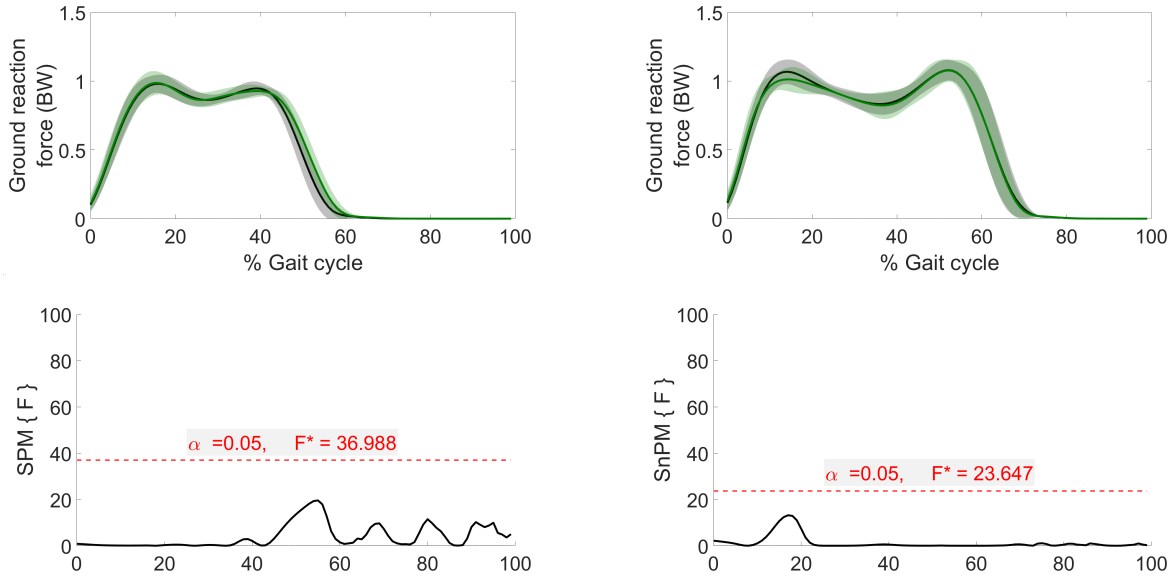
Figure 6.13: Top: Pelvic Internal (Int)/External (Ext) Rotation (Rot) angles with ICRC (black) and TaKeuP (green) prostheses. Bottom: Statistical parametric mapping results.

	ICRC Mean ± SD *Median [95% CI]*		TaKeuP Mean ± SD *Median [95% CI]*	
Biomechanical parameter	Prosthetic side	Intact side	Prosthetic side	Intact side
P2P pelvic rotation (°)	10.77 ± 3.08	*9.34 [8.10-14.84]*	10.88 ± 2.25	*10.39 [8.85-14.48]*

Table 6.13: Transverse plane pelvic kinematics.
CI, confidence interval. P2P, peak-to-peak.

6.3.5 Kinetics

Figure 6.14 and Table 6.14 shows the ground reaction forces (GRF) over the course of the gait cycle, with no significant differences between prosthesis fitting cases.



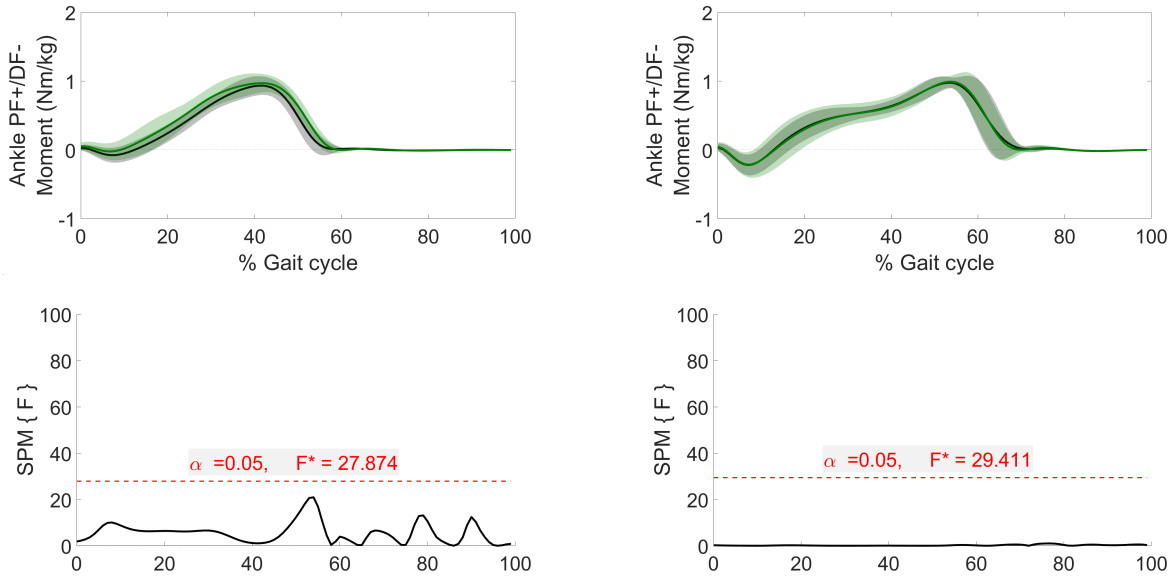
(a) Prosthetic side **(b)** Intact side

Figure 6.14: Top: Ground reaction forces (GRF) with ICRC (black) and TaKeuP (green) prostheses. Bottom: Statistical parametric mapping results.

	ICRC Mean ± SD		TaKeuP Mean ± SD	
Biomechanical parameter	Prosthetic side	Intact side	Prosthetic side	Intact side
First peak GRF (BW)	1.02 ± 0.06	1.11 ± 0.07	1.02 ± 0.09	1.05 ± 0.07
Second peak GRF (BW)	0.96 ±0.04	1.11 ± 0.07	0.94 ± 0.03	1.12 ± 0.09

Table 6.14: Ground reaction forces (GRF).

Figure 6.15 and Table 6.15 show the sagittal plane ankle moments over the course of the gait cycle, with no significant differences between prosthesis fitting cases.



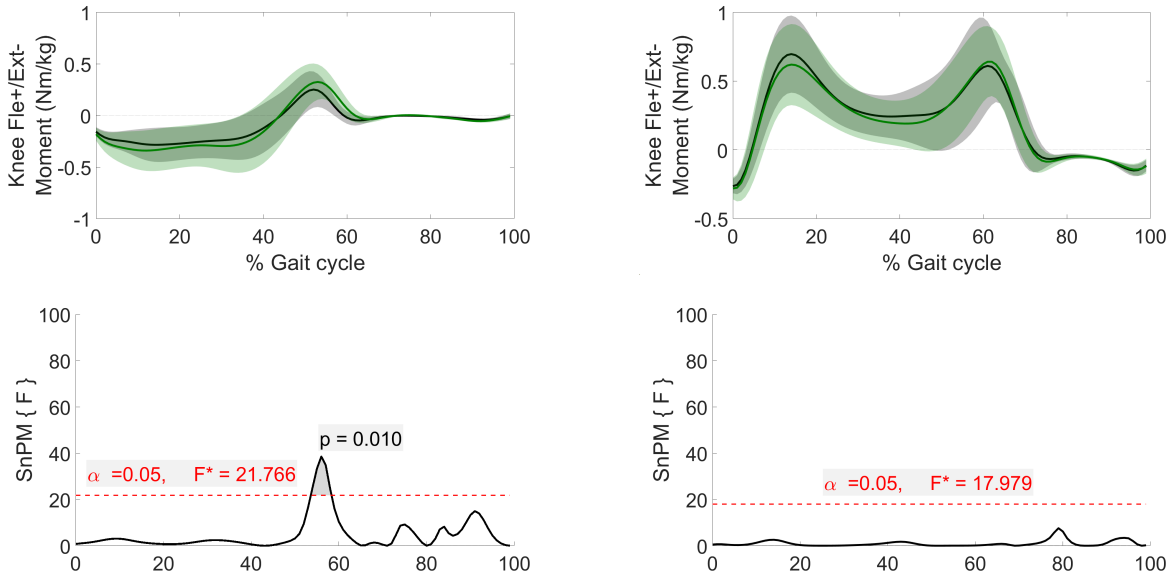
(a) Prosthetic side **(b)** Intact side

Figure 6.15: Top: Ankle Plantar flexion (PF)/Dorsiflexion (DF) moments with ICRC (black) and TaKeuP (green) prostheses. Bottom: Statistical parametric mapping results.

	ICRC Mean ± SD *Median [95% CI]*		TaKeuP Mean ± SD *Median [95% CI]*	
Biomechanical parameter	Prosthetic side	Intact side	Prosthetic side	Intact side
Peak ankle plantar flexion moment (Nm/kg)	0.95 ± 0.13	1.04 ± 0.11	1.00 ± 0.14	1.06 ± 0.11
Peak ankle dorsiflexion moment (Nm/kg)	*0.09 [0.04-0.17]*	0.23 ± 0.13	*0.05 [0.01-0.15]*	0.25 ± 0.15

Table 6.15: Sagittal plane ankle moments.
CI, confidence interval.

Figure 6.16 show the sagittal plane knee moments over the course of the gait cycle. SPM reported higher proshetic knee flexion moments for TaKeuP than ICRC in late stance (p=.010). When comparing discrete values in Table 6.16, the peak prosthetic knee flexion moments were higher for TaKeuP by 0.1 Nm/kg than ICRC (0.3 Nm/kg, p=.033). There were no significant differences in the intact knee sagittal plane moments between prosthesis fitting cases.



(a) Prosthetic side **(b)** Intact side

Figure 6.16: Top: Knee Flexion (Fle)/Extension (Ext) moments with ICRC (black) and TaKeuP (green) prostheses. Bottom: Statistical parametric mapping results.

	ICRC Mean ± SD		TaKeuP Mean ± SD	
Biomechanical parameter	Prosthetic side	Intact side	Prosthetic side	Intact side
Peak knee flexion moment (Nm/kg)	0.30 ± 0.13 ***p=.033**	0.83 ± 0.23	0.37 ± 0.14	0.81 ± 0.22
Peak knee extension moment (Nm/kg)	0.37 ± 0.14	0.27 ± 0.06	0.43 ± 0.21	0.30 ± 0.08

Table 6.16: Sagittal plane knee moments.
*Statistically significant prosthetic side differences between prosthesis fitting cases (p<.05).

Figure 6.17 and Table 6.17 show the coronal plane intact knee moments over the course of the gait cycle, with no significant differences between prosthesis fitting cases.

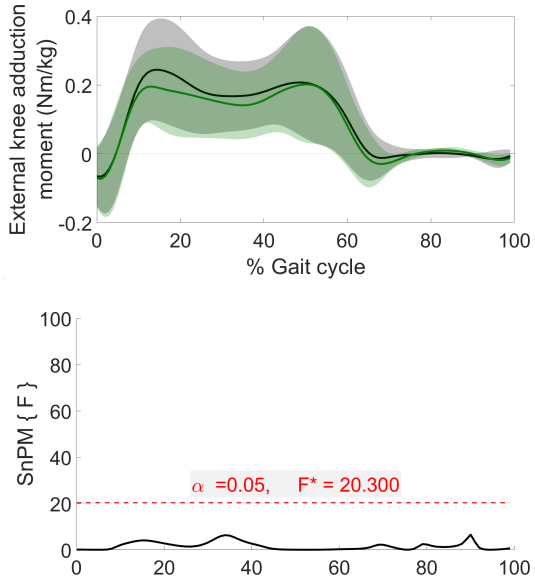
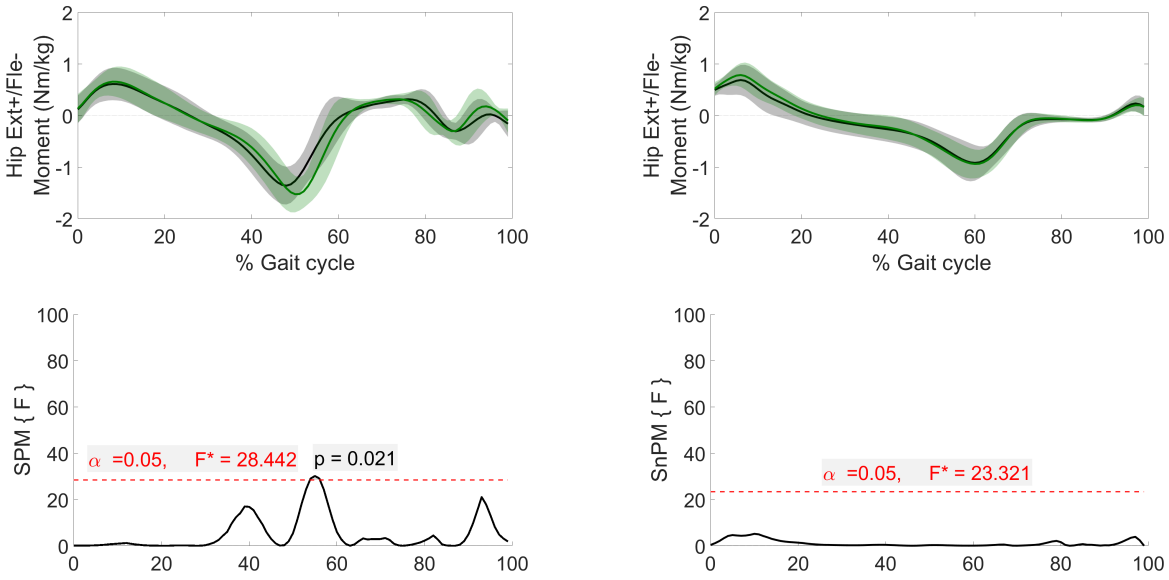


Figure 6.17: Top: External intact knee adduction moments with ICRC (black) and TaKeuP (green) prostheses. Bottom: Statistical parametric mapping results.

Biomechanical parameter	ICRC Mean ± SD	TaKeuP Mean ± SD
Peak knee adduction moment (Nm/kg)	0.28 ± 0.15	0.27 ± 0.15
Peak knee loading rate (Nm/kg.s)	3.72 ± 1.41	3.71 ± 1.30

Table 6.17: Coronal plane intact knee moments and loading rate.

Figure 6.18 shows the sagittal plane hip joint moments over the course of the gait cycle. SPM reported higher prosthetic side hip flexion moments in late stance with TaKeuP than ICRC (p=.021). When comparing discrete values in Table 6.18, the peak prosthetic side hip flexion moments were larger by 0.2 Nm/kg with TaKeuP than ICRC (1.6 Nm/kg, p=.017). There were no significant differences in the intact side hip sagittal plane moments between prosthesis fitting cases.



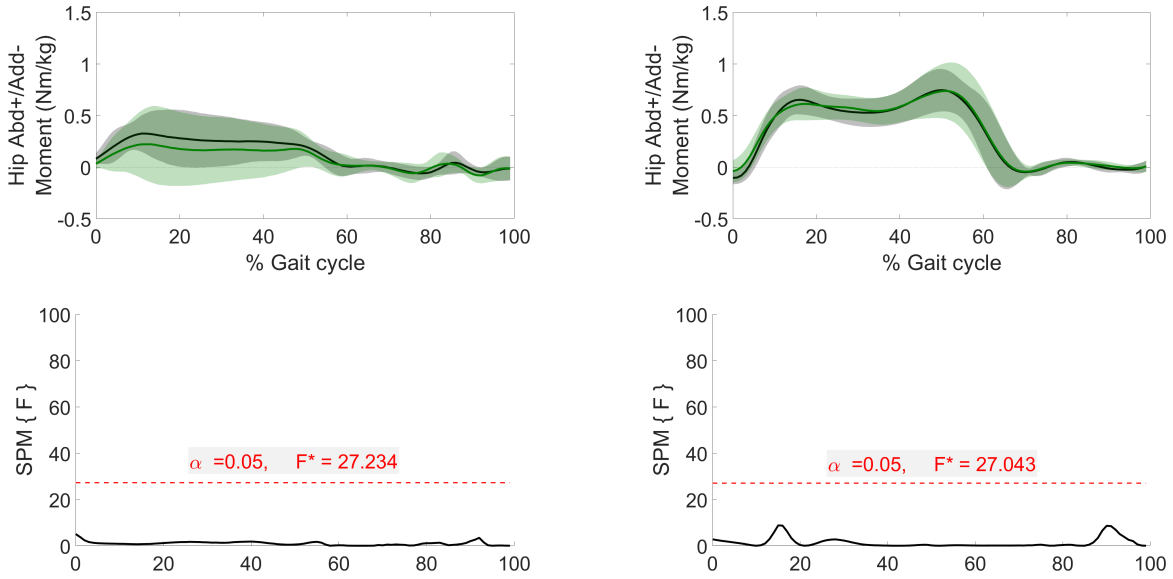
(a) Prosthetic side **(b)** Intact side

Figure 6.18: Top: Hip Extension (Ext)/Flexion (Fle) moments with ICRC (black) and TaKeuP (green) prostheses. Bottom: Statistical parametric mapping results.

	ICRC Mean ± SD		TaKeuP Mean ± SD	
Biomechanical parameter	Prosthetic side	Intact side	Prosthetic side	Intact side
Peak hip extension moment (Nm/kg)	0.69 ± 0.27	0.73 ± 0.26	0.77 ± 0.23)	0.82 ± 0.20
Peak hip flexion moment (Nm/kg)	1.59 ± 0.25 ***p=.017**	1.01 ± 0.29	1.74 ± 0.28	1.03 ± 0.23

Table 6.18: Sagittal plane hip moments.
*Statistically significant prosthetic side differences between prosthesis fitting cases (p<.05).

Figure 6.19 and Table 6.19 show the coronal plane hip moments over the course of the gait cycle, with no significant differences between prosthesis fitting cases.



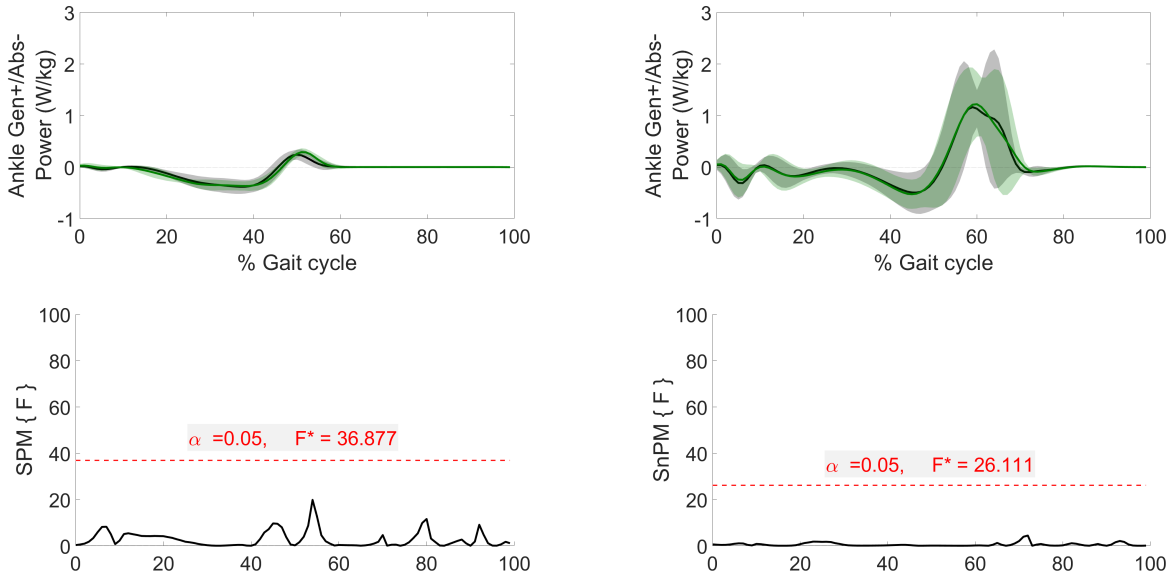
(a) Prosthetic side **(b)** Intact side

Figure 6.19: Top: Hip Abduction (Abd)/Adduction (Add) moments with ICRC (black) and TaKeuP (green) prostheses. Bottom: Statistical parametric mapping results.

	ICRC Mean ± SD *Median [95% CI]*		TaKeuP Mean ± SD *Median [95% CI]*	
Biomechanical parameter	Prosthetic side	Intact side	Prosthetic side	Intact side
Peak hip abduction moment (Nm/kg)	0.44 ± 0.19	0.78 ± 0.20	0.39 ± 0.28	0.76 ± 0.37
Peak hip adduction moment (Nm/kg)	0.11 ± 0.06	*0.41 [0.20-0.65]*	0.19 ± 0.08	*0.36 [0.17-0.61]*

Table 6.19: Coronal plane hip moments.
CI, confidence interval.

Figure 6.20 and Table 6.20 show the calculated sagittal plane ankle power over the course of the gait cycle, with no significant differences between prosthesis fitting cases.



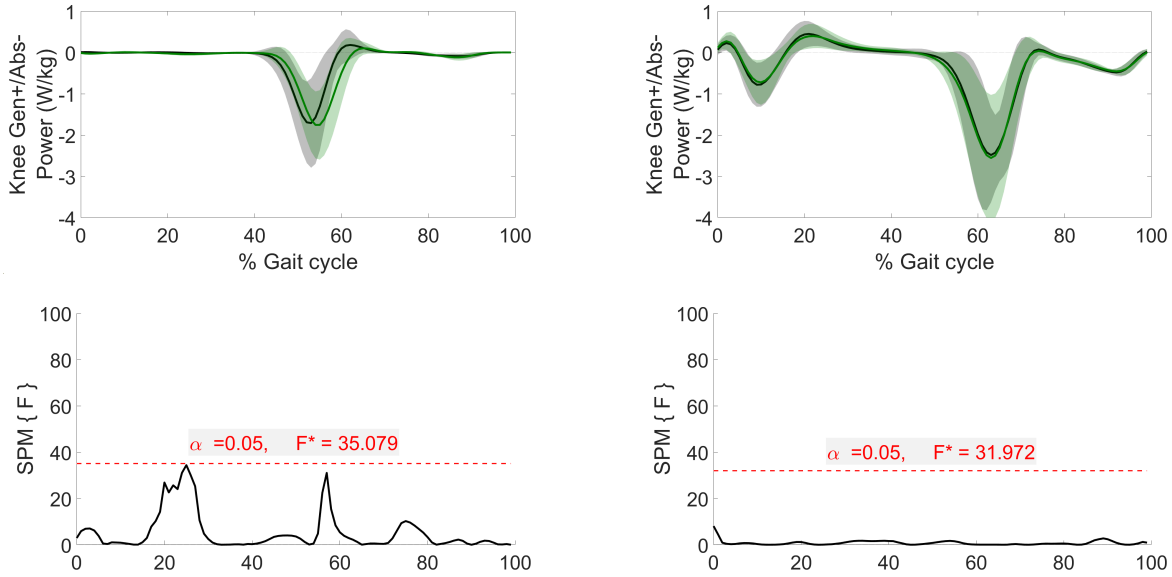
(a) Prosthetic side **(b)** Intact side

Figure 6.20: Top: Ankle Generated (Gen)/Absorbed (Abs) power with ICRC (black) and TaKeuP (green) prostheses. Bottom: Statistical parametric mapping results.

	ICRC Mean ± SD		TaKeuP Mean ± SD	
Biomechanical parameter	Prosthetic side	Intact side	Prosthetic side	Intact side
Peak ankle generated power (W/kg)	0.31 ± 0.07	2.13 ± 0.75	0.33 ± 0.06	2.17 ± 0.50
Peak ankle absorbed power (W/kg)	0.43 ± 0.14	0.71 ± 0.36	0.43 ± 0.08	0.67 ± 0.27

Table 6.20: Sagittal plane ankle power.

Figure 6.21 and Table 6.21 show the sagittal plane knee power over the course of the gait cycle. TaKeuP presented lower peak knee generated power by 0.1 W/kg than the ICRC knee (0.4 W/kg, p=.009). There were no significant differences in the intact knee power between prosthesis fitting cases.



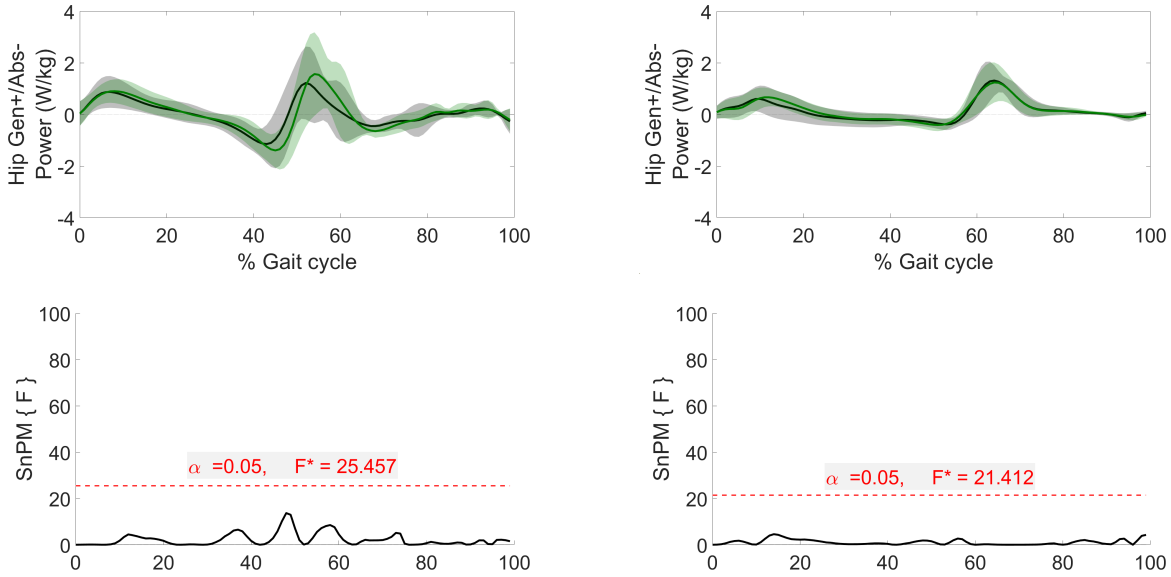
(a) Prosthetic side **(b)** Intact side

Figure 6.21: Top: Knee Generated (Gen)/Absorbed (Abs) power with ICRC (black) and TaKeuP (green) prostheses. Bottom: Statistical parametric mapping results.

	ICRC Mean ± SD		TaKeuP Mean ± SD	
Biomechanical parameter	Prosthetic side	Intact side	Prosthetic side	Intact side
Peak knee generated power (W/kg)	0.36 ± 0.15 ***p=.009**	0.66 ± 0.17	0.23 ± 0.10	0.60 ± 0.18
Peak knee absorbed power (W/kg)	2.07 ± 0.97	3.22 ± 0.97	2.09 ± 0.76	3.29 ± 1.14

Table 6.21: Sagittal plane knee power.
*Statistically significant prosthetic side differences between prosthesis fitting cases (p<.05).

Figure 6.22 and Table 6.22 show the calculated hip power over the course of the gait cycle. When walking with TaKeuP, the peak prosthetic side hip generated power was higher at push-off by 0.4 W/kg than ICRC (2.3 W/kg, p=.016). There were no significant differences in the intact side hip power between prosthesis fitting cases.



(a) Prosthetic side **(b)** Intact side

Figure 6.22: Top: Hip Generated (Gen)/Absorbed (Abs) power with ICRC (black) and TaKeuP (green) prostheses. Bottom: Statistical parametric mapping results.

	ICRC Mean ± SD		TaKeuP Mean ± SD	
Biomechanical parameter	Prosthetic side	Intact side	Prosthetic side	Intact side
Peak hip generated power (W/kg)	2.25 ± 0.76 ***p=.016**	1.66 ± 0.45	2.65 ± 0.74	1.63 ± 0.39
Peak hip absorbed power (W/kg)	1.75 ± 0.54	0.51 ± 0.28	1.89 ± 0.62	0.52 ± 0.23

Table 6.22: Sagittal plane hip power.
*Statistically significant prosthetic side differences between prosthesis fitting cases (p<.05).

Figure 6.23 and Table 6.23 show the intact ankle joint contact forces and impulse. No significant differences were identified between prosthesis fitting cases.

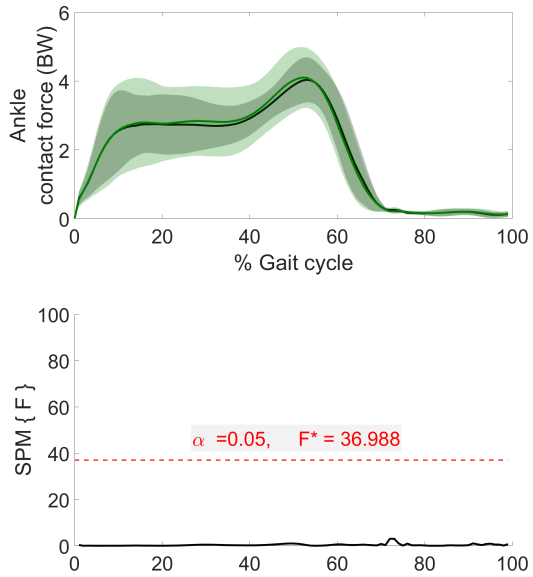


Figure 6.23: Top: Intact ankle joint contact forces of UTF with ICRC (black) and TaKeuP (green) prostheses. Bottom: Statistical parametric mapping results.

Biomechanical parameter	ICRC Mean ± SD *Median [95% CI]*	TaKeuP Mean ± SD *Median [95% CI]*
First peak ankle contact force (BW)	*2.96 [2.23-4.15]*	*2.66 [2.00-4.27]*
Second peak ankle contact force (BW)	4.23 ± 0.62	4.37 ± 0.74
Ankle contact force impulse (BW.s)	187.93 ± 33.03	190.48 ± 52.84
Normalised ankle contact force impulse (BW.s/m)	*137.11 [122.36-164.44]*	*127.85 [108.32-176.42]*

Table 6.23: Intact ankle joint contact forces and impulse.
CI, confidence interval.

Figure 6.24 and Table 6.24 show the medial intact knee joint contact forces and impulse. No significant differences were identified between prosthesis fitting cases.

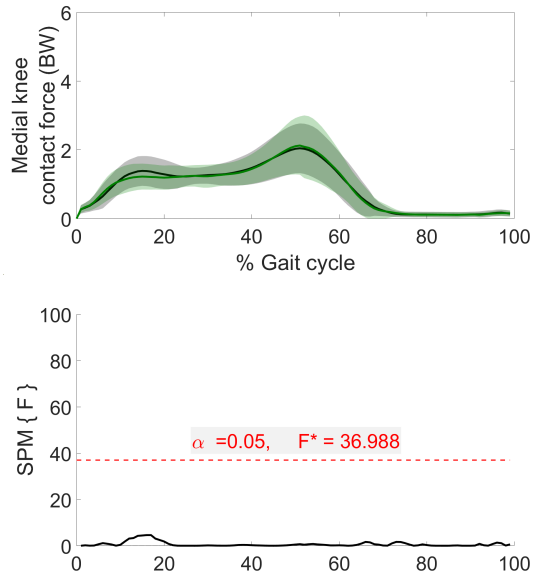


Figure 6.24: Top: Medial compartment of the intact knee joint contact forces with ICRC (black) and TaKeuP (green) prostheses. Bottom: Statistical parametric mapping results.

Biomechanical parameter	ICRC Mean ± SD	TaKeuP Mean ± SD
First peak medial knee contact force (BW)	1.49 ± 0.44	1.39 ± 0.41
Second peak medial knee contact force (BW)	2.13 ± 0.78	2.27 ± 0.83
Medial knee contact force impulse (BW.s)	90.41 ± 21.41	90.26 ± 19.93
Normalised medial knee contact force impulse (BW.s/m)	68.74 ± 15.33	67.75 ± 15.59

Table 6.24: Medial compartment of the intact knee contact forces and impulse.

Figure 6.25 and Table 6.25 show the lateral intact knee joint contact forces and impulse. No significant differences were identified between prosthesis fitting cases.

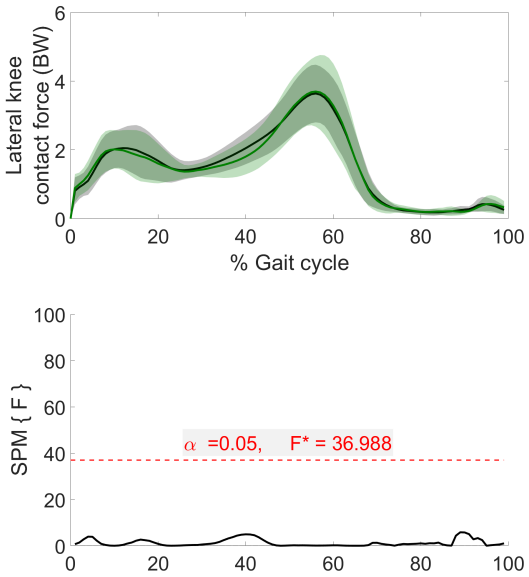


Figure 6.25: Top: Lateral compartment of the intact knee joint contact forces with ICRC (black) and TaKeuP (green) prostheses. Bottom: Statistical parametric mapping results.

Biomechanical parameter	ICRC Mean ± SD *Median [95% CI]*	TaKeuP Mean ± SD *Median [95% CI]*
First peak lateral knee contact force (BW)	*2.35 [1.74-2.77]*	*2.11 [1.71-2.77]*
Second peak lateral knee contact force (BW)	3.82 ± 0.82	3.97 ± 1.00
Lateral knee contact force impulse (BW.s)	150.43 ± 23.30	147.86 ± 23.10
Normalised lateral knee contact force impulse (BW.s/m)	114.81 ± 14.19	110.40 ± 14.92

Table 6.25: Lateral compartment of the intact knee contact forces and impulse.

Figure 6.26 and Table 6.26 present the total intact knee contact forces and impulse. No significant differences were identified between prosthesis fitting cases.

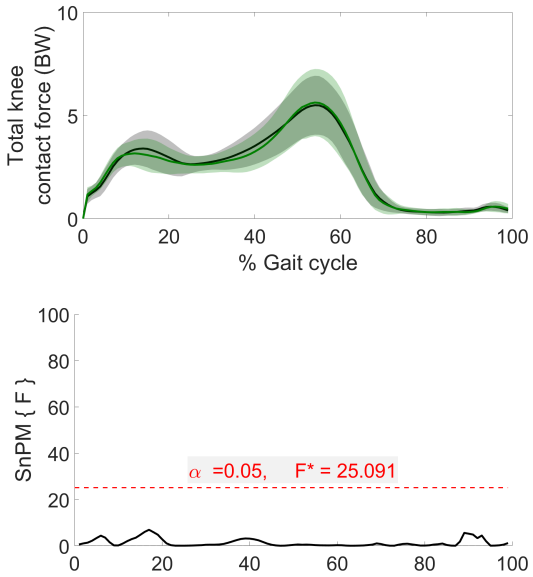
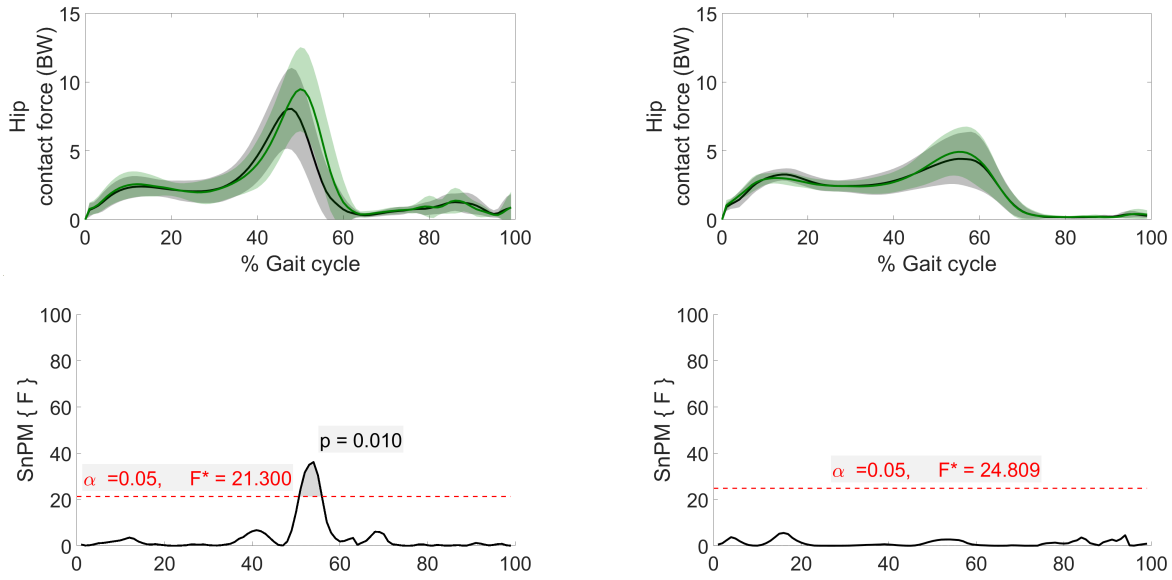


Figure 6.26: Top: Total intact knee joint contact forces with ICRC (black) and TaKeuP (green) prostheses. Bottom: Statistical parametric mapping results.

Biomechanical parameter	ICRC Mean ± SD	TaKeuP Mean ± SD
First peak total knee contact force (BW)	3.74 ± 0.71	3.63 ± 0.50
Second peak total knee contact force (BW)	5.95 ± 1.48	6.24 ± 1.68
Total knee contact force impulse (BW.s)	240.84 ± 41.20	238.12 ± 38.45
Normalised total knee contact force impulse (BW.s/m)	183.55 ± 27.91	178.15 ± 27.65

Table 6.26: Total intact knee contact forces and impulse.

Figure 6.27 shows the hip joint contact forces over the course of the gait cycle. SPM reported higher prosthetic side hip contact forces with TaKeuP than ICRC in late stance (p=.010). When comparing discrete values in Table 6.27, the second peak of the prosthetic side hip joint contact force was larger by 1.3 BW than ICRC (9.1 BW, p=.027). The prosthetic side hip contact force impulse was larger by 21.6 BW.s with TaKeuP than ICRC (223.0 BW.s, p=.036). There were no differences in the intact side hip contact forces and impulse between prosthesis fitting cases.



(a) Prosthetic side **(b)** Intact side

Figure 6.27: Top: Hip joint contact forces with ICRC (black) and TaKeuP (green) prostheses. Bottom: Statistical parametric mapping results.

	ICRC Mean ± SD		TaKeuP Mean ± SD	
Biomechanical parameter	Prosthetic side	Intact side	Prosthetic side	Intact side
First peak hip contact force (BW)	2.71 ± 0.69	3.43 ± 0.43	2.75 ± 0.63	3.22 ± 0.36
Second peak hip contact force (BW)	9.10 ± 2.65 ***p=.027**	4.76 ± 2.00	10.36 ± 2.45	5.26 ± 1.90
Second peak hip contact force normalised by speed (BW/(m/s))	8.79 ± 2.08	4.64 ± 1.47	9.77 ± 1.84	5.09 ± 1.63
Hip contact force impulse (BW.s)	223.03 ± 46.71 ***p=.036**	207.00 ± 48.52	244.66 ± 40.67	210.63 ± 38.93
Normalised hip contact force impulse (BW.s/m)	167.81 ± 28.30	156.72 ± 30.28	180.48 ± 27.83	157.61 ± 28.43

Table 6.27: Hip joint contact forces and impulse.
*Statistically significant prosthetic side differences between prosthesis fitting cases ($p<.05$).

6.4 Discussion

This chapter investigated amputee musculoskeletal system function, loading and prosthesis user satisfaction with low-cost polycentric prosthetic knees (TaKeuP and ICRC) with different extension assist mechanisms. Conventional prosthetic polycentric knees, such as ICRC, use an extension assist mechanism that pushes the knee towards flexion once it reaches a certain angle. Conversely, the TaKeuP knee uses a novel spring extension mechanism that pushes the knee towards extension for all knee angles. The results demonstrate that design choices can improve functionality and gait symmetry in unilateral above- and through-knee amputees. The key findings of this chapter are presented in Table 6.28.

1. Participants reported higher levels of satisfaction for functionality and appearance with TaKeuP than ICRC.
2. TaKeuP showed higher walking speed by 0.1 m/s than ICRC.
3. TaKeuP showed longer percentage stance time in the prosthetic limb gait cycle by 1.6% than ICRC.
4. TaKeuP introduced a smaller difference between the intact and prosthetic knee flexion angle by 5.5% than ICRC.
5. There were no differences in the intact ankle and knee joint loading between walking with TaKeuP and ICRC.
6. TaKeuP showed larger prosthetic side hip joint contact forces by 1.3 BW than ICRC.

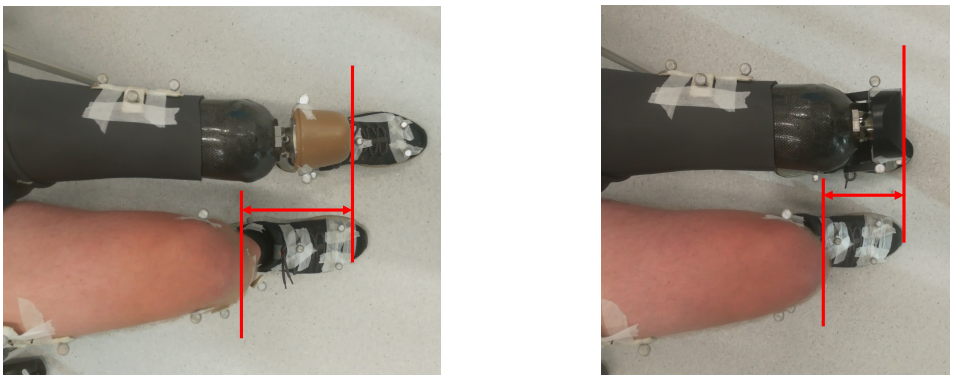
Table 6.28: Key differences between the biomechanical effect of the TaKeuP and ICRC prosthetic knees.

Participants were able to walk faster with the TaKeuP knee than ICRC. TaKeuP's spring extension assist mechanism pushed the knee towards extension and prevented excessive knee flexion in the early swing phase of the gait cycle, leading to lower peak prosthetic knee flexion by 16% than ICRC. As a consequence, UTF did not need to wait for the TaKeuP knee to come back to the extended position from a position of higher flexion, and so, were able to walk faster. Additionally, the novel extension assist mechanism introduced more symmetrical gait patterns than the conventional extension assist used by the ICRC knee. Firstly, the peak TaKeuP knee flexion angle was more similar to the peak intact knee flexion, with a difference of 8.9° between limbs. Conversely, the difference between the peak ICRC and intact knee flexion angle was 19.0°. Secondly, UTF spent a larger percentage of the gait cycle in the prosthetic limb stance phase with TaKeuP than ICRC. Due to the ability to push-off the prosthetic toe for a longer time, amputees showed higher prosthetic side peak hip extension angles with TaKeuP than ICRC. This led to larger prosthetic side hip flexion moments and 14% larger second peak of the hip joint contact force with TaKeuP compared to ICRC. This increase might be detrimental, as high and repetitive loading may lead to tissue degeneration (Ewers et al. 2001, Kerin et al. 2003). However, the long-term effect of this difference is unknown and the small number of participants impedes generalization. Future prosthetic knee design work could investigate the possibility of reducing the hip joint contact forces whilst maintaining the

observed functional abilities.

Chapter 4 demonstrated higher loading of the lateral compartment of the knee of UTF compared to able-bodied persons. Additionally, UTF presented higher intact ankle, lateral and total intact knee loading when walking with ICRC knees and SACH feet compared to walking with microprocessor-controlled knee units and dynamic response prosthetic feet (Chapter 5). The analysis presented in this chapter did not identify any significant differences in the intact ankle and knee joints contact forces between walking with TaKeuP and ICRC, and the similarity might be due to the fact that although some design features are different, both prosthetic knees have polycentric four-bar linkage mechanisms.

There are aspects that the biomechanical tools presented in this thesis could not take into account. As the current ICRC polycentric knee design is not through-knee centred, it has a bulky top component that is part of the thigh segment. This design feature introduced knee level asymmetry in the seated position between the intact and prosthetic sides for through-knee amputees and amputees with long residual limbs, as illustrated in Figure 6.28a. The knee level asymmetry may lead to cosmetic issues and negative social perception. Conversely, the TaKeuP knee is adequate for both through- and above-knee amputees, regardless of the residuum length. As the TaKeuP knee unit is composed of one thin top component that moves with the thigh and one bigger component that moves with the shank, the design reduced the thigh length asymmetry (Figure 6.28b). Additionally, the improved thigh length symmetry and range of motion allowed study participants to kneel - a specific requirement of lower limb amputees in LMICs, which is constrained by the ICRC knee mechanism (Radcliffe et al. 2016).



(a) ICRC knee. **(b)** TaKeuP knee.

Figure 6.28: Thigh length discrepancy of one unilateral through-knee amputee fitted with ICRC and TaKeuP prosthetic knees.

Based on the results from the SAT-PRO prosthesis satisfaction questionnaire, participants were generally more satisfied with the TaKeuP prosthetic knee than ICRC. Although statistical significance was not reached due to the small number of participants and variability between them, the median scores were used as descriptive measures. Participants were more satisfied with TaKeuP's functionality and appearance. The improve-

ment in the cosmetic appearance is beneficial in LMICs, as prosthetic users often face stigmatisation. As both prosthetic knees were new to the participants and the familiarization periods were equal between prostheses, the observed biomechanical and clinical differences between prostheses were purely a consequence of the prosthetic design. The long-term effects are not known and one could only speculate if differences were to diverge or converge over time. Future work could consider additional questions in the self-reported questionnaires regarding the perception of the mass of the prosthesis, squeaking or clicking sounds caused by the prosthetic knee, balance, ability to walk on uneven terrains, walk up and down the stairs, sit down and stand up from a chair.

As the same prosthetic socket and SACH foot were used for each participant between trials with the two prostheses, the observed differences between fitting conditions were due to the prosthetic knee specifications alone. As detailed in Chapter 5, the high risk of tripping in the UTF population has been associated with the minimum toe clearance in the swing phase of the gait cycle (Riveras et al. 2020). Previous work aimed to improve toe clearance in polycentric knees for developing countries (Marisami & Venkatachalam 2021), where optimal stability is especially required on uneven terrains. Both TaKeuP and ICRC knees have polycentric designs that allow for shank shortening and higher toe clearance compared to monocentric prosthetic knees (Riveras et al. 2020, Bellmann et al. 2020). Future work could investigate the minimum toe clearance differences between the TaKeuP and ICRC prostheses.

6.5 Limitations

This study has protocol related limitations, which were previously detailed in Chapter 5. Briefly, study participants completed a familiarization period with the prostheses in the laboratory setting on the day of data collection. Although well known that prosthesis learning requires prolonged use, a biomechanical comparison between two prosthetic knees that were both new to the participants was equitable. Limitations of the musculoskeletal modelling process were discussed in previous chapters.

6.6 Conclusion

This chapter provides biomechanical analyses of amputee function and loading with low-cost polycentric prosthetic knees that use different spring extension assist mechanisms: the ICRC knee with a conventional mechanism that pushes the knee towards flexion past a certain knee flexion angle, and the TaKeuP knee with a novel mechanism that pushes the knee towards extension across the full knee range of motion. The new extension assist mechanism improved the symmetry between the intact and prosthetic knee angles by preventing excessive prosthetic knee flexion in early swing. When using the new extension assist, participants did not need to wait for the knee to come back from a position of higher flexion and therefore could walk faster. The improved functionality of the new spring extension assist mechanism is also supported by the findings of the SAT-PRO questionnaires.

Chapter 7

Conclusion. Generalizing learning of amputee musculoskeletal function and loading

This chapter uses statistical analyses to investigate the effect of prosthetic and anatomical parameters on functional abilities and joint contact loading of unilateral and bilateral above/through-knee traumatic amputees. The results form the basis of the overall thesis discussion, where the key findings of this thesis are summarised and future work is proposed to aid prosthesis design and prescription for lower limb amputees.

7.1 Thesis summary and motivation for generalizing learning

The Global Burden of Disease has reported significant numbers of persons living with traumatic lower limb amputations (Mcdonald et al. 2020). These individuals vary significantly with regards to aspects such as cause and level of amputation, physical condition, activity level, age, rehabilitation pathway and prosthetic devices. Although amputees can restore function through intensive rehabilitation and use of prosthetic devices, the body is required to adopt compensatory movement and loading strategies, which may lead to musculoskeletal complications such as osteoarthritis (Norvell et al. 2005, Gailey et al. 2008, Kulkarni & Adams 1998).

Computational musculoskeletal modelling is a powerful tool that has previously been used to investigate lower limb amputee musculoskeletal system loading (Ding et al. 2020, Henson 2020). Although subject-specific model development based on magnetic resonance imaging (MRI) can improve model outcomes, it is time and computationally intensive. **Chapter 2** developed an MRI based anatomical-atlas of above/through-knee amputee datasets and anthropometry based regression models which can be used to identify the best dataset to linearly scale a model to obtain model outcomes with clinically insignificant errors. This study, combined with advanced musculoskeletal modelling software, provides robust tools to perform accurate biomechanical analyses of musculoskeletal mechanics for lower limb above/through-knee amputees in a time efficient manner, without the need for costly imaging-derived anatomies. Using this musculoskeletal modelling and linear scaling to a model with the most anthropometric similarity, valuable information about joint contact loading can be obtained and used to explain the high rates of osteoarthritis in the lower limb amputee population.

Abnormal and repetitive joint loading may lead to tissue degeneration (Ewers et al. 2001, Kerin et al. 2003). Due to loss of muscle, ankle and knee joints, bilateral above/through-knee amputees (BTF) rely on the hip spanning muscles for propulsion. **Chapter 3** used the anatomical dataset developed in Chapter 2 and demonstrated that this compensatory mechanism significantly increases the second peak of the hip joint contact force when walking with full-length articulated prostheses compared to persons without limb loss. Conversely, fore-shortened non-articulated stubbies introduce hip joint loading similar to able-bodied persons during one gait cycle, but present lower functional abilities than full-length articulated prostheses.

Unilateral lower limb amputees have high prevalence rates of knee osteoarthritis in the intact limb (Norvell et al. 2005, Gailey et al. 2008). **Chapter 4** used biomechanical tools to understand the incidence of knee osteoarthritis in the unilateral above/through-knee amputee population (UTF) and identified higher loading of the lateral compartment of the intact knee and lower medial to lateral intact knee loading dose ratio than able-bodied matched controls. This loading distribution indicates that UTF might be susceptible to lateral knee osteoarthritis. The higher functional demand of the intact limb was a

consequence of the adopted movement strategies as required by anatomical factors and prosthetic requirements.

This thesis demonstrated that the above/through-knee amputee musculoskeletal function and loading are influenced by the prosthetic design. As so many amputees worldwide are unable to access high-cost prostheses, it is imperative to investigate the biomechanical effect of more widely available appropriate technologies. Therefore, **Chapter 5** compared the biomechanical effects of microprocessor-controlled knee (MPK) units coupled with dynamic response feet and International Committee of the Red Cross (ICRC) mechanical polycentric knees coupled with solid-ankle-cushioned-heel (SACH) feet. MPK units with dynamic response feet presented less gait deviations and consequently improved (reduced) loading of the ankle, lateral and total knee joints of the intact limb compared to ICRC knees coupled with SACH feet. The conventional extension assist mechanism used by the ICRC knee limited the ability to walk fast, highlighting the need to investigate the effect of this design feature on amputee function. Thus the work in Chapter 6 was proposed.

Chapter 6 investigated the biomechanical effect of different spring extension assist mechanisms in polycentric prosthetic knees: the ICRC knee with a conventional mechanism that pushes the knee towards flexion past a certain knee flexion angle, and the TaKeuP knee with a novel mechanism that pushes the knee towards extension across the full knee range of motion. TaKeuP's spring extension assist improved the symmetry between the prosthetic and intact knee flexion angles, and allowed amputees to walk faster compared to the conventional extension assist used by the ICRC knee.

The aforementioned musculoskeletal abnormalities and functional limitations may be mitigated through appropriate prosthesis design and prescription. However, prosthesis prescription is often based on manufacturer claims and anecdotal evidence, with little research-based evidence of the effect of prosthetic design on the amputee musculoskeletal system function. Prosthetic devices have many design variations, and this thesis showed that key features of the prosthetic design influence amputee functional abilities and joint loading. Amputee anatomy is another key feature that affects both function and loading during ambulation. This chapter seeks to combine the learning to date by conducting a statistical analysis of all the available datasets to identify significant anatomical and prosthetic parameters that explain functional abilities and intact joint loading measures that are of clinical importance for BTF and UTF. Linear regression analysis is a gold standard approach commonly used in biomechanics to model relationships between independent explanatory variables and a dependent outcome variable (Manal et al. 2015, Carse et al. 2021, Charlton & Johnson 2006). This chapter will also use this statistical approach.

Lower limb amputation inevitably introduces limitations in functional abilities, which may be assessed using clinical measures such as the amputee mobility predictor (Gailey et al. 2002) and 2-minute or 6-minute walking tests. As these measures were not included in this thesis' data collection protocols, this thesis considered cadence, self-selected walk-

ing speed and fast walking speed as indicators of amputee functional abilities. The second peak of the hip joint contact force profile and the hip joint impulse normalised to walked distance were considered relevant indicators of BTF joint health, and the normalised lateral knee contact force impulse was considered a relevant indicator of joint health for the UTF cohort. The justification for these measures is that these were significantly different from able-bodied persons and also significantly different between prostheses in the previous chapters. The joint loading measures are especially relevant as joint degeneration and osteoarthritis have previously been linked to mechanical loading (Felson 2013, Ewers et al. 2001, Kerin et al. 2003, Ding et al. 2020, Gailey et al. 2008, Morgenroth et al. 2012, Norvell et al. 2005). The findings of this statistical analysis form the basis of the overall thesis discussion.

7.2 Database and analytical approach

Table 7.1 and Table 7.2 show the UTF and BTF study participant details. The data presented in the previous chapters were included in this study, with the addition of data collected from two additional participants: one participant fitted with the mechanical KX06 prosthetic knee (Blatchford, United Kingdom) and SACH prosthetic foot, and one participant fitted with KX06 and dynamic response foot. The gait data of these two participants were analysed following the modelling pipeline detailed in Chapter 4.

Part. No. (Gender)	Age (y)	Adj. mass (kg)	Height[a] (m)	Amp. level Stump length (cm) L, R	Prosth. socket	Trialled prostheses
BTF 1 (Male)	36	89	1.87	TK, AK 55, 44	Quad	Genium X3 with Triton LP Sidekicks stubbies
BTF 2 (Male)	41	64	1.64	AK, AK 36, 39	IC	Genium X3 with Triton LP
BTF 3 (Male)	40	93	1.80	AK, AK 42, 41	IC	Genium X3 with Triton LP
BTF 4 (Male)	32	68	1.71	AK, AK 40, 41	Quad	Genium X3 with Taleo Sidekicks stubbies
BTF 5 (Male)	34	84	1.80	AK, TK 36, 47	IC (L), Quad (R)	Genium X3 with Triton LP Sidekicks stubbies
BTF 6 (Male)	41	86	1.87	TK, AK 50, 33	Quad	Genium X3 with Triton LP Sidekicks stubbies
BTF 7 (Male)	38	95	1.80	AK, AK 39, 25	IC	Sidekicks stubbies
BTF 8 (Male)	31	78	1.70	AK, AK 34, 36	IC	Sidekicks stubbies
BTF 9 (Male)	27	80	1.75	TK, TK 47, 46	Quad	Sidekicks stubbies
BTF 10 (Male)	33	79	1.75	AK, AK 41, 14	IC	Sidekicks stubbies
BTF 11 (Male)	27	85	1.85	AK, AK 34, 43	IC	Genium X3 with Triton LP
BTF 12 (Male)	33	97	1.82	TK, TK 45, 48	Quad	Genium X3 with Triton LP

Table 7.1: BTF database details.
[a]Pre-injury height. L, left. R, right. TF, transfemoral. TK, through-knee. IC, ischial containment. Quad, quadrilateral. LP, low profile.

Part. No. (Gender)	Age (y)	Adj. mass (kg)	Height (m)	Amp. level Stump length (cm)	Prosth. socket	Trialled prostheses
UTF 1 (Male)	33	81	1.78	TF 39	IC	Rheo XC with Vari-Flex ICRC with SACH TaKeuP with SACH
UTF 2 (Male)	41	77	1.78	TK 51	Quad	Genium X3 with Pacifica LP ICRC with SACH TaKeuP with SACH
UTF 3 (Male)	66	69	1.73	TF 37	IC	Orion3 with Echelon VT ICRC with SACH TaKeuP with SACH
UTF 4 (Male)	57	73	1.65	TF 32	IC	Orion3 with Echelon ICRC with SACH TaKeuP with SACH
UTF 5 (Female)	55	102	1.72	TK 41	Quad	Genium X3 with Triton LP ICRC with SACH TaKeuP with SACH KX06 with dynamic foot
UTF 6 (Male)	47	95	1.76	TF 37	IC	Genium X3 with Triton ICRC with SACH TaKeuP with SACH
UTF 7 (Male)	57	94	1.76	TF 34	IC	C-leg with Triton ICRC with SACH TaKeuP with SACH
UTF 8 (Male)	34	101	1.80	TK 51	Quad	KX06 with SACH ICRC with SACH TaKeuP with SACH

Table 7.2: UTF database details.
TF, transfemoral. TK, through-knee. IC, ischial containment. Quad, quadrilateral. LP, low profile.

Linear regression analysis was used to investigate the biomechanical effect of prosthetic and anatomical factors on the above/through-knee amputee functional abilities and musculoskeletal system loading. Data were clustered, as each participant tested one or more prostheses in a repeated measures design. The observations were not independent, and so the output dependent variables varied at multiple levels: prosthesis level, participant level and limb level (for BTF). Therefore, stepwise multiple regression models could not be used, as the assumption of independence would have been violated. In order to account for the variance at each level, multilevel (mixed) modeling analysis was used. Interaction terms were allowed in the analysis to account for cases when the effect of a predictor on the dependent variable changes depending on the value of another predictor. Analyses

were performed separately for the BTF and UTF cohorts.

The input parameters in the two-level (prosthesis level and participant level) regression models that explain BTF functional abilities (cadence, self-selected walking speed) were the following:

- Anatomical parameters
  - Estimated intact mass (kg)
  - Pre-injury height (m)
  - Estimated intact body mass index (BMI, kg/m^2)
  - Age (years)
  - Gender (female = 0, male = 1)
  - Amputation type (above-knee/above-knee = 0, above-knee/through-knee = 1, through-knee/through-knee = 2)
  - Average of left and right stump lengths (cm)
  - Shortest stump length (cm)
  - Longest stump length (cm)
- Prosthetic parameters
  - Prosthesis type (fore-shortened non-articulated stubbies = 0, full-length articulated microprocessor knees and dynamic response feet = 1)
  - Shock absorber (no = 0, yes = 1)

As the hip contact force is specific to one limb, the BTF hip joint loading regression analysis was performed at three levels: prosthesis level, participant level and limb level. The input parameters in the multilevel regression models that explain BTF hip joint loading for each limb were the following:

- Anatomical parameters
  - Estimated intact mass (kg)
  - Pre-injury height (m)
  - Estimated intact body mass index (BMI, kg/m^2)
  - Age (years)
  - Gender (female = 0, male = 1)
  - Amputation level (above-knee = 0, through-knee = 1)
  - Stump length (cm)
- Prosthetic parameters

  - Prosthesis type (fore-shortened non-articulated stubbies = 0, full-length articulated microprocessor knees and dynamic response feet = 1)
  - Shock absorber (no = 0, yes = 1)
  - Prosthetic socket type (ischial containment = 0, quadrilateral = 1)

The input parameters in the multilevel regression models that explain UTF functional abilities and loading were the following:

- Anatomical parameters
  - Estimated intact mass (kg)
  - Height (m)
  - Estimated intact body mass index (BMI, kg/m^2)
  - Age (years)
  - Gender (female = 0, male = 1)
  - Amputation level (above-knee = 0, through-knee = 1)
  - Stump length (cm)
  - Stump length/intact thigh length ratio (%)
- Prosthetic parameters
  - Prosthetic foot type (SACH = 0, dynamic response = 1)
  - Shock absorber (no = 0, yes = 1)
  - Knee control (mechanical = 0, microprocessor = 1)
  - Knee axis (polycentric = 0, monocentric = 1)
  - Prosthetic socket type (ischial containment = 0, quadrilateral = 1)

One two-level (prosthesis level and participant level) regression model was developed for each of the following dependent variables:

- Functional abilities
  - Cadence (steps/min)
  - Self-selected walking speed (m/s)
  - Fast walking speed (m/s)
- Musculoskeletal system loading
  - Lateral knee impulse normalised to walked distance (BW.s/m)

As all through-knee amputees were fitted with ischial containment sockets and all above-knee amputees were fitted with quadrilateral sockets, the socket type parameter was equal to the amputation level parameter. Similarly, as all mechanical prosthetic knees were polycentric and all microprocessor prosthetic knees were monocentric, the knee axis type was captured by the prosthetic knee type parameter.

Each parameter was added and removed one at a time in the multilevel regression model. Parameters were included in the final regression model if statistical significance of the associated coefficients was reached, and if the model was improved from the previous one. This was decided based on the Akaike Information Criterion (AIC) value, where a decrease in more than 2 AIC units from the previous model is considered a significant improvement. Multilevel models account for variances at two or more levels, so the traditional R^2 could not be used. The following assumptions in the multilevel statistical analysis were checked: linearity between the dependent variable and each independent variable, multicollinearity, normality of residuals, homoscedasticity, independence of observations between levels, no significant outliers. One outlier was identified in the UTF cohort for the lateral knee impulse variable, but was not excluded from the regression model as valuable information can be obtained from the data. The biomechanical results for this study participant (fitted with a different prosthetic foot type from the other participants) are presented in the case study in Section 4.3.5, Chapter 4.

7.3 Results

7.3.1 Individuals with bilateral transfemoral amputation

Table 7.3 shows the identified multilevel regression model for BTF self-selected walking speed. The prosthesis type was the only significant predictor (p=.001), where the walking speed was higher with full-length articulated prosthesis versus stubbies.

Parameter	Coefficient estimate	Std. error	Sig.	95% Confidence interval
Intercept	0.85	0.04	<.001	(0.76 0.94)
Prosthesis type	0.30	0.04	.001	(0.19 0.41)

Table 7.3: Multilevel regression model (n=16).
Dependent variable: self-selected walking speed (m/s).

Table 7.4 shows the identified multilevel regression model for BTF cadence, with the estimated intact BMI as the only significant predictor (p=.014), where the cadence was higher with lower BMI.

Parameter	Coefficient estimate	Std. error	Sig.	95% Confidence interval
Intercept	188.95	31.39	.001	(121.63 256.27)
Intact BMI	-3.38	1.21	.014	(-5.97 -0.79)

Table 7.4: Multilevel regression model (n=16).
Dependent variable: cadence (steps/min).

Table 7.5 shows the identified multilevel regression model for the second peak of the BTF hip joint contact force during level-ground walking. The prosthesis type was the only significant predictor (p<.001), where the contact force was higher with full-length articulated prostheses versus stubbies.

Parameter	Coefficient estimate	Std. error	Sig.	95% Confidence interval
Intercept	4.47	0.58	<.001	(3.24 5.70)
Prosthesis type	3.48	0.48	<.001	(2.42 4.54)

Table 7.5: Multilevel regression model (n=32).
Dependent variable: second peak hip joint contact force (BW).

Table 7.6 shows the identified multilevel regression model for BTF hip joint impulse normalised to walked distance. The prosthesis type was the only significant predictor (p=.016), where the normalised hip impulse was higher with stubbies versus full-length articulated prostheses.

Parameter	Coefficient estimate	Std. error	Sig.	95% Confidence interval
Intercept	252.95	11.98	<.001	(227.48 278.41)
Prosthesis type	-35.73	12.55	.016	(-63.40 -8.06)

Table 7.6: Multilevel regression model (n=32).
Dependent variable: normalised hip joint impulse (BW.s/m).

7.3.2 Individuals with unilateral transfemoral amputation

Multilevel regression analysis identified two regression models for UTF cadence, where the AIC difference between models was less than 2 units, indicating similar strength between models. Table 7.7 shows the first multilevel regression model for UTF cadence. The only significant predictor was the prosthetic knee type (p<.001), where cadence was higher with microprocessor-controlled prosthetic knees compared to mechanical knees. Table 7.8 shows the second multilevel regression model for UTF cadence. The only significant predictor was the prosthetic foot type (p<.001), where cadence was higher with dynamic response prosthetic feet versus SACH prosthetic feet.

Parameter	Coefficient estimate	Std. error	Sig.	95% Confidence interval
Intercept	93.29	2.16	<.001	(88.29 98.28)
Knee type	7.97	1.58	<.001	(4.63 11.30)

Table 7.7: Multilevel regression model (n=25).
Dependent variable: cadence (steps/min). AIC=146.509

Parameter	Coefficient estimate	Std. error	Sig.	95% Confidence interval
Intercept	93.19	2.18	<.001	(88.14 98.24)
Foot type	7.46	1.61	<.001	(4.04 10.88)

Table 7.8: Multilevel regression model (n=25).
Dependent variable: cadence (steps/min). AIC=148.347

Multilevel regression analysis identified two regression models for UTF self-selected walking speed, where the AIC difference between models was less than 2 units, indicating similar strength between models. Table 7.9 shows the first regression model for UTF self-selected walking speed, with the prosthetic knee type (p=.002) and age (p=.005) as significant predictors. In this model, the walking speed was higher with microprocessor knees (versus mechanical knees) and higher age. Table 7.10 shows the second regression model for UTF walking speed, with the prosthetic knee type (p=.002) and stump length (p=.024) as significant predictors. In this model, the walking speed was higher with microprocessor knees (versus mechanical knees) and longer stumps.

Parameter	Coefficient estimate	Std. error	Sig.	95% Confidence interval
Intercept	1.48	0.10	<.001	(1.22 1.74)
Knee type	0.11	0.03	.002	(0.04 0.17)
Age	-0.01	0.002	.005	(-0.01 -0.003)

Table 7.9: Multilevel regression model (n=25).
Dependent variable: self-selected walking speed (m/s). AIC = -34.742.

Parameter	Coefficient estimate	Std. error	Sig.	95% Confidence interval
Intercept	0.50	0.18	.032	(0.06 0.95)
Knee type	0.11	0.03	.002	(0.05 0.17)
Stump length	0.01	0.004	.024	(0.002 0.02)

Table 7.10: Multilevel regression model (n=25).
Dependent variable: self-selected walking speed (m/s). AIC=-32.816.

Table 7.11 shows the multilevel regression model for UTF fast walking speed, with the prosthetic knee type (p<.001) and age (p=.021) as significant predictors. The walking speed was higher with microprocessor knees (versus mechanical knees) and higher age.

Parameter	Coefficient estimate	Std. error	Sig.	95% Confidence interval
Intercept	1.86	0.20	<.001	(1.36 2.36)
Knee type	0.17	0.03	<.001	(0.10 0.24)
Age	-0.01	0.004	.021	(-0.02 -0.002)

Table 7.11: Multilevel regression model (n=23).
Dependent variable: fast walking speed (m/s).

Table 7.12 shows the multilevel regression model for UTF lateral knee impulse normalised to walked distance. The prosthetic knee type was the only significant predictor (p=.006), where the lateral knee normalised impulse was higher with mechanically-controlled prosthetic knees compared to microprocessor knees.

Parameter	Coefficient estimate	Std. error	Sig.	95% Confidence interval
Intercept	112.51	5.38	<.001	(99.96 125.07)
Knee type	-11.74	3.72	.006	(-19.63 -3.86)

Table 7.12: Multilevel regression model (n=25).
Dependent variable: normalised lateral knee impulse (BW.s/m).

7.4 Thesis discussion and concluding remarks

7.4.1 Individuals with bilateral transfemoral amputation

The available prostheses for BTF are the fore-shortened non-articulated stubbies and full-length articulated prostheses (MPK units coupled with dynamic response feet). Expectedly, multilevel regression analysis identified the prosthesis parameter to be a significant predictor of BTF walking speed. Chapter 3 showed that the BTF walking speeds

were lower with stubbies than MPK due to the inability to achieve larger stride lengths with stubbies. However, cadence was lower with higher body mass index adjusted for amputation, and was not correlated with the prosthesis type parameter. This was expected, as Chapter 3 showed that amputees who were able to walk with both articulated and non-articulated prostheses presented higher cadence with stubbies than prosthetic knees in an attempt to maintain similar walking speeds to those achieved with prosthetic knees. Conversely, stubbies-only users presented lower cadence than the rest of the BTF cohort, indicating lower functional abilities of this amputee subgroup. Stubbies-only users presented lower hip flexion angles and higher sagittal plane pelvic motions than other amputees walking with stubbies. The lordotic posture might either be a consequence of possibly tight rectus femoris reattachment or of the reduced rectus femoris muscle volume observed in this subgroup. It is known that, unlike full-length articulated prostheses, stubbies do not allow for continuous stretching of muscles during gait, which might lead to atrophy. However, based on the biomechanical analysis presented in Chapter 3, it is still unclear whether the reduced muscle volume is a cause or an effect of stubbies-only use, and future work could investigate this.

Due to loss of muscle and joints, BTF rely on the muscles spanning the hip for propulsion, leading to significantly higher second peak of the hip joint contact force profile than persons without limb loss, as demonstrated in Chapter 3. Multilevel regression analysis identified the prosthesis type parameter as the most significant predictor of hip joint loading, where the second peak of the hip joint contact force was higher with MPK units coupled with dynamic response feet than stubbies. This was demonstrated in Chapter 3, which provided an in-depth biomechanical analysis of walking with full-length articulated prostheses and non-articulated stubbies. The larger step lengths with MPK led to higher hip extension angles, which in turn led to higher flexion moments and contact forces at the hip. The hip joint loading during one gait cycle with stubbies was similar to that of persons without limb loss. However, multilevel regression analysis showed that the hip impulse normalised to walked distance was higher with non-articulated compared to full-length articulated prostheses, indicating that a greater hip loading dose was required with stubbies than prosthetic knees for equal distances. Non-articulated stubby prostheses may improve hip joint loading and health only if used for short distances. Moreover, they present limited functional abilities and cosmetic appearance. Conversely, full-length articulated prostheses improve appearance and functionality, but may increase osteoarthritis risk for highly-active BTF amputees. There is anecdotal evidence that amputees sometimes prefer to use stubbies at home or when they feel tired, supporting the finding that stubbies may be more appropriate for short distances only. Future work could investigate factors related to fatigue. The choice of appropriate prosthesis should be based on musculoskeletal health, functionality objectives and cosmesis preference. The balance between these varies per individual.

7.4.2 Individuals with unilateral transfemoral amputation

Chapter 4 demonstrated that UTF with MPK units and dynamic response feet walk at similar speeds and cadence to persons without limb loss. However, Chapter 5 and Chapter

6 showed lower speeds and cadence when walking with mechanically-controlled prosthetic knees (ICRC, TaKeuP) coupled with solid-ankle-cushioned-heel (SACH) feet. Therefore, it was expected for multilevel regression analysis to identify the prosthetic knee type and prosthetic foot type as significant predictors of walking speeds and cadence. The findings are in accordance with previous literature that showed that MPK units present faster walking speeds than mechanical knees (Sawers & Hafner 2013). Microprocessor-controlled knee units allow for variable walking speeds by adjusting the knee damping to the amputee's gait using in-built sensors. Conversely, mechanically-controlled knees use a hinge mechanism, and the lack of internal control reduces the level of biological realism compared to MPK, which can replicate knee kinematics in both stance and swing phases of the gait cycle.

Variations in prosthetic knee designs may affect amputee function. For instance, the choice of the spring extension assist mechanism can improve the gait of unilateral trans-femoral amputees. Conventional four-bar polycentric prosthetic knees, such as the ICRC knee (presented in Chapter 5 and Chapter 6), use an extension assist that links one of the bars to the body of the prosthesis. This design feature causes the spring to push the knee towards flexion past a certain knee angle. Other four-bar polycentric knees such as TaKeuP (presented in Chapter 6) use an extension assist mechanism that links the bottom and top parts of knee and pushes the prosthetic knee towards extension throughout the full range of motion. Chapter 6 investigated the effect of this design feature on amputee function, and demonstrated that TaKeuP's extension assist prevented excessive prosthetic knee flexion in early swing, thus improving the symmetry between the intact and prosthetic knee flexion angles. By reducing the prosthetic knee peak flexion angles, amputees were not required to wait for the knee to come back to the extension position, allowing them to walk fast. When participants attempted to walk faster with the conventional extension assist spring, they felt that the risk of falling was high.

Dynamic response feet present faster walking speeds and cadence than SACH feet (Hafner et al. 2002). The advanced design of dynamic feet use elastic materials that deform under load and return to the original shape when unloaded. This feature enhances the prosthetic ankle power at the push-off phase of the gait cycle (as presented in Chapter 5). Conversely, the SACH foot has the simplest design, consisting of a rigid forefoot and compressive heel that do not allow for energy storage and return. Therefore, dynamic feet restore more functionality of the anatomical foot and ankle compared to SACH, and may improve reliance on the prosthetic limb during gait through longer stance time and higher ground reaction forces. In this study's cohort, MPK units were coupled with dynamic response feet, and mechanical knees were most commonly coupled with SACH feet. Therefore, as the prosthetic foot parameter was equal to the prosthetic knee parameter in 24 out 25 observations (the exception was one mechanical knee coupled with a dynamic response foot), it was not possible to clearly differentiate between the effects of the prosthetic foot and prosthetic knee on the investigated outcome variables. If these mixed feet/knees options were available, it would be expected for dynamic response feet to show higher cadence and walking speeds than SACH feet given the same type of prosthetic knee is used. Similarly, it would be expected for microprocessor knees to show

higher cadence and walking speeds than mechanical knees given the same type of prosthetic foot is used.

The stump length was also identified as a significant predictor of self-selected walking speed, where speed increased with residuum length. This demonstrates that the degree of functional disability increases with the amputation level. Longer residual limbs may have stronger musculature for propulsion and longer lever arms that allow for better suspension of the prosthesis, enhancing comfort and allowing amputees to achieve higher walking speeds. Of course, stump length is not the only anatomical feature that may be important, as different surgical procedures and muscle re-attachment locations might lead to stronger musculature for shorter stumps than longer stumps (Ranz et al. 2017). Amputees have a wide anatomical variability and the sample size in this study did not allow for differences in surgical procedures to be taken into account. Finally, it was observed that functional abilities decreased with increasing age, in concordance with previous literature (Batten et al. 2019). Age and stump length were inversely correlated in this dataset and therefore, their coefficients in a regression model that contained both parameters were not statistically significant, indicating that the information that the stump length parameter could have provided was already encoded in the age parameter; the small sample size limited the stump length parameter to provide further significant information in the combined model. Although through-knee amputations are now more common than above-knee amputations, the time since amputation was not related to age. The observed moderate correlation between age and stump length might just be a characteristic of the current dataset, and might not be observed with a larger sample size. Future work could build a larger database to increase the statistical power of the observed results. Interestingly, the stump length was not a significant predictor of fast walking speeds. When participants were instructed to walk as fast as they could, the limitation imposed by the stump length was overcome, and so the ability to walk fast was only influenced by the prosthetic knee type and age.

Unlike bilateral amputees, unilateral amputees adopt compensation strategies that are dominated by the intact limb (Henson et al. 2021). The internal mechanical loading of the intact limb knee is a variable of interest as abnormal joint contact forces may relate to tissue degeneration (Ewers et al. 2001, Kerin et al. 2003), osteoarthritis development and progression (Ding et al. 2020). Chapter 4 demonstrated higher lateral knee impulse (loading dose) for UTF than persons without limb loss, suggesting that high-functioning UTF might be more susceptible to lateral knee osteoarthritis. Therefore, mitigation strategies need to be proposed to improve (reduce) intact knee loading, which might be influenced by asymmetry between the intact and prosthetic limbs. Multilevel regression analysis identified the prosthetic knee type to be the only significant predictor of lateral knee impulse normalised to walked distance, where higher lateral knee loading was observed with mechanically-controlled knees than MPK units. This was expected, as MPK units have been shown in Chapter 5 and literature (Uchytil et al. 2014) to present lower asymmetry than mechanically-controlled knees. Nonetheless, the lateral knee loading dose when walking with MPK units and dynamic response feet was still significantly higher than persons without limb loss due to the different biomechanics (hip hiking, vaulting)

adopted to compensate for the insufficient prosthetic toe clearance. One possible solution that may reduce these gait deviations is a coupling mechanism of the prosthetic knee and foot, which would allow the prosthetic ankle to plantar flex whilst the knee flexes in the swing phase of the gait cycle. This would improve prosthetic toe clearance, removing the need to adopt hip hiking and vaulting for successful task completion. This in turn might improve the loading of the lateral compartment of the knee and reduce the risk of knee osteoarthritis in the UTF population.

The lowest lateral knee loading dose in the UTF cohort was observed for one study participant fitted with the microprocessor Rheo Knee and Re-Flex prosthetic foot. Unlike other dynamic response prosthetic feet, Re-Flex provides high levels of vertical and rotational shock absorption using the integrated titanium coil. Chapter 4 showed that this design characteristic led to improved symmetry in ground reaction forces compared to a study participant with similar amputation, but who was fitted with a Genium microprocessor knee and Triton prosthetic foot without a shock absorber. Given this observation, a parameter that accounts for the effect of shock absorbing components was added in the regression analysis. However, as only one study participant used a prosthetic foot with a shock absorber, statistical significance could not be reached. Future work could focus on gait analysis for UTF using high impact shock absorbing prosthetic components to investigate their biomechanical effect on joint loading.

All study participants were fitted with prosthetic sockets, and the effect of different fixation methods has not been investigated. Walking with bone-anchored prostheses can improve functional abilities and quality of life (McMenemy et al. 2020). As the implant transmits the load directly to the bone, prosthetic feet with vertical and rotational shock absorbing components should be recommended in order to reduce the impact at the implant-bone interface. Due to the ability to axially load the femur, gait asymmetry might be lower for amputees with osseointegration than amputees with socket-anchored prostheses. As prosthetic sockets cannot distribute the weight axially through the femur, transfemoral amputees are at risk of osteopenia (Rush et al. 1994), which can lead to fragility fractures. Osseointegration may reduce the risk of overuse injuries of the intact limb and promote long-term health and user satisfaction. Future work could investigate the loading profiles and bone mineral density of above/through-knee amputees with bone-anchored prostheses.

In summary, this thesis demonstrated that MPK units and dynamic response feet with shock absorbing components provide optimal functional abilities and improved loading of the sound limb, and therefore should be recommended for active traumatic amputees. However, as these prosthetic devices are expensive, amputees in low-to-middle income countries (LMICs) may not be able to afford these. Additionally, high-cost prosthetic devices may not be appropriate for specific requirements in LMICs, as they may not be waterproof, dustproof and require regular charging. Therefore, there is an immediate need for adequate prosthetic devices for LMICs that consider functional abilities, joint health and cost. The International Committee of the Red Cross (ICRC) prosthetic polycentric knee joint is an affordable option for persons with limb loss in LMICs. The

ICRC knee uses a conventional spring extension assist mechanism that links one of the bars to the prosthesis body. This design feature leads to significantly higher prosthetic knee flexion angles than the intact limb, requiring prosthetic users to wait for the knee to return to the extended position for heel strike, thus limiting the ability to walk fast. Chapter 6 showed that the choice of the extension assist design affects walking speeds. The novel spring extension assist used by the TaKeuP polycentric knee joint links the bottom and top parts of knee. This mechanism presented lower prosthetic knee flexion angles than ICRC, and improved the symmetry between the prosthetic and intact knee flexion angles. TaKeuP demonstrated improved functional abilities and level of user satisfaction than ICRC. However, there were no significant differences in the loading of the intact limb between prostheses, which was expected given that both prosthetic knees use a four-bar linkage system. Biomechanical analyses gave many interesting results in Chapter 5 when comparing mechanical knees coupled with SACH feet to microprocessor knees coupled with dynamic response feet, but few in Chapter 6 when comparing two different mechanical polycentric knee joints. This demonstrates that subtle differences are not just biomechanical, but also about perception of the prosthesis, which is why self-reported questionnaires are also very important when assessing a prosthesis.

This thesis focused on understanding the bilateral and unilateral above/through-knee traumatic amputee function and loading. However, the biomechanical and statistical tools presented in this thesis could also be used in future work to investigate the musculoskeletal function and loading of bilateral and unilateral transtibial amputees with different prostheses. The significant anatomical and prosthetic parameters that explain function and loading could be identified, thus ensuring optimal function and musculoskeletal health through adequate prosthetic design and prescription.

7.5 Future work

The summary of the future work proposed throughout the thesis is the following:

- Establish biomechanical tools for non-linear scaling of lower limb amputee models.
- Investigate muscular volume adaptations of UTF amputees.
- Develop an anatomical atlas based scaling study to accurately predict UTF muscle and joint contact forces.
- Investigate lower limb amputee function and loading during various activities of daily living, and not just gait.
- Analyse muscle forces and dosage for lower limb amputees, and investigate whether detrimental muscle dosage can be reduced, whilst maintaining similar peak muscle forces.
- Investigate the effect of fatigue on amputee function and loading.

- Investigate the upper body compensatory mechanism and loading of the lumbar spine for UTF and BTF.
- Investigate biomechanical data of female lower limb amputees to account for gender differences in musculoskeletal system function and loading.
- Investigate differences in musculoskeletal function and loading between traumatic unilateral through- and above-knee amputees.
- Investigate the biomechanical effect of prosthetic devices on amputee walking capacity over a longer period of time and in real-world conditions, removing the time and space constraints of the laboratory setting.
- Investigate loading profiles of UTF with high-cost mechanical prosthetic knees and provide comparisons to loading profiles with microprocessor-controlled knees.
- Investigate loading profiles of UTF fitted with prosthetic feet with vertical and rotational shock absorbing components.
- Design and test a prosthetic knee and foot coupling mechanism to improve toe clearance and reduce gait deviations.
- Design and test low-cost prosthetic feet with improved functionality for LMICs.
- Investigate the loading criteria of different prosthetic feet and knees and assess the appropriateness of the current ISO standards for strength for lower limb prostheses.
- Investigate the loading profiles of amputees with bone-anchored prostheses.
- Assess bone health of above/through-knee amputees with socket- and bone-anchored prostheses.
- Include unilateral and bilateral transtibial amputee biomechanical data and increase the size of the presented amputee biomechanical database to generalize learning of the biomechanical effect of anatomical and prosthetic parameters on the amputee function and loading for any type of amputation.

7.6 Broader context

This thesis presented efficient computational tools that were used to analyse functional abilities and joint loading. Lower limb amputees are at risk of functional disability and musculoskeletal disorders. This modelling approach can be used to investigate the biomechanical effect of different prosthetic devices on the unilateral and bilateral above/through amputee musculoskeletal system and propose strategies to ensure optimal function and musculoskeletal health.

Different mitigation strategies can be proposed to improve long term musculoskeletal health and function. The findings of this thesis can be used in clinical settings for adequate prosthesis prescription in a subject-specific manner to meet the specific requirements of lower limb amputees. In accordance with review studies (Stevens & Wurdeman 2019, Stevens et al. 2018, Sedki & Fisher 2015), this thesis recommends MPK and dynamic response feet to be used by amputees with high activity levels and potential for ambulation across variable speeds in order to improve functional abilities and sound limb health. This work can be used to justify the cost of microprocessor-controlled knees for highly-active amputees. Additionally, high-performance prosthetic feet with shock absorbing components might be suitable for amputees with bone-anchored prostheses in order to reduce the impact to the residual bone and the risk of intact knee degeneration. Finally, prosthetic manufacturers could use this work to improve prosthetic design to ensure optimal outcomes for lower limb amputees.

Appendices

Appendix A

Detailed muscle parameters of each anatomical dataset

Muscle	Muscle volume (V_m, cm^3)	Muscle length (L_m, cm)	Fibre length to muscle length ratio (L_f/L_m)	Pennation angle (θ, deg)	Sarcomere length (L_s, μM)	PCSA (cm^2)
Adductor brevis	233.85	15.23	0.68	6.10	2.91	24.20
Adductor longus	245.87	23.45	0.50	7.10	3.00	23.12
Adductor magnus	772.11	35.13	0.39	15.50	2.19	44.04
Biceps femoris long head	405.27	31.77	0.28	11.60	2.35	38.84
Gemellus	18.70	9.25	1.00	0.00	2.70	2.02
Gluteus maximus	1771.10	32.51	0.62	21.90	2.60	78.49
Gluteus medius	619.92	21.39	0.37	20.50	2.40	65.19
Gluteus minimus	215.74	14.39	1.00	0.00	2.70	14.99
Gracilis	184.58	36.07	0.79	8.20	3.24	7.69
Iliacus	396.18	28.12	0.56	14.30	3.02	27.17
Obturator externus	79.86	11.02	1.00	0.00	2.70	7.24
Obturator internus	149.42	8.88	1.00	0.00	2.70	16.83
Pectineus	123.13	14.29	1.00	0.00	2.70	8.61
Piriformis	86.30	10.75	1.00	0.00	2.70	8.03
Psoas minor						1.10
Psoas major	370.96	36.82	0.50	10.60	3.11	22.82
Quadratus femoris	69.55	8.13	1.00	0.00	2.70	8.56
Rectus femoris	340.43	35.88	0.21	13.90	2.42	39.31
Sartorius	305.81	58.87	0.90	1.30	3.11	6.65
Semimembranosus	471.53	30.46	0.24	15.10	2.61	60.19
Tensor fasciae latae	165.90	17.75	1.00	0.00	2.70	9.34

Table A.1: Muscle parameters of anatomical dataset 1.

Muscle	Muscle volume (V_m, cm^3)	Muscle length (L_m, cm)	Fibre length to muscle length ratio (L_f/L_m)	Pennation angle (θ, deg)	Sarcomere length (L_s, μM)	PCSA (cm^2)
Adductor brevis	210.04	15.23	0.68	6.10	2.91	21.73
Adductor longus	262.81	23.45	0.50	7.10	3.00	24.71
Adductor magnus	694.71	35.13	0.39	15.50	2.19	39.63
Biceps femoris long head	292.94	31.77	0.28	11.60	2.35	28.08
Gemellus	21.21	9.25	1.00	0.00	2.70	2.29
Gluteus maximus	1457.61	32.52	0.62	21.90	2.60	64.60
Gluteus medius	577.51	21.39	0.37	20.50	2.40	60.73
Gluteus minimus	163.93	14.39	1.00	0.00	2.70	11.39
Gracilis	145.56	36.07	0.79	8.20	3.24	6.07
Iliacus	376.13	28.12	0.56	14.30	3.02	25.80
Obturator externus	78.47	11.02	1.00	0.00	2.70	7.12
Obturator internus	151.92	8.88	1.00	0.00	2.70	17.11
Pectineus	105.99	14.29	1.00	0.00	2.70	7.41
Piriformis	104.09	10.75	1.00	0.00	2.70	9.69
Psoas minor						1.10
Psoas major	380.99	36.82	0.50	10.60	3.11	23.43
Quadratus femoris	56.47	8.13	1.00	0.00	2.70	6.95
Rectus femoris	338.33	35.88	0.21	13.90	2.42	39.07
Sartorius	224.44	58.87	0.90	1.30	3.11	4.88
Semimembranosus	391.10	30.46	0.24	15.10	2.61	49.93
Tensor fasciae latae	141.15	17.75	1.00	0.00	2.70	7.95

Table A.2: Muscle parameters of anatomical dataset 2.

Muscle	Muscle volume (V_m, cm^3)	Muscle length (L_m, cm)	Fibre length to muscle length ratio (L_f/L_m)	Pennation angle (θ, deg)	Sarcomere length (L_s, μM)	PCSA (cm^2)
Adductor brevis	153.31	14.83	0.68	6.10	2.91	16.29
Adductor longus	189.46	22.84	0.50	7.10	3.00	18.29
Adductor magnus	486.12	34.21	0.39	15.50	2.19	28.48
Biceps femoris long head	133.46	30.93	0.28	11.60	2.35	13.14
Gemellus	1.29	9.01	1.00	0.00	2.70	0.14
Gluteus maximus	1088.82	31.67	0.62	21.90	2.60	49.56
Gluteus medius	457.69	20.83	0.37	20.50	2.40	49.43
Gluteus minimus	128.50	14.01	1.00	0.00	2.70	9.17
Gracilis	58.67	35.12	0.79	8.20	3.24	2.51
Iliacus	282.00	27.48	0.56	14.30	3.02	19.86
Obturator externus	48.72	10.74	1.00	0.00	2.70	4.54
Obturator internus	107.62	8.64	1.00	0.00	2.70	12.45
Pectineus	83.41	13.92	1.00	0.00	2.70	5.99
Piriformis	63.76	10.46	1.00	0.00	2.70	6.09
Psoas minor						1.10
Psoas major	239.73	35.85	0.50	10.60	3.11	15.14
Quadratus femoris	41.61	7.92	1.00	0.00	2.70	5.26
Rectus femoris	174.71	34.94	0.21	13.90	2.42	20.72
Sartorius	173.68	57.32	0.90	1.30	3.11	3.88
Semimembranosus	178.76	29.66	0.24	15.10	2.61	23.44
Tensor fasciae latae	84.44	17.29	1.00	0.00	2.70	4.88

Table A.3: Muscle parameters of anatomical dataset 3.

Muscle	Muscle volume (V_m, cm^3)	Muscle length (L_m, cm)	Fibre length to muscle length ratio (L_f/L_m)	Pennation angle (θ, deg)	Sarcomere length (L_s, μM)	PCSA (cm^2)
Adductor brevis	187.86	18.60	0.68	6.10	2.91	15.91
Adductor longus	259.18	24.09	0.50	7.10	3.00	23.73
Adductor magnus	672.24	34.09	0.39	15.50	2.19	39.51
Biceps femoris long head	564.66	36.18	0.28	11.60	2.35	47.53
Gemellus	1.52	7.40	1.00	0.00	2.70	0.21
Gluteus maximus	1578.15	29.19	0.62	21.90	2.60	77.91
Gluteus medius	522.85	19.58	0.37	20.50	2.40	60.09
Gluteus minimus	170.93	12.28	1.00	0.00	2.70	13.91
Gracilis	126.27	22.51	0.79	8.20	3.24	8.43
Iliacus	332.96	27.04	0.56	14.30	3.02	23.83
Obturator externus	80.87	12.01	1.00	0.00	2.70	6.73
Obturator internus	102.12	10.85	1.00	0.00	2.70	9.42
Pectineus	102.59	13.85	1.00	0.00	2.70	7.41
Piriformis	80.86	15.22	1.00	0.00	2.70	5.31
Psoas minor						1.10
Psoas major	268.93	25.29	0.50	10.60	3.11	24.08
Quadratus femoris	70.93	8.89	1.00	0.00	2.70	7.98
Rectus femoris	325.10	32.45	0.21	13.90	2.42	41.51
Sartorius	220.34	41.97	0.90	1.30	3.11	6.72
Semimembranosus	266.87	27.92	0.24	15.10	2.61	37.17
Tensor fasciae latae	119.52	17.57	1.00	0.00	2.70	6.80

Table A.4: Muscle parameters of anatomical dataset 5.

Muscle	Muscle volume (V_m, cm^3)	Muscle length (L_m, cm)	Fibre length to muscle length ratio (L_f/L_m)	Pennation angle (θ, deg)	Sarcomere length (L_s, μM)	PCSA (cm^2)
Adductor brevis	173.93	16.27	0.68	6.10	2.91	16.84
Adductor longus	244.97	24.93	0.50	7.10	3.00	21.67
Adductor magnus	612.31	27.66	0.39	15.50	2.19	44.37
Biceps femoris long head	378.38	25.53	0.28	11.60	2.35	45.13
Gemellus	1.50	5.65	1.00	0.00	2.70	0.27
Gluteus maximus	1366.65	28.78	0.62	21.90	2.60	68.43
Gluteus medius	489.28	18.98	0.37	20.50	2.40	58.02
Gluteus minimus	126.98	12.01	1.00	0.00	2.70	10.57
Gracilis	101.48	17.27	0.79	8.20	3.24	8.83
Iliacus	301.55	24.70	0.56	14.30	3.02	23.63
Obturator externus	74.52	12.26	1.00	0.00	2.70	6.08
Obturator internus	103.06	16.46	1.00	0.00	2.70	6.26
Pectineus	87.14	12.66	1.00	0.00	2.70	6.88
Piriformis	69.55	13.02	1.00	0.00	2.70	5.34
Psoas minor						1.10
Psoas major	270.69	23.71	0.50	10.60	3.11	25.85
Quadratus femoris	66.00	9.84	1.00	0.00	2.70	6.71
Rectus femoris	269.22	23.14	0.21	13.90	2.42	48.20
Sartorius	222.71	39.86	0.90	1.30	3.11	7.15
Semimembranosus	188.07	15.56	0.24	15.10	2.61	47.00
Tensor fasciae latae	110.66	16.58	1.00	0.00	2.70	6.68

Table A.5: Muscle parameters of anatomical dataset 6.

Muscle	Muscle volume (V_m, cm^3)	Muscle length (L_m, cm)	Fibre length to muscle length ratio (L_f/L_m)	Pennation angle (θ, deg)	Sarcomere length (L_s, μM)	PCSA (cm^2)
Adductor brevis	154.31	15.99	0.68	6.10	2.91	15.21
Adductor longus	212.61	23.54	0.50	7.10	3.00	19.92
Adductor magnus	585.20	35.19	0.39	15.50	2.19	33.33
Biceps femoris long head	156.41	19.39	0.28	11.60	2.35	24.56
Gemellus	2.66	5.38	1.00	0.00	2.70	0.49
Gluteus maximus	1133.17	30.90	0.62	21.90	2.60	52.85
Gluteus medius	419.83	19.52	0.37	20.50	2.40	48.39
Gluteus minimus	121.62	12.81	1.00	0.00	2.70	9.50
Gracilis	53.85	19.32	0.79	8.20	3.24	4.19
Iliacus	219.38	26.41	0.56	14.30	3.02	16.08
Obturator externus	64.58	9.59	1.00	0.00	2.70	6.74
Obturator internus	109.36	18.17	1.00	0.00	2.70	6.02
Pectineus	68.06	10.09	1.00	0.00	2.70	6.74
Piriformis	58.06	11.44	1.00	0.00	2.70	5.08
Psoas minor						1.10
Psoas major	187.67	23.61	0.50	10.60	3.11	18.00
Quadratus femoris	53.73	7.51	1.00	0.00	2.70	7.15
Rectus femoris	120.91	27.44	0.21	13.90	2.42	18.25
Sartorius	98.25	39.32	0.90	1.30	3.11	3.20
Semimembranosus	187.35	27.54	0.24	15.10	2.61	26.45
Tensor fasciae latae	89.42	15.52	1.00	0.00	2.70	5.76

Table A.6: Muscle parameters of anatomical dataset 7.

Muscle	Muscle volume (V_m, cm^3)	Muscle length (L_m, cm)	Fibre length to muscle length ratio (L_f/L_m)	Pennation angle (θ, deg)	Sarcomere length (L_s, μM)	PCSA (cm^2)
Adductor brevis	135.83	16.14	0.68	6.10	2.91	13.27
Adductor longus	134.73	16.57	0.50	7.10	3.00	17.93
Adductor magnus	490.49	22.69	0.39	15.50	2.19	43.33
Biceps femoris long head	24.10	8.82	0.28	11.60	2.35	8.32
Gemellus	4.08	6.98	1.00	0.00	2.70	8.32
Gluteus maximus	1124.42	29.00	0.62	21.90	2.60	55.87
Gluteus medius	407.94	18.74	0.37	20.50	2.40	48.99
Gluteus minimus	104.53	11.74	1.00	0.00	2.70	8.90
Gracilis	29.71	10.14	0.79	8.20	3.24	4.41
Iliacus	214.60	26.51	0.56	14.30	3.02	15.67
Obturator externus	64.12	11.37	1.00	0.00	2.70	5.64
Obturator internus	96.51	15.55	1.00	0.00	2.70	6.21
Pectineus	68.44	12.29	1.00	0.00	2.70	5.57
Piriformis	51.67	11.47	1.00	0.00	2.70	4.50
Psoas minor						1.10
Psoas major	145.36	24.44	0.50	10.60	3.11	13.47
Quadratus femoris	58.15	7.42	1.00	0.00	2.70	7.84
Rectus femoris	89.12	17.25	0.21	13.90	2.42	21.40
Sartorius	41.96	24.04	0.90	1.30	3.11	2.23
Semimembranosus	53.26	14.60	0.24	15.10	2.61	14.19
Tensor fasciae latae	76.20	14.92	1.00	0.00	2.70	5.11

Table A.7: Muscle parameters of anatomical dataset 8.

Muscle	Muscle volume (V_m, cm^3)	Muscle length (L_m, cm)	Fibre length to muscle length ratio (L_f/L_m)	Pennation angle (θ, deg)	Sarcomere length (L_s, μM)	PCSA (cm^2)
Adductor brevis	169.26	17.27	0.68	6.10	2.91	15.45
Adductor longus	207.38	25.58	0.50	7.10	3.00	17.88
Adductor magnus	758.47	41.84	0.39	15.50	2.19	36.33
Biceps femoris long head	191.59	28.22	0.28	11.60	2.35	20.67
Gemellus	5.61	5.97	1.00	0.00	2.70	0.94
Gluteus maximus	1119.45	28.13	0.62	21.90	2.60	57.36
Gluteus medius	467.60	21.51	0.37	20.50	2.40	48.92
Gluteus minimus	170.20	13.99	1.00	0.00	2.70	12.17
Gracilis	48.47	15.29	0.79	8.20	3.24	4.77
Iliacus	295.62	28.30	0.56	14.30	3.02	20.22
Obturator externus	45.24	8.54	1.00	0.00	2.70	5.30
Obturator internus	112.63	16.48	1.00	0.00	2.70	6.83
Pectineus	83.74	15.36	1.00	0.00	2.70	5.45
Piriformis	77.13	14.64	1.00	0.00	2.70	5.27
Psoas minor						1.10
Psoas major	246.57	28.01	0.50	10.60	3.11	19.93
Quadratus femoris	41.29	7.25	1.00	0.00	2.70	5.69
Rectus femoris	253.89	31.19	0.21	13.90	2.42	33.52
Sartorius	175.02	40.12	0.90	1.30	3.11	5.58
Semimembranosus	281.00	31.50	0.24	15.10	2.61	34.70
Tensor fasciae latae	118.47	17.47	1.00	0.00	2.70	6.78

Table A.8: Muscle parameters of anatomical dataset 9.

Muscle	Muscle volume (V_m, cm^3)	Muscle length (L_m, cm)	Fibre length to muscle length ratio (L_f/L_m)	Pennation angle (θ, deg)	Sarcomere length (L_s, μM)	PCSA (cm^2)
Adductor brevis	139.21	18.13	0.68	6.10	2.91	12.10
Adductor longus	217.64	26.05	0.50	7.10	3.00	18.42
Adductor magnus	692.81	37.98	0.39	15.50	2.19	36.56
Biceps femoris long head	222.61	26.94	0.28	11.60	2.35	25.16
Gemellus	4.18	7.66	1.00	0.00	2.70	0.55
Gluteus maximus	1211.95	29.40	0.62	21.90	2.60	59.41
Gluteus medius	485.86	20.04	0.37	20.50	2.40	54.56
Gluteus minimus	140.77	13.71	1.00	0.00	2.70	10.27
Gracilis	115.18	26.44	0.79	8.20	3.24	6.55
Iliacus	304.70	27.62	0.56	14.30	3.02	21.36
Obturator externus	79.72	9.96	1.00	0.00	2.70	8.00
Obturator internus	102.77	16.18	1.00	0.00	2.70	6.35
Pectineus	94.87	15.93	1.00	0.00	2.70	5.96
Piriformis	92.54	14.67	1.00	0.00	2.70	6.31
Psoas minor						1.10
Psoas major	276.33	28.06	0.50	10.60	3.11	22.30
Quadratus femoris	40.89	6.25	1.00	0.00	2.70	6.54
Rectus femoris	215.61	28.39	0.21	13.90	2.42	31.47
Sartorius	215.12	43.81	0.90	1.30	3.11	6.28
Semimembranosus	333.08	30.82	0.24	15.10	2.61	42.03
Tensor fasciae latae	137.09	17.99	1.00	0.00	2.70	7.62

Table A.9: Muscle parameters of anatomical dataset 10.

Muscle	Muscle volume (V_m, cm^3)	Muscle length (L_m, cm)	Fibre length to muscle length ratio (L_f/L_m)	Pennation angle (θ, deg)	Sarcomere length (L_s, μM)	PCSA (cm^2)
Adductor brevis	195.84	18.04	0.68	6.10	2.91	17.11
Adductor longus	241.18	21.57	0.50	7.10	3.00	24.66
Adductor magnus	740.00	24.24	0.39	15.50	2.19	61.18
Biceps femoris long head	272.74	31.35	0.28	11.60	2.35	26.49
Gemellus	2.38	4.13	1.00	0.00	2.70	0.58
Gluteus maximus	1482.10	31.09	0.62	21.90	2.60	67.81
Gluteus medius	464.29	20.78	0.37	20.50	2.40	50.27
Gluteus minimus	94.83	13.20	1.00	0.00	2.70	7.19
Gracilis	113.62	22.15	0.79	8.20	3.24	7.71
Iliacus	324.33	28.24	0.56	14.30	3.02	22.23
Obturator externus	75.29	97.44	1.00	0.00	2.70	7.73
Obturator internus	87.69	14.02	1.00	0.00	2.70	6.25
Pectineus	115.05	13.93	1.00	0.00	2.70	8.26
Piriformis	61.43	11.06	1.00	0.00	2.70	5.56
Psoas minor						1.10
Psoas major	437.47	37.57	0.50	10.60	3.11	26.37
Quadratus femoris	69.50	9.81	1.00	0.00	2.70	7.09
Rectus femoris	268.38	32.72	0.21	13.90	2.42	33.99
Sartorius	216.21	44.96	0.90	1.30	3.11	6.15
Semimembranosus	472.56	32.43	0.24	15.10	2.61	56.66
Tensor fasciae latae	92.81	14.70	1.00	0.00	2.70	6.31

Table A.10: Muscle parameters of anatomical dataset 11.

Muscle	Muscle volume (V_m, cm^3)	Muscle length (L_m, cm)	Fibre length to muscle length ratio (L_f/L_m)	Pennation angle (θ, deg)	Sarcomere length (L_s, μM)	PCSA (cm^2)
Adductor brevis	225.79	16.90	0.68	6.10	2.91	21.06
Adductor longus	221.26	19.56	0.50	7.10	3.00	24.94
Adductor magnus	634.19	26.34	0.39	15.50	2.19	48.25
Biceps femoris long head	347.47	31.99	0.28	11.60	2.35	33.07
Gemellus	7.24	6.65	1.00	0.00	2.70	1.09
Gluteus maximus	1359.98	30.67	0.62	21.90	2.60	63.90
Gluteus medius	425.35	20.56	0.37	20.50	2.40	46.55
Gluteus minimus	114.68	13.38	1.00	0.00	2.70	8.57
Gracilis	144.70	23.76	0.79	8.20	3.24	9.16
Iliacus	335.14	26.99	0.56	14.30	3.02	24.03
Obturator externus	75.06	10.45	1.00	0.00	2.70	7.19
Obturator internus	79.59	17.39	1.00	0.00	2.70	4.58
Pectineus	129.47	13.34	1.00	0.00	2.70	9.71
Piriformis	81.35	14.98	1.00	0.00	2.70	5.43
Psoas minor						1.10
Psoas major	439.79	39.61	0.50	10.60	3.11	25.14
Quadratus femoris	67.54	9.63	1.00	0.00	2.70	7.01
Rectus femoris	263.52	32.04	0.21	13.90	2.42	34.08
Sartorius	228.88	43.39	0.90	1.30	3.11	6.75
Semimembranosus	364.46	33.18	0.24	15.10	2.61	42.71
Tensor fasciae latae	108.93	14.25	1.00	0.00	2.70	7.65

Table A.11: Muscle parameters of anatomical dataset 12.

Muscle	Muscle volume (V_m, cm^3)	Muscle length (L_m, cm)	Fibre length to muscle length ratio (L_f/L_m)	Pennation angle (θ, deg)	Sarcomere length (L_s, μM)	PCSA (cm^2)
Adductor brevis	97.57	17.85	0.68	6.10	2.91	8.61
Adductor longus	161.67	28.35	0.50	7.10	3.00	12.58
Adductor magnus	552.99	34.26	0.39	15.50	2.19	32.35
Biceps femoris long head	233.38	32.84	0.28	11.60	2.35	21.64
Gemellus	4.51	6.22	1.00	0.00	2.70	0.72
Gluteus maximus	912.94	29.67	0.62	21.90	2.60	44.34
Gluteus medius	367.21	21.09	0.37	20.50	2.40	39.17
Gluteus minimus	99.16	11.17	1.00	0.00	2.70	8.88
Gracilis	89.17	29.26	0.79	8.20	3.24	4.58
Iliacus	213.00	25.65	0.56	14.30	3.02	16.07
Obturator externus	42.89	10.37	1.00	0.00	2.70	4.14
Obturator internus	54.68	14.13	1.00	0.00	2.70	3.87
Pectineus	48.38	14.69	1.00	0.00	2.70	3.29
Piriformis	40.20	10.33	1.00	0.00	2.70	3.89
Psoas minor						1.10
Psoas major	225.01	35.91	0.50	10.60	3.11	14.19
Quadratus femoris	75.22	10.13	1.00	0.00	2.70	7.43
Rectus femoris	199.43	33.95	0.21	13.90	2.42	24.34
Sartorius	176.55	50.77	0.90	1.30	3.11	4.45
Semimembranosus	344.29	35.04	0.24	15.10	2.61	38.21
Tensor fasciae latae	74.17	18.44	1.00	0.00	2.70	4.02

Table A.12: Muscle parameters of anatomical dataset 13.

Muscle	Muscle volume (V_m, cm^3)	Muscle length (L_m, cm)	Fibre length to muscle length ratio (L_f/L_m)	Pennation angle (θ, deg)	Sarcomere length (L_s, μM)	PCSA (cm^2)
Adductor brevis	102.27	16.70	0.68	6.10	2.91	9.65
Adductor longus	124.70	24.70	0.50	7.10	3.00	11.13
Adductor magnus	584.51	31.60	0.39	15.50	2.19	37.07
Biceps femoris long head	194.41	23.36	0.28	11.60	2.35	25.34
Gemellus	7.68	6.34	1.00	0.00	2.70	1.21
Gluteus maximus	887.37	27.96	0.62	21.90	2.60	45.74
Gluteus medius	335.86	18.04	0.37	20.50	2.40	41.89
Gluteus minimus	124.52	11.23	1.00	0.00	2.70	11.09
Gracilis	62.71	21.99	0.79	8.20	3.24	4.29
Iliacus	224.57	25.81	0.56	14.30	3.02	16.84
Obturator externus	43.57	8.13	1.00	0.00	2.70	5.36
Obturator internus	59.26	14.30	1.00	0.00	2.70	4.14
Pectineus	51.41	14.34	1.00	0.00	2.70	3.59
Piriformis	30.76	9.82	1.00	0.00	2.70	3.13
Psoas minor						1.10
Psoas major	213.84	34.88	0.50	10.60	3.11	13.88
Quadratus femoris	71.83	6.27	1.00	0.00	2.70	11.45
Rectus femoris	165.90	30.36	0.21	13.90	2.42	22.64
Sartorius	156.94	46.85	0.90	1.30	3.11	4.29
Semimembranosus	337.22	31.32	0.24	15.10	2.61	41.87
Tensor fasciae latae	100.86	16.70	1.00	0.00	2.70	6.04

Table A.13: Muscle parameters of anatomical dataset 14.

Muscle	Muscle volume (V_m, cm^3)	Muscle length (L_m, cm)	Fibre length to muscle length ratio (L_f/L_m)	Pennation angle (θ, deg)	Sarcomere length (L_s, μM)	PCSA (cm^2)
Adductor brevis	113.78	20.79	0.68	6.10	2.91	8.63
Adductor longus	153.31	22.63	0.50	7.10	3.00	14.94
Adductor magnus	549.17	39.93	0.39	15.50	2.19	27.56
Biceps femoris long head	195.36	27.08	0.28	11.60	2.35	21.97
Gemellus	0.28	4.63	1.00	0.00	2.70	0.06
Gluteus maximus	871.81	31.45	0.62	21.90	2.60	39.95
Gluteus medius	271.18	17.06	0.37	20.50	2.40	35.78
Gluteus minimus	92.41	9.56	1.00	0.00	2.70	9.67
Gracilis	66.77	21.47	0.79	8.20	3.24	4.68
Iliacus	207.84	28.13	0.56	14.30	3.02	14.30
Obturator externus	54.91	12.02	1.00	0.00	2.70	4.57
Obturator internus	72.50	14.54	1.00	0.00	2.70	4.99
Pectineus	34.62	12.73	1.00	0.00	2.70	2.72
Piriformis	33.70	11.50	1.00	0.00	2.70	2.93
Psoas minor						1.10
Psoas major	254.78	34.26	0.50	10.60	3.11	16.84
Quadratus femoris	33.84	7.68	1.00	0.00	2.70	4.41
Rectus femoris	195.41	25.25	0.21	13.90	2.42	32.06
Sartorius	108.82	36.41	0.90	1.30	3.11	3.82
Semimembranosus	145.87	26.92	0.24	15.10	2.61	21.07
Tensor fasciae latae	76.81	13.25	1.00	0.00	2.70	5.80

Table A.14: Muscle parameters of anatomical dataset 15.

Muscle	Muscle volume (V_m, cm^3)	Muscle length (L_m, cm)	Fibre length to muscle length ratio (L_f/L_m)	Pennation angle (θ, deg)	Sarcomere length (L_s, μM)	PCSA (cm^2)
Adductor brevis	57.50	8.54	0.68	6.10	2.91	10.61
Adductor longus	15.11	4.82	0.50	7.10	3.00	6.91
Adductor magnus	57.45	6.79	0.39	15.50	2.19	16.95
Biceps femoris long head	18.48	4.61	0.28	11.60	2.35	12.22
Gemellus	1.81	3.84	1.00	0.00	2.70	0.47
Gluteus maximus	617.08	23.00	0.62	21.90	2.60	38.66
Gluteus medius	196.88	16.09	0.37	20.50	2.40	27.53
Gluteus minimus	71.99	10.35	1.00	0.00	2.70	6.96
Gracilis	3.81	3.81	0.79	8.20	3.24	1.50
Iliacus	181.53	26.61	0.56	14.30	3.02	13.21
Obturator externus	56.21	11.44	1.00	0.00	2.70	4.91
Obturator internus	69.24	14.48	1.00	0.00	2.70	4.78
Pectineus	39.86	12.75	1.00	0.00	2.70	3.13
Piriformis	28.69	6.81	1.00	0.00	2.70	4.21
Psoas minor						1.10
Psoas major	216.33	28.46	0.50	10.60	3.11	17.21
Quadratus femoris	21.43	7.30	1.00	0.00	2.70	2.93
Rectus femoris	43.04	10.01	0.21	13.90	2.42	17.82
Sartorius	47.57	47.95	0.90	1.30	3.11	4.07
Semimembranosus	0.57	1.43	0.24	15.10	2.61	1.55
Tensor fasciae latae	47.78	9.30	1.00	0.00	2.70	5.14

Table A.15: Muscle parameters of anatomical dataset 16.

Muscle	Muscle volume (V_m, cm^3)	Muscle length (L_m, cm)	Fibre length to muscle length ratio (L_f/L_m)	Pennation angle (θ, deg)	Sarcomere length (L_s, μM)	PCSA (cm^2)
Adductor brevis	109.08	15.16	0.68	6.10	2.91	11.34
Adductor longus	177.29	23.86	0.50	7.10	3.00	16.39
Adductor magnus	487.00	28.69	0.39	15.50	2.19	34.01
Biceps femoris long head	214.73	22.37	0.28	11.60	2.35	29.23
Gemellus	3.54	5.95	1.00	0.00	2.70	0.59
Gluteus maximus	935.40	28.45	0.62	21.90	2.60	47.38
Gluteus medius	373.18	20.67	0.37	20.50	2.40	40.64
Gluteus minimus	88.07	11.25	1.00	0.00	2.70	7.83
Gracilis	69.95	19.43	0.79	8.20	3.24	5.41
Iliacus	254.36	26.16	0.56	14.30	3.02	18.82
Obturator externus	52.54	7.97	1.00	0.00	2.70	6.59
Obturator internus	69.95	46.99	1.00	0.00	2.70	4.12
Pectineus	59.29	13.27	1.00	0.00	2.70	4.47
Piriformis	40.60	14.80	1.00	0.00	2.70	2.74
Psoas minor						1.10
Psoas major	232.40	38.73	0.50	10.60	3.11	13.59
Quadratus femoris	31.98	8.08	1.00	0.00	2.70	3.96
Rectus femoris	162.70	26.94	0.21	13.90	2.42	25.02
Sartorius	127.70	37.32	0.90	1.30	3.11	4.38
Semimembranosus	252.50	29.59	0.24	15.10	2.61	33.19
Tensor fasciae latae	76.40	17.87	1.00	0.00	2.70	4.28

Table A.16: Muscle parameters of anatomical dataset 17.

Muscle	Muscle volume (V_m, cm^3)	Muscle length (L_m, cm)	Fibre length to muscle length ratio (L_f/L_m)	Pennation angle (θ, deg)	Sarcomere length (L_s, μM)	PCSA (cm^2)
Adductor brevis	98.42	16.02	0.68	6.10	2.91	9.68
Adductor longus	182.32	23.24	0.50	7.10	3.00	17.30
Adductor magnus	511.00	29.58	0.39	15.50	2.19	34.62
Biceps femoris long head	246.79	27.46	0.28	11.60	2.35	27.36
Gemellus	2.26	6.82	1.00	0.00	2.70	0.33
Gluteus maximus	896.56	30.05	0.62	21.90	2.60	42.99
Gluteus medius	387.41	20.46	0.37	20.50	2.40	42.62
Gluteus minimus	95.50	12.59	1.00	0.00	2.70	7.59
Gracilis	80.52	21.74	0.79	8.20	3.24	5.57
Iliacus	192.79	25.45	0.56	14.30	3.02	14.66
Obturator externus	57.35	10.13	1.00	0.00	2.70	5.66
Obturator internus	67.14	15.36	1.00	0.00	2.70	4.38
Pectineus	50.71	12.32	1.00	0.00	2.70	4.12
Piriformis	37.45	13.49	1.00	0.00	2.70	2.78
Psoas minor						1.10
Psoas major	169.69	38.16	0.50	10.60	3.11	10.07
Quadratus femoris	33.51	6.86	1.00	0.00	2.70	4.89
Rectus femoris	178.96	30.37	0.21	13.90	2.42	24.41
Sartorius	133.30	40.08	0.90	1.30	3.11	4.25
Semimembranosus	291.39	29.23	0.24	15.10	2.61	38.76
Tensor fasciae latae	73.60	18.54	1.00	0.00	2.70	3.97

Table A.17: Muscle parameters of anatomical dataset 18.

Appendix B

Validation of each subject-specific musculoskeletal model

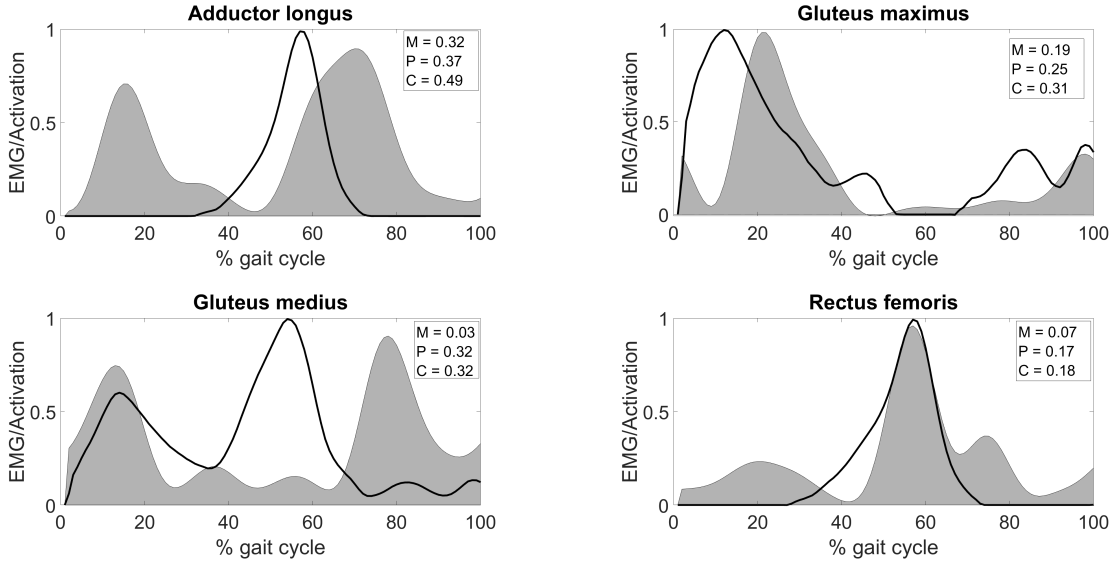


Figure B.1: Predicted muscle activations (solid line) and normalised EMG data (shaded area) for model 2. M, P and C represent the magnitude, phase and combined Sprague and Geers errors.

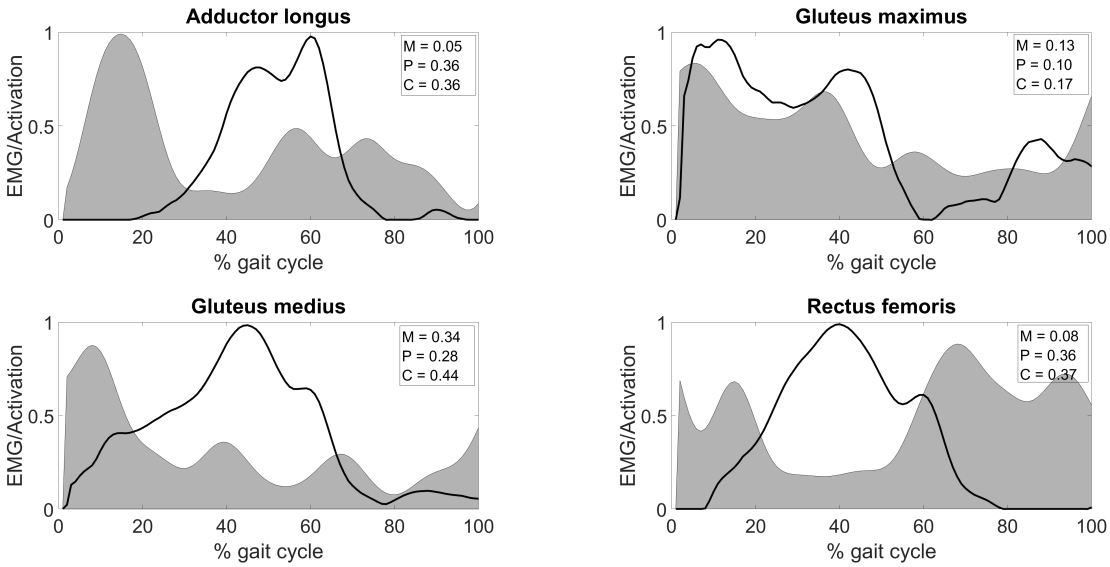


Figure B.2: Predicted muscle activations (solid line) and normalised EMG data (shaded area) for model 3. M, P and C represent the magnitude, phase and combined Sprague and Geers errors.

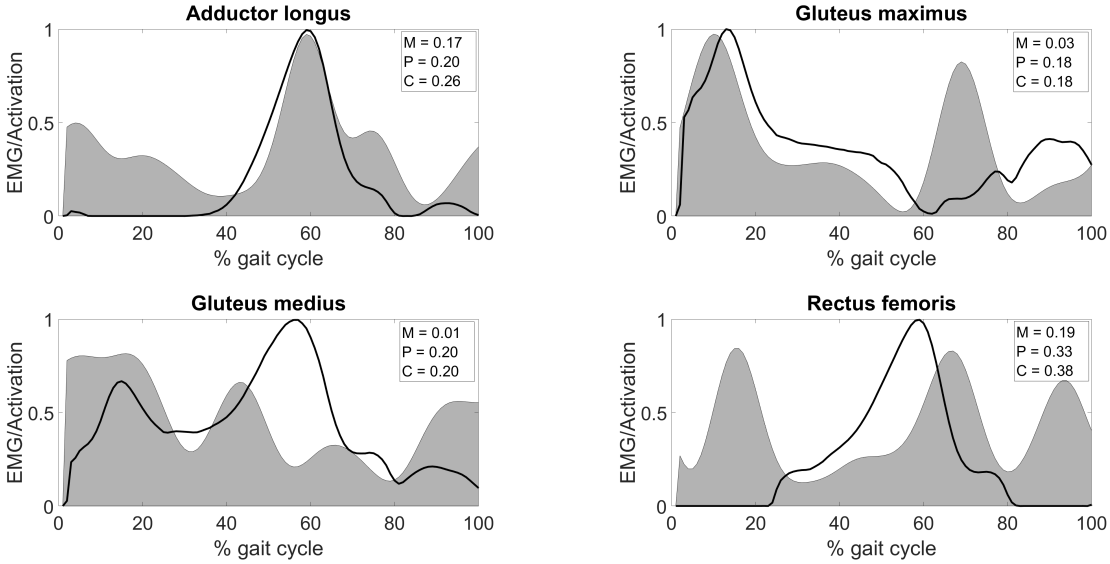


Figure B.3: Predicted muscle activations (solid line) and normalised EMG data (shaded area) for model 4. M, P and C represent the magnitude, phase and combined Sprague and Geers errors.

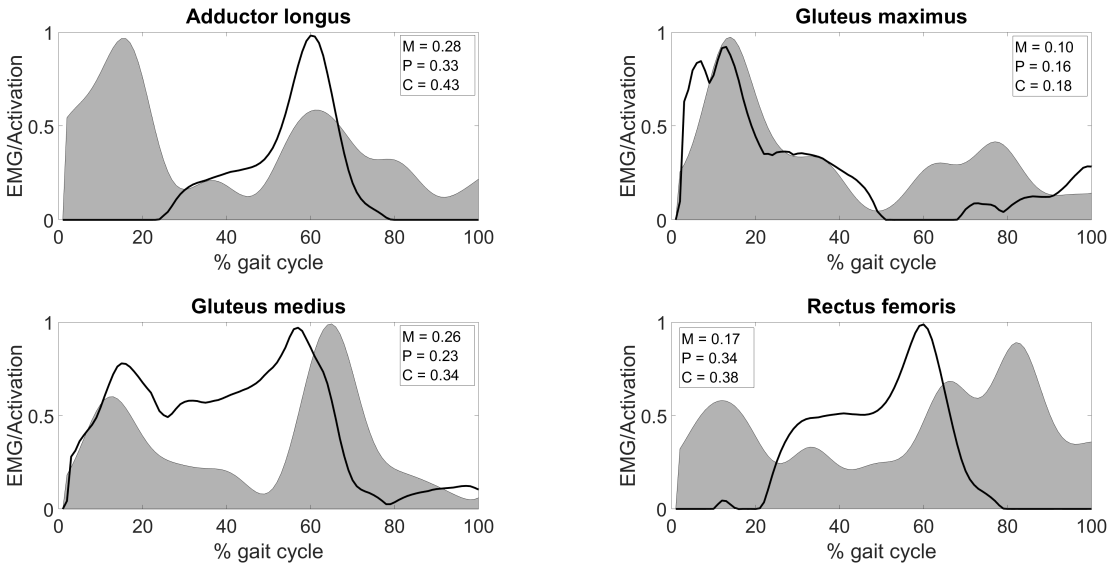


Figure B.4: Predicted muscle activations (solid line) and normalised EMG data (shaded area) for model 5. M, P and C represent the magnitude, phase and combined Sprague and Geers errors.

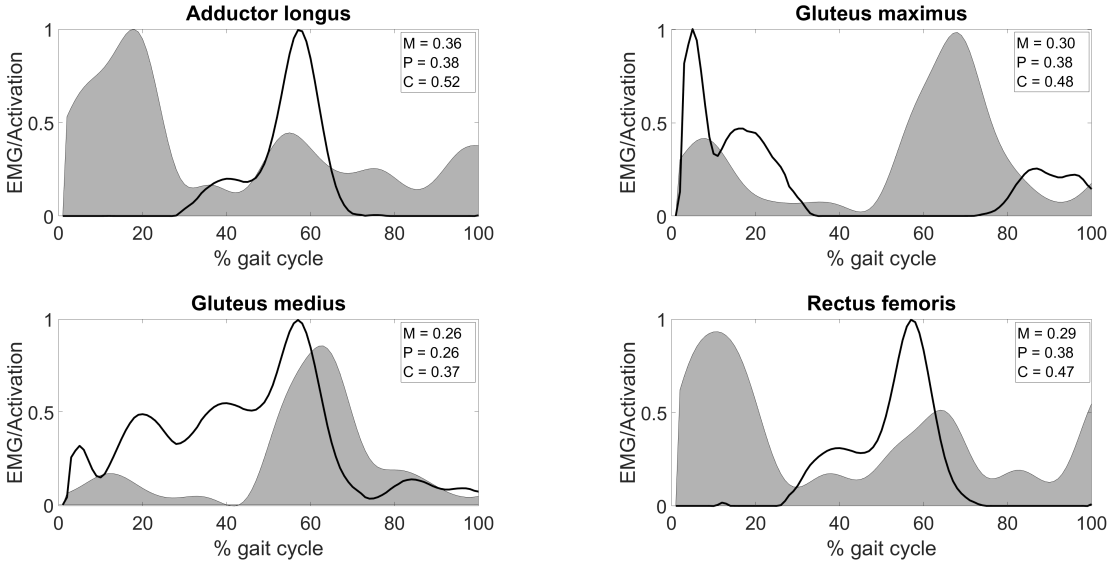


Figure B.5: Predicted muscle activations (solid line) and normalised EMG data (shaded area) for model 6. M, P and C represent the magnitude, phase and combined Sprague and Geers errors.

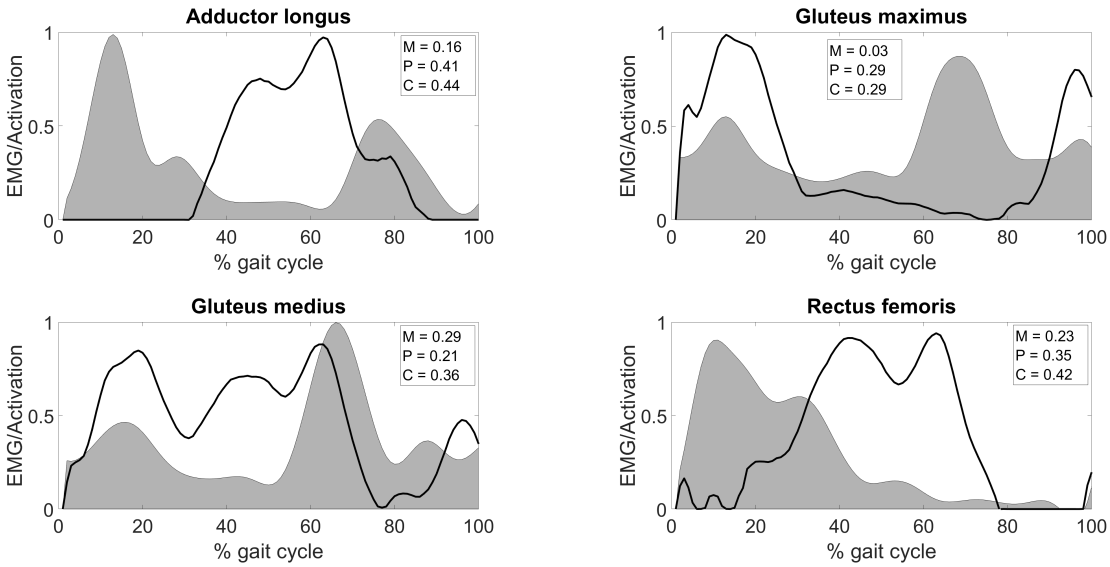


Figure B.6: Predicted muscle activations (solid line) and normalised EMG data (shaded area) for model 7. M, P and C represent the magnitude, phase and combined Sprague and Geers errors.

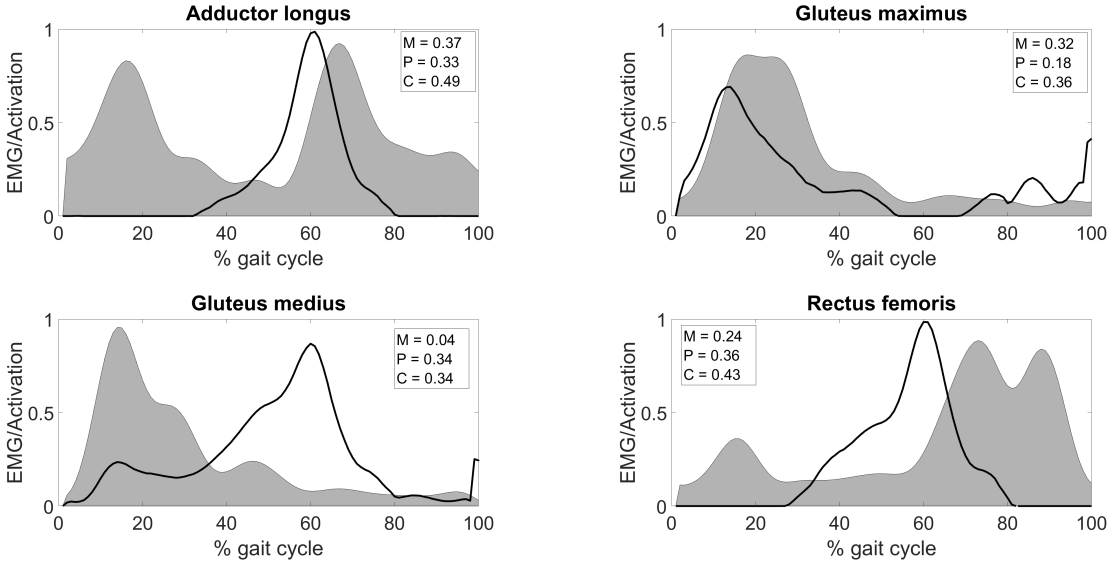


Figure B.7: Predicted muscle activations (solid line) and normalised EMG data (shaded area) for model 9. M, P and C represent the magnitude, phase and combined Sprague and Geers errors.

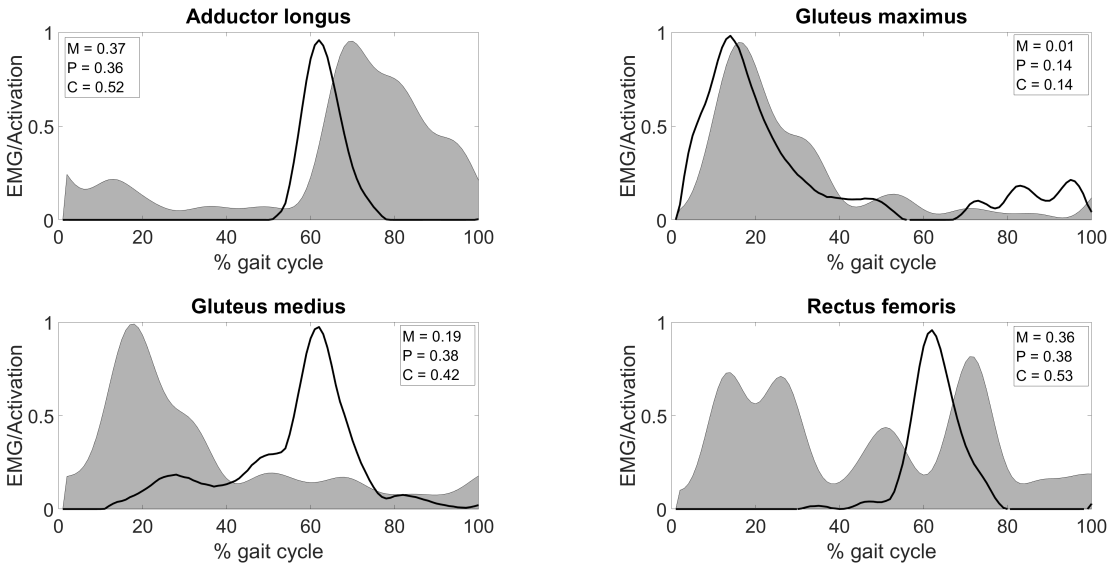


Figure B.8: Predicted muscle activations (solid line) and normalised EMG data (shaded area) for model 10. M, P and C represent the magnitude, phase and combined Sprague and Geers errors.

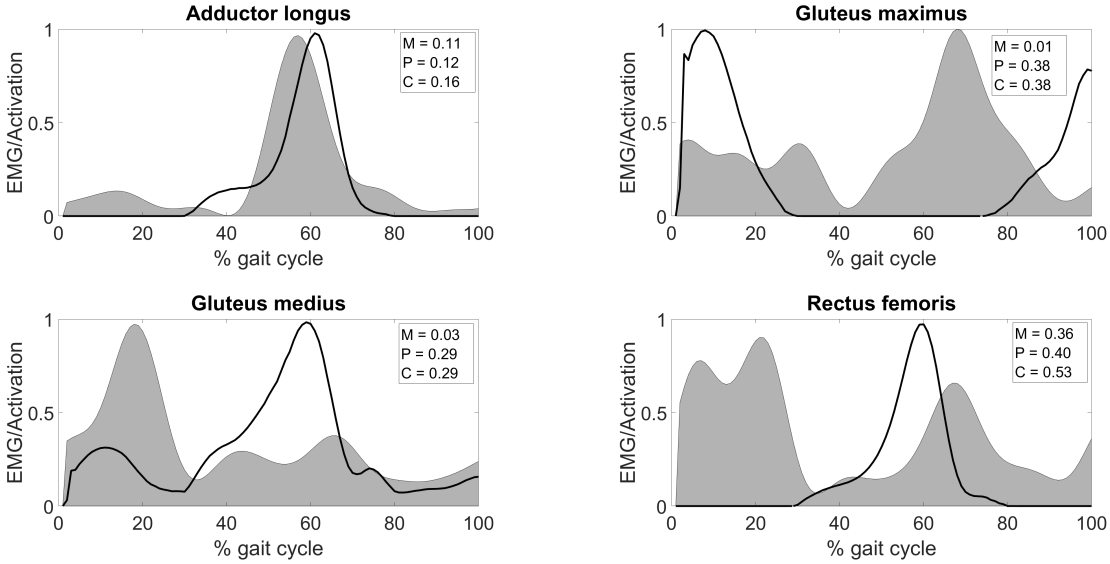


Figure B.9: Predicted muscle activations (solid line) and normalised EMG data (shaded area) for model 11. M, P and C represent the magnitude, phase and combined Sprague and Geers errors.

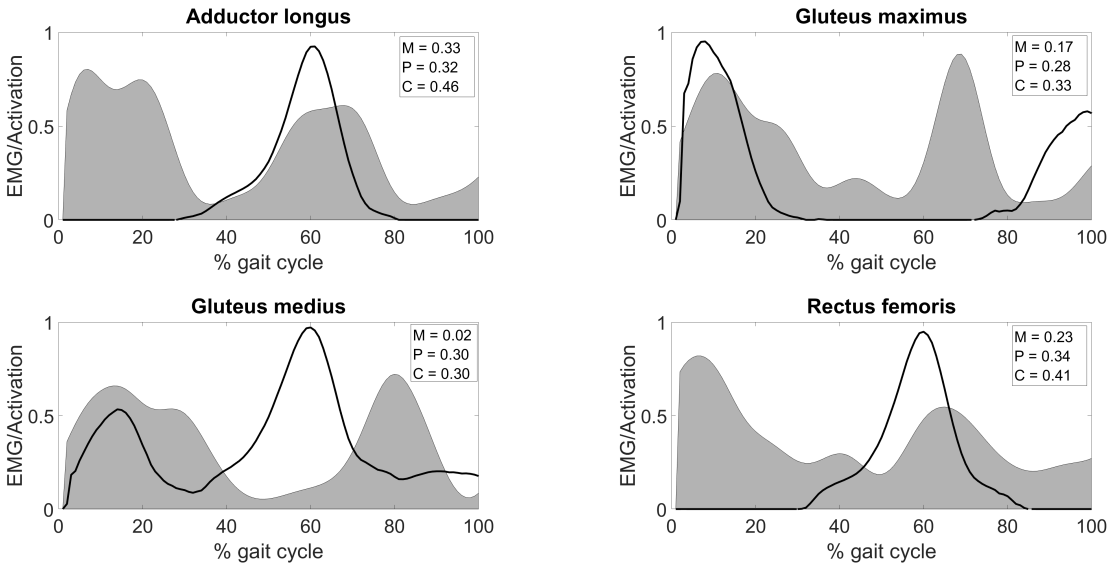


Figure B.10: Predicted muscle activations (solid line) and normalised EMG data (shaded area) for model 12. M, P and C represent the magnitude, phase and combined Sprague and Geers errors.

Appendix C

SAT-PRO prosthesis satisfaction questionnaire

Date:

Participant ID number:

SATISFACTION WITH PROSTHESIS (SAT-PRO) QUESTIONNAIRE

For each question, please **circle the number** that best describes your satisfaction with your prosthesis.

1. My prosthesis is comfortable
    1) Totally agree
    2) Rather agree
    3) Rather disagree
    4) Totally disagree

2. When I am in the presence of people other than my family, I am at ease wearing my prosthesis.
    1) Totally agree
    2) Rather agree
    3) Rather disagree
    4) Totally disagree

3. My prosthesis is easy to clean.
    1) Totally agree
    2) Rather agree
    3) Rather disagree
    4) Totally disagree

4. My prosthesis works well regardless of the weather.
    1) Totally agree
    2) Rather agree
    3) Rather disagree
    4) Totally disagree

5. My prosthesis is easy to put on.
    1) Totally agree
    2) Rather agree
    3) Rather disagree
    4) Totally disagree

6. There are chances that I will hurt myself with my prosthesis.
    1) Totally agree
    2) Rather agree
    3) Rather disagree
    4) Totally disagree

7. I find it easy to move with my prosthesis.
    1) Totally agree
    2) Rather agree
    3) Rather disagree
    4) Totally disagree

8. The repairs/adjustments to my prosthesis are done in reasonable time.
    1) Totally agree
    2) Rather agree
    3) Rather disagree
    4) Totally disagree

9. My prosthesis will last me a long time.
    1) Totally agree
    2) Rather agree
    3) Rather disagree
    4) Totally disagree

10. When I wear my prosthesis, I can accomplish more things than without it.
    1) Totally agree
    2) Rather agree
    3) Rather disagree
    4) Totally disagree

11. I am satisfied with the look of my prosthesis.
    1) Totally agree
    2) Rather agree
    3) Rather disagree
    4) Totally disagree

12. I find it easy to use my prosthesis with or without a walker/cane.
    1) Totally agree
    2) Rather agree
    3) Rather disagree
    4) Totally disagree

13. It was easy to understand how to use my prosthesis.
    1) Totally agree
    2) Rather agree
    3) Rather disagree
    4) Totally disagree

14. My prosthesis causes me physical pain or discomfort.
    1) Totally agree
    2) Rather agree
    3) Rather disagree
    4) Totally disagree

15. In general, I am satisfied with my prosthesis.
    1) Totally agree
    2) Rather agree
    3) Rather disagree
    4) Totally disagree

END OF QUESTIONNAIRE

Appendix D

List of publications and conference presentations

Diana Toderita, David P. Henson, Christian Klemt, Ziyun Ding, Anthony MJ Bull. "An anatomical atlas-based scaling study for quantifying muscle and hip joint contact forces in above and through-knee amputees using validated musculoskeletal modelling". In: IEEE Transactions on Biomedical Engineering. 2021. 68(11):3447-3456.

Diana Toderita, David P. Henson, Clement D. Favier, Vasiliki Vardakastani, Biranavan Sivapuratharasu, Alison H. McGregor, Alexander N. Bennett, Anthony MJ Bull. "Biomechanical assessment of bilateral transfemoral amputee gait using stubby prostheses and microprocessor-controlled knee units". 9th World Congress of Biomechanics 2022, Taipei.

Diana Toderita, Clement D. Favier, Giovanni S. Milandri, Vasiliki Vardakastani, David P. Henson, Anthony MJ Bull. "Biomechanical effect of high- and low-cost prostheses for transfemoral amputees". BioMedEng Conference 2022, London, UK.

References

Abou-Zamzam, A. M., Teruya, T. H., Killeen, J. D. & Ballard, J. L. (2003), 'Major lower extremity amputation in an academic vascular center', *Annals of Vascular Surgery* **17**(1), 86–90.

Adams, M., Bogduk, N., Burton, K. & Dolan, P. (2007), *The Biomechanics of Back Pain*, Churchill Livingstone.

Agrawal, V., Gailey, R., Toole, C. O., Gaunaurd, I. & Dowell, T. (2009), 'Symmetry in External Work (SEW): A novel method of quantifying gait differences between prosthetic feet', *Prosthetics and Orthotics International* **33**(2), 148–156.

Arnold, E. M., Hamner, S. R., Seth, A., Millard, M. & Delp, S. L. (2013), 'How muscle fiber lengths and velocities affect muscle force generation as humans walk and run at different speeds', *Journal of Experimental Biology* **216**(11), 2150–2160.

ATscale (2020), Product narrative: Protheses, Technical Report April.
URL: *https://atscale2030.org/*

Balk, E. M., Gazula, A., Markozannes, G., Kimmel, H. J., Saldanha, I. J., Resnik, L. J. & Trikalinos, T. A. (2018), *Lower Limb Prostheses: Measurement Instruments, Comparison of Component Effects by Subgroups, and Long-Term Outcomes*, number 213.
URL: *http://www.ncbi.nlm.nih.gov/pubmed/30285344*

Batten, H. R., McPhail, S. M., Mandrusiak, A. M., Varghese, P. N. & Kuys, S. S. (2019), 'Gait speed as an indicator of prosthetic walking potential following lower limb amputation', *Prosthetics and Orthotics International* **43**(2), 196–203.

Behr, J., Friedly, J., Molton, I., Morgenroth, D., Jensen, M. P. & Smith, D. G. (2009), 'Pain and pain-related interference in adults with lower-limb amputation: Comparison of knee-disarticulation, transtibial, and transfemoral surgical sites', *J Rehabil Res Dev* **46**(7), 963–972.
URL: *https://www.ncbi.nlm.nih.gov/pmc/articles/PMC3624763/pdf/nihms412728.pdf*

Bellmann, M., Blumentritt, S. & Köhler, T. M. (2020), 'Polycentric exoprosthetic knee joints - Extent of shortening during swing phase', *Canadian Prosthetics and Orthotics Journal* **3**(1).

Bennell, K. L., Bowles, K. A., Wang, Y., Cicuttini, F., Davies-Tuck, M. & Hinman, R. S. (2011), 'Higher dynamic medial knee load predicts greater cartilage loss over 12 months in medial knee osteoarthritis', *Annals of the Rheumatic Diseases* **70**(10), 1770–1774.

Bilodeau, S., Hébert, R. & Desrosiers, J. (1999), 'Questionnaire sur la satisfaction des personnes amputees du membre inferieur face a leur prothese: Developpement et validation', *Canadian Journal of Occupational Therapy* **66**(1), 23–32.

Bowker, H. & Michael, J. (1992), *Atlas of Limb Prosthetics: Surgical, Prosthetic, and Rehabilitation Principles*, 2 edn, American Academy of Orthopedic Surgeons.

Brånemark, R., Brånemark, P. I., Rydevik, B. & Myers, R. R. (2001), 'Osseointegration in skeletal reconstruction and rehabilitation: A review', *Journal of Rehabilitation Research and Development* **38**(2), 175–181.

Buckwalter, J. A. (1992), 'Mechanical Injuries of Articular Cartilage', *The Iowa Orthopaedic Journal* **12**, 50.

Burke, M. J., Roman, V. & Wright, V. (1978), 'Bone and joint changes in lower limb amputees', *Annals of the Rheumatic Diseases* **37**(3), 252–254.

Carbone, V., Van Der Krogt, M. M., Koopman, H. F. J. M. & Verdonschot, N. (2016), 'Sensitivity of subject-specific models to Hill muscle – tendon model parameters in simulations of gait', *Journal of Biomechanics* **49**(9), 1953–1960.
URL: *http://dx.doi.org/10.1016/j.jbiomech.2016.04.008*

Carroll, M. K., Carroll, K., Rheinstein, J. & Highsmith, M. J. (2018), 'Functional differences of bilateral transfemoral amputees using full-length and stubby-length prostheses', *Technol Innov* **20**, 75–83.

Carse, B., Scott, H., Davie-Smith, F., Brady, L. & Colvin, J. (2021), 'Minimal clinically important difference in walking velocity, gait profile score and two minute walk test for individuals with lower limb amputation', *Gait and Posture* **88**(November 2020), 221–224.
URL: *https://doi.org/10.1016/j.gaitpost.2021.06.001*

Castro, M. P. D., Soares, D. & Mendes, E. (2014), 'Plantar Pressures and Ground Reaction Forces During Walking of Individuals With Unilateral Transfemoral Amputation', *American Academy of Physical Medicine and Rehabilitation* pp. 1–11.
URL: *http://dx.doi.org/10.1016/j.pmrj.2014.01.019*

Cavanagh, P. R. & Komi, P. V. (1979), 'Electromechanical delay in human skeletal muscle under concentric and eccentric contractions', *European Journal of Applied Physiology and Occupational Physiology* **42**(3), 159–163.

Chang, Y. H., Bae, T. S., Kim, S. K., Mun, M. S. & Lee, W.-h. (2011), 'Intact Hip and Knee Joint Moment in Coronal Plane with Unilateral Transfemoral Amputee', *International Journal of Precision Engineering and Manufacturing* **12**(1), 129–134.

Charlton, I. W. & Johnson, G. R. (2006), 'A model for the prediction of the forces at the glenohumeral joint', *Proceedings of the Institution of Mechanical Engineers, Part H: Journal of Engineering in Medicine* **220**(8), 801–812.

Chen, H. C., Ashton-Miller, J. A., Alexander, N. B. & Schultz, A. B. (1991), 'Stepping over obstacles: Gait patterns of healthy young and old adults', *Journals of Gerontology* **46**(6), 196–203.

Christie, H. J., Kumar, S. & Warren, S. A. (1995), 'Postural aberrations in low back pain', *Archives of Physical Medicine and Rehabilitation* **76**(3), 218–224.

Cleather, D. J. & Bull, A. M. J. (2012), 'The development of lower limb musculoskeletal models with clinical relevance is dependent upon the fidelity of the mathematical description of the lower limb. Part 2: Patient-specific geometry', *Proceedings of the Institution of Mechanical Engineers, Part H: Journal of Engineering in Medicine* **226**(2), 133–145.

Cleather, D. J. & Bull, A. M. J. (2015), 'The development of a segment-based musculoskeletal model of the lower limb: Introducing FREEBODY', *Royal Society Open Science* **2**(6).

Crossley, K. M., Dorn, T. W., Ozturk, H., van den Noort, J., Schache, A. G. & Pandy, M. G. (2012), 'Altered hip muscle forces during gait in people with patellofemoral osteoarthritis', *Osteoarthritis and Cartilage* **20**(11), 1243–1249.
URL: *http://dx.doi.org/10.1016/j.joca.2012.07.011*

Crowninshield, R. D. & Brand, R. A. (1981), 'A physiologically based criterion of muscle force prediction in locomotion', *J Biomech* **14**(11), 793–801.

Czerniecki, M. (1996), 'Rehabilitation in Limb Deficiency . 1 . Gait and Motion Analysis', *American Academy of Physical Medicine and Rehabilitation* **77**(3), S3–S8.

Davis, K. G. & Marras, W. S. (2000), 'The effects of motion on trunk biomechanics', *Clinical Biomechanics* **15**(10), 703–717.

Day, J. W., Smidt, G. L. & Lehmann, T. (1984), 'Effect of pelvic tilt on standing posture', *Physical Therapy* **64**(4), 510–516.

De Leva, P. (1996), 'Adjustments to Zarsiorsky-Seluyanov's segment inertia parameters', *International Journal of Imaging Systems and Technology* **29**(9), 1223–1230.

Devan, H., Dillon, M. P., Carman, A. B., Hendrick, P., Hale, L., Boocock, M. & Ribeiro, D. C. (2017), 'Spinal and pelvic kinematics during gait in people with lower-limb amputation, with and without low back pain: an exploratory study', *Journal of Prosthetics and Orthotics* **29**(3), 121–129.

Ding, Z., Jarvis, H. L., Bennett, A. N., Baker, R. & Bull, A. M. (2020), 'Higher knee contact forces might underlie increased osteoarthritis rates in high functioning amputees: A pilot study', *Journal of Orthopaedic Research* (May), 1–11.

Ding, Z., Nolte, D., Tsang, C. K., Cleather, D. J., Kedgley, A. E. & Bull, A. M. J. (2016), 'In vivo knee contact force prediction using patient-specific musculoskeletal geometry in a segment-based computational model', *Journal of Biomechanical Engineering* **138**(2), 1–9.

Ding, Z., Tsang, C. K., Nolte, D., Kedgley, A. E. & Bull, A. M. J. (2019), 'Improving musculoskeletal model scaling using an anatomical atlas: the importance of gender and anthropometric similarity to quantify joint reaction forces', *IEEE Transactions on Biomedical Engineering* **66**(12), 1–13.

Drevelle, X., Villa, C., Bonnet, X., Loiret, I., Fodé, P. & Pillet, H. (2014), 'Vaulting quantification during level walking of transfemoral amputees', *Clinical Biomechanics* **29**(6), 679–683.
URL: *http://dx.doi.org/10.1016/j.clinbiomech.2014.04.006*

Duda, G. N., Brand, D., Freitag, S., Lierse, W. & Schneider, E. (1996), 'Variability of femoral muscle attachments', *Journal of Biomechanics* **29**(9), 1185–1190.

Duffell, L. D., Hope, N. & McGregor, A. H. (2014), 'Comparison of kinematic and kinetic parameters calculated using a cluster-based model and Vicon's plug-in gait', *Proceedings of the Institution of Mechanical Engineers, Part H: Journal of Engineering in Medicine* **228**(2), 206–210.

Eberly, V. J., Mulroy, S. J., Gronley, J. K., Perry, J., Yule, W. J. & Burnfield, J. M. (2014), 'Impact of a stance phase microprocessor- controlled knee prosthesis on level walking in lower functioning individuals with a transfemoral amputation', *Prosthetics and Orthotics International* **38**(4), 447–455.

Edwards, D. S., Phillip, R. D., Bosanquet, N., Bull, A. M. J. & Clasper, J. C. (2015), 'What is the magnitude and long-term economic cost of care of the british military Afghanistan amputee cohort?', *Clinical Orthopaedics and Related Research* **473**(9), 2848–2855.
URL: *http://dx.doi.org/10.1007/s11999-015-4250-9*

Ehde, D. M., Smith, D. G., Czerniecki, J. M., Campbell, K. M., Malchow, D. M., Robinson, L. R., Dm, A. E., Dg, S. & Jm, C. (2001), 'Back Pain as a Secondary Disability in Persons With Lower Limb Amputations', *Arch Phys Med Rehabil* **82**(June), 731–734.

Ephraim, P. L., Wegener, S. T., MacKenzie, E. J., Dillingham, T. R. & Pezzin, L. E. (2005), 'Phantom pain, residual limb pain, and back pain in amputees: Results of a national survey', *Archives of Physical Medicine and Rehabilitation* **86**(10), 1910–1919.

Ewers, B. J., Dvoracek-Driksna, D., Orth, M. W. & Haut, R. C. (2001), 'The extent of matrix damage and chondrocyte death in mechanically traumatized articular cartilage explants depends on rate of loading', *Journal of Orthopaedic Research* **19**(5), 779–784.

Fatone, S., Caldwell, R., Angelico, J., Stine, R., Kim, K. Y., Gard, S. & Oros, M. (2021), 'Comparison of Ischial Containment and Subischial Sockets on Comfort, Function,

Quality of Life, and Satisfaction With Device in Persons With Unilateral Transfemoral Amputation: A Randomized Crossover Trial', *Archives of Physical Medicine and Rehabilitation* **102**(11), 2063–2073.e2.
URL: *https://doi.org/10.1016/j.apmr.2021.05.016*

Felson, D. T. (2013), 'Osteoarthritis as a disease of mechanics', *Osteoarthritis and Cartilage* **21**(1), 10–15.
URL: *http://dx.doi.org/10.1016/j.joca.2012.09.012*

Fiodorenko-Dumas, Z., Dumas, I., Kowal, M., Machnikowska, A., Gieysztor, E., Winiarski, S. & Paprocka-Borowicz, M. (2021), 'Using Stubby Prosthesis after Bilateral Transfemoral Amputation: A Biomechanical Case Study', *Applied Sciences* **11**(3671), 1–9.

Friston, K., Ashburner, J., S.J., K., Nichols, T. & Penny, W. (2007), *Statistical Parametric Mapping: The Analysis of Functional Brain Images*, Elsevier, London.

Gailey, R., Allen, K., Castles, J., Kucharik, J. & Roeder, M. (2008), 'Review of secondary physical conditions associated with lower-limb amputation and long-term prosthesis use', *Journal of Rehabilitation Research and Development* **45**(1), 15–30.

Gailey, R. S., Roach, K. E., Applegate, E., Cho, B., Cunniffe, B., Licht, S., Maguire, M. & Nash, M. S. (2002), 'The Amputee Mobility Predictor: An instrument to assess determinants of the lower-limb amputee's ability to ambulate', *Archives of Physical Medicine and Rehabilitation* **83**(5), 613–627.

Gard, S. A. (2006), 'Use of quantitative gait analysis for the evaluation of prosthetic walking performance', *Journal of Prosthetics and Orthotics* **18**(6), 93–104.

Gard, S. A., Childress, D. S. & Uellendahl, J. E. (1996), 'The influence of four-bar linkage knees on prosthetic swing-phase floor clearance', *Journal of Prosthetics and Orthotics* **8**(2), 34–40.

Gauthier-Gagnon, C., Grisé, M. C. & Potvin, D. (1999), 'Enabling factors related to prosthetic use by people with transtibial and transfemoral amputation', *Archives of Physical Medicine and Rehabilitation* **80**(6), 706–713.

Giarmatzis, G., Jonkers, I., Wesseling, M., Van Rossom, S. & Verschueren, S. (2015), 'Loading of Hip Measured by Hip Contact Forces at Different Speeds of Walking and Running', *Journal of Bone and Mineral Research* **30**(8), 1431–1440.

Gitter, A., Paynter, K., Walden, G. & Darm, T. (2002), 'Influence of rotators on the kinematic adaptations in stubby prosthetic gait', *American Journal of Physical Medicine and Rehabilitation* **81**(4), 310–314.

Griffin, F. M., Math, K., Scuderi, G. R., Insall, J. N. & Poilvache, P. L. (2000), 'Anatomy of the epicondyles of the distal femur', *The Journal of Arthroplasty* **15**(3), 354–359.

Grimmer, M., Holgate, M., Holgate, R., Boehler, A., Ward, J., Hollander, K., Sugar, T. & Seyfarth, A. (2016), 'A powered prosthetic ankle joint for walking and running', *BioMedical Engineering Online* **15**(3), 37–52.

Gupta, N., Castillo-Laborde, C. & Landry, M. D. (2011), 'Health-related rehabilitation services: Assessing the global supply of and need for human resources', *BMC Health Services Research* **11**(276), 1–11.

Haas, A. E. (1928), *Introduction to theoretical physics*, Constable Limited.

Hafner, B. J., Sanders, J. E., Czerniecki, J. & Fergason, J. (2002), 'Energy storage and return prostheses: does patient perception correlate with biomechanical analysis?', *Clinical Biomechanics* **17**, 325–344.

Handsfield, G. G., Meyer, C. H., Hart, J. M., Abel, M. F. & Blemker, S. S. (2014), 'Relationships of 35 lower limb muscles to height and body mass quantified using MRI', *Journal of Biomechanics* **47**(3), 631–638.

Hanspal, R. (2003), Report of the Working Party. Amputee and Prosthetic Rehabilitation - Standards and Guidelines, Technical report, British Society of Rehabilitation Medicine (2nd Edition).

Hanspal, R. S. & Sullivan, J. (2021), *Essentials of Foot and Ankle Surgery. Chapter: Principles of lower limb prosthetics and rehabilitation*, 1st editio edn, CRC Press.

Hendershot, B. D., Shojaei, I., Acasio, J. C., Dearth, C. L. & Bazrgari, B. (2018), 'Walking speed differentially alters spinal loads in persons with traumatic lower limb amputation', *J Biomech* (70), 248–254.

Hendershot, B. D. & Wolf, E. J. (2014), 'Three-dimensional joint reaction forces and moments at the low back during over-ground walking in persons with unilateral lower-extremity amputation', *Clinical Biomechanics* **29**(3), 235–242.
URL: *http://dx.doi.org/10.1016/j.clinbiomech.2013.12.005*

Henson, D. P. (2020), Understanding the musculoskeletal function of bilateral through and above-knee amputees: methods to improve the optimisation and individualisation of intervention techniques and therapeutic device design for lower-limb amputees, PhD thesis, Imperial College London.

Henson, D. P., Edgar, C., Ding, Z., Sivapuratharasu, B., Le Feuvre, P., Finnegan, M. E., Quest, R., McGregor, A. H. & Bull, A. M. (2021), 'Understanding lower limb muscle volume adaptations to amputation', *Journal of Biomechanics* **125**, 110599.
URL: *https://doi.org/10.1016/j.jbiomech.2021.110599*

Hospital episode statistics NHS digital (2020), 'http://content.digital.nhs.uk/hes (accessed 29 July 2020)'.
URL: *http://content.digital.nhs.uk/hes*

Ikeda, A. J., Grabowski, A. M., Lindsley, A. & Reisinger, K. D. (2014), 'A scoping literature review of the provision of orthoses and prostheses in resource- limited environments 2000 – 2010 . Part one : Considerations for success', *Prosthetics and Orthotics International* **38**(4), 269–286.

Inman, V. T. (1966), 'Human locomotion', *Canadian Medical Association Journal* **94**(20), 1047.

Isakov, E., Keren, O. & Benjuya, N. (2000), 'Trans-tibial amputee gait: Time-distance parameters and EMG activity', *Prosthetics and Orthotics International* **24**(3), 216–220.

Jaegers, S. M., Arendzen, J. H. & de Jongh, H. J. (1995), 'Changes in hip muscles after above-knee amputation', *Clinical orthopaedics and related research* **319**, 276–284.

Jaegers, S. M., Vos, L. D., Rispens, P. & Hof, A. L. (1993), 'The relationship between comfortable and most metabolically efficient walking speed in persons with unilateral above-knee amputation', *Archives of Physical Medicine and Rehabilitation* **74**(5), 521–525.

Jarvis, H. L., Bennett, A. N., Twiste, M., Phillip, R. D., Etherington, J. & Baker, R. (2017), 'Temporal spatial and metabolic measures of walking in highly functional individuals with lower limb amputations', *Archives of Physical Medicine and Rehabilitation* **98**(7), 1389–1399.
URL: *http://dx.doi.org/10.1016/j.apmr.2016.09.134*

Jarvis, H. L., Reeves, N. D., Twiste, M., Phillip, R. D., Etherington, J. & Bennett, A. N. (2020), 'Can high-functioning amputees with state-of-the-art prosthetics walk normally? A kinematic and dynamic study of 40 individuals', *Annals of physical and rehabilitation medicine* pp. 4–11.
URL: *https://doi.org/10.1016/j.rehab.2020.04.007*

Jensen, J. S. & Treichl, H. B. (2007), 'Mechanical testing of prosthetic feet utilized in low-income countries according to ISO-10328 standard', *Prosthetics and Orthotics International* **31**(2), 177–206.

Kaptein, B. L. & Van Der Helm, F. C. T. (2004), 'Estimating muscle attachment contours by transforming geometrical bone models', *J Biomech* **37**, 263–273.

Kaufman, K. R., Frittoli, S. & Frigo, C. A. (2012), 'Gait asymmetry of transfemoral amputees using mechanical and microprocessor-controlled prosthetic knees', *Clinical Biomechanics* **27**(5), 460–465.
URL: *http://dx.doi.org/10.1016/j.clinbiomech.2011.11.011*

Kerin, A. J., Coleman, A., Wisnom, M. R. & Adams, M. A. (2003), 'Propagation of surface fissures in articular cartilage in response to cyclic loading in vitro', *Clinical Biomechanics* **18**(10), 960–968.

Klein Horsman, M. D., Koopman, H. F., van der Helm, F. C., Prosé, L. P. & Veeger, H. E. J. (2007), 'Morphological muscle and joint parameters for musculoskeletal modelling of the lower extremity', *Clinical Biomechanics* **22**(2), 239–247.

Klemt, C., Nolte, D., Ding, Z., Rane, L., Quest, R. A., Finnegan, M. E., Walker, M., Reilly, P. & Bull, A. M. (2019), 'Anthropometric scaling of anatomical datasets for subject-specific musculoskeletal modelling of the shoulder', *Annals of Biomedical Engineering* **47**(4), 924–936.

Kulkarni, J. & Adams, J. (1998), 'Association between amputation , arthritis and osteopenia in British male war veterans with major lower limb amputations', *Clinical Rehabilitation* **12**, 348–353.

Kulkarni, J., Gaine, W. J., Buckley, J. G., Rankine, J. J. & Adams, J. (2005), 'Chronic low back pain in traumatic lower limb amputees', *Clinical Rehabilitation* **19**(1), 81–86.

Leardini, A., Berti, L., Begon, M. & Allard, P. (2013), 'Effect of trunk sagittal attitude on shoulder, thorax and pelvis three-dimensional kinematics in able-bodied subjects during gait.', *PloS one* **8**(10), 1–7.

Lieber, R. L., Loren, G. J. & Friden, J. (1994), 'In vivo measurement of human wrist extensor muscle sarcomere length changes', *Journal of Neurophysiology* **71**(3), 874–881.

Lohman, T. H., Roche, A. F. & Martorell, R. (1988), *Anthropometric standardization reference manual*, Human Kinetics Books, Champaign, IL.

Long, M. J., Papi, E., Duffell, L. D. & McGregor, A. H. (2017), 'Predicting knee osteoarthritis risk in injured populations', *Clinical Biomechanics* **47**(June), 87–95.

Mâaref, K., Martinet, N., Grumillier, C., Ghannouchi, S., André, J. M. & Paysant, J. (2010), 'Kinematics in the Terminal Swing Phase of Unilateral Transfemoral Amputees: Microprocessor-Controlled Versus Swing-Phase Control Prosthetic Knees', *Archives of Physical Medicine and Rehabilitation* **91**(6), 919–925.
URL: *http://dx.doi.org/10.1016/j.apmr.2010.01.025*

Manal, K., Gardinier, E., Buchanan, T. S. & Snyder-Mackler, L. (2015), 'A more informed evaluation of medial compartment loading: The combined use of the knee adduction and flexor moments', *Osteoarthritis and Cartilage* **23**(7), 1107–1111.
URL: *http://dx.doi.org/10.1016/j.joca.2015.02.779*

Marisami, P. & Venkatachalam, R. (2021), 'Towards optimal toe-clearance in synthesizing polycentric prosthetic knee mechanism', *Computer Methods in Biomechanics and Biomedical Engineering* **0**(0), 1–12.
URL: *https://doi.org/10.1080/10255842.2021.1972291*

Mcdonald, C. L., Westcott-mccoy, S., Weaver, M. R., Haagsma, J. & Kartin, D. (2020), 'Global prevalence of traumatic non-fatal limb amputation', *Prosthetics and Orthotics International* pp. 1–20.

McMenemy, L., Ramasamy, A., Sherman, K., Mistlin, A., Phillip, R., Evriviades, D. & Kendrew, J. (2020), 'Direct Skeletal Fixation in bilateral above knee amputees following blast: 2 year follow up results from the initial cohort of UK service personnel', *Injury* **51**(3), 735–743.
URL: *https://doi.org/10.1016/j.injury.2020.01.006*

Meanley, S. (1995), 'Different approaches and cultural considerations in third world prosthetics', *Prosthetics and Orthotics International* **19**(3), 176–180.

Melcer, T., Belnap, B., Jay Walker, G., Konoske, P. & Galarneau, M. (2011), 'Heterotopic ossification in combat amputees from Afghanistan and Iraq wars: Five case histories and results from a small series of patients', *Journal of Rehabilitation Research and Development* **48**(1), 1–12.

Mensch, G. (1983), 'Physiotherapy following through-knee amputation', *Prosthetics and Orthotics International* **7**(2), 79–87.

Mitsiopoulos, N., Baumgartner, R. N., Heymsfield, S. B., Lyons, W., Gallagher, D. & Ross, R. (1998), 'Cadaver validation of skeletal muscle measurement by magnetic resonance imaging and computerized tomography', *Journal of Applied Physiology* **85**(1), 115–122.

Miyazaki, T., Wada, M., Kawahara, H., Sato, M., Baba, H. & Shimada, S. (2002), 'Dynamic load at baseline can predict radiographic disease progression in medial compartment knee osteoarthritis', *Annals of the Rheumatic Diseases* **61**(7), 617–622.

Morgenroth, D. C., Gellhorn, A. C. & Suri, P. (2012), 'Osteoarthritis in the Disabled Population: A Mechanical Perspective', *American Academy of Physical Medicine and Rehabilitation* **4**(May), 20–27.

Muller, M. (2016), *Atlas of amputations and limb deficiencies: surgical, prosthetic and rehabilitation principles*, 4th ed. edn, Rosemont: American Academy of Orthopaedic Surgeons.

Nakahara, I., Takao, M., Sakai, T., Nishii, T., Yoshikawa, H. & Sugano, N. (2011), 'Gender differences in 3D morphology and bony impingement of human hips', *Journal of Orthopaedic Research* **29**(3), 333–339.

Nolan, L. & Lees, A. (2000), 'The functional demands on the intact limb during walking for active trans-femoral and trans-tibial amputees', *Prosthetics and Orthotics International* **24**, 117–125.

Nolan, L., Wit, A., Dudzin, K., Lees, A., Lake, M. & Wychowan, M. (2003), 'Adjustments in gait symmetry with walking speed in trans-femoral and trans-tibial amputees', *Gait and Posture* **17**, 142–151.

Nolte, D., Tsang, C. K., Zhang, K. Y., Ding, Z., Kedgley, A. E. & Bull, A. M. J. (2016), 'Non-linear scaling of a musculoskeletal model of the lower limb using statistical shape

models', *Journal of Biomechanics* **49**(14), 3576–3581.
URL: *http://dx.doi.org/10.1016/j.jbiomech.2016.09.005*

Norvell, D. C., Czerniecki, J. M., Reiber, G. E., Maynard, C., Pecoraro, J. A. & Weiss, N. S. (2005), 'The prevalence of knee pain and symptomatic knee osteoarthritis among veteran traumatic amputees and nonamputees', *Archives of Physical Medicine and Rehabilitation* **86**(3), 487–493.
URL: *http://dx.doi.org/10.1016/j.apmr.2004.04.034*

Papi, E., Bull, A. M. & McGregor, A. H. (2020), 'Alteration of movement patterns in low back pain assessed by Statistical Parametric Mapping', *Journal of Biomechanics* **100**, 109597.
URL: *https://doi.org/10.1016/j.jbiomech.2019.109597*

Pataky, T. C., Robinson, M. A. & Vanrenterghem, J. (2013), 'Vector field statistical analysis of kinematic and force trajectories', *Journal of Biomechanics* **46**(14), 2394–2401.
URL: *http://dx.doi.org/10.1016/j.jbiomech.2013.07.031*

Penn-Barwell, J. G. (2011), 'Outcomes in lower limb amputation following trauma: a systematic review and meta-analysis.', *International Journal of the Care of the Injured* **42**(12), 1474–1479.

Perotto, A. (2011), *Anatomical guide for the electromyographer: the limbs and trunk*, Charles C Thomas Publisher.

Perry, J., Burnfield, J. M., Newsam, C. J. & Conley, P. (2004), 'Energy expenditure and gait characteristics of a bilateral amputee walking with C-leg prostheses compared with stubby and conventional articulating prostheses', *Archives of Physical Medicine and Rehabilitation* **85**(10), 1711–1717.

Physical Rehabilitation Programme, I. (2020), PHYSICAL REHABILITATION, Technical report, International Committee of the Red Cross.

Potter, B. K., Burns, T. C., Lacap, A. P., Granville, R. R. & Gajewski, D. (2006), 'Heterotopic ossification in the residual limbs of traumatic and combat-related amputees', *Journal of the American Academy of Orthopaedic Surgeons* **14**(10), 191–197.

Pruziner, A. L., Werner, K. M., Copple, T. J., Hendershot, B. D. & Wolf, E. J. (2014), 'Does intact limb loading differ in servicemembers with traumatic lower limb loss?', *Clinical orthopaedics and related research* **472**(10), 3068–3075.

Radcliffe, C. W. (1977), 'Above-knee prosthetics', *Prosthetics and Orthotics International* (1), 146–160.

Radcliffe, C. W. (1994), 'Four-bar linkage prosthetic knee mechanisms: Kinematics, alignment and prescription criteria', *Prosthetics and Orthotics International* **18**(3), 159–173.

Radcliffe, I., Grigoriadis, G. & Natt, C. (2016), Designing an Improved Prosthesis for Knee Disarticulation Amputees, Technical report, Department of Bioengineering, The Dyson School of Design Engineering, Imperial College London.

Ranz, E. C., Wilken, J. M., Gajewski, D. A. & Neptune, R. R. (2017), 'The influence of limb alignment and transfemoral amputation technique on muscle capacity during gait', *Computer Methods in Biomechanics and Biomedical Engineering* **20**(11), 1167–1174.
URL: *https://doi.org/10.1080/10255842.2017.1340461*

Riveras, M., Ravera, E., Ewins, D., Shaheen, A. F. & Catalfamo-Formento, P. (2020), 'Minimum toe clearance and tripping probability in people with unilateral transtibial amputation walking on ramps with different prosthetic designs', *Gait and Posture* **81**(July), 41–48.
URL: *https://doi.org/10.1016/j.gaitpost.2020.07.005*

Rouhani, A. & Mohajerzadeh, S. (2013), 'An epidemiological and etiological report on lower extremity amputation in northwest of Iran', *Archives of Bone and Joint Surgery* **1**(2), 103–106.

Rush, P. J., Wong, J. S. W., Kirsh, J. & Devlin, M. (1994), 'Osteopenia in patients with above knee amputation', *Archives of Physical Medicine and Rehabilitation* **75**(1), 112–115.

Russell Esposito, E., Aldridge Whitehead, J. M. & Wilken, J. M. (2015), 'Sound limb loading in individuals with unilateral transfemoral amputation across a range of walking velocities', *Clinical Biomechanics* **30**(10), 1049–1055.
URL: *http://dx.doi.org/10.1016/j.clinbiomech.2015.09.008*

Sarin, H., Kokkolaras, M., Hulbert, G., Papalambros, P., Barbat, S. & Yang, R. J. (2010), 'Comparing time histories for validation of simulation models: Error measures and metrics', *Journal of Dynamic Systems, Measurement and Control, Transactions of the ASME* **132**(6), 1–10.

Sawers, A. B. & Hafner, B. J. (2013), 'Outcomes associated with the use of microprocessor-controlled prosthetic knees among individuals with unilateral transfemoral limb loss: A systematic review', *J Rehabil Res Dev* **50**(3), 273–314.

Scheys, L., Spaepen, A., Suetens, P. & Jonkers, I. (2008), 'Calculated moment-arm and muscle-tendon lengths during gait differ substantially using MR based versus rescaled generic lower-limb musculoskeletal models', *Gait and Posture* **28**(4), 640–648.

Schumacher, C., Berry, A., Lemus, D., Rode, C., Seyfarth, A. & Vallery, H. (2019), 'Biarticular muscles are most responsive to upper-body pitch perturbations in human standing', *Scientific Reports* **9**(1), 1–14.

Sedki, I. & Fisher, K. (2015), 'Developing prescribing guidelines for microprocessor-controlled prosthetic knees in the South East England', *Prosthetics and Orthotics International* **39**(3), 250–254.

Shaw, J., Challa, S., Conway, D., Liu, M., Haonga, B., Eliezer, E., Morshed, S. & Shearer, D. (2018), 'Quality of life and complications in lower limb amputees in Tanzania: results from a pilot study', *The Lancet Global Health* **6**(Suppplement 2), S18.
URL: *http://dx.doi.org/10.1016/S2214-109X(18)30147-5*

Sherk, V. D., Bemben, M. G. & Bemben, D. A. (2008), 'BMD and Bone Geometry in Transtibial and Transfemoral Amputees', *Journal of Bone and Mineral Research* **23**(9), 1449–1457.

Shojaei, I., Hendershot, B. D., Wolf, E. J. & Bazrgari, B. (2016), 'Persons with unilateral transfemoral amputation experience larger spinal loads during level-ground walking compared to able-bodied individuals', *Clinical Biomechanics* **32**, 157–163.

Sivapuratharasu, B., Bull, A. M. & McGregor, A. H. (2019), 'Understanding Low Back Pain in Traumatic Lower Limb Amputees: A Systematic Review', *Archives of Rehabilitation Research and Clinical Translation* **1**(1-2), 100007.
URL: *https://doi.org/10.1016/j.arrct.2019.100007*

Smith, D. G. (2004), 'The knee disarticulation: It's better when it's better and it's not when it's not', *inMotion* **14**(1), 56–62.

Smith, D. G., Legro, M. W., Reiber, G. E., Aguila, M., Boone, D. A. & Mph, C. (1999), 'Phantom Limb , Residual Limb , and Back Pain After Lower Extremity Amputations', *Clinical Orthopaedics and Related Research* **361**, 29–38.

Smith, J. D., Ferris, A. E., Heise, G. D., Hinrichs, R. N. & Martin, P. E. (2014), 'Oscillation and reaction board techniques for estimating inertial properties of a below-knee prosthesis', *Journal of Visualized Experiments* **87**, 1–15.

Steeper Group (2022), 'Seattle SACH Catalague'.

Stevens, P. M., Rheinstein, J. & Wurdeman, S. R. (2018), 'Prosthetic Foot Selection for Individuals with Lower-Limb Amputation: A Clinical Practice Guideline', *Journal of Prosthetics and Orthotics* **30**(4), 175–180.

Stevens, P. M. & Wurdeman, S. R. (2019), 'Prosthetic Knee Selection for Individuals with Unilateral Transfemoral Amputation: A Clinical Practice Guideline', *Journal of Prosthetics and Orthotics* **31**(1), 2–8.

Struyf, P. A., van Heugten, C. M., Hitters, M. W. & Smeets, R. J. (2009), 'The Prevalence of Osteoarthritis of the Intact Hip and Knee Among Traumatic Leg Amputees', *Archives of Physical Medicine and Rehabilitation* **90**(3), 440–446.
URL: *http://dx.doi.org/10.1016/j.apmr.2008.08.220*

Summers, G. D., Morrison, J. D. & Cochrane, G. M. (1987), 'Foot loading characteristics of amputees and normal subjects', *Prosthetics and Orthotics International* **11**(1), 33–39.

Taghipour, H., Moharamzad, Y., Mafi, A. R. & Amini, A. (2009), 'Quality of Life Among Veterans With War-Related Unilateral Lower Extremity Amputation : A Long-Term Survey in a Prosthesis Center in Iran', *J Orthop Trauma* **23**(7), 525–530.

Tang, J., McGrath, M., Laszczak, P., Jiang, L., Bader, D. L., Moser, D. & Zahedi, S. (2015), 'Characterisation of dynamic couplings at lower limb residuum/socket interface using 3D motion capture', *Medical Engineering and Physics* **37**(12), 1162–1168.
URL: *http://dx.doi.org/10.1016/j.medengphy.2015.10.004*

Tzamaloukas, A. H., Patron, A. & Malhotra, D. (1994), 'Body mass index in amputees', *Journal of Parenteral and Enteral Nutrition* **18**(4), 355–358.

Uchytil, J., Jandacka, D., Zahradnik, D. & Janura, M. (2014), 'Temporal – spatial parameters of gait in transfemoral amputees : Comparison of bionic and mechanically passive knee joints', *Prosthetics and Orthotics International* **38**(3), 199–203.

Valente, G., Pitto, L., Testi, D., Seth, A., Delp, S. L., Stagni, R., Viceconti, M. & Taddei, F. (2014), 'Are subject-specific musculoskeletal models robust to the uncertainties in parameter identification?', *PLoS ONE* **9**(11).

Ward, S. R., Eng, C. M., Smallwood, L. H. & Lieber, R. L. (2009), 'Are current measurements of lower extremity muscle architecture accurate?', *Clinical Orthopaedics and Related Research* **467**(4), 1074–1082.

Weinert-Aplin, R. A., Twiste, M., Jarvis, H. L., Baker, R. J., Twiste, M., Jarvis, H. L., Bennett, A. N., Bennett, A. N. & Bennett, A. N. (2017), 'Medial-lateral centre of mass displacement and base of support are equally good predictors of metabolic cost in amputee walking', *Gait and Posture* **51**, 41–46.
URL: *http://dx.doi.org/10.1016/j.gaitpost.2016.09.024*

White, D. R., Woodard, H. Q. & Hammond, S. M. (1987), 'Average soft-tissue and bone models for use in radiation dosimetry', *Br. J. Radiol.* **60**, 907–13.

Whittle, M. W. (2006), *Gait analysis: an introduction*, 4 edn, Butterworth-Heinemann Elsevier, USA.

Yamaguchi, G. (2005), *Dynamic modelling of musculoskeletal motion: a vectorized approach for biomechanical analysis in three dimensions*, Springer Science & Business Media.

Yeung, L. F., Leung, A. K., Zhang, M. & Lee, W. C. (2012), 'Long-distance walking effects on trans-tibial amputees compensatory gait patterns and implications on prosthetic designs and training', *Gait and Posture* **35**(2), 328–333.
URL: *http://dx.doi.org/10.1016/j.gaitpost.2011.10.004*

Yu, B., Gabriel, D., Noble, L. & An, K. N. (1999), 'Estimate of the optimum cutoff frequency for the Butterworth low-pass digital filter', *Journal of Applied Biomechanics* **15**(3), 318–329.

Zuk, M., Syczewska, M. & Pezowicz, C. (2018), 'Influence of uncertainty in selected musculoskeletal model parameters on muscle forces estimated in inverse dynamics-based static optimization and hybrid approach', *Journal of Biomechanical Engineering* **140**(12), 1–12.